

**Characterization of the conformational dynamics of the Nek2 leucine zipper
domain**

Thesis submitted for the degree of
Doctor of Philosophy
at the University of Leicester

By

Rebecca Croasdale B.Sc. (Hons.)
Department of Biochemistry
University of Leicester

2013

Characterization of the conformational dynamics of the Nek2 leucine zipper domain

REBECCA CROASDALE

ABSTRACT

Nek2 is a cell cycle regulated protein kinase. Its expression and activity peak in S and G2 phase before the protein is targeted for degradation in mitosis. Nek2 activity promotes centrosome separation and bipolar spindle formation, processes that are essential for maintaining the fidelity of chromosome segregation and cell division.

Importantly, Nek2 inhibition results in increased apoptosis and senescence in cancer cell lines and tumour xenografts making Nek2 an attractive target for chemotherapeutic intervention.

The α -helix is the most common secondary structure in proteins, with 2-3% of all proteins adopting a coiled-coil structure. The coiled-coil motif mediates a diverse range of functions including DNA transcription, intracellular protein shuttling, membrane signalling, and coordination of the cell cycle. Nek2 contains two coiled-coil motifs in its C-terminal non-catalytic domain, the first of which forms a leucine zipper structure, whilst the second has recently been classified as a SARAH domain. The leucine zipper spans residues 304-340 and is responsible for Nek2 dimerization, autophosphorylation and activation.

The Nek2 leucine zipper contains an unusual pattern of charged residues in the dimerization interface. Through studies on isolated fragments, we found that the Nek2 leucine zipper exists primarily as a dimer in solution, albeit with concentration dependent higher order oligomerization. However, the positioning of charged residues enabled the helices to undergo a register shift between two alternative heptad conformations on a timescale of 17s^{-1} . This represents slow-intermediate exchange on the NMR timescale, greatly increasing the transverse and longitudinal relaxation rates leading to enhanced loss of signal intensity. As this precluded structure determination through NMR studies on wild-type fragments, a K309C mutant was generated that ‘locked’ the leucine zipper into one conformation. The significantly reduced relaxation rates confirming the presence of conformational dynamics and making structural determination possible in the future.

ACKNOWLEDGMENTS

I would initially like to thank my supervisors Prof. Andrew Fry and Dr. Mark Pfuhl, for all their support and guidance in completing the thesis. I also would like to thank the Hope Foundation for Cancer Research, for the hard work to raise money to fund research projects such as this.

I would also like to thank all the members of the Fry Lab and also the Pfuhl Lab, past and present, we had many good and great times whilst working together. These times I will remember fondly.

I would like to express my deep gratitude to my family, especially my parents Stephen and Denise, Sister Rachael and grandparents Elsie and James who have supported me every step of the way through this process.

Thank you to my Grandparents Eva and Dennis who would have been so proud of this moment, for all their support and encouragement throughout all stages of my education.

Lastly, the members of 11 Tower Street, I will never forget Carla, Jon, Rob, Paul and Claudia for being superb company and making such lovely food. I miss you all!

CONTENTS

ABSTRACT.....	II
ACKNOWLEDGMENTS	III
CONTENTS	IV
FIGURES.....	VII
ABBREVIATIONS.....	IX
1 INTRODUCTION	1
1.1 The Molecular Biology of Cancer.....	2
1.1.1 Cellular Proliferation	2
1.1.2 Genetic Instability	3
1.2 Centrosomes.....	9
1.2.1 The functions of the Centrosome	11
1.2.2 Centrosomes and cancer	13
1.2.3 Regulation of centrosome duplication.....	15
1.3 Nek Protein Kinases	17
1.3.1 Nek2: a centrosome kinase.....	18
1.3.2 Functions of Nek2 at the centrosome.....	21
1.3.3 Regulation of Nek2 by phosphorylation	24
1.3.4 Regulation of Nek2 by oligomerization.....	25
1.3.5 Structural studies on Nek2.....	31
1.3.6 Nek2 and Cancer	34
1.4 Kinase inhibitors	36
1.5 Aims and Objectives.....	37
2 MATERIALS AND METHODS	41
2.1 Molecular Biology Techniques	42
2.1.1 Polymerase chain reaction (PCR)	42
2.1.2 Restriction digestion	42
2.1.3 Ligation.....	43
2.1.4 Bacterial transformation.....	43
2.1.5 PCR screening of clones	45
2.1.6 Cloning performed	46

2.1.7	Site-directed mutagenesis	46
2.1.8	DNA gel electrophoresis.....	48
2.1.9	Plasmid preparation.....	48
2.1.10	Preparation of chemically competent bacteria	48
2.2	Analysis of proteins	49
2.2.1	SDS-PAGE	49
2.2.2	Coomassie Blue staining	49
2.2.3	Protein determination	49
2.3	Protein expression and Purification	50
2.3.1	Competent cells transformation for protein expression	50
2.3.2	Expression in Luria- Bertani (LB) medium.....	50
2.3.3	Expression in Minimal medium M9 (Marley Method).	51
2.3.4	Protein Purification	52
2.3.5	Purification methods using chromatography	52
2.3.6	Removal of the Histidine tag.....	53
2.3.7	Buffer exchange for Circular Dichroism (CD) analysis.....	55
2.4	Spectroscopic analysis	55
2.4.1	Circular Dichroism (CD) spectroscopy.....	55
2.4.2	NMR spectroscopy	56
2.4.3	Analytical ultracentrifugation	72
2.5	Bioinformatics software	73
3	BIOPHYSICAL PROPERTIES OF THE NEK2 LEUCINE ZIPPER	74
3.1	Results.....	75
3.1.1	Rationale for the design of the Nek2 leucine zipper constructs.....	75
3.1.2	Molecular biology of the Nek 2 Leucine zipper constructs.....	77
3.1.3	Preliminary characterisation of the Nek2 leucine zipper constructs	80
3.1.4	Generation of the Nek2 LZ5 domain mutants	88
3.1.5	Expression and purification of the Nek 2 Leucine zipper constructs	89
3.1.6	Average expression yields of the Nek 2 leucine zipper constructs.....	95
3.1.7	Bioinformatics analysis of the sequence of the Nek2 LZ domain	100
3.1.8	Circular dichroism (CD) of the wild-type Nek2 leucine zipper constructs	107
3.1.9	Circular dichroism (CD) of the mutated Nek2 leucine zipper constructs	108
3.1.10	Analytical ultracentrifugation of Nek2 LZ domain	112
3.2	Discussion	114
3.2.1	Biophysical analysis of Nek2 leucine zipper.....	114
4	CHARACTERIZATION OF THE DYNAMIC NATURE OF THE NEK2 LEUCINE ZIPPER USING NMR	118

4.1	Results	119
4.1.1	Rationale to explore the dynamics of the leucine zipper domain	119
4.1.2	^{15}N LZ5 Expression and Purification	119
4.1.3	2D homonuclear TOCSY/NOESY with LZ2	122
4.1.4	^{15}N HSQC reference spectra.....	125
4.1.5	^{15}N HSQC showing the effect of dilution on LZ5	135
4.1.6	^1H 1D showing the effect of dilution on LZ2	139
4.1.7	2D $^1\text{H}/^{15}\text{N}$ HSQC of LZ5 studying the effect of temperature upon exchange	142
4.1.8	2D $^1\text{H}/^{15}\text{N}$ HSQC of LZ5 studying the effect of acetonitrile upon exchange	145
4.1.9	The effect of increasing temperature at 30% acetonitrile concentration	146
4.1.10	The effect of decreasing temperature at 30% acetonitrile concentration	150
4.1.11	The influence of pH upon HSQC line widths and the number of peaks present	154
4.1.12	Investigating the nature of exchange in LZ5	156
4.1.13	Investigation of the exchange in ‘locked’ LZ5 conformations through mutation.....	161
4.2	Discussion	165
4.2.1	Exchange dynamics present in the Nek2 leucine zipper.....	165
4.2.2	Investigation into the NMR oligomerization state of the Nek2 leucine zipper	165
5	FINAL DISCUSSION	167
5.1	Final discussion	168
5.1.1	Sequence specific interactions within the Nek2 leucine zipper	168
5.1.2	The Nuclear export signal of the Nek2 protein.....	170
5.1.3	Nek2 leucine zipper - a dynamic domain	171
5.1.4	Probing the oligomerization state of the Nek2 leucine zipper	174
5.1.5	Manipulation of the kinetic equilibrium using temperature	179
5.1.6	Frequency of exchange dynamics observed by NMR	180
5.1.7	Characterization of the Nek2 mutants.....	182
5.1.8	Functional relevance of the conformational dynamics of the Nek2 leucine zipper ...	184
6	BIBLIOGRAPHY	189
7	APPENDIX.....	221

FIGURES

FIGURE 1.1 THE SPINDLE ASSEMBLY CHECKPOINT	6
FIGURE 1.2 CENTROSOME ORGANISATION	10
FIGURE 1.3 THE DOMAIN ORGANISATION OF THE THREE NEK2 SPLICE VARIANTS	20
FIGURE 1.4 ALPHA HELIX GEOMETRY	27
FIGURE 1.5 RESIDUE INTERACTIONS IN TWO-STRANDED COILED-COILS	29
FIGURE 1.6 STRUCTURE OF THE NEK2 PROTEIN KINASE DOMAIN	33
FIGURE 2.1 PETM-11 VECTOR MAP	44
FIGURE 2.2 BOLTZMANN DISTRIBUTION IN A MAGNETIC FIELD B_0	58
FIGURE 2.4 RELAXATION PROCESSES	63
FIGURE 3.1 MOLECULAR BIOLOGY OF LEUCINE ZIPPER CONSTRUCTS	79
FIGURE 3.2 1D ^1H NMR CHARACTERIZATION OF LZ0	82
FIGURE 3.3 1D ^1H NMR CHARACTERIZATION OF LZ2	83
FIGURE 3.4 1D ^1H NMR CHARACTERIZATION OF LZ3	84
FIGURE 3.5 1D ^1H NMR CHARACTERIZATION OF LZ4	85
FIGURE 3.6 1D ^1H NMR CHARACTERIZATION OF LZ5	86
FIGURE 3.7 1D ^1H NMR CHARACTERIZATION OF LZ6	87
FIGURE 3.8 MUTAGENESIS TO LOCK HEP1 AND HEP1I REPEATS IN LZ5	90
FIGURE 3.9 AFFINITY PURIFICATION OF LZ0-LZ6 USING FAST FLOW 6 NI-NTA BEADS	93
FIGURE 3.10 PURIFICATION OF LEUCINE ZIPPER CONSTRUCTS 0 AND 2	94
FIGURE 3.11 CALIBRATING THE BCA PROTEIN ASSAY TO THE LEUCINE ZIPPER CONSTRUCTS	97
FIGURE 3.12 REDUCED COMPATIBILITY BCA ASSAY CALIBRATION CURVE WITH 2 MM DTT	98
FIGURE 3.13 LEVELS OF PROTEIN EXPRESSION BETWEEN NEK2 LEUCINE ZIPPER CONSTRUCTS	99
FIGURE 3.14 LEVELS OF PROTEIN YIELD BETWEEN NEK2 LEUCINE ZIPPER CONSTRUCTS	102
FIGURE 3.15 SEQUENCE ANALYSIS OF THE NEK2 LEUCINE ZIPPER	103
FIGURE 3.16 SEQUENCE ANALYSIS OF THE POTENTIAL INTERFACES OF THE NEK2 LEUCINE ZIPPER	104
FIGURE 3.17 NEK2 LZ SEQUENCE ANALYSIS OF A POTENTIAL NUCLEAR EXPORT SIGNAL (NES)	106
FIGURE 3.18 CIRCULAR DICHROISM (CD) COMPARISON OF LEUCINE ZIPPER CONSTRUCTS LZ0 AND LZ5	109
FIGURE 3.19 THERMAL MELTING TEMPERATURE OF THE NEK2 LZ5 MUTANT K309C	110
FIGURE 3.20 THERMAL MELTING TEMPERATURE OF THE NEK2 LZ5 MUTANT E310C	111
FIGURE 3.21 SEDIMENTATION VELOCITY AUC OF LZ0, LZ5 AND LZ5K309C/C335A	113
FIGURE 4.1 PURIFICATION OF THE HIS-TAGGED 15N NEK2 LEUCINE ZIPPER DOMAIN 5	121
FIGURE 4.2 2D TOCSY/NOESY ^{15}N NEK2 LEUCINE ZIPPER DOMAIN 2 (LZ2)	124
FIGURE 4.3 2D $^1\text{H}/^{15}\text{N}$ HSQC OF NEK2 LZ0	126
FIGURE 4.4 2D $^1\text{H}/^{15}\text{N}$ HSQC OF NEK2 LZ1	127
FIGURE 4.5 2D $^1\text{H}/^{15}\text{N}$ HSQC OF NEK2 LZ2	128
FIGURE 4.6 2D $^1\text{H}/^{15}\text{N}$ HSQC OF NEK2 LZ4	129
FIGURE 4.7 2D $^1\text{H}/^{15}\text{N}$ HSQC OF NEK2 LZ5	130
FIGURE 4.8 2D $^1\text{H}/^{15}\text{N}$ HSQC OF NEK2 LZ5 C335AK309C OXIDISED	131
FIGURE 4.9 2D $^1\text{H}/^{15}\text{N}$ HSQC OF NEK2 LZ5 C335AK309C REDUCED	132
FIGURE 4.10 2D $^1\text{H}/^{15}\text{N}$ HSQC OF NEK2 LZ5 C335AE310C OXIDISED	133
FIGURE 4.11 2D $^1\text{H}/^{15}\text{N}$ HSQC OF NEK2 LZ5 C335AE310C REDUCED	134
FIGURE 4.12 2D $^1\text{H}/^{15}\text{N}$ HSQC OF NEK2 LZ5	136
FIGURE 4.13 2D $^1\text{H}/^{15}\text{N}$ HSQC OF THE NEK2 LZ5 SHOWING THE EFFECT OF DILUTION ON OLIGOMERISATION	138
FIGURE 4.14 1H 1D SPECTRUM OF THE NEK2 LZ2 SHOWING THE EFFECT OF DILUTION ON OLIGOMERISATION	140
FIGURE 4.15 2D $^1\text{H}/^{15}\text{N}$ HSQC SPECTRA OF THE NEK2 LZ2 SHOWING THE EFFECT OF DILUTION ON OLIGOMERISATION	141
FIGURE 4.16 2D $^1\text{H}/^{15}\text{N}$ HSQC OF NEK2 LZ5 SHOWING THE EFFECT OF TEMPERATURE	144
FIGURE 4.17 2D $^1\text{H}/^{15}\text{N}$ HSQC OF NEK2 LZ5 SHOWING THE EFFECT OF ACETONITRILE CONCENTRATION	147
FIGURE 4.18 1D ^{15}N SLICE OF LZ5 SHOWING THE EFFECT OF ACETONITRILE CONCENTRATION UPON LINE BROADENING	148
FIGURE 4.19 2D $^1\text{H}/^{15}\text{N}$ HSQC OF LZ5 SHOWING THE EFFECT OF INCREASING TEMPERATURE WITH 30% ACETONITRILE	149
FIGURE 4.20 2D $^1\text{H}/^{15}\text{N}$ HSQC OF LZ5 SHOWING THE EFFECT OF DECREASING TEMPERATURE WITH 30% ACETONITRILE	152
FIGURE 4.21 1D SLICE OF AN HSQC OF LZ5 SHOWING THE EFFECT OF DECREASING TEMPERATURE WITH 30% ACETONITRILE	153
FIGURE 4.22 2D $^1\text{H}/^{15}\text{N}$ HSQC OF LZ5 SHOWING THE EFFECT OF PH	155
FIGURE 4.23 2D HETERONUCLEAR CORRELATION EXPERIMENT OF NEK2 LZ5 REFERENCE HSQC	158
FIGURE 4.24 ^{15}N RELAXATION EXPERIMENTS USING LZ5	159

FIGURE 4.25 ^{15}N RELAXATION EXPERIMENTS USING LZ5 FOR PEAKS #12 AND #43	160
FIGURE 4.26 2D $^1\text{H}/^{15}\text{N}$ HSQC OF LZ5, LZ5K309C AND LZ5E310C	162
FIGURE 4.27 ^{15}N HETERONUCLEAR CORRELATION EXPERIMENTS USING LZ5K309C.....	164
FIGURE 5.1 EXAMPLE SPECTRA DISPLAYING DIFFERING EXCHANGE RATES RELATED TO CHEMICAL SHIFT.....	177
FIGURE 5.2 TWO STATE DYNAMIC PROCESS INVOLVING THE NEK2 LEUCINE ZIPPER	178
FIGURE 5.3 MODEL DEPICTING THE THEORETIC CONFORMATIONS OF THE NEK2 LEUCINE ZIPPER	187
FIGURE 5.4 MUTAGENESIS TO LOCK HEP1 AND HEP2 REPEATS IN LZ5	188

ABBREVIATIONS

Abelson murine leukaemia viral oncogene homolog 1	ABL1
Analytical ultracentrifugation	AUC
Anaphase-promoting factor complex/cyclosome	APC/C
Asterless/CEP152	Asl
Bicinchoninic acid assay	BCA assay
Bovine serum albumin	BSA
Breakpoint cluster region	BCR
Burkitt's lymphoma	BL
Centrosomal Nek2-associated protein 1	C-Nap1
Centrosomes amplification	CA
Chemical shift anisotropy	CSA
Chromosome instability	CIN
Chronic myeloid leukaemia	CML
Circular dichroism	CD
Cyclin-dependent kinase	CDK
Cyclin dependent kinase 1	CDK1
Deoxyribonucleic acid	DNA
Deoxyribonucleotide triphosphates	dNTPs
Dithiothreitol	DTT
Epidermal growth factor receptor	EGFR
European Molecular Biology Laboratory	EMBL
Extracellular matrix	ECM
Extracellular regulated kinases 2	ERK2
Fast flow 6	FF6
Free induction decay	FID
Hidden Markov model algorithm	HMM
Highly expressed in cancer-1	Hec-1
Immobilized Metal ion Affinity Chromatography	IMAC
Immunoglobulin	Ig
Leucine zipper	LZ

Luria- Bertani	LB
Mammalian sterile 20-like kinase	Mst
Methionine-arginine	MR
Microtubule-organising centre	MTOC
Mitotic Arrest Deficient	Mad
Mitotic checkpoint complex	MCC
Monopolar spindle 1	Mps1
Myelocytomatosis viral oncogene	c-myc
Neural network algorithm	NN
Nuclear export signal	NES
Nuclear magnetic resonance	NMR
Nuclear overhauser effect	NOE
Nuclear overhauser enhanced spectroscopy	NOESY
Nucleotide excision repair	NER
One dimensional	1D
Pericentriolar material	PCM
Polo-like kinase	Plk
Polymerase chain reaction	PCR
Protein phosphatase 1	PP1
Radio frequency	RF
Retinoblastoma	Rb
Salvador/Ras-association domain family/hippo	SARAH
Scaffold protein Salvador	hSav1
Sedimentation coefficient	S
Small molecule inhibitor	SMI
Spindle assembly checkpoint	SAC
Standard deviation	SD
Three dimensional	3D
Total correlation spectroscopy	TOSCY
Two dimensional heteronuclear single quantum coherence	2D-HSQC
Ultraviolet	UV

CHAPTER 1

INTRODUCTION

1.1 The Molecular Biology of Cancer

1.1.1 Cellular Proliferation

Many normal cells hyperproliferate (hyperplasia) on occasions but retain their normal behaviour and appearance due to the effect of internal and external inhibitory signals.

Neoplasm or tumour can be used to describe the abnormal growth of cells. Tumours can be divided into two groups benign or malignant. Benign tumours are associated with a better prognosis and remain localised, although can be precursors of malignant tumours. Cancer clinically describes a malignant tumour, malignant tumours have the ability to invade surrounding tissue and metastasise to other distant organs. The malignant tumour overcomes normal inhibitory signals to possess a growth advantage over the normal cells which surround it. Often these are self sufficiency in growth signals, insensitivity to growth inhibition signals, a reduction in cell death (resistance to apoptosis), unlimited proliferation and membrane modifications resulting in loss of cell-cell contact interactions and the production of proteases to facilitate movement through the extracellular matrix (ECM) termed invasion leading to metastasis (Hanahan and Weinberg, 2000). Malignant tumours often utilise extracellular ligands to stimulate the growth of new blood vessels (angiogenesis) to support a dense tumour mass. The invasive properties of a malignant tumour are what distinguish it from a benign tumour with metastasis being the primary cause of death in cancer.

1.1.2 Genetic Instability

Chromosomal instability (CIN) occurs at a high rate in human tumours. It has been postulated that CIN gives tumour cells their increased ability to proliferative, invasive advantage and also plays a role in drug resistance. However, the exact mechanisms behind chromosomal rearrangement are still largely unclear.

There are different types of genetic alterations which are thought to contribute to the development of human tumours, which can be divided into categories.

The first being sequence changes in the genome. Typically, these involve base substitutions, deletions or insertions of a few nucleotides. In patients with Xeroderma pigmentosum nucleotide excision repair (NER) enzymes have been found to be mutated and non-functional (Freidberg et al., 2006). Upon exposure to ultraviolet light (UV) light any mutations in the genome cannot be corrected with the defective NER enzymes. For example, when this occurs to p53 (Williams et al., 1998) or N-Ras (Karnoub and Weinberg, 2008) it could increase the propensity to induce neoplastic transformation. In pancreatic tumours, a genomic analysis revealed predominantly missense mutations in primary tumours taken from a patient group of 24 (Jones et al., 2008). One of the core pathways found to be mutated was K-Ras allowing for the downstream activation of the mitogen-activated protein kinase (MAPK) and extracellular signal-regulated kinases (ERK) pathways allowing the pancreatic tumour cells the ability to initiate growth signals and aid differentiation.

A second type of genetic alteration is an elevated rate of the gain or loss of whole chromosomes. Changes in chromosome numbers are observed in nearly all human tumours (Lengauer et al., 1998). Aneuploidy is the state of having abnormal chromosome number.

The mitotic checkpoint or spindle assembly checkpoint (SAC) is the primary mechanism by which cells safeguard against chromosome missegregation (Kops et al., 2005; Musacchio and Salmon, 2007). The SAC delays the onset of anaphase until all chromosomes are stably attached to the microtubule spindle. In organisms such as flies (*Drosophila*) or fission yeast with low chromosome numbers, the SAC is non-essential because of the short time taken to achieve correct chromosome attachment to the spindles (Buffin et al., 2007). In higher eukaryotes the attachment of all chromosomes to the spindle can take hours (Rieder et al., 1994), in these cell types the SAC is essential.

The mitotic checkpoint complex (MCC) consists of Mitotic Arrest Deficient (Mad) 1-3, in humans Mad3 is called BUBR1. Mad mutants progress through mitosis in the presence of unattached kinetochores (Li and Murray, 1991). When a cell undergoing mitosis possesses extra chromosomes and/or centrosomes this phenotype greatly increases the time required for spindle assembly (Yang et al., 2008). In the event of this occurring, unless mitotic exit is delayed the progeny will be aneuploid. Data which supports this theory in mammals, shows that inactivation of the mitotic checkpoint in Mad2 null mice leads to aneuploidy and apoptosis (Dobles et al., 2000). This would indicate that any mutations in the MCC proteins could lead to aneuploidy and eventually to CIN in tumour cells. However, a high percentage of tumours possess a functional SAC and have a normal mitotic checkpoint (Gascoigne and Taylor, 2008). Therefore, could *bona fide* MCC proteins be responsible for aneuploidy? In theory if mutated SAC proteins could affect the integrity of the genome aneuploidy could arise, however, the data indicates that this is not the case and altered expression levels are more common. A more plausible explanation could be that in cells which display CIN the errors originate from abnormal spindle microtubule dynamics or possibly in the proteins

that repair incorrect kinetochore attachment or both simultaneously (Bakhoum et al., 2009). The SAC negatively regulates the ability of CDC20 to activate the anaphase-promoting factor complex/cyclosome (APC/C). The APC/C polyubiquitinates two key components, cyclin B and securin, inactivation of the APC/C would serve to inhibit the degradation of these proteins by the 26S proteosome. Securin is an inhibitor of the protease separase. Separase cleaves the cohesin complex that holds sister chromatids together (Figure 1.1), only upon cohesin cleavage can the cell progress into anaphase. Therefore, mutations found in the cyclin B family of proteins, CDK1, securin or separase including any regulatory proteins involved could induce premature exit from mitosis resulting in aneuploidy but are rare in human tumours.

An alternative perspective of where aneuploidy originates from can be obtained when considering the attachment of microtubules to the kinetochore. For proper segregation microtubules attach to a kinetochore from a single spindle pole. However, in some instances one kinetochore can attach to both spindle poles simultaneously. The result is termed a merotelic attachment. Merotelic attachments have been identified as the main, if not only, cause of lagging chromosomes in anaphase (Cimini et al., 2001). Merotelic attachments do not mediate cell cycle arrest or apoptosis readily via activation of SAC related effectors (Cimini, 2008). Moreover, mechanisms to correct merotely are not completely efficient (Cimini et al., 2006; Knowlton et al., 2006). What is striking is that merotely does not activate the SAC, it is therefore logical to assume that improper microtubule attachment to kinetochore leads to loss in fidelity of chromosome segregation and finally to the generation of aneuploid progeny.

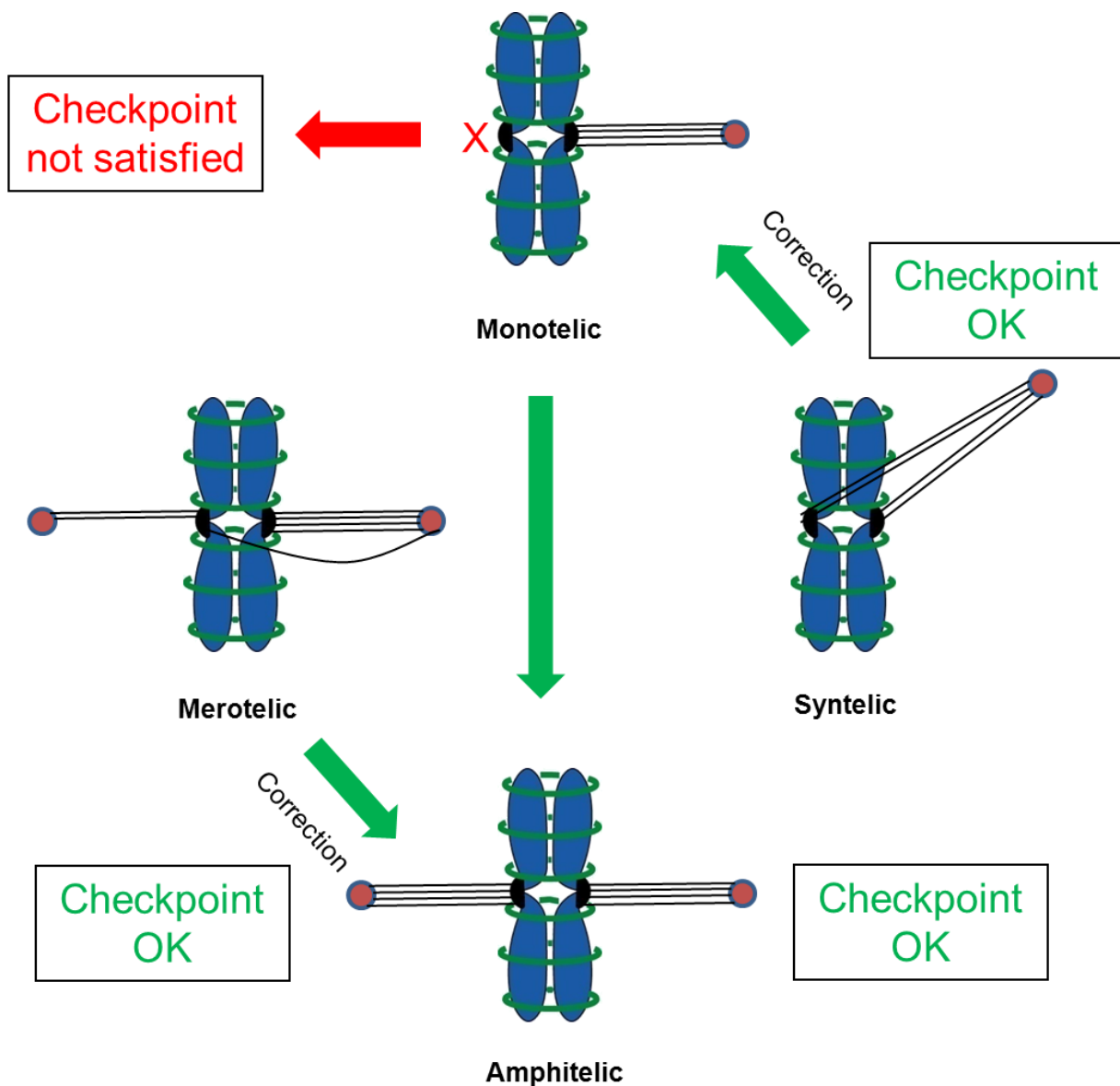


Figure 1.1 The spindle assembly checkpoint

Amphitelic attachment of spindle microtubules to the kinetochores of sister chromatids is required for chromosome segregation. Under these conditions, the SAC is satisfied. However, the SAC is not activated under certain conditions conducive to chromosome misalignment as indicated above in the merotelic and syntelic examples of spindle misattachment. According to this model, the SAC is only activated upon detection of a monotelic attachment, whereafter, mitosis is delayed until the SAC is satisfied.

The third category of genetic instability includes mechanisms of chromosome translocations; As early as 1914 Theodor Boveri first suggested that chromosome abnormalities may be a causative factor in cancers (Boveri, 1929). Indeed, many years later chromosome translocations and inversions appear to be the most common type of genetic abnormalities in human tumours (Yunis, 1986). Chromosome translocations can be described as the movement of genetic information from one chromosome to another. The first consistently identified chromosome translocation is found in the genesis of human chronic myeloid leukaemia (CML). In this disease a reciprocal translocation between chromosome 9 and 22 creates abnormal versions of both chromosomes, and is termed Philadelphia chromosome (Nowell and Hungerford, 1961). In this genetic abnormality found in CML, the Abelson murine leukaemia viral oncogene homolog 1 (ABL1) normally found on chromosome 9 switches to the breakpoint cluster region (BCR) of chromosome 22 (Klein et al., 1982; Bartram et al., 1983). The BCR-ABL fusion protein exhibits a higher enzymatic activity than ABL due to the replacement of the amino terminal of ABL with the domain from BCR, and therefore, an altered gene product (Konopka and Witte, 1985). The significance of the identification of this chromosome translocation can be put into perspective when considering the treatment for CML, where targeted tyrosine kinase inhibitors such as Imatinib show approximately 92% survival rate over 8 years (Gambacorti-Passerini et al., 2011), indicating the significance of the chromosome translocation of ABL in this disease.

The chromosome translocation in CML described the change in gene product, however, in Burkitt's lymphoma (BL) an insertion in the promoter region of c-myc results in an altered regulation. In 80% of cases chromosome 8 and 14 are involved, the breakpoint is located

upstream of the c-myc gene and is translocated to the Immunoglobulin (Ig) gene on chromosome 14 (Yunis, 1986; Haluska et al, 1987), the strong Ig promoter upregulates the c-myc gene resulting in an overexpression of c-myc protein.

Alterations in chromosomes are often used as a prognostic marker for tumour progression in highly invasive advanced human tumours (Mitelman, 2000; Ried et al., 1999), due to the high rate of occurrence. Interesting, centrosome abnormalities are not only found in advanced invasive cancers alongside chromosome abnormalities, but are common in low grade tumours and *in situ* carcinomas (Pihan et al., 2001; Lingle et al., 2002; Pihan et al., 2003). This provides evidence that centrosome abnormalities are present early in a tumours evolution and poses the question, are chromosome abnormalities or chromosome instability (CIN) caused by centrosome irregularities? This leads to a fourth category of potential mechanisms of cancer development, in human somatic cells coordination of the centrosome and chromosome duplication cycles appear to be under the control of the retinoblastoma pathway through hyperphosphorylation of the Rb protein (Meraldi et al., 1999) and subsequent activation of cyclin-dependent kinase 2 (CDK2) (Hinchcliffe et al., 1999; Matsumoto et al., 1999; Pihan et al., 2001). In terms of tumourigenesis, mutations in the Rb tumour suppressor protein could lead to deregulation in these key S-phase events enhancing the likelihood of supernumerary centrosomes and chromosome instability in human cancer cells.

Centrosomes have a dominant role in the formation of the mitotic spindle apparatus when present in cells (described in detail in section 1.2), with multipolar spindles being a common phenotype of tumour cells. Abnormal spindle formation can therefore be thought to contribute to errors in chromosome segregation, however, which occurs as the primary

event remains under investigation. With supernumerary centrosomes being found in tetraploid cells and are thought to enhance the potential for chromosome missegregation (Meraldi et al., 2002).

1.2 Centrosomes

Theodor Boveri in 1888 first coined the term ‘centrosome’ when he described a single extremely minute body, or more commonly a pair of bodies, staining intensely with haematoxylin, surrounded by a cytoplasmic radiating aster’. Advances in technologies such as fluorescence microscopy, electron microscopy, and proteomics allow the protein components of the highly dynamic structure of the centrosome to be identified. A clearly visible membranous boundary cannot be seen in the centrosome, this is unusual in that they are the only non-membranous organelles in vertebrate cells.

Centrosomes occupy a volume of $1\text{-}2\mu\text{m}^3$ and are usually in close proximity to the nucleus. In vertebrates, these consist of two substructures, centrioles and pericentriolar material (PCM) (Andersen, 1999). Each centriole consists of a nine-fold symmetrical array of triplet microtubules (blades) that make up the barrel, together with other elements. The centrioles lie perpendicular to each other and in close proximity at one end (proximal). This end of the centriole contains the ‘cartwheel’, a set of nine spokes connected to a central axis, the proximal end is the site of new centriole assembly. The older centriole is called the mother or maternal centriole, and contains distal appendages. The distal end also contains the plus-ends of the centriolar microtubules, these provide the template for the assembly of cilia and flagella when the centrioles turn into basal bodies (Figure 1.2A and B).

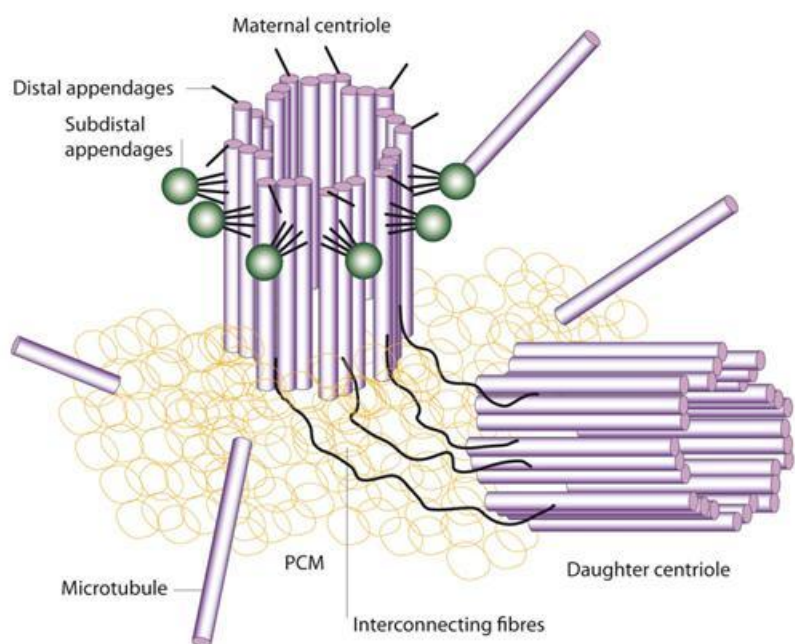
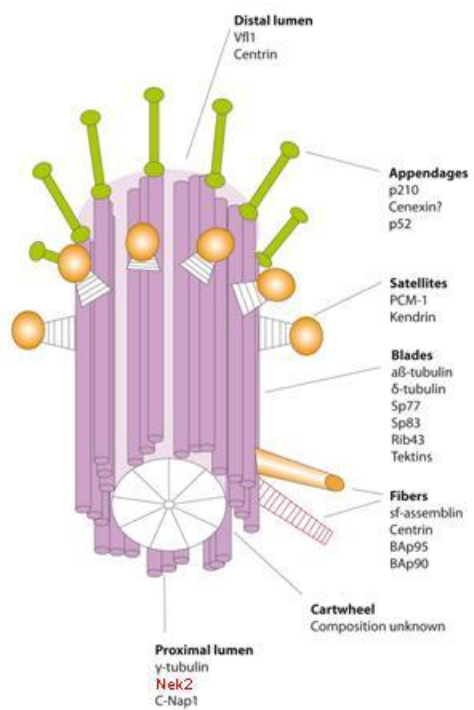
A**B**

Figure 1.2 Centrosome organisation

A. This schematic represents a pair of centrioles. Each centriole has pericentriolar material that nucleates around the ends closest to one another. A series of interconnecting fibres link the closest ends of the two centrioles, the fibrous linkage connecting the proximal ends of the centrioles together is made up of large proteins which contain coiled coil domains. Panel B the maternal centriole that bears distal and sub-distal appendages, core proteins identified by proteomic analysis are labelled. Cenexin is not present on the daughter centriole. Reproduced from Doxsey (2001).

Proteomic studies have suggested the existence of more than a hundred centrosome components present in cells (Andersen et al., 2003). Indeed despite the fact that the centrosome has now been studied for over 100 years, and the organisation and regulation of this mysterious organelle will take many years still to elucidate.

1.2.1 The functions of the Centrosome

The centrosome is associated with a number of major functions that include microtubule nucleation, anchoring and release. It also is thought to participate in mitotic spindle assembly, positioning of the mitotic spindle, cytokinesis and possibly G1/S control.

The PCM is a fibrous lattice composed of coiled-coil proteins which can anchor signalling molecules and components of the γ -tubulin ring complex (γ -TuRC). γ -tubulin ring complexes act as the site from which microtubules are nucleated (reviewed in Zimmermann et al., 1999). γ -TuRCs are concentrated in the PCM and therefore the PCM acts as the microtubule-organising centre (MTOC), which nucleates the microtubule array in interphase and the spindle microtubules during mitosis (Euteneurer and McIntosh, 1981). Microinjection of antibodies raised against poly-glutamylated tubulin into HeLa cells leads to the disassembly of the centrioles (Bobinnec et al., 1998), In turn this causes the collapse of the PCM and MTOC, indicating that it is the function of the centriole to focus the PCM and regulate the number of MTOCs in the cell.

Since centrosomes function to nucleate and organise microtubules and also associate with the spindle poles, it would be logical to assume that centrosomes have an essential role in spindle assembly. However, in mammalian cells centrosomes are not essential for spindle assembly (Hinchcliffe et al., 2001, Khodjakov et al., 2000) indicating that a non-centrosomal pathways of spindle organisation exist. Nevertheless, when centrosomes are present they

act dominantly to organise spindle poles and so centrosome numbers dictate the polarity of the spindle assembled, with amplified centrosomes causing formation of multipolar spindles (Heald et al., 1997).

Positioning of the mitotic spindle is also thought to be fundamentally important for processes including, accurate segregation of chromosomes, normal and asymmetrical cell division and defining the plane of cytokinesis. A common feature of mammalian and yeast cell spindle positioning systems is the interaction of molecules at the plus ends of centrosome-associated astral microtubules, with cytoplasmic dynein located at the cell cortex (Schuyler and Pellman, 2001). In mammalian cells lacking centrosomes, no astral microtubules are produced and spindles become positioned incorrectly causing problems in cytokinesis (Khodjakov and Reider, 2001). However, in studies in Drosophila it seems that non-centrosomal mechanisms for spindle positioning also exist (Giansanti et al., 2001, Roegiers et al., 2001). When centrosomes are eliminated from interphase vertebrate cells using laser ablation (Khodjakov et al., 2000), mitotic cells can still assemble mitotic spindles but approximately half fail to complete cytokinesis, linking the centrosome loosely with completion of cytokinesis. To elucidate the role of centrosomes in cytokinesis further research is required.

Redundant pathways could provide a mechanism to ensure high fidelity of chromosome segregation. Mistakes in chromosome distribution can lead to severe consequences for the organism. Genomic instability due to whole chromosome losses or gains can lead to loss of tumour suppressor genes and amplification of oncogenes that can promote unregulated growth characteristics (Brinkley, 2001, Nigg, 2002). Genomic instability due to unequal

chromosome distribution at mitosis is thought to be a major driving force in multi-step carcinogenesis (Lengauer et al., 1998, D'Assoro et al., 2002, Pihan et al., 2003).

1.2.2 Centrosomes and cancer

Centrosomes, in mammalian cells, have an essential role in the formation of the mitotic spindle and chromosome segregation, primarily because it is the primary site of microtubule nucleation (Bornens, 2002; Doxsey, 2001). A common characteristic of tumour cells is the presence of multipolar spindles which are often associated with abnormal centrosome number or architecture (Kuo et al., 2000; Lingle et al., 1998; Pihan et al., 1998; Pihan et al., 2001; Sato et al., 2001).

Supernumerary centrosomes are frequently present in tumour cell lines which also contain an abnormal number of chromosomes (aneuploidy); which process occurs first is still a matter of intense debate. However, the acquisition of supernumerary centrosomes could be generated either by direct uncoupling of the centrosome duplication cycle or tetraploidization as occurs in cells which fail to undergo cytokinesis (Brinkley, 2001; Lingle et al., 1998; Lingle and Salsbury, 1999; Nigg, 2002; Pihan and Doxsey, 1999). In cells lacking in p53 and Rb pocket proteins, tetraploid cells progress into mitosis which results in the generation of multipolar spindles (Borel et al., 2002). This falls in line with the finding that in osteosarcoma cell lines cells with mutant p53, cells containing supernumerary centrosomes also had an increased incidence of abnormal mitosis and aneuploidy (Al-Romaih et al., 2003). Abnormal chromosome content also known as aneuploidy and chromosome instability (CIN) are two of the most common abnormalities in cancer cells. The genetic instability seen in cancer cells can arise from an accelerated rate of mutation, arising from defects in DNA repair, to chromosome missegregation. Chromosome segregation errors

may lead to abnormal chromosome content, usually two or three times the content of a normal diploid cell (Rajagopalan and Lengauer, 2004). These aneuploid cells may then go on to exhibit CIN, a phenotype characterised by the gain or loss of chromosomes at each cell division. CIN is thought to promote the Darwinian genomic evolution characteristic of cancer, whereby proto-oncogene mutations accumulate, and normal alleles of mutated tumour suppressor genes are lost (Pihan et al., 1998; Cahill et al., 2002; Hahn et al., 2002). CIN is thought to facilitate the inexorable evolution of cancers towards cellular states that support tumour cell growth, dissemination, and resistance to therapy. A common element in the chain of events associated with the loss of fidelity in chromosome segregation is centrosome dysfunction (Brinkley et al., 2001; Doxsey et al., 2001; Lingle et al., 2000). Centrosome defects, aneuploidy and chromosomal instability (CIN) are dominant features of human primary tumours, and have been reported even in early pre-invasive tumours (Ghadimi et al., 2000; Lingle et al., 2002; Pihan et al., 2003a). The analysis of primary invasive breast tumours revealed regions of centrosome amplification in 89% of patient samples. Moreover, the greatest degree of centrosome amplification was observed in aggressive, oestrogen independent disease with lymph node involvement (Schneeweiss et al., 2003). The identification of mutated pathways that promote centrosomal amplification could lead to innovative ways to treat patients, especially for disease such as triple negative breast tumours, for which currently, no successful treatment strategies exist.

The effect of extra centrosomes upon the duration of mitosis was studied. A population of tumour cells has a higher percentage of cells in mitosis when compared to normal tissue, the reasons for this was systematically analysed. It was found that doubling the number of chromosomes to 4N resulted in the duration of mitosis being increased from 20 minutes to

30 minutes, whereas, doubling the centrosomes number increased mitosis by approximately 30 minutes or more (Yang et al., 2008). This data indicates that the presence of extra centrosomes influences the duration of mitosis more than chromosome content, and that extra centrosomes are dominant in extending cell division in tumour cells.

1.2.3 Regulation of centrosome duplication

For successful mitosis to occur, it is of utmost importance to assemble a bipolar spindle, hence, two centrosomes should be present at the onset of mitosis to ensure faithful segregation of the chromosomes. Each centrosome forms the pole of the bipolar spindle, which upon completion of mitosis, leaves each daughter cell to inherit a single centrosome. Therefore a cycling cell must duplicate centrosomes before the next division. Centrosome regulation through the cell cycle depends on three events: disorientation, duplication and disjunction. Interestingly, all three events are regulated in a large part by protein phosphorylation.

Centriole disorientation, also termed centriole disengagement, has been proposed to be the step which “licences” subsequent duplication (Tsou and Stearns, 2006). Experiments using *Xenopus laevis* cell free extracts indicated a role for separase, a protease indirectly regulated by the anaphase-promoting factor complex/cyclosome (APC/C) through securin, in the promotion of centriole disorientation during anaphase (Tsou and Stearns, 2006). However, further studies using cultured cells revealed a crucial role for polo-like kinase 1 (Plk1) in centriole disorientation (Rapley et al., 2005).

After disorientation the centrioles that have lost their perpendicular orientation are able to initiate template formation for the generation of new procentrioles. The synthesis of procentrioles occurs alongside DNA replication in S phase and is initiated at the G₁/S

transition. Again, this occurs in response to protein phosphorylation. In mammalian cells, CDK2/Cyclin A activity has been found to be essential for centrosome duplication (Meraldi et al., 1999), whilst in, *X. laevis* extracts and cultured *C. griseus* cells, CDK2/Cyclin E activity was required for duplication to occur (Lacey et al., 1999; Matsumoto et al., 1999). Using the NIH3T3 murine fibroblast cell line, the addition of an antibody blocking the phosphorylation of nucleophosmin by CDK2/Cyclin E in turn blocked centriole duplication (Tarapore et al., 2002). There is now considerable evidence that CDK2 plays a major role in centriole duplication events. However, the publication of data showing that mice lacking CDK2 were viable and healthy yet infertile, indicates that CDK2 is non-essential in somatic cells and essential only in meiosis (Ortega et al., 2003; Berthet et al., 2003). Despite the fact that CDK2 is abundantly expressed in all dividing cells and is highly conserved through multicellular organisms, its role in the cell cycle can be replaced by CDK1 (Hochegger et al., 2007; Krasinska et al., 2008). Indeed, through gene targeting experiments in mice, only CDK1 knockout of all the CDKs was lethal to the developing mice embryos (Santamaria et al., 2007), indicating that only CDK1 has an absolutely essential role in cell division.

In addition to CDK2, RNAi mediated knockdown of Plk4 in HeLa human cervical cells resulted in a progressive loss of centrioles at each division cycle (Habedanck et al., 2005), Conversely, overexpression of active Plk4 induced centriole duplication in U2OS (human osteosarcoma) and HeLa cell lines. Recently, a novel protein Asterless (Asl) or CEP152 has been identified, which has been proven to bind to Plk4 to promote centrosomes duplication. An Asl mutant deficient in Plk4 binding prevented centriole duplication in cultured cells and embryos (Dzhindzhev et al., 2010).

The final stage of the centriole cycle is disjunction. During interphase, the centrioles are connected by a putative tether. The purification of paired centrosomes and the visualisation of a physical linkage through electron microscopy suggest a protein linkage between mother and daughter centrioles (Fry, 2002). Currently the fibrous linkage is not fully defined but it has been suggested that the protein centrosomal Nek2-associated protein 1 (C-Nap1), provides a platform for a second protein called rootletin (Bahe et al., 2005; Mayor et al., 2003). The disassembly of the inter-centriolar linkage at the G2/M transition is regulated by phosphorylation of the two core proteins C-Nap1 and rootletin. The Nek2 kinase is directly involved in the phosphorylation of both C-Nap1 and rootletin in vitro and in cultured cell lines (Bahe et al., 2005; Faragher and Fry et al., 2003; Fry et al., 1998). Motor proteins, such as kinesin, then facilitate the physical movement of centrosomes to the spindle poles after Nek2 induced severance of the linker (Sharp et al., 2000).

1.3 Nek Protein Kinases

A family of serine/threonine protein kinases that regulate the cell cycle are the NIMA (*Never In Mitosis A*) related kinases, there are eleven genes encoding NIMA kinases in humans. NIMA was identified in the filamentous fungus *Aspergillus nidulans* as a protein kinase that is required for mitotic entry (Fry and Nigg, 1995). Cells with a temperature-sensitive copy of the gene *nimA* arrest in G2 when cultured at the restrictive temperature, and enter mitosis synchronously when released from the block. Overexpression of NIMA drives cells into mitosis from any point in the cell cycle, phenotypically this is characterized by premature nuclear envelope breakdown, chromatin condensation, and mitotic spindle formation (Osmani et al., 1988, Osmani et al., 1988, Lu and Means 1994).

Of the eleven human NIMA-related kinases, they are mainly conserved in their catalytic domains. The most closely related is Nek2 which shares 47% sequence homology with NIMA across the catalytic domain (Schultz et al., 1994). NIMA and Nek2 have similar biochemical and substrate specificity *in vitro*, both target β -casein preferentially instead of the α -casein isoform, and utilize ATP instead of GTP for the phosphate donor (Fry et al., 1995). NIMA and Nek2 display similar cell cycle-dependant expression patterns, both are present in a low concentration in G1 and increase throughout S and G2 finally reaching a peak at G2/M (Schultz et al., 1994, Osmani et al., 1991).

1.3.1 Nek2: a centrosome kinase

A study performed by Fry et al (1998) provided the first evidence that Nek2 associated with the centrosome. U2OS cells treated with nocodazole which depolymerises cytoplasmic microtubules were examined by immunofluorescence microscopy, this demonstrated that Nek2 was a *bona fide* centrosomal protein which preferentially localized at the proximal ends of both centrioles. Nek2, however, is not exclusively confined to the centrosome and up to 90% of the total pool of cellular Nek2 is not located at the centrosome. When Nek2 is overexpressed the non-centrosomal pool is found exclusively in the cytoplasm of some cells and the nucleus of others (Fry et al., 1998b).

Human Nek2 is a 48 KDa (445 amino acid) protein, the catalytic kinase domain is located at the N-terminus, while the C-terminal non-catalytic domain contains two regions predicted to form coiled-coils, the first is located immediately downstream of the kinase domain and contains a putative leucine zipper (LZ), the second coiled-coil is at the end of the C-terminus. Initial work with *Xenopus laevis*, the African clawed toad, revealed two variants of Nek2, Nek2A (48 KDa) and Nek2B (44 KDa) (Uto et al. 1999). This study found that Nek2B is present

in oocytes and early embryos whereas Nek2A is expressed after gastrula-neurula transition, suggesting that the two variants of Nek2 may engage in meiotic and mitotic roles in a sequential manner during *Xenopus* development.

Human Nek2 was also found to exist in two different splice variants, which exhibited distinct expression patterns in mitosis (Hames and Fry, 2002). More recently, an additional splice variant has been identified in testis and was termed Nek2-T (Fardila et al., 2004). Originally thought to be testis specific, this isoform was renamed Nek2-C after its discovery in other tissues (Wu, 2007). Nek2A matched the expression pattern of Nek2 first described by Schultz, et al., 1994. In detail, it is now clear that Nek2A protein is almost undetectable in G1 but accumulates rapidly at the G1/S transition remaining high until late G2 and decreasing at the onset of mitosis. Nek2B expression differs in that detectable levels remain in cells arrested in mitosis (Hames and Fry, 2002). Nek2A decreases upon entry to mitosis due to the presence of destruction motifs in the C-terminus which are not present in Nek2B (Hames et al., 2001). The destruction motifs present in Nek2A are a C-terminal methionine-arginine (MR) dipeptide tail and a KEN box which are both targeted by the anaphase promoting complex (Hames et al., 2001; Hayes et al., 2006). Nek2B is lacking in the C-terminus destruction motifs present in Nek2A and Nek2C, but contains the kinase domain, LZ and a microtubule binding and centrosomal localisation domain (Figure 1.3).

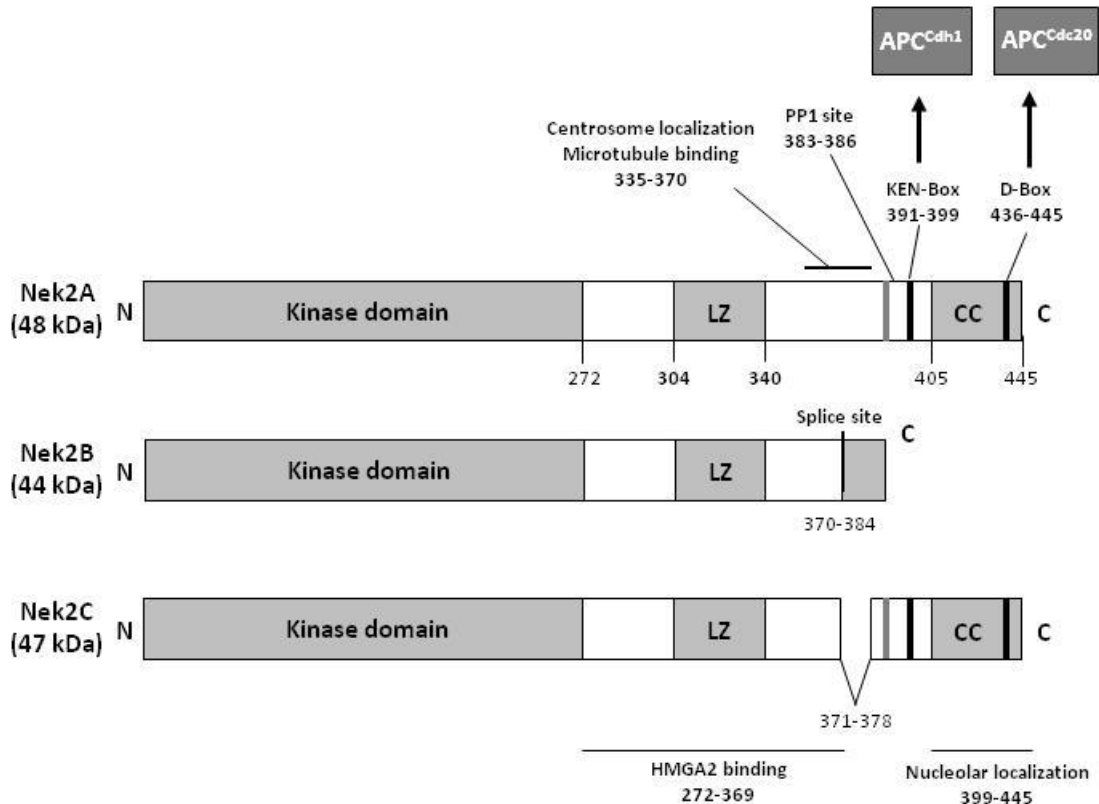


Figure 1.4 The Domain Organisation of the three Nek2 splice variants

Three splice variants of human Nek2 have been described: Nek2A, Nek2B and Nek2C. The splice variants all carry an identical N-terminal catalytic kinase domain followed by a leucine zipper (LZ) dimerization motif. Nek2A and Nek2C contain an additional coiled-coil domain (CC) at the extreme C-terminus. A splice site after amino acid 370 leads to the generation of Nek2B with the last amino acid being 384, and a short internal truncation in Nek2C. Both Nek2A and Nek2C contain PP1 binding motifs and motifs for protein degradation mediated by APC/CCdc20 or APC/CCdh1. The non-catalytic domain of Nek2 also confer centrosome and nucleolar localization sequences. Reproduced from Hayward and Fry (2005).

1.3.2 Functions of Nek2 at the centrosome

In Xenopus embryos Nek2B is the only isoform of Nek2, and is necessary for centrosome maturation (Fry et al., 2000; Twomey et al., 2004). How this occurs is still unclear, if it is through phosphorylation mediated signalling or solely a structural role through the leucine zipper domain. One factor remains clear, Nek2B is essential for the maintenance of centrosomal architecture and plays a role in bipolar spindle formation, given that microinjection of Nek2B antibodies or the addition of excess kinase-dead Nek2B resulted in fragmentation of centrosomes and disrupted bipolar spindle formation (Uto and Sagata, 2000). In human HeLa cells, Nek2B is required for mitotic exit (Fletcher et al., 2005).

Nek2 isoforms are best characterised as core centrosomal components, as they localise independently of microtubules throughout the cell cycle to centrosomes (Fry et al., 1998). Whilst Nek2B has a role in the maintenance of the structural integrity of centrosomes, Nek2A is an important kinase governing centrosome cohesion. Overexpression of recombinant Nek2A results in premature centrosome disjunction. In U2OS cells overexpressing Nek2A, a five-fold increase in premature centrosomes disjunction in interphase was observed. Conversely, overexpression of the kinase-dead, Nek2A-K37R, did not induce this phenotype (Faragher and Fry, 2003; Fry et al., 1998). Furthermore, the experiments by Faragher and Fry (2003) revealed that cells expressing an inactive Nek2A kinase exhibited an increased incidence of monopolar spindles, centrosomes remaining paired surrounded by a rosette of chromosomes. The cells increased in ploidy and an increase in the G2/M population was reported (Faragher and Fry, 2003).

Nek2 represents the most well studied of the human NIMA related kinases. Nek2 plays a core role in the regulation of centrosomes disjunction. Centrosomal-Nek2 associated

protein (C-Nap1) was isolated from a yeast two-hybrid screen to using Nek2 as the bait (Fry et al., 1998). Following the generation of antibodies, it was seen that C-Nap1 is a centrosomal protein in interphase. However, a reduction in staining at mitotic spindle poles confirmed that C-Nap1 is displaced from centrosomes during mitosis before it reaccumulates following telophase. C-Nap1 is a large coiled-coil protein (281 KDa) with globular N- and C-terminal domains. Nek2 phosphorylates C-Nap1 at both the N- and C-termini *in vitro* and *in vivo* (Fry et al., 1998; Hames et al., 2002). Overexpression of a truncated C-Nap1 construct or depletion of C-Nap1 by RNAi induces premature centrosome separation (Bahe et al., 2005; Mayor et al., 2000). Hence, the current hypothesis is that when the activity of Nek2 peaks in G2/M, C-Nap1 becomes phosphorylated and is displaced from the centrosome leading to disassembly of the linker (Mayor et al., 2002).

A second substrate of Nek2 located at the inter-centriolar linkage is rootletin. Rootletin was first identified as a component of basal bodies in ciliated cells where it forms the major component of the ciliary rootlet. The C-terminal coiled coil domain bears sequence homology to human C-Nap1 (Yang et al., 2002). Andersen et al (2003) then identified rootletin in a proteomic analysis of human centrosomes. Rootletin also localises to the proximal ends of centrioles and rootletin has been found to interact with both C-Nap1 and Nek2 (Bahe et al., 2005), indicating that rootletin is a *bona fide* component of the centriolar link. The current literature suggests that Nek2, when released from PP1 inhibition, phosphorylates C-Nap1 and rootletin at the G2/M transition and therefore induces their displacement from centrioles leading to the perturbation of the inter-centriolar linkage, and finally centrosome disjunction.

Recently, Nek2A has been reported to be a target of Hippo pathway component which may facilitate the dissolution of the centriolar linkage (Mardin et al., 2010). It is proposed that the mammalian sterile 20-like kinase-1 (Mst1), mammalian sterile 20-like kinase-2 (Mst2) and the scaffold protein Salvador (hSav1) are functioning as a module to control the localised activity of Nek2A at centrosomes. This functional interaction is thought to be mediated through the Salvador/Ras-association domain family/hippo (SARAH) domains of hSav1 and Mst1/Mst2 with the second coiled-coil domain in Nek2A and Nek2C. Phosphorylation of Nek2A by Mst2 induces the recruitment of Nek2A to the centrosomes, and it has been postulated that this could potentially increase the localized activity of Nek2A to a threshold needed to facilitate centrosome disjunction at the G2/M transition (Mardin et al., 2010). In this regard, it is interesting that whilst high doses of an Eg5 inhibitor block bipolar spindle function, low doses do not except under conditions when Nek2 is also depleted. Hence, the Eg5 motor protein and Nek2 cooperate at G2/M to provide the forces required to break apart the centriolar linkage (Mardin et al., 2010).

Nek2 is thought to have a role in maintaining fidelity of chromosome attachment to the kinetochore during mitosis. The spindle checkpoint complex regulates the correct amphitelic attachment of microtubules to the kinetochore. The spindle checkpoint proteins Mad1 and Hec1 are reported to interact with Nek2. Highly expressed in cancer-1 (Hec-1) is a coiled-coil protein that is essential for the recruitment of monopolar spindle 1 (Mps1) and Mad1/2 complexes to the kinetochore (Martin-Lluesma et al., 2002). Nek2 has been shown to bind to and phosphorylate Hec1 in human cells (Chen et al., 2002). Currently, screening of novel inhibitors or Nek2/Hec1 analogues is on-going (Qiu et al., 2009).

Nek2A has also been documented to be a binding partner of a member of the MAPK pathway, Erk2 (Lou et al., 2004). This interaction occurs via residues K414 and K415, and therefore will not be relevant to Nek2B which is lacking in the C-terminal domain residues 385-446. The inhibition of extracellular regulated kinases 2 (ERK2) did not affect the recruitment of Nek2A to the centrosomes (Lou et al., 2004). It remains unclear what functional role this interaction mediates *in vivo*.

1.3.3 Regulation of Nek2 by phosphorylation

The activity of Nek2A peaks in S and G2 and is due in part to increased transcription, but also relates to kinase activity which is modulated by phosphorylation and dephosphorylation. The C-terminus of Nek2A contains a binding site for protein phosphatase 1 (PP1); this was identified by performing a yeast two-hybrid screen with PP1 and confirmed following the co-immunoprecipitation of full length GST-Nek2A and PP1. A PP1 binding motif, KVHF, is present in the Nek2A C-terminus located at residues 383-386, with an F386A mutation resulting in the abolition of PP1 binding (Helps et al., 2000). The position of the KVHF motif means that this site is not present in Nek2B. The PP1 binding site is present in Nek2A and Nek2C but not Nek2B indicating that Nek2B is not undergoing regulation by PP1 (Hames and Fry, 2002). PP1 is itself regulated in a cell cycle dependent manner by Inh2. Inh2 is a 198 amino acid heat stable protein whose cellular expression peaks prior to mitosis. Inh2 forms a complex with PP1C:Nek2A/C. Inh2 binds to PP1C and inhibits phosphatase activity, consequentially releasing the inhibition on Nek2A/C and allowing Nek2 autophosphorylation (Eto et al., 2002).

Nek2A dimerization depends upon the presence of a coiled-coil motif located immediately C-terminal to the kinase domain (Fry et al., 1999). The motif resembles a leucine zipper (LZ) by having a heptad repeat of leucine residues. The autophosphorylation of Nek2 predominantly on serine residues had previously been observed (Fry et al., 1995; Gallant et al., 1995). To understand if the leucine zipper played a role in autophosphorylation, immunoprecipitation followed by *in vitro* kinase assays was performed. It was observed that the Nek2 C-terminal domain construct became strongly phosphorylated when mixed with wild-type Nek2 but not catalytically inactive mutant, Nek2-K37R, or a Nek2-ΔLZ construct without the LZ motif. This indicates that the kinase domain is responsible for catalysing a trans-phosphorylation reaction and this takes place only in the presence of Nek2 with an intact LZ (Fry et al., 1999).

Interestingly, Fry et al (1999) also found that the ability of the Nek2-ΔLZ construct to phosphorylate β-casein was five-fold reduced when compared to the wild-type Nek2, indicating that the presence of the LZ motif significantly increased kinase activity. Another finding was that the Nek2 dimer was stable and salt resistant to 500 mM NaCl, indicating that hydrophobic rather than ionic interactions were primarily responsible for dimerization at the LZ interface.

1.3.4 Regulation of Nek2 by oligomerization

The coiled-coil α-helical motif mediates oligomerization of a wide variety of proteins. Analysis of primary structure indicates that 2-3% of protein residues form coiled-coils (Wolf et al., 1997). The coiled-coil domain has a diverse range of functions including the maintenance of the cytoskeleton of eukaryotic cells, α-keratin for example (McArthur, 1943), the movement of protein within the cell via motor proteins such as myosin, kinesin

and dynein (Cohen and Parry, 1998; Kozielski et al., 1997; Samso et al., 1998), membrane transport using soluble NSF Attachment Protein (SNARE) (Lin and Scheller, 1997), and most famously GCN4 and c-myc-max in DNA transcription (Lavigne et al., 1995; O'Shea, 1991) making the coiled coil a common and versatile domain found in human cells. Two stranded parallel coiled-coils are the most common motif involved in protein oligomerization (Lupas, 1996). Leucine zippers were first identified as dimerization domains in bZIP transcription factors with a sequence motif consisting of leucines every 7 amino acids (Landschulz et al., 1988). The relevance of the repeating heptad sequence was clarified when it was shown that leucine zippers assume a coiled coil fold (Oas et al., 1990; Saudek et al., 1990; O'Shea et al., 1991).

The canonical coiled-coil consists of two-right handed amphipathic α -helices which supercoil around each other in a left-handed orientation. The hydrophobic interface of the coiled-coil drives coiled-coil assembly, therefore the amphipathic nature of α -helices is important. Parallel left handed α -helices are characterized by a seven-residue periodicity AbcDefg (heptad repeat), in which the hydrophobic residues are spaced in a 3 + 4 pattern (i.e. HPPHPPP – H = hydrophobic and P = polar). Conversely, it has been observed that right handed coiled coils possess an undecated eleven residue repeat (Harbury et al., 1998; Stetefeld et al., 2000). Stability of α -helices is mediated by a distinct ‘knobs into holes’ packing of the apolar side chains into a hydrophobic core (Crick, 1953). Each turn of a standard α -helix is comprised of 3.6 residues per turn, however, the average spacing of hydrophobic residues in a heptad repeat is 3.5 due to the left-handed coiling of the helices around each other in a coiled-coil (Figure 1.4A, B and C).

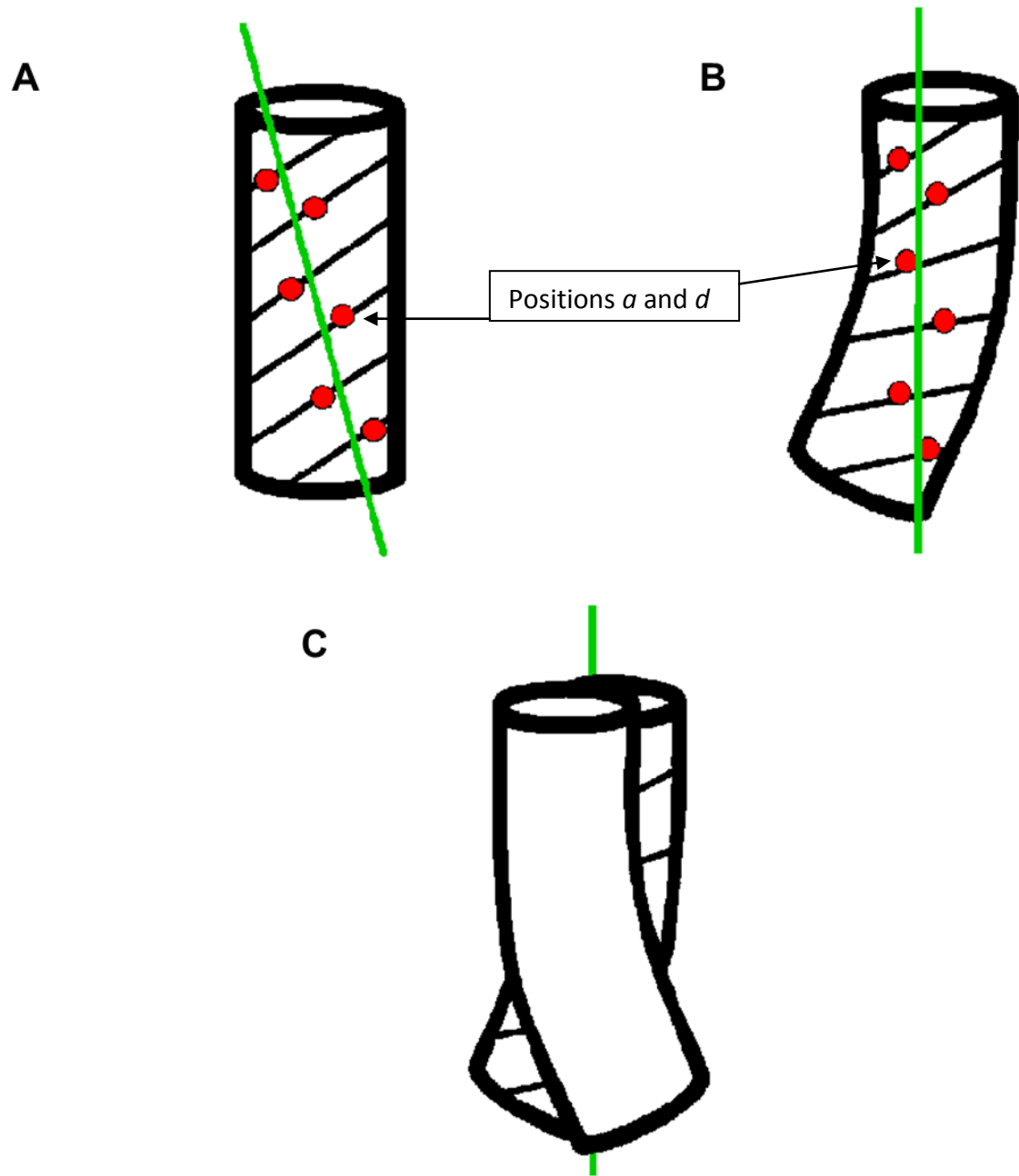


Figure 1.5 Alpha helix geometry

A. The heptad helical repeat AbcDefg is shown representing the interface of an dimeric alpha helix, positions *a* and *d* are indicated by the red balls. B. The interface of dimeric alpha helices are able to contact due to the presence of a coiled-coil fold creating vertical alignment of positions *a* and *d* shown by the vertical green line. C. A representation of a two stranded left handed coiled-coil structure based on the GCN4 structure by O'Shea and colleagues (1991).

O’Shea in 1991 outlined the simplest parameters for coiled-coil formation and named this the “Peptide Velcro (PV) hypothesis”. The interface *a*- and *d*-positions should contain hydrophobic residues for maximum stability. In addition it was postulated that the residues at positions *e* and *g* are often occupied by charged residues that can form salt bridges. These residues form interhelical electrostatic interactions that further stabilize the coiled-coil and mediate the degree of specificity of coiled-coil interaction (Figure 1.5). The solvent exposed face of the helix which encompasses positions *b*, *c*, and *f* must be hydrophilic. In nature, wide sequence variations from this fundamental model exist and influence the oligomerization state of coiled coils. Leucine zippers show great versatility as they can exist as dimmers, trimers, tetramers, can be homo- or hetero-oligomers and can form parallel and anti-parallel complexes (Adamson et al., 1993; Alber, 1992; Mason and Arndt, 2004). Interestingly, examples of dynamic motion in leucine zippers has been documented in the literature; the fast dynamics of the rotation of an asparagine side chain in GCN4 and c-jun (Junius et al., 1996; Junius et al., 1995; Saudek et al., 1991; Saudek et al., 1990), and the slow dynamics of the Mnt repressor which exists in two conformations, with the dimeric and tetrameric structure generated by a staggered assembly of two coiled-coil dimers that are packed into a distorted four helical coiled coil (Nooren et al., 1999).

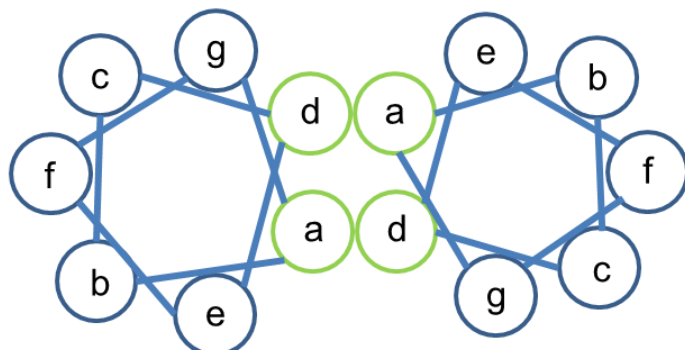
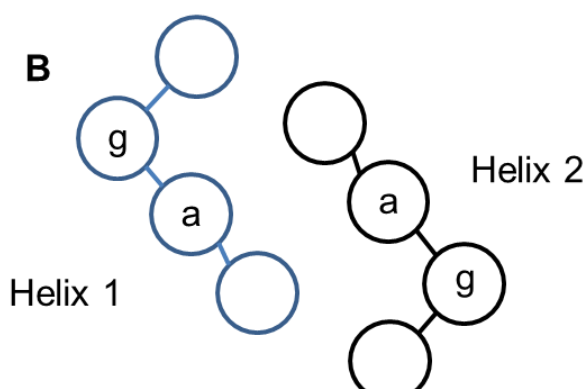
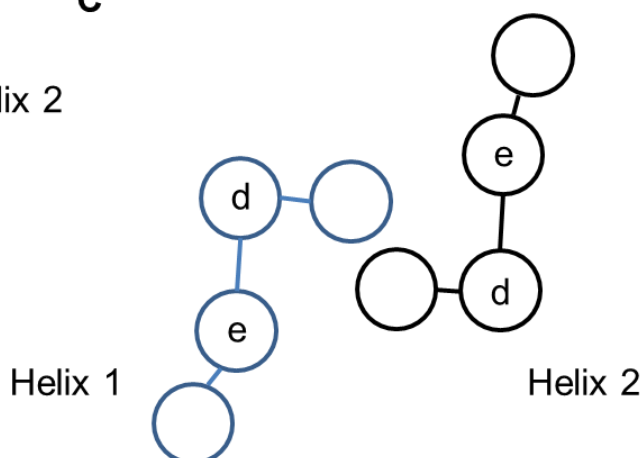
A**B****C**

Figure 1.6 Residue interactions in two-stranded coiled-coils

A. The alpha helical structure represented as a helical wheel shows the residue arrangement of the seven heptad repeat. Positions *a* and *d* are shown to be the primary residues involved in the formation of the interface in 2-stranded coiled coils. B. Alternative interactions which are thought to occur between the side-chains of core and non-core residues in positions *a* and *g* are shown (helix 1 is coloured blue and helix 2 black). C. A representation of the packing of the *d*-layer in relation to the *e*-layer in a two-stranded coiled-coil. Reproduced from Walshaw and Woolfson (2003).

As discussed above, Nek2 contains a putative parallel homodimeric leucine zipper domain with an atypical organization of charged residues (Fry et al., 1999). The effect of the coiled-coil motif on the oligomerization state of Nek2 was first tested by Fry and colleagues (Fry et al., 1999). Glycerol gradient centrifugation of endogenous and recombinant Nek2 indicated that Nek2 existed as a 6S complex, the predicted size of a homodimer. Deletion of the leucine zipper region resulted in the formation of a 4S complex consistent with a Nek2 monomer. A yeast two-hybrid screen supported this theory by finding that the Nek2 leucine zipper strongly interacted with itself and the Nek2 wild-type protein; control experiments using a mutant devoid of the leucine zipper motif gave no interaction. Interestingly, the Nek2-ΔLZ deletion mutant dramatically reduced kinase activity up to five-fold, establishing a link for the first time between the leucine zipper domain, dimerization and the function of the kinase.

Using the GCN4 coiled-coil structure as a basis, a model was generated with the conformation of the residues adjusted to the most energetically favourable values (Fry et al., 1999). They predicted the leucine zipper to be a parallel homodimer with leucine-leucine interactions at the interface. However, a remarkable feature of the Nek2 leucine zipper is the conservation of a stretch of five glutamic acid residues which occupy the *a* position. This deviation from standard coiled-coils which primarily contain hydrophobic residues in the *a* position, is thought to be compensated by the glutamic acids in the *a* position forming salt bridges with the basic residues in the *g'* position of the opposite helix. Antiparallel formation was postulated to be unfavourable due to the positioning of like-charged residues in close proximity (Fry et al., 1999).

The unusual sequence arrangement in the Nek2 leucine zipper could be to maintain specificity which is of utmost importance to maintain function. It appears the positioning of the acidic, basic and hydrophobic residues is critical to function due to the conservation between human, mouse and *Xenopus* Nek2 sequences (Fry et al., 1999). Charged residues occupying the α position have also been found in the coiled coil of myosin II, although the charged amino acids are not highly conserved throughout species as in Nek2 (Blankenfeldt et al., 2006; Li et al., 2003). This highly unusual sequence conservation present in an α -helix represents a novel approach to coiled-coil formation which has not previously been described, making structural determination of the Nek2 leucine zipper a high priority.

1.3.5 Structural studies on Nek2

Nek2 activity is subject to regulation via phosphorylation events and this mechanism of regulation was investigated through the generation of the three-dimensional structure complexed with small molecule inhibitors (Rellos et al., 2007; Westwood et al., 2009). Upon solving the structure of the Nek2 kinase domain, Rellos and colleagues found a rather unusual structure in the area around the conserved DFG motif located at the N-terminal end of the T-loop. This motif functions to anchor the N-terminal end of the T-loop and allows aspartate (D) to act as a ligand for a bound divalent metal ion (Figure 1.6A). In inactive kinases, the DFG motif adopts an extended conformation as seen in Aurora-A, with which the Nek2 kinase domain shares 31% structural similarity. In Nek2, the DFG motif and the following five residues constitute an extended motif which folds into an unusual α T helix in preference to a short beta-sheet (Figure 1.6B). This interesting modification at the end of the T-loop could provide a novel mechanism to utilize in the event of drug design to improve specificity. A comparison of the 500 kinase domain structures known to date indicate that

such a motif is only also present in the Cdk2 and EGFR kinase domains. Interestingly, though, the residue N-terminal to the DFG motif is a glycine which is present in less than 10% of kinase domains. This is thought to confer flexibility to the DFG motif and activation loop which was observed in several different conformations (Westwood et al., 2009). These conformational changes could be targeted to develop Nek2 specific inhibitors which lock the kinase into an inactive state or inhibit the active state of the kinase by the steric hindrance of ATP binding.

The catalytic sites of kinase domains are notoriously difficult to inhibit using small molecules targeting the ATP binding site without the presence of unusual structural features. This is due to the classical design of such molecules which function to compete for binding with ATP in the nucleotide binding cleft of the kinase. Determination of the structure generates essential information needed to attempt to design small molecules which are highly specific, however, even with structural information the development of a specific small molecule remains challenging.

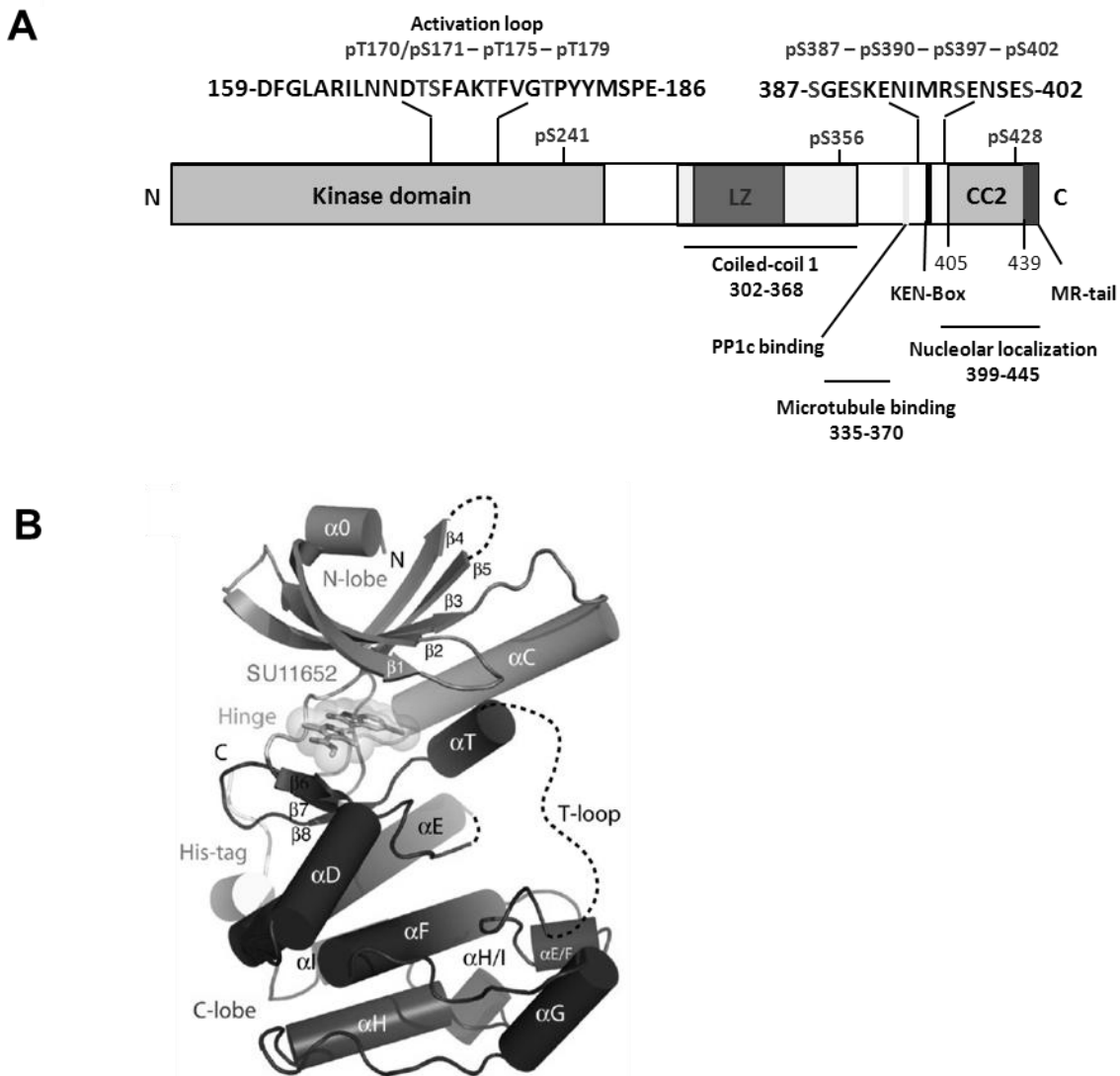


Figure 1.7 Structure of the Nek2 protein kinase domain

A. A schematic diagram displaying the major domains and functional features of the Nek2A protein. Autophosphorylation sites within the catalytic domain and the C-terminal region are indicated. B. The structure of the Nek2 kinase domain is shown in complex with a pyrrole-indolinone inhibitor, SU11652. The N-lobe is followed by the hinge region with the inhibitor in close proximity; finally, the C-lobe is indicated at the bottom left of the structure. Disordered regions are displayed using dashed lines. Adapted from Rellos et al. (2007).

1.3.6 Nek2 and Cancer

Amongst the first studies to implicate Nek2 in human proliferative disease arose from microarray analysis of mRNA abundance in 1,700 genes, where it was revealed that there was a marked upregulation of Nek2 in cell lines derived from Ewing's tumours (Wai et al., 2002). Hayward et al (2004) examined the levels of protein expression of Nek2 in cell lines derived from breast, cervical and prostate carcinomas where an elevation in Nek2 protein of 2-5 fold was reported. Interestingly, examination of 20 high grade invasive ductal carcinoma (IDC) breast tumours by immunohistochemistry revealed marked Nek2 upregulation in 16 samples. Comparative genomic hybridisation (CGH) analysis of 44 archival breast tumours showed a common amplification of region 1q32, the locus of the human Nek2 gene (Schultz et al., 1994), with 32 patient samples showing a gain or loss of up to six copies (Lou et al., 2004). With Nek2 protein levels being upregulated in some human tumours, it is interesting to speculate what effect Nek2 overexpression may have on cancer progression. Overexpression of Nek2 in HBL-100 immortalized breast cells can induce aneuploidy, and there is a 5-10 fold increase in cells with multiple or enlarged nuclei (Hayward et al., 2004). In this cell type multiple centrosomes are a typical phenotype and may have resulted from an abortive mitosis and/or a failure in cytokinesis.

Nek2 expression has been reported to be increased in a number of human tumour cells, these include Ewings tumour (Wai et al., 2002) and primary breast carcinoma (Hayward et al., 2004). In non-Hodgkin lymphomas it has been documented that Nek2 is present in high levels and that this correlates with a poor prognosis (de Vos et al., 2003). The link between Nek2 and tumour progression highlights Nek2 as an attractive target for tumour therapy,

and is reinforced by the observation that Nek2 depletion in HeLa cells leads to cell cycle arrest and an increase in apoptosis (Fletcher et al., 2005; Fletcher et al., 2004).

Zeng et al (2010) recently investigated the origins of centrosomes amplification (CA) in mammary tumorigenesis. Overexpression of K-Ras-G12D induces CA in mammary precursor lesions. However, when the expression of cyclin D1, Cdk4 or Nek2 was abrogated in human mammary epithelial cells (MCF10A) expressing H-Ras-G12V, Ras-induced CA was inhibited. The ability of K-Ras-G12D to initiate CA in mammary precursor lesions indicates that CA precedes tumorigenesis and is specific to certain oncogenes. Moreover, c-myc did not induce CA in premalignant lesions but induced CA in tumours, and the overexpression of c-myc induced an upregulation of Nek2 (Zeng et al., 2010). This interesting work indicates that in premalignant lesions with oncogene specific mutations which facilitate an increased rate of CA, a Nek2 inhibitor could be beneficial to abrogate CA, and therefore, reduce aneuploidy to protect against the progression towards cancer. Nek2 clearly plays an important role in cell division, especially in spindle formation and chromosome segregation.

Nek2 inhibitor screens are currently underway and it will be interesting to see if a small molecule inhibitor of Nek2 activity can reduce or halt tumour cell proliferation, or activate a pathway that can force the cells into apoptosis (Innocenti et al., 2012; Solanki et al., 2011; Whelligan et al., 2010). However, the use of a cyclic cytotoxic compound could not be used in combination with a therapeutic that causes cellular senescence, due to the requirement that the tumour cells would need to be cycling in order for a Nek2 inhibitor to have efficacy.

1.4 Kinase inhibitors

The first small molecule inhibitors (SMIs) of protein kinases were developed in the early 1980s, all of these novel compounds were found to be ATP competitive (Hidaka et al., 1984). It became apparent after the elucidation of the structure of Protein Kinase A (Knighton et al., 1991), that the first SMIs developed as ATP competitors struggled to reach sufficient intracellular potency and therefore most designed ATP inhibitors could not successfully out compete intracellular ATP resulting in a loss of efficacy. Furthermore, due to the similarity of the residues which are involved in the binding of ATP, sufficient specificity between the different protein kinases cannot be achieved with these early ATP competitive substrates, termed Type I SMIs. Around 1992, the first SMI targeting the inactive state of the Abelson tyrosine kinase (ABL) domain was developed by Nick Lyndon and his team at Novartis (Buchdunger et al., 1996). Although the drug Imatinib also targeted the highly conserved amino-terminal region of the binding loop and could be classed as an ATP competitor, and therefore a Type I SMI, upon binding it induces a structural transition to 'lock' the kinase into the inactive conformation. However, in terms of specificity, Imatinib also inhibits the c-KIT and PDGF-receptor tyrosine kinases (Buchdunger et al., 2000) with similar potency, indicating that specificity could be improved. Efforts to improve specificity by enhancing SMI design came with the development of non-ATP competitive SMIs (reviewed in Harrison et al., 2008). Type II SMIs target the ATP binding site but the binding is directed also partially towards an allosteric pocket, whereas, Type III SMIs target an allosteric region close to the ATP binding site or another pocket important for activation, distant to the ATP binding site. The change in strategy with regards to SMI design results in an improvement in efficacy for cancer patients, however, the most successful SMI in cancer with regards to efficacy is the

Type I SMI Imatinib, which is the first line treatment for CML with a 90% 5 year survival rate.

1.5 Aims and Objectives

The goal of this research project was to determine if the Nek2 leucine zipper domain is a suitable candidate to be considered as a target for a chemotherapeutic agent in human cancer.

The leucine zipper motif of Nek2 is known to modulate the kinase activity of Nek2 by facilitating dimerization and allowing subsequent trans-activation by phosphorylation (Fry et al., 1999). To date, structural information only exists for the kinase domain but it is of mounting importance to elucidate the structure of the Nek2 leucine zipper and subsequently the full-length protein. One could speculate that the Nek2 leucine zipper may be responsible for releasing the inhibition of the αT helix on the αC catalytic domain as receptor dimerization has been shown to mediate the activation of the epidermal growth factor receptor (EGFR) (Zhang et al., 2006). In the proposed model of EGFR activation that results from the interaction between the EGFR kinase domains, an αT helix of one monomer packs against the αC of the opposing monomer, thereby releasing the inhibitory effect of the αT helix and allowing kinase domain activation. Perhaps the leucine zipper of Nek2 functions in a similar manner where dimerization through the leucine zipper could release the block mediated by the αT helix, either by eliciting a conformational change which draws the αT helix from the αC directly or by mediating an association between opposite αC domains.

Once the structure has been elucidated it could then be used to design a small molecule which could function to specifically inhibit dimerization of Nek2, and therefore reduce kinase activity. Owing to the unusual sequence of the leucine zipper which is not reciprocated in any other protein documented to date, a highly specific small molecule inhibitor could be generated. Therapeutics which maintain specificity are usually associated with the reduction of side-effects because of the reduction of “off-target” effects. Previously, multi-specific small molecules were thought to be the most effective in reducing tumour progression. Whilst in part this is true, many compounds fail in development due to high levels of toxicity to normal cells in patients. Therefore, an inhibitor developed to target the coiled-coil motif and prevent dimerization would represent a novel mechanism by which to inhibit kinase activity.

Previous attempts to crystallize the leucine zipper domain failed due to the possible existence of conformational dynamics. In this project, I focused upon determining the nature of the dynamics of this domain using nuclear magnetic resonance (NMR) spectroscopy and attempted to optimize NMR parameters to allow the subsequent elucidation of the three-dimensional structure of the Nek2 leucine zipper.

The specific project objectives were as follows:

1. To investigate the domain boundaries of the leucine zipper domain

Using bioinformatics software the predicted leucine zipper domain boundaries were determined. This allowed the design of multiple constructs of the leucine zipper with various lengths. These were expressed and analysed with respect to productivity, aggregation, and stability.

2. To investigate the biophysical nature of the interactions in the Nek2 leucine zipper

Circular dichroism (CD) and analytical ultracentrifugation (AUC) were performed to determine the melting temperature of the different leucine zipper constructs and the Kd and concentration dependent oligomeric state of the leucine zipper.

3. To determine the kinetics of the dynamics using NMR spectroscopy

One dimensional (1D) and two dimensional heteronuclear single quantum coherence (2D-HSQC) experiments and 2D relaxation experiments were undertaken to elucidate the timescale of the relaxation of the Nek2 leucine zipper dimer. Specifically, the rate of exchange of the proposed two different conformations was determined using two engineered leucine zipper mutants which lock the dimer into one of the two predicted conformation, respectively.

4. To characterize the optimal parameters for structural determination

Temperature, field strength, pH and protein concentration were systematically analysed using NMR. 2D HSQC experiments were performed to determine the effects of variation

upon spectral quality with respect to line broadening and the number of peaks present. These experiments would function to determine the optimal conditions, in relation to the signal to noise ratio, and potentially in the future the determination of the three dimensional (3D) structure of the Nek2 leucine zipper.

CHAPTER 2

MATERIALS AND METHODS

2.1 Molecular Biology Techniques

2.1.1 Polymerase chain reaction (PCR)

Platinum® Pfx deoxyribonucleic acid (DNA) Polymerase system was used in the PCR. 200 ng of template DNA was subjected to amplification (initial denaturation 2 minutes at 94°C then 94°C, 15 seconds, 60°C, 30 seconds, 68°C, 30 seconds for 30 cycles with a final extension of 12 minutes at 72°C) using Platinum® Pfx DNA polymerase (2.5U polymerase, 500 nM each primer, 1.2 mM deoxyribonucleotide triphosphates (dNTP) mix, 1 mM MgSO₄). Amplification was confirmed by gel electrophoresis. The PCR products were purified using QIAquick PCR purification kit according to the manufacturers' protocol, eluted in a volume of 20 µl in TE buffer.

2.1.2 Restriction digestion

The entry plasmid pETM-11 (European Molecular Biology Laboratory - EMBL) and the PCR products were restricted using the endonucleases BamHI and Ncol. Only Roche endonucleases were used for restriction. Buffer B at pH 8.0 (Tris-HCl 10 mM, MgCl₂ 5 mM, NaCl 100 mM and 2-Mercaptoethanol 1 mM) was chosen to perform a double digest of the vector and the PCR product. The enzyme efficiency of Ncol in buffer B was 50% - 75% and for BamHI was 100%. 1.5 µg of the pETM-11 vector was digested; 20 µl of the vector in TE buffer, 4 µl distilled water, 3 µl Buffer B, 1.5 µl BamHI, 1.5 µl Ncol were placed in a reaction vial and mixed thoroughly, briefly centrifuged and incubated for 2 hours at 37°C. Gel electrophoresis was then performed and the vector and PCR product were further purified using QIAquick gel extraction kit, the amount of DNA was quantified using ultraviolet (UV) spectrophotometry at 260 nm.

2.1.3 Ligation

The amplified genes were ligated into the digested pETM-11 vector (Figure 2.1) using the Rapid DNA ligation kit (Roche). 50 ng of pETM-11 vector was ligated to 150 ng of PCR insert at a ratio of 1:3 vector:insert. 2 µl vector and 6 µl PCR insert was dissolved in 2 µl 1 x DNA dilution buffer. T4 DNA ligation buffer was mixed thoroughly and 10 µl was added to the reaction vial and mixed again. 1 µl T4 DNA ligase was added and mixed thoroughly, the vial was incubated for 5-10 minutes at RT. If the initial volume of the vector and PCR product exceeds 10 µl the T4 ligation buffer and T4 ligase must be scaled up appropriately in a DNA dilution buffer mix:T4 ligation buffer:T4 ligase enzyme in a 1:1:0.1 ratio, the incubation time must also be increased to 30 minutes at RT.

2.1.4 Bacterial transformation

Following incubation the ligation reaction was used immediately for transformation or stored at -20°C, 2 µl of the reaction volume used to transform 100 µl chemically competent *E. coli* DH5α (F-, φ80lacZΔM15, Δ(lacZYA-argF), U169, recA1, deoR, endA1, hsdR17(rk-, mk+), phoA, supE44, thi-1, gyrA96, relA1) were thawed from -80°C on ice. 100 ng DNA was added and mixed by gentle stirring before incubation on ice for 30 minutes. Plasmid uptake was induced by incubation at 42°C for 1 minute in a water bath followed by re-incubation on ice for 5 minutes. Pre-warmed LB media was added and the transformation incubated at 37°C, 225 rpm for 1 hour before aliquots were spread onto kanamycin-LB agar plates (34 µg/µl) and incubated overnight at 37°C.

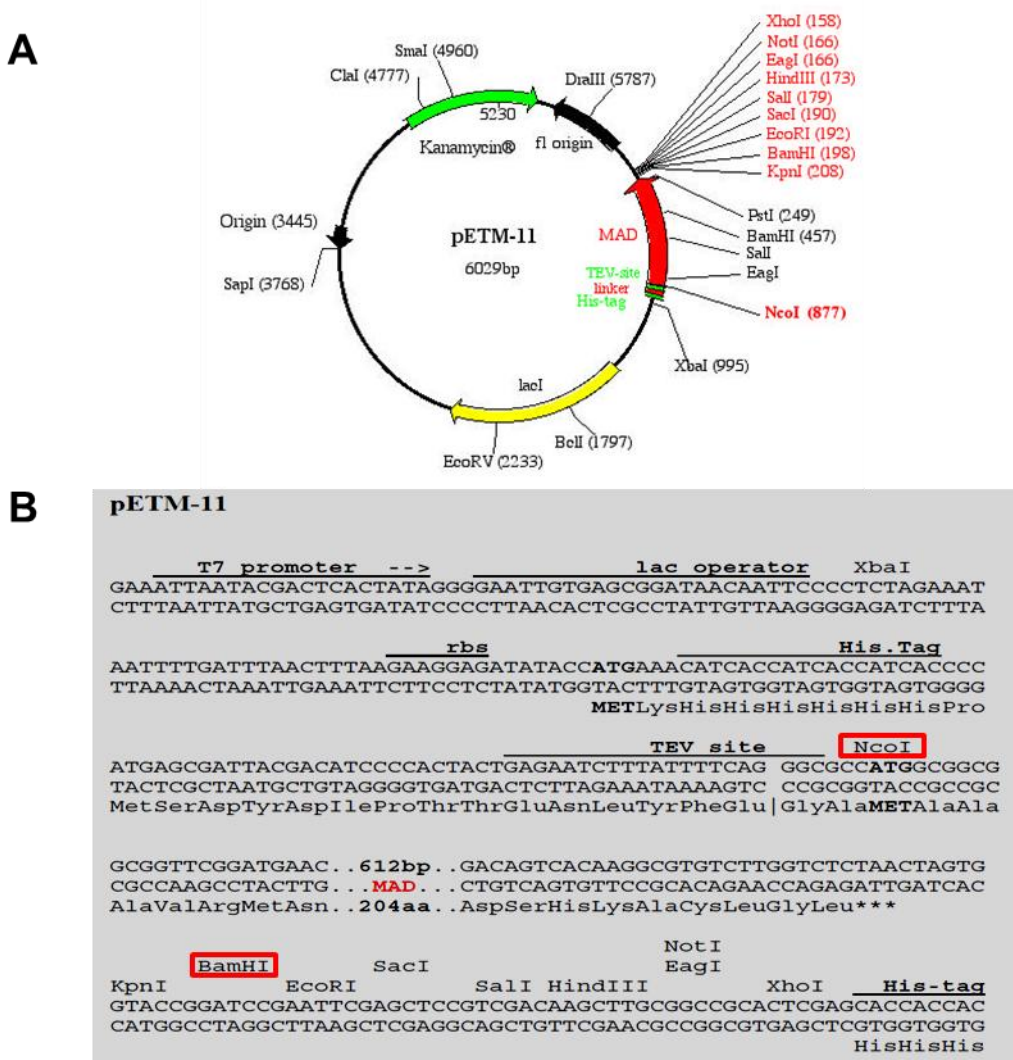


Figure 2.1 pETM-11 vector map

A. The pETM-11 vector map, highlighted in red is the multiple cloning site (MCS) used to insert the leucine zipper gene into the vector is shown. The vector contains kanamycin resistance. B. The T7 promoter region followed by the lac operator to initiate T7 RNA polymerase synthesis in the host bacterial cells is labelled, the ribosome binding site (rbs) is displayed followed by the 6 x Histidine tag. A short linker sequence precedes the TEV protease site used to remove the 6 x Histidine tag in a post-purification step. Ncol and BamHI were the preferred restriction endonuclease sites utilised to insert the Nek2 LZ DNA sequence into the MCS, and therefore, the pETM-11 vector.

2.1.5 PCR screening of clones

To identify bacterial clones containing the Nek2 LZ insert a PCR screening step was performed. A printed paper numbered squared grid was attached to the underside of a Kanamycin-LB plate, individual colonies were picked from the plate and resuspended in vial 1 containing 50 µl distilled water. The pipette tip was immediately taken out of the water and stabbed into the plate at position number 1, this continued until between 6 to 12 colonies had been chosen for each construct. The plate was then incubated overnight at 37°C. The vials of resuspended bacterial clones were then used for the PCR reaction. In a clean 0.2 µl thin walled PCR tube 10 µl bacterial clone, 1.5 µl distilled water, 500 µM LZ forward primer (0.5 µl), 500 µM LZ reverse primer (0.5 µl), 12.5 µl REDTaq® ReadyMix™ PCR Reaction Mix with MgCl₂ (Sigma-Aldrich®) was added and the reagents thoroughly mixed and centrifuged briefly. The PCR parameters were as follows: cycle 1 - 94°C for 5 mins; cycle 2 - 94°C for 30 sec, 60°C for 30 sec, 72°C for 30 sec repeated 30 times and cycle 3 - 72°C for 8 mins and to hold temperature at 4°C when cycling was complete . The PCR products were analysed using gel electrophoresis. Two positive clones indicated by a band at approximately 126 bp were chosen and used to inoculate a 5 ml LB-Kanamycin culture to be used to isolate the plasmid DNA described in 2.1.9, and 500 ng of each clone was sent to PNACL (University of Leicester) for sequencing.

2.1.6 Cloning performed

Name of Construct (Residue number)	Type of cloning performed	Cloned by Rebecca Croasdale	Sequence confirmed by PNACL
LZ0 (288-358)	Sub-cloned from pET-22b into pETM-11 vector	+	+
LZ3 (304-340)	Cloning of PCR fragment into pETM-11	+	+
LZ4 (302-340)	Cloning of PCR fragment into pETM-11	+	+
LZ5 (302-343)	Cloning of PCR fragment into pETM-11	+	+
LZ6 (299-340)	Cloning of PCR fragment into pETM-11	+	+

2.1.7 Site-directed mutagenesis

The mutagenesis primers used to generate the LZ5 mutants LZ5K309C and LZ5E310C were as follows:

C335A: CAGAAAGAACAGGAGCTT**G**CAGTTCGTGAGAGACTAG and
GTCTCTCACGAAC**TG**CAAGCTCCTGTTCTTCTG;

K309C : CTGTATTGAGTGAGCTGAAACT**TG**TGTGAAATTCAAGTTACAGGAGCGAGA and
TCTCGCTCCTGTAACTGAATTTCACACAGTTTCAGCTCACTCAATACAG;

E310C: ATTGAGTGAGCTGAAACTGAAGT**G**TATTCAAGTTACAGGAGCGAGAGC and
GCTCTCGCTCCTGTAACTGAATA**C**ACTTCAGTTTCAGCTCACTCAAT

(the mutated codon is indicated in bold font). Point mutations were introduced at two positions in the original LZ5 plasmid using the Quikchange kit (Stratagene). Before commencing with the PCR the *E.coli* species in which the template was propagated contained the enzyme Dam methylase i.e. LZ5 plasmid in DH5 α , to ensure that the template DNA will be methylated on adenine residues. The reagent composition for PCR in 0.2 μ l PCR tubes was the following: 5 μ l 10 x reaction buffer, 1 μ l LZ5 template (50ng), 1.25 μ l forward primer (125 ng), 1.25 μ l reverse primer (125 ng), 40.5 μ l distilled water and 1 μ l dNTP mix thoroughly mixed and pulse centrifuged. The PCR parameters for the mutagenesis were: cycle 1 - 95°C for 30 seconds; cycle 2 - 95°C for 30 sec, 55°C for 1 min, 68°C for 5 minutes 30 seconds (1 min/kb of plasmid length – LZ5 5,476 bp) repeated 12 times. Following temperature cycling the mutagenesis reaction was cooled on ice for 2 minutes. 1 μ l of the DpnI enzyme was added to each reaction, mixed, centrifuged for 1 minute and incubated at 37 °C for 1 hour. 14 ml BD Falcon tubes were cooled on ice prior to the transformation, 1 μ l of the DpnI digested DNA was added to 50 μ l XL1-Blue supercompetent cells, swirled gently, incubated on ice for 30 minutes and heat pulsed at 42 °C in a water bath for exactly 45 seconds and then placed immediately on ice for 2 minutes. LB medium was preheated to 37 °C in an incubator and 0.5 ml was added to each tube containing the XL1-Blue cells and incubated at 37 °C for 1 hour shaking at 225 rpm. The whole volume of each transformation reaction was plated onto pre-warmed LB-Kanamycin (34 μ g/ μ) agar plates in 250 μ l on each plate and incubated overnight at 37 °C. The integrity of the mutated plasmids was confirmed by DNA sequencing at PNACL (University of Leicester) using a T7 forward primer and a BGH reverse primer.

2.1.8 DNA gel electrophoresis

DNA in loading buffer (50% v/v Glycerol, 100 mM EDTA, 0.3% v/v Bromophenol blue) was resolved by electrophoresis on a gel of 1% (w/v) agarose dissolved in 1 x TBE (89 mM Tris-HCl, 89 mM Boric acid, 1 mM EDTA pH 8.0) supplemented with ethidium bromide (0.5 µg/ml) alongside 1 µl diluted 1:10 of the 1 Kb Plus DNA molecular weight marker in lane 1 (Invitrogen). The gel was immersed in 1 x TBE and DNA resolved by electrophoresis at 80V for 45 minutes. Gels were subject to UV transillumination (302 nm) and images acquired with a Gene Genius CCD gel documentation system (Syngene, Cambridge, UK).

2.1.9 Plasmid preparation

Small and large scale preparations of DNA were made using QIAgen miniprep and QIAfilter maxiprep kits, respectively, according to the manufacturers' instructions. Overnight cultures of the appropriate transformed bacterial strain were grown overnight in LB medium (Bacto-tryptone 10 g/l, Yeast extract 5 g/l, NaCl 10 g/l) at 37°C, plasmid DNA extracted and purified, and eluted in TE buffer. Maxiprep yield was quantified by measuring OD₂₆₀ and diluted to a final concentration of 1 µg/µl.

2.1.10 Preparation of chemically competent bacteria

DH5α *E. coli* were streaked on LB agar plates and incubated overnight at 37 °C. 2 ml LB medium was inoculated with a single isolated colony and incubated at 37°C, 225 rpm for 9 hours. The entire starter cultured was used to inoculate a further 500 ml LB containing 10 mM MgCl₂. This 500 ml culture was incubated at room temperature with gentle shaking at 125 rpm until an OD₆₀₀ of 0.5, then cooled rapidly in ice water. The bacterial cells were collected by centrifugation at 3000 rpm, 0°C, in a pre-chilled Sorvall GS3 rotor. The culture media was decanted and the pellet resuspended in 150 ml ice cold transformation buffer

(15 mM CaCl₂, 250 mM KCl, 10 mM PIPES, 55 mM MnCl₂, pH 6.7), centrifuged again as before and resuspended in 40 ml ice cold transformation buffer. 5 ml DMSO was added and mixed by gentle swirling before aliquoting and flash freezing using liquid nitrogen prior to storage at -80°C.

2.2 Analysis of proteins

2.2.1 SDS-PAGE

NuPAGE 4-12% gels (Invitrogen) were used to resolve the protein samples. 50ml MES running buffer was added to 950 ml of water, 500 µl of reducing agent was added to the central chamber of the tank. Lastly, 20 µl of the protein sample was loaded into the well of the gel, and a constant voltage of 200V was applied to the unit for 35 minutes.

2.2.2 Coomassie Blue staining

Following electrophoresis the stacking gel was discarded and the resolving gel soaked in Coomassie Brilliant Blue solution (0.25% Coomassie Brilliant Blue (w/v), 40% IMS, 10% acetic acid (v/v)) for a minimum of 30 minutes. Protein bands were visualized by washing in destaining solution (25% IMS, 7.5% acetic acid (v/v)) to remove background gel staining.

2.2.3 Protein determination

Total protein content of solutions was determined by BCA assay, which exploits the quantitative colorimetric interaction of reduced copper sulphate, bicinchoic acid and peptide bonds. 5 µl of protein solution was incubated with 1 ml BCA assay reagent at 60°C for 30 minutes, allowed to cool and the absorbance determined at 562 nm. A serial dilution of BSA standards similarly assayed allowed construction of a standard curve relating absorption to protein concentration.

2.3 Protein expression and Purification

2.3.1 Competent cells transformation for protein expression

The competent cells were thawed for 1 hour on ice before inoculating with 2 µl of the vector containing the desired cDNA fragment. After leaving the cells on ice for 30 minutes, they were heat shocked at 42°C for 30 seconds, and then 250 µl of SOC medium (Invitrogen) were added. After incubation at 37°C for 60 minutes, 20 µl of the transformed cells were plated out using coli-rollers (Novagen) onto LB-Agar plates containing appropriate antibiotic.

2.3.2 Expression in Luria- Bertani (LB) medium

Plasmids encoding the leucine zipper constructs were transformed into the *E.coli* strain BL21 Rosetta2pLysS (Novagen). 100 µL of the cultures were plated onto LB-agar plates containing Kanamycin (Kan) (50 µg/ml) to enable selective growth of the pETM-11 plasmid (provided by EMBL Heidelberg) with Chloramphenicol (Cam) to limit bacterial growth to the BL21 Rosetta2pLysS strain (34 µg/ml). The plates were incubated overnight (12-16 hours) at 37°C and the resulting colonies were used to inoculate a sterile 5 ml LB culture containing the appropriate antibiotics was incubated for 8 hours at 37°C with a rotational speed of 225 rpm, and then grown in 200 ml LB cultures overnight. 20 ml of the bacterial culture was transferred to 2 x 2 L conical flasks both containing 500 ml LB medium and Kan/Cam antibiotics. The conical flasks were incubated at 37°C with an agitation speed of 225 rpm until an optical density A₆₀₀ of 0.75, upon detection of the late-log phase of bacterial growth protein expression was induced with the addition of 0.5 mM IPTG, after 4 hours the cultures were harvested at 6000 rpm (9782 g) for 15 minutes in Sorvall rotor SLC-6000 at 4°C. The pellet was stored at -20°C until purification.

Expression conditions and solubility status of LZ constructs

Name of construct	Expression temperature	Solubility status
LZ0	37°C	Soluble fraction
LZ2	37°C	Soluble fraction
LZ3	37°C	Soluble fraction
LZ4	37°C	Soluble fraction
LZ5	37°C	Soluble fraction
LZ6	37°C	Soluble fraction

2.3.3 Expression in Minimal medium M9 (Marley Method)

M9 medium composition

The 20x salt solution consists of; Na₂HPO₄ 120 g, KH₂PO₄ 60 g and NaCl 10 g dissolved in a volume of 1 L using distilled water and subsequently autoclaved.

Vitamins dissolved in 100 ml autoclaved water: choline chloride 0.4 g, folic acid 0.5 g

Micronutrients dissolved in 100 ml autoclaved water: NaMoO₄ 0.73 mg, H₃BO₃ 24.7 mg, CoCl₂ 7.1 mg, CuSO₄ 2.5 mg, MnCl₂ 15.8 mg and ZnSO₄ 2.9 mg.

To prepare the M9 medium 50 ml of the previously prepared 20x salt solution were added to a 1 L shaker flask and autoclaved, after cooling the following components were added whilst stirring; MgSO₄ 1M 2 ml, CaCl₂ 0.1M 100 µl, Glucose 6 g (dissolved in 50 ml of H₂O and sterile filtered using a syringe with a Millipore 0.2 µM filter), NH₄Cl 1 g the solution was mixed for 15 minutes at RT. 1 ml aliquots of the vitamin and micronutrient solutions had been prepared and stored at -20 °C, 1 ml of each was thawed and added to the solution. The M9 medium was subsequently used for expression.

1 L M9 Minimal medium was used to obtain ^{15}N labelled protein as previously described. The same procedure for protein expression in LB was repeated as described in the section above, until reaching an optical density of 0.8, after which the cultures were spun down at 5000 rpm ($9782 \times g$) for 8 minutes in a Sorvall rotor SLC-6000. After centrifugation the pellets were resuspended in 1X M9 salts and then spun down again for 8 minutes at 5000 rpm. The pellet has been re-suspended in 50 ml minimal medium (M9), containing $^{15}\text{NH}_4\text{Cl}$ to ^{15}N labelled protein, and then transferred in the M9 medium and left in the shaker at 37°C for 1 hour prior to induction with 1 ml IPTG 0.75M (Isopropyl Isopropyl β -D-1-thiogalactopyranoside) (Melford laboratories). After 4 hours the cells were harvested by centrifugation for 15 minutes at 6000 rpm and kept at -20°C until needed for the purification.

2.3.4 Protein Purification

The bacterial pellet obtained from 4 L of LB culture was re-suspended in 10 ml fast flow 6 (FF6) wash buffer (PO_4 20 mM, NaCl 500 mM, Imidazole 10 mM, β -ME 2.5 mM, NaN_3 0.02% (w/v), pH = 7.5-8.0), after which the solution was sonicated for 2 minutes (20 sec on, 20 sec off, 10 amplitude) and centrifuged for 90 minutes at 18,000 rpm ($59,768 \times g$) to rupture the cell membrane and release the overexpressed proteins of interest. SDS-PAGE (Sodium Dodecyl Sulphate PolyAcrylamide Gel Electrophoresis) analysis was performed to screen for solubility.

2.3.5 Purification methods using chromatography

The LZ supernatants were purified by Immobilized Metal ion Affinity Chromatography (IMAC) using Ni Sepharose 6 Fast Flow columns (Amersham), due to the presence of the hexa-histidine tag. The resin contained in each column consists of 90 mm beads of agarose

with a coupled chelating group, which has been charged with Ni²⁺ ions. The gravity flow columns were packed using 4 ml of re-suspended Ni-NTA resin, corresponding to 2 ml of resin in each column. Each leucine zipper construct had been assigned a specific Ni-NTA column for the duration of the study. The protein suspension, was loaded onto pre-equilibrated Ni-NTA columns (20 ml FF6 wash buffer) and allowed to bind, was washed with 40 ml of FF6 wash buffer (Phosphate 20 mM, NaCl 500 mM, Imidazole 500 mM, β-ME 2.5 mM, NaN₃ 0.02% (w/v), pH = 7.5-8.0), and eluted with 8 ml of FF6 elution buffer (Phosphate 20 mM, NaCl 500 mM, Imidazole 500 mM, β-ME 2.5 mM, NaN₃ 0.02% (w/v), pH = 7.5-8.0). Further purification was achieved using Size Exclusion Chromatography (SEC) on a Superdex 75 HiLoad 16/60 pre-packed column. The Superdex 75 HiLoad 16/60 was calibrated using the gel filtration standard (BIORAD cat#151-1901): 250 µl of the molecular weight standard was loaded into the 250 µl sample loop and subsequently injected onto the column at a flow rate of 0.5 ml/min, the standard consists of five proteins thyroglobulin (670 kDa), γ-globulin (158 kDa), Ovalbumin (44 kDa), Myoglobin (17 kDa) and Vitamin B₁₂ (1.35 kDa), the chromatogram used to calculate the molecular weight of the LZ protein by cross-referencing the elution volumes of standards (Ovalbumin (44 kDa at 52 ml), Myoglobin (17 kDa at 64 ml) and Vitamin B₁₂ (1.35 kDa at 88 ml) against the elution volume of the LZ proteins to interpret molecular weights of the SEC peaks.

2.3.6 Removal of the Histidine tag

All LZ constructs were expressed with an N-terminal 6 x Histidine tag to enable a final purification of over 99% prior to NMR analysis. To avoid any interference with dimerization of the leucine zipper, we decided to remove the histidine tag completely. After the histidine tag and immediately preceding the leucine zipper an AcTev protease site was present. AcTev

protease (Invitrogen) was used to cleave the leucine zipper proteins in the following way:
The leucine zipper sample was concentrated down to a volume of 500 µl in a centrifuge at
4,000 rpm at 10°C using Vivaspin columns (MWCO 3,000 Da).

Actev digestion parameters

Leucine zipper	6 mg (in 500 µl)
20x TEV buffer	30 µl
0.1M DTT	6 µl
AcTEV protease	(30 U) 3 µl
Water	61 µl Total volume 600 µl

The reaction was incubated for 10 hours at 30°C. Post incubation with AcTEV an IMAC purification step was required to remove both the protease and the cleaved histidine tag. The 2 ml Ni-NTA columns underwent an equilibration step by the addition of 20 ml of FF6 wash buffer before the addition of the cleaved LZ–AcTEV solution to the column, prior to the addition of the protein solution a clean collection tube was placed to collect the flow-through after the protein solution was added which contained the cleaved leucine zipper constructs (the AcTEV protease contains a His tag for removal after cleavage, the LZ construct contained a His tag which also binds to the NiNTA resin. Only pure LZ flowed through), once the protein sample had ran through the column the Ni-NTA was washed with 5 ml of FF6 wash buffer (Phosphate 20 mM, NaCl 500 mM, Imidazole 500 mM, β-ME 2.5 mM, NaN₃ 0.02%, pH = 7.5-8.0) which was also collected, 20 ml FF6 wash buffer was added and not collected, the protease and free His tag were eluted with 16 ml of FF6 elution buffer (Phosphate 20 mM, NaCl 500 mM, Imidazole 500 mM, β-ME 2.5 mM, NaN₃ 0.02%, pH = 7.5-8.0). The column was washed with 20 ml FF6 buffer and finally stored in 20% ethanol at 4°C for future use.

2.3.7 Buffer exchange for Circular Dichroism (CD) analysis

To perform CD spectroscopy the proteins for analysis were dialysed against CD buffer using cassettes (PIERCE Slide-A-Lyzer Dialysis Cassettes MWCO; 3,500, 3-12 ml), the sample was loaded using an 18-gauge needle attached to a syringe. The buffer was exchanged three times using 1 L of CD buffer each (Phosphate 20 mM, NaCl 50 mM, DTT 1 mM, pH = 7.0). Finally, the proteins were concentrated by centrifugation (Vivaspin MWCO: 3,000, 20 ml).

The LZ5 mutants (K309C and E310C) were analysed by CD under reducing and oxidising conditions. The reducing buffer composition was as previously described (Phosphate 20 mM, NaCl 50 mM, DTT 1 mM, pH = 7.0); the oxidising buffer was made as follows (Phosphate 20 mM, NaCl 50 mM, pH = 7.0), with oxygen flowed through the buffer during dialysis overnight. In each example the 1 L buffer was replaced 3 times with the final exchange running overnight at 4°C.

To run the NMR experiments, all the proteins were dialysed against NMR buffer using dialysis membrane cassettes (PIERCE Slide-A-Lyzer Dialysis Cassettes MWCO; 3,500, 3-12 ml) as previously described. The buffer was exchanged three times using 1 L of NMR buffer each (Phosphate 20 mM, NaCl 50 mM, DTT 2mM, pH = 7.0). Finally, the proteins were concentrated by centrifugation (Vivaspin MWCO: 3,000, 20 ml).

2.4 Spectroscopic analysis

2.4.1 Circular Dichroism (CD) spectroscopy

All CD experiments were recorded on a JASCO700 instrument fitted with a Peltier temperature control system. Square cuvettes with 0.1 or 1 mm pathlength were used with

protein concentrations ranging from 20-200 µM. Spectra were calibrated using software provided by the manufacturer. To measure thermal unfolding curves, samples were heated at 1°C/min while the CD signal at a constant wavelength of 222 nm was measured. Unfolding curves were fitted to the equation for a two-state unfolding reaction using a home written Mathematica macro documented in section 3.1.9 to ascertain at which temperatures the transition from folded to unfolded began. In alpha helices a broad transition area is normally seen, due to the sequential unwinding of the helix from the N-or the C-terminus or both simultaneously.

2.4.2 NMR spectroscopy

NMR spectroscopy is a tool used for the determination of atomic resolution structures of biological molecules i.e. proteins and nucleic acids. The first 3D structure of a protein was ascertained by Kurt Wüthrich in 1985 (Havel and Wüthrich, 1985), using NOE data in combination with a distance geometry programme (DISGEO). Since this date, the evolution of NMR hardware (increased magnetic field strength and cryoprobes) and NMR methodology, added to the advances in molecular biology and biochemical methods for the production and ability to isotope label recombinant proteins, has led to an increase in demand for NMR technology to determine the three dimensional structure of proteins. Moreover, NMR spectroscopy can be used to provide information regarding conformational dynamics and exchange processes of proteins in solution, and is most effective in determining sites of ligand binding and mapping surfaces where important protein/ligand interactions occur.

2.4.2.1 Principles of NMR spectroscopy

Isotopes which are most commonly used in NMR are ^1H , ^{13}C , and ^{15}N , these have a nuclear spin (I) of a $\frac{1}{2}$. Atoms of biomolecules with a nuclear spin $I = \frac{1}{2}$ possess an associated magnetic dipole moment (μ) which is equal to the gyromagnetic ratio (γ) multiplied by the nuclear spin (I), ($\mu = \gamma I$) in a magnetic field (B_0). Consequently, when quantized can have two possible orientations ($I_z = \pm\frac{1}{2}$), these two energy levels are populated according to the Boltzmann distribution (Figure 2.2). The difference in energy levels (ΔE) between α/β is field dependent and relative population differences between the high and low energy states is small approximately 10^{-4} , making NMR a rather insensitive method in spectroscopy. Sensitivity can be improved by reducing the signal to noise ratio. This can be performed by increasing the number of spins in the sample by increasing the concentration, and also an increase in the magnetic field strength (B_0).

As previously described when a nucleus is placed in a magnetic field there is an interaction between the nuclear magnetic moment and the applied field. The energy of this interaction is dependent on the angle between the magnetic moment and the field (with the highest energy being when the magnetic moment is at an angle of 180 degrees to the field and the lowest energy when the magnetic moment parallel, and therefore 0 degrees to the field). However, random thermal motion acts to disrupt this alignment and drive the system to where the magnetic moments have random orientations. Since it is more probable that the nuclear spin is driven towards a lower energy state, the thermal motion of is slightly more bias towards magnetic moments with a parallel alignment to the field. Eventually, this leads to an anisotropic distribution of nuclear spin polarisations, termed thermal equilibrium.

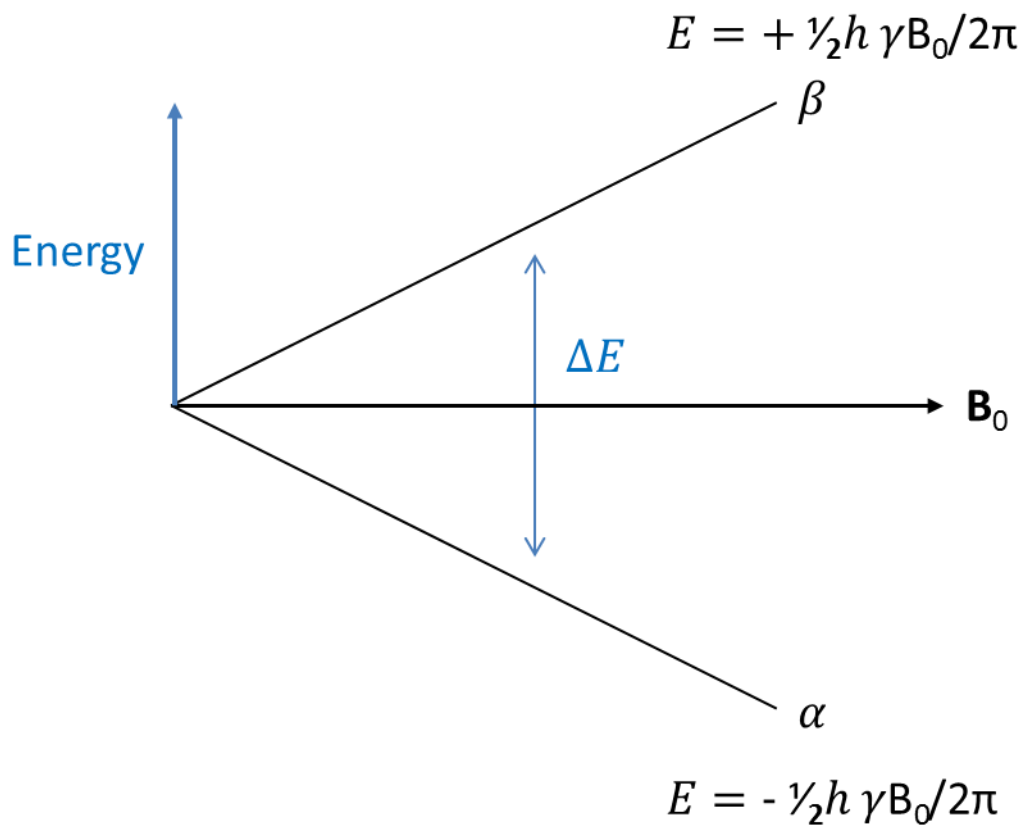


Figure 2.2 Boltzmann distribution in a magnetic field B_0

The probable distribution of magnetisation energy (E) in two populations α and β are shown (h = Planck's constant). The difference between population α and β are small (of the order 10^{-4}), however, it is the difference in population states that produces an effective magnetisation along the z-axis

Therefore, the whole sample has a net magnetisation along the direction of the applied magnetic field which is represented by a bulk magnetisation vector. When the sample is placed in a magnetic field it takes time for the equilibrium magnetisation to build up and for the bulk magnetisation to have a net magnetisation along the z – axis. However, even though a net magnetism is induced in the z-axis only there is no overall net magnetisation in the x- or y-directions because the precession frequencies of the individual nuclei are out of phase, not correlated and generate an average of zero. Transverse magnetisation can be observed only when the system is perturbed and therefore an x or y magnetisation is generated, for example by a radio frequency (RF) pulse.

The nuclear Larmor frequency (ω_0) can be measured in hertz (Hz), also termed cycles per second, and can be related to γ the gyromagnetic ratio (proportionality constant) and the applied magnetic field (B_0) using the equation $\omega_0 = -\gamma B_0$. This can be expressed either in the units of radians per second or Hz when ω_0 is multiplied by 2π (Ernst, 1987; Abraham, 1961). Therefore, the differences in the gyromagnetic ratio lead to different Larmor frequencies when using spectrometers of differing field strengths (the Larmor frequency is proportional to the magnetic field). To counteract this, frequencies are expressed in units independent of the field strength, the measured peak frequencies are calibrated against the frequency of a known reference compound TMS for each NMR spectrometer operating using a different field strength. Therefore, the chemical shift δ (ppm) = $10^6 \times ((v - v_{ref}) / v_{ref})$ where v is the measured frequency and v_{ref} is the TMS reference frequency in Hz.

The precession of the magnetisation vector forms the basis of detection in NMR. A small wire coil is mounted around the sample and in the xy-plane, as the magnetisation vector cuts the wire coil (mounted in the spectrometer around the sample) a current is induced,

this is then subsequently amplified and recorded. This is called the free induction decay (FID). Fourier transformation of these signals would give us a single NMR resonance lines at a frequency in Herz (Hz) in the spectrum. Detailed equations depicting the components of magnetisation can be found in Chapter 2 from Freeman, R. (1997).

2.4.2.2 Basic NMR experiments

A pulsed NMR spectrum is recorded in the following way: a delay is used in order to allow the spins reach equilibrium and is called the relaxation delay, t_r (few seconds). A burst of radio frequency (RF) power is applied to the sample which normally lasts no more than 20 μ s per scan, the excited transient signal, FID, is subsequently recorded for a time known as the acquisition time t_{acq} , between 50 ms to a few seconds. When the FID is processed using the Fourier transformation the spectrum is visible. The experiment is repeated a set number of times (N) to improve the signal to noise ratio (time averaging), the noise adds up more slowly than the signal by a factor of \sqrt{N} . A closer look at the pulse sequence can divide this into three parts, in the first the magnetisation builds up along the z-axis and reaches equilibrium, in the second a $90^\circ(x)$ pulse is applied and rotates the magnetisation into the y-axis, in the third stage the magnetisation precesses around the transverse plane at the offset (Ω). The magnetisation can be calculated using: $M_y = M_0\cos\Omega t$ and $M_x = M_0\sin\Omega t$. The Fourier transform will give the spectrum peaks appearing at frequency Ω . When the spectrum has multiple peaks each can be assigned with a separate magnetisation vector each. These vectors will be rotated onto the transverse plane after the hard pulse and the detected signal is the sum of these components. Every NMR experiment must undergo pulse calibration prior to the initiation of the pulse sequence, the length of the 90° pulse or P_1 must be determined. A modified pulse-acquisition experiment is performed with a flip

angle β of 180° to find a null, this is then divided by two to calculate the length of a 90° degree pulse (P_1).

2.4.2.3 Spin echo

The spin echo sequence at the end of the second delay places all magnetisation along the same axis, independent of the length of τ (delay) or the offset Ω . The spin echo can briefly be described as a technique where the offset has been refocused and at the end of the sequence the magnetisation, and appears to not have evolved and the offset is zero. If a magnetisation vector has precessed away from the $-y$ -plane through an angle of ϕ it has acquired a phase ϕ , if a $180^\circ(x)$ pulse is applied it has no effect on the x -component (this is aligned with the B_1 field) but it rotates the y -component to the opposite axis, therefore from $-y$ to $+y$ and has a position in terms of phase ϕ of $\pi - \phi$. The pulse sequence starts with a $90^\circ(x)$ pulse which places the magnetisation along the $-y$ -axis. If the offset is positive the magnetisation precesses from the $-y$ towards x through the angle $\Omega\tau$ (phase). After the $180^\circ(x)$ pulse the magnetisation has shifted to the y -axis with a phase of $\Omega\tau$, when measured from the $-y$ -axis this is calculated by $\pi - \Omega\tau$, the phase at the end of the sequence is given by $(\pi - \Omega\tau) + \Omega\tau = \pi$ a magnetisation vector aligned on the y -axis. The intervention of the 180° pulse causes the phases to cancel one another out.

Pulses can also be applied in the y -plane and are written as $90^\circ(y)$ for example. A pulse about the y -axis will position the magnetisation along the x -axis. Interestingly a 180° pulse about any axis in the transverse lane will position the magnetisation from $+z$ - to the $-z$ -axis.

2.4.2.4 Fourier transformation

An NMR experiment gives us the superposition of all the spins as a function of time $F(t)$. The Fourier transform is performed to convert the intensities FID as a function of frequencies and obtain the $F(\omega)$. A mathematical operator is used to convert a function from a time domain into a frequency domain: $F(t)$ into $F(\omega)$.

2.4.2.5 Relaxation

Once a spin has been perturbed, it tends to relax back to its equilibrium state over a period of time. Every spin has two different kind of relaxation (Figure 2.4); longitudinal or spin-lattice relaxation the decay of spin-magnetization back to the Boltzmann distribution equilibrium and transverse or spin-spin relaxation which is the decay of coherences or the loss of phase. In isolated spin $\frac{1}{2}$ there are two time constants associated with these two types of relaxation and these are: spin-lattice relaxation time constant T_1 and the transverse relaxation time constant T_2 . To understand relaxation processes one must first consider the some causes of relaxation: these are dipole-dipole and chemical shift anisotropy (CSA). Dipole-dipole coupling can be direct where the spin influences its neighbor due to the magnetic fields present or indirect with J-coupling in which nuclear spins are coupled together through electrons. Direct dipole-dipole coupling can be visualized since every nuclear spin is magnetic and therefore, generated a magnetic field in the direction of its spin magnetic moment. For example, a magnetic field generated by spin *A* would interact with the magnetic field of spin *B* through space. This type of coupling may be intra- or intermolecular. The dipole-dipole coupling constant takes into account the distance between the two nuclei and it is this reason why it can be used to generate geometric data for the determination of the structure of molecules.

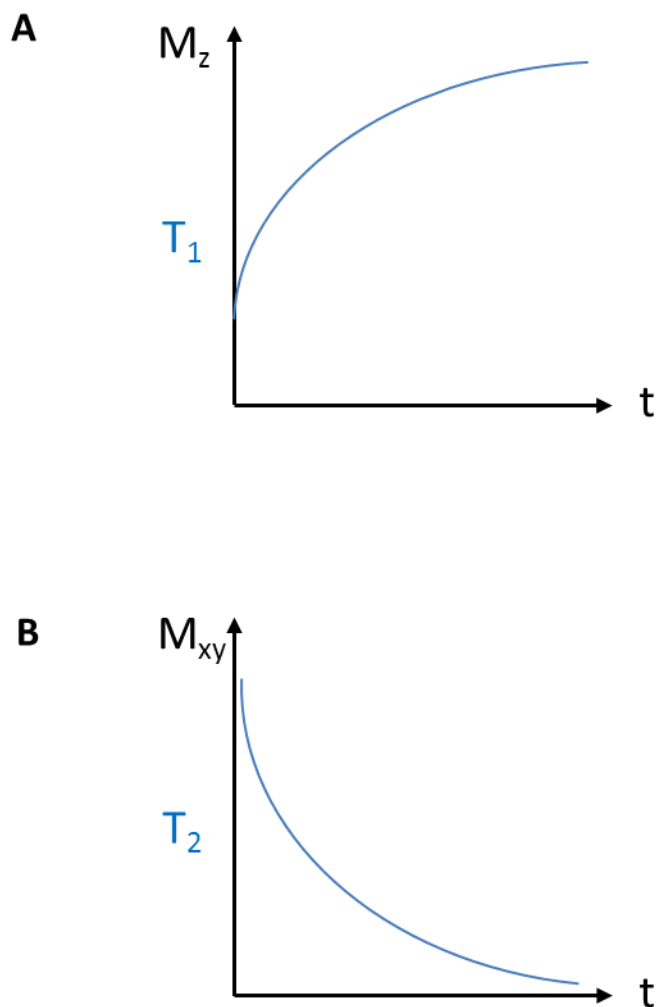


Figure 2.3 Relaxation processes

A. The T_1 relaxation is shown the magnetisation on the z-axis decays exponentially to the equilibrium Boltzmann distribution. B. The M_{xy} magnetisation decays exponentially as the magnetisation loses coherence in the y-axis, T_2 relaxation occurs.

The chemical shift is the variation of the magnetic field on the nuclei of an atom caused by the electrons which surround it. The B_0 field induces currents in the electrons surrounding the molecule and the molecular currents then generate a magnetic field called the induced field B_i . The induced field is linearly dependent on the applied field. The chemical shift tensor relates the induced field to the external field and is linearly dependent on the applied field. Three principle axes are derived from when the induced field is parallel to the external field, if the principle values for z, x, and y are equal then the chemical shift tensor is said to be isotropic. If two or more principle values are different then it is anisotropic. CSA increases its effect on relaxation as the magnetic field strength increases and can compete with dipole-dipole relaxation.

The autocorrelation function is a means of calculating how rapidly the transverse field fluctuates. The parameter τ_c is the correlation time of the fluctuations, the correlation time also corresponds to the length of time a molecule takes to rotate one radian. Slow fluctuations have large values of τ_c whereas, fast fluctuations have a small value. The correlation time τ_c depends on the parameters of the experiment like temperature, the τ_c is in general decreased by increasing temperature and increased by lowering the temperature. The spectral density function $J(\omega)$ is defined as twice the FT of the autocorrelation function and tells us the amount of motion present at a certain Larmor frequency. If the correlation time τ_c is short then the spectral density function $J(\omega)$ is broad.

Spin-lattice (longitudinal) relaxation rate constants R_1 as previously described this corresponds to how quickly the system will return to the Boltzmann equilibrium along the z-axis to its starting position. Spin-spin (transverse) relaxation rate constants R_2 describe the decay of transverse magnetization ($x-y$ -plane) to zero. The Bloch equations present

relaxation theoretically (Bloch, 1946): $M(t)$ represents the nuclear magnetization vector and $B(t)$ is the applied magnetic field.

$$\frac{dMz(t)}{dt} = \gamma(M(t) \times B(t))z - R1(Mz(t) - M_0)$$

$$\frac{dMx(t)}{dt} = \gamma(M(t) \times B(t))x - R2Mx(t)$$

$$\frac{dMy(t)}{dt} = \gamma(M(t) \times B(t))y - R2My(t)$$

R_1 and R_2 values are reciprocals of each other and therefore $T_1 = \frac{1}{R_1}$ and $T_2 = \frac{1}{R_2}$. The values of

R_2 governs the length of time the FID can be observed, whilst, R_1 rates govern the time taken for equilibrium to be restored. Once the correlation time has been calculated and subsequently the spectral density, dynamic information can be extracted from the NMR experiments. To perform such a study the model independent analysis (Lipari and Szabo, 1982a; Lipari and Szabo, 1982a; Clore et al., 1990) can be used to calculate the parameters; S – the general order parameter which is a measure of the spatial restriction of the motion and τ_c - the effective correlation time which measures the rate of motion

The equation for determining S is as follows: Model 1

$$J(\omega) = \frac{2}{5} \left[\frac{S^2 \tau_c}{1 + (\omega \tau_c)^2} \right]$$

The spectral density can be used to calculate the specific relaxation rates and relies on the motion being isotropic. When the molecule is not globular, for example, an elongated protein structures motion can be described as anisotropic, such anisotropic motion can function to bias the relaxation rates giving reduced accuracy in the calculated τ_c values

which in turn leads to the calculation of J the spectral density being different from the actual experimental value.

$$R_1 = \left(\frac{d^2}{4}\right) [3J(\omega_N) + 7J(\beta_1\omega_H) + c^2J(\omega_N)]$$

$$R_2 = \left(\frac{d^2}{8}\right) [4J(0) + 3J(\omega_H) + 13J(\beta_2\omega_H)] + \frac{c^2}{6} [4J(0) + 3J(\omega_H)]$$

$$\text{NOE} = \left(\frac{d^2}{4}\right) 5J(\beta_3\omega_H)$$

d = dipolar relaxation contribution and $\beta_1 = 0.921$, $\beta_2 = 0.955$ and $\beta_3 = 0.87$ for ^{15}N nuclei.

Therefore, a factor which can directly affect T_1 relaxation is an increase in field strength B_0 that extends the T_1 relaxation period.

2.4.2.6 Chemical exchange

An early definition of described that for chemical exchange to occur motional properties involve the making and breaking of chemical bonds are present. Therefore, if a dynamic process takes one nuclei from one magnetic environment to another the NMR spectrum will show this due to the chemical shifts and J-coupling changing, if on an appropriate time-scale. The term chemical exchange can also used when the conformation of a molecule changes, however, more recently it is described as conformational exchange. The study of chemical exchange is well documented (Gutowsky and Holm, 1956; McConnell, 1958), early work showed the effects of chemical exchange on NMR spectra in relation to temperature using para-nitrosodimethylaniline (Buckley et al., 1974; Furness et al., 1975). The spins show scalar coupling but the nitroso group can flip from one side to the other of the plane of the ring, when it flips the chemical shifts and couplings are swapped. Therefore, all lines are

broadened with the transition into a different magnetic environment. In this case the term mutual exchange is used because the molecule is identical in both cases. The leucine zipper exchange could also be referred to as mutual exchange as the molecule remains the same whilst the conformation changes over time.

Using the measured variable of chemical shift, the exchange between two states can be characterised by shifts δ_A and δ_B , slow exchange occurs if the exchange rate $k \ll |\delta_A - \delta_B|$, and intermediate exchange if $k = |\delta_A - \delta_B|$ (reviewed in Bain, 2003).

2.4.2.7 Nuclear overhauser enhanced spectroscopy (NOESY)

The nuclear overhauser effect (NOE) is the transfer of magnetisation from one nuclei to another through space via cross relaxation (Anderson and Freeman, 1962; Overhauser, 1953). This distance is approximately 5Å. Briefly, in a NOESY spectrum the peaks seen are due to cross relaxation due to direct dipolar coupling and not through chemical bond, therefore the technique indicates which protons are near to each other (Jeener, 1979; Wagner and Wüthrich, 1982). A basic NOESY pulse sequence has three $\pi/2$ (90 degree) pulses. The first pulse creates transverse spin magnetization. This precesses during the evolution time t_1 . The second rotates the transverse magnetization in the x-y-plane to longitudinal magnetization z-axis and allows cross relaxation to occur where magnetisation is transferred for the mixing period τ_m . In the case of the NOESY experiments performed for the leucine zipper the τ_m was kept constant at 80 ms (Macura & Ernst, 1980). The third pulse creates transverse magnetisation from the remaining longitudinal magnetisation, after which acquisition begins and the transverse magnetization is observed as a function of the

time t_2 . The NOESY spectrum is generated by a 2D Fourier transform with respect to t_1 and t_2 .

2.4.2.8 Total correlation spectroscopy (TOCSY)

The first indications that the Nek2 leucine zipper was subject to exchange dynamics were generated from early experiments using $^1\text{H}/^{15}\text{N}$ TOCSY for the construct LZ2. The TOCSY experiment gave rise to crosspeaks between signals from backbone amide groups, which can only arise through chemical exchange processes (Feeney et al., 1991). The peaks were of equal intensity indicating that the exchanging species were present in equal populations. Normally a TOCSY spectrum gives information on spin systems connected through chemical bonds and therefore through J-coupling. The TOCSY pulse sequence consists of an initial $\pi/2$ pulse and t_1 evolution, followed by a series of short π pulses throughout the entire mixing time τ_m , in the case of the TOCSY performed on the leucine zipper this was 50 ms, the series of short pulses during the τ_m , this series of 180 pulses continually rotates the magnetisation about the z-axis and effectively holds it there, this is called “spin-lock”, any magnetisation which is not orientated along the z-axis eventually decays due to the inhomogeneity in the B_1 field, leaving only the magnetisation which has arisen through coupling present during the acquisition phase t_2 (Braunschweiler & Ernst, 1983).

2.4.2.9 $^1\text{H}-^{15}\text{N}$ HSQC

An $^1\text{H}-^{15}\text{N}$ heteronuclear single quantum coherence (HSQC) is the most commonly performed experiment in NMR (Bodenhausen and Ruben, 1980). A 2D- $^1\text{H}-^{15}\text{N}$ HSQC spectrum gives us the characteristic map of the hydrogen and nitrogen chemical shifts and corresponds to the number of residues in the protein observed, with the exception of

proline residues which do not possess a free NH. Amino acids which contain NH groups within their side chains, such as Arginine (R), give rise to additional signals.

Initially, the experiment starts with an insensitive nuclei enhanced by polarization transfer (INEPT) experiment. The size of the magnetisation that is detected at the end of the experiment depends on the equilibrium magnetisation we start with, this in turn depends on the B_1 field and also the gyromagnetic ratio, therefore, a proton has a higher gyromagnetic ratio and therefore equilibrium magnetisation than nitrogen. The INEPT pulse utilises this by transferring polarization from the 1H nuclei to the ^{15}N via $1J$ coupling (Morris and Freeman, 1979), during the t_1 evolution period the anti-phase ^{15}N magnetisation precesses under the effect of the nitrogen chemical shift, the heteronuclear couplings are then refocused by applying a 180 degree 1H pulse in the middle of t_1 . A reverse-INEPT block is then used to convert ^{15}N magnetisation into in-phase 1H magnetisation, in the final stage of the experiment the acquisition is performed with nitrogen decoupling so that only the 1H signal is recorded.

2.4.2.10 Summary of NMR experiments

NMR spectra were acquired from 0.35 mL samples of 2 mM or 0.1 mM leucine zipper constructs LZ0 – LZ5 complex in a 20 mM sodium phosphate, 100 mM sodium chloride and 0.02% (w/v) sodium azide buffer at pH 7, containing either 10% D₂O. All NMR data were acquired at 298 K, unless specified differently, on either an 800 MHz Varian Inova or a 600 MHz Bruker Avance spectrometer. The 2D spectra recorded to characterise the leucine zipper constructs were: 1H TOCSY (Braunschweiler & Ernst, 1983) with mixing times of 50 ms, and NOESY (Macura & Ernst, 1980) with an NOE mixing time of 80 ms; $^{15}N/^1H$ HSQC (Bodenhausen & Ruben, 1980); 2D 1H experiments over 24-48 hours and $^{15}N/^1H$ HSQC

spectra over about 16 hours. Typical acquisition times in 2D experiments were either 75 ms (^{15}N) or 35 ms (^1H) in F_1 and 140 ms in F_2 (^1H). The WATERGATE method was used to suppress the water signal when required (Piotto *et al.*, 1992). The NMR data were processed using Topspin (Bruker) or in the case of the 2D ^1H - ^{15}N heteronuclear correlation experiment (Farrow *et al.*, 1994), with the collaborative computing project (CCPN) (Vranken *et al.*, 2005).

2.4.2.11 Analysis of Protein dynamics using NMR

Spectra were recorded at a temperature of 298K on Bruker Advance 600 and 800 MHz spectrometers fitted with 5 mm cryoprobes. Exchange experiments were as previously described (Farrow *et al.*, 1994), Farrow and colleagues present an accurate method for determining rate constants in a two state exchange system, a 2D ^1H - ^{15}N heteronuclear correlation experiment is used to estimate both chemical exchange and longitudinal exchange and is based on the transfer of longitudinal ^{15}N magnetisation (N_z) between the exchanging conformations, based on a method previously described in the literature by Montelione and Wagner (1989). The pulse sequence used in this experiment has been reported elsewhere for the measurement of longitudinal relaxation rates (Kay *et al.*, 1989; Palmer *et al.*, 1991a). Artefacts and water signals were suppressed by using pulse field gradients (Bax and Pochapsky, 1992; John *et al.*, 1992); supplementary to this, the gradient g1, which follows the first ^{15}N $\pi/2$ pulse ensures that only proton magnetisation has a signal. Selective pulse on the water resonance were used to minimise the saturation of water (Grzesiek and Bax, 1993a); Kay *et al.*, 1994). The ^{15}N 90_y pulse (prior to the gradient g4) creates z nitrogen magnetisation which then relaxes/exchanges during the mixing time T. The pulse scheme employed during T applies 1H 180 degree pulses every few milliseconds

and are applied as cosine-modulated pulses (Smallcombe, 1993). These have broad excitation null on resonance on the water. After T evolution the magnetisation is returned to the NH proton for detection via an INEPT pulse scheme (Morris and Freeman, 1979). WATERGATE was applied to suppress the water signal prior to detection to return the water magnetisation to the +z axis (Piotto et al., 1992).

For the quantitative analysis of the exchange rates a series of mixing times were used: 8, 16, 24, 32, 64, 96 and 160 ms. Peak volumes were used to characterise the decay of the magnetisation through the mixing time. To perform this, the Bloch equations for chemical exchange between two sites were used (Hahn and Maxwell, 1952; Gutowsky et al., 1953; McConnell, 1958; Hull and Sykes, 1975). The intensities of the auto peaks for the Nek2 leucine zipper conformer A (Hepl) and conformer B (Hepll) are calculated using equations 1a and 1b depicted in Farrow et al., 1994. A mixing time of 64 ms was used for the NMR experiment.

The intensities of the exchange peaks that corresponded to a transfer of magnetisation from conformation A to conformation B were calculated using equation 1c and 1d (Farrow et al., 1994).

The longitudinal and exchange rates were extracted by fitting the equations to the measured auto and exchange peaks, the auto peaks were generated by recording the spectrum under fully relaxed conditions with no T mixing time. The spectra were modified further to increase the dispersion of the peaks by changing from a $^{15}\text{N}-^1\text{H}$ view to a $^1\text{H}-^1\text{H}$ NOESY-like view and also by combining both views into a 3D experiment (F. W. Muskett, R. A. Croasdale, A. M. Fry, M. Pfuhl, unpublished results). Diagonal and cross peak intensities for sufficiently well resolved systems of exchanging amide resonances were extracted using

CCPN analysis (Vranken et al., 2005) and fitted to standard equations for slow exchange (Farrow et al., 1994) using a home written Mathematica macro (M. Pfuhl) to yield exchange rates and ^{15}N longitudinal relaxation rates. ^{15}N longitudinal (R_1) and transversal (R_2) were also measured directly in the standard manner using delays of 16, 48, 96, 192, 288, 384, 512, 704, 880, 1120, and 1440 ms for R_1 and 5, 10, 15, 20, 31, 41, 61, 82, 102, 133, 154 ms for R_2 .

2.4.3 Analytical ultracentrifugation

The sedimentation velocity experiments were carried out on a Beckman XL-I centrifuge using an An50-Ti rotor at 4°C and a speed of 42,000 rpm (LZ0) and an An-60 Ti rotor at 20°C and a speed of 60,000 rpm (LZ5 and LZ5 mutants). Scans were recorded using the interference optical system until no further sedimentation occurred. Sample concentrations were about 10-200 μM in standard NMR buffers. Protein partial specific volume and buffer density and viscosity were calculated using SEDNTERP (Laue et al., 1992). The experimental data were analysed using Sedfit (Schuck, 2000) by fitting to the $c(s)$ and $c(s,f/f_0)$ models with one discrete component (LZ0) and results for some samples confirmed by 2-dimensional spectrum analysis, enhanced van-Holde-Weischet analysis and Genetic Algorithm analysis using UltraScan (Demeler, 2005). The AUC experiments were performed by Tina Daviter at the University of London.

2.5 Bioinformatics software

Leucine zipper prediction was performed with the 2ZIP server (Bornberg-Bauer et al., 1998) (<http://2zip.molgen.mpg.de/index.html>).

The coiled-coil prediction was performed with the COILS server (Lupas et al., 1991) (http://www.ch.embnet.org/software/COILS_form.html). Single helix preference as well as N- and C-caps were calculated with the web based version of AGADIR (Munoz and Serrano, 1994) (<http://www.embl-heidelberg.de/Services/serrano/agadir/agadir-start.html>).

Pattern searches were performed with the program pattinprot (http://npsa-pbil.ibcp.fr/cgi-bin/npsa_automat.pl?page=npsa_pattinprot.html) (Bucher et al., 1996).

Nuclear export sequences were analysed using the program NetNES 1.1 (<http://www.cbs.dtu.dk/services/NetNES/>) (La Cour et al., 2004).

CHAPTER 3

BIOPHYSICAL PROPERTIES OF THE NEK2 LEUCINE ZIPPER

3.1 Results

3.1.1 Rationale for the design of the Nek2 leucine zipper constructs

In total several leucine zipper variants were designed, the initial construct LZ1 had been described by Fry et al. (1999) where a bioinformatics screen COILS (Ferré-D'Amaré et al., 1993) with a window function of 28 residues was performed to identify the LZ domain boundaries, this predicted residues 306-334 comprised the Nek2 leucine zipper. Initial 2D-HSQC experiments using a ¹⁵N isotope labelled sample of LZ1 had revealed a significant number of overlapping peaks, more than the expected 28 for the dimeric coiled-coil, indicating the necessity to initially extend the domain boundary in the case that LZ1 was partially unfolded. In parallel, studies were undertaken by Frank Ivins (MRC Mill Hill, London) in order to attempt to crystallise the leucine zipper motif of Nek2. In these studies the calculated domain boundaries of the leucine zipper was predicted to be between residues 302-368, using the COILS software, which discounted a trough in the coil prediction of 0.2-0.4 probability at residue 335. To ascertain if the trough in the COILS prediction was of significance to the leucine zipper structure, the technique of limited proteolysis was performed on the full-length Nek2 protein kinase by F. Ivins (Croasdale et al., 2011). The data indicated the presence of an 8 kDa fragment resistant to Trypsin cleavage after 1 hour. The 8 kDa fragment was the only significant fragment remaining after 1 hour incubation at 37°C; when excised and subsequently analysed by MALDI-TOF mass spectroscopy, the spectrum revealed that the resistant fragment of 8 kDa spanned residues 302-368 of Nek2 and was named CC1. All attempts to crystallise the leucine zipper motif of Nek2 to date have failed. To address this issue the powerful tool of NMR spectroscopy was chosen to examine

the possibility of dynamics in the motif and elucidate the parameters to solve the 3D structure. 2D-HSQC experiments using ¹⁵N labelled samples performed at the University of Leicester revealed an increased number of peaks than the 66 expected from CC1 construct. The expression plasmid pET-22b encoding the CC1 protein was kindly donated from F. Ivins, the recombinant CC1 protein has a non-cleavable C-terminal 6 x histidine tag, this was re-cloned into PETM-11 vector containing a cleavable 6 x His tag on the N-terminus (to avoid potential interference in the NMR analysis) and was renamed LZ0. 2D ¹⁵N HSQC NMR experiments revealed a significant reduction in peak dispersion when compared to LZ1, adding additional complexity to the previously observed effects of line broadening with LZ1. Therefore, the software AGADIR (Muñoz and Serrano, 1994; Muñoz and Serrano, 1997; Lacroix et al., 1998) was chosen to aid the engineering of the leucine zipper by predicting the beginning and end of the helix, this reduced the size of the LZ motif in order to reduce the spectral overlap due to the poor peak dispersion common to helices. Specifically, this was used to predict the location of the N-cap which represents an important feature of all α -helices, and can be used to determine the beginning of the coiled-coil. Since the first four backbone NH groups and final four backbone CO groups residues are unable to form the $i \rightarrow i + 4$ hydrogen bonds to other backbone groups present throughout the α -helix, polar side chains at the ends of helices can replace this interaction and function as a hydrogen bonding partner. This is termed N-capping and C-capping. The design of the leucine zipper constructs was such that all constructs extended at least 10 amino acid residues, past the predicted end of the coiled-coil and therefore the C-cap. However, AGADIR analysis revealed the presence of two possible N-cap sites in close succession to one another. The first was predicted to begin at serine 300 and the second at serine 304. Interestingly, in helix design the residues conferring the greatest stability to the N-cap are S, D, T, N, G, P, with another

eleven residues being strongly avoided (V, I, F, A, K, L, Y, R, E, M, and Q). Serine, aspartic acid and threonine are the most favoured residues for N-capping (Kumar and Bansal, 1998). Aurora and Rose, 1998 provided an example of a stable N-cap motif, Ser-Xaa-Xaa-Glu. It was found that the addition of hydrophobic residues preceding the N-cap added stability to the helix. When comparing the Nek2 leucine zipper constructs it can be seen that the second predicted N-cap (SELK) is preceded by a stretch of hydrophobic residues PVL(SELK), which are omitted from the constructs LZ3, LZ4 and LZ5, indicating that the second predicted N-cap is likely the *bona-fide* N-cap of the Nek2 leucine zipper and that constructs LZ0, LZ2 and LZ6 may theoretically possess increased stability.

The first rationally designed leucine zipper construct was LZ2 which showed the best NMR spectra with approximately 80 peaks visible in the 2D ^{15}N HSQC analysis. However, although this was an improvement from the spectrum of both LZ0 and LZ1 the expected number of peaks was in the region of 49 and an area of unresolved peaks remained. Therefore, for the PhD project four more variants of the Nek2 leucine zipper LZ3, LZ4, LZ5 and LZ6 were designed. These varied at the N- and C-terminus to include or discount the first predicted N-cap at position 300 and extend beyond the C-capping residues, with the goal to improve peak dispersion and decrease the complexity of the spectra.

3.1.2 Molecular biology of the Nek 2 Leucine zipper constructs

The pETM-11 vector containing an N-terminal hexa-histidine tag was used as the master plasmid for all the leucine zipper constructs, specifically these constructs encoded the Nek2 leucine zipper (residues 288-358- LZ0, residues 296-343-LZ2, residues 301-340-LZ3, residues 299-340-LZ4, residues 299-343-LZ5, and residues 296-340-LZ6), and was used to express the polypeptides in E.coli. Figure 3.14 shows the amino acid composition of leucine zipper 0 to 6

constructs. The cloning procedure has been described in detail in sections 2.1.1 – 2.1.7 of the materials and methods, the cloning procedure remained exactly the same for all constructs. The PCR product of the temperature cycling of LZ5 using the polymerase Platinum Pfx (Invitrogen) were analysed on 1% agarose gels stained with ethidium bromide (Figure 3.1A), an annealing temperature of 55°C yielded produced a product with a molecular weight of 126 bp corresponding to LZ5 with the restriction site Ncol 3' and BamHI 5'. The PCR product yield could be improved when increasing the annealing temperature to 60°C (Figure 3.1B). LZ0 was generated using gradient temperature cycling PCR and can be seen by a band at the size 225 bp, the annealing temperature was performed using a range of values 55°C, 60°C, 62°C, 64°C and 66°C (Figure 3.1C). The optimal annealing temperature for the PCR reaction of LZ0 is between 60°C and 62°C. The PCR product (LZ0) and the pETM-11 vector (containing LZ5) were subsequently digested with BamHI and Ncol for two hours and the analysed on by electrophoresis prior to ligation (Figure 3.1D). In this example after digestion the vector should yield two products of sizes 5350 bp (to be isolated) and 126 bp (discarded), the 126 bp fragment is often difficult to visualise due to its small size and lower fluorescent intensity, however, when the exposure was increased a band was present. The PCR product yields three fragments of 5 bp, 7 bp and 213 bp, only the band of 213 bp is visible. To screen which of the newly formed pETM-11-LZ0 recombinant vectors to send for analysis by DNA sequencing a PCR was performed on the bacterial colonies generated after transformation (Figure 3.1E). In this example, of the six picked LZ0 clone six were positive for the correct insert (LZ0), indicating that none of the colonies were the original pETM-11 vector containing LZ5 (undigested vector) or re-ligated vector without the insert. Two were chosen to send for sequencing at PNACL (University of Leicester).

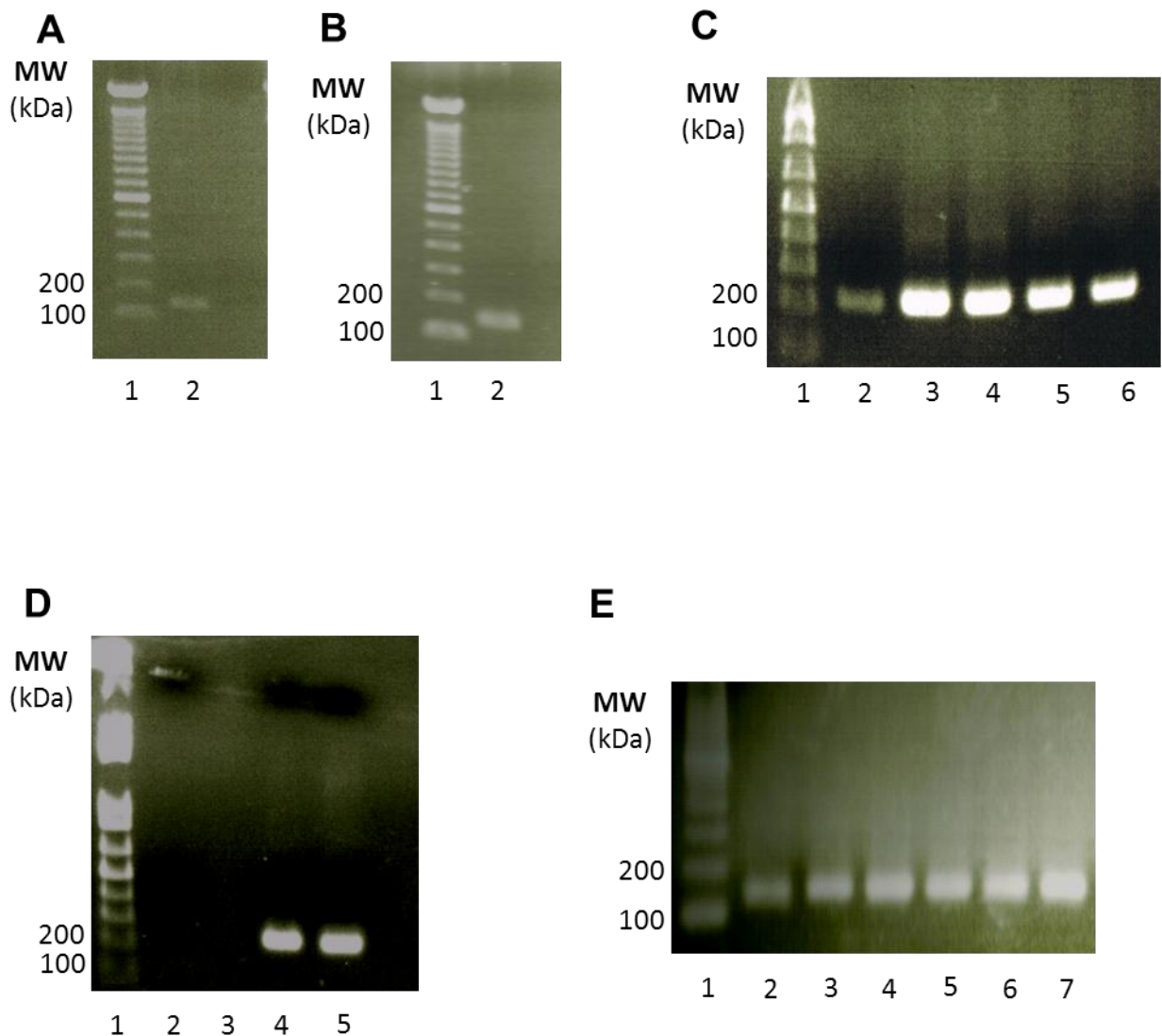


Figure 3.1 Molecular biology of leucine zipper constructs

A. The PCR products of Nek2 LZ construct 5 are shown, lane 1 contains 1 μ l of 1 Kb plus DNA ladder (Invitrogen), 2 - PCR reaction with an annealing temperature of 55°C. B. PCR of Nek2 LZ5, 1 – 1 μ l 1Kb plus DNA ladder and Lane 2 Nek2 LZ5 cycled with an annealing temperature of 60°C. C. A gradient temperature cycling PCR of LZ0 is displayed Lane 1 - 1 μ l of 1 Kb plus DNA ladder, 2 - annealing temperature of 55°C, 3 - 60°C, 4 - 62°C, 5 - 64°C, 6 - 66°C. D. A restriction digest using BamHI and Ncol is shown prior to band excision for DNA isolation, 1 – DNA ladder, 2 – Nek2 LZ5 a band at 5350 bp (to be isolated) and 126 bp (discarded), 3 – empty, 4 – LZ0 annealed at 60°C, 5 - LZ0 annealed at 62°C, the LZ0 had a band size of 225 bp. E. The PCR screening step employed for all LZ constructs prior to DNA sequencing are shown. 1 – 1 μ l 1Kb plus DNA ladder, 2 – PCR product of LZ5 clone 1, 3 – LZ5 clone 2, 4 - LZ5 clone 3, 5 – LZ5 clone 4, 6 – LZ5 clone 5, 7 – LZ5 clone 6.

3.1.3 Preliminary characterisation of the Nek2 leucine zipper constructs

Proteins are routinely examined by 1D ^1H NMR spectroscopy to assess suitability for structure determination using NMR (Page et al., 2005; Peti et al., 2004). 1D ^1H NMR spectra can be used to characterize the folded state of proteins in a rapid screening method without the need for isotope labelling, in a time frame of seconds to minutes. Ideally, a 1D ^1H NMR spectrum of a folded, monomeric, protein would display significant dispersion of resonance lines in the three spectral regions where ring current-shifted methyl resonances (0.5-1.5 ppm), downfield-shifted α -proton resonances (3.5-6 ppm), and downfield-shifted amide proton resonances (6-10 ppm) which would indicate that the protein was not globular and the structure could be elucidated using standard NMR spectroscopy experiments (McDonald et al., 1967; Wüthrich, 1986). In the case of the Nek2 leucine zipper motif, the 1D ^1H NMR spectra were performed for each leucine zipper construct to minimise sample processing time in the buffer 20 mM sodium phosphate, 100 mM sodium chloride and 0.02% (w/v) sodium azide buffer at pH 7, containing 10% D₂O and at 1 mM and 0.1 mM sample concentrations: LZ0 (Figure 3.2); LZ2 (Figure 3.3); LZ3 (Figure 3.4); LZ4 (Figure 3.5); LZ5 (Figure 3.6); LZ6 (Figure 3.7). All the 1D ^1H NMR experiments were obtained at 298K and recorded with water presaturation. The spectra display line broadening over the entire spectrum for each LZ construct (LZ0 – LZ6) with no high field shifts due to the absence of aromatic residues, normally indicative of intrinsic large size, aggregation or oligomerization (Wüthrich, 1986). However, before the start of the project it was evident from the combination of AUC, CD spectroscopy and 2D NMR analysis performed on LZ1 (as previously described in 3.1.1), that the Nek2 leucine zipper motif was of a small size (approximately 5.4

kDa), was properly folded indicated by CD spectroscopy, and was dimeric in solution at 1 mM (AUC). Moreover, the line broadening observed indicated a significant increase in relaxation rates due to a slow-intermediate exchange effect, which was indicated in the 2D HSQC by the reduction of the expected peak number from 49 to 35 peaks and a calculation of relaxation rates using a NOESY experiment with a 80 ms mixing time indicates an exchange rate of between 10 and 100 s^{-1} (performed prior to the onset of the PhD project by Mark Pfuhl). The 1D ^1H NMR spectra were therefore used as a selection tool to observe if the variation of the domain boundaries in the Nek2 LZ constructs had improved or worsened the line broadening. Nek LZ5 was therefore chosen for all subsequent NMR optimization upon due to the low number of amino acids compared to other LZ constructs and good ^{15}N expression levels.

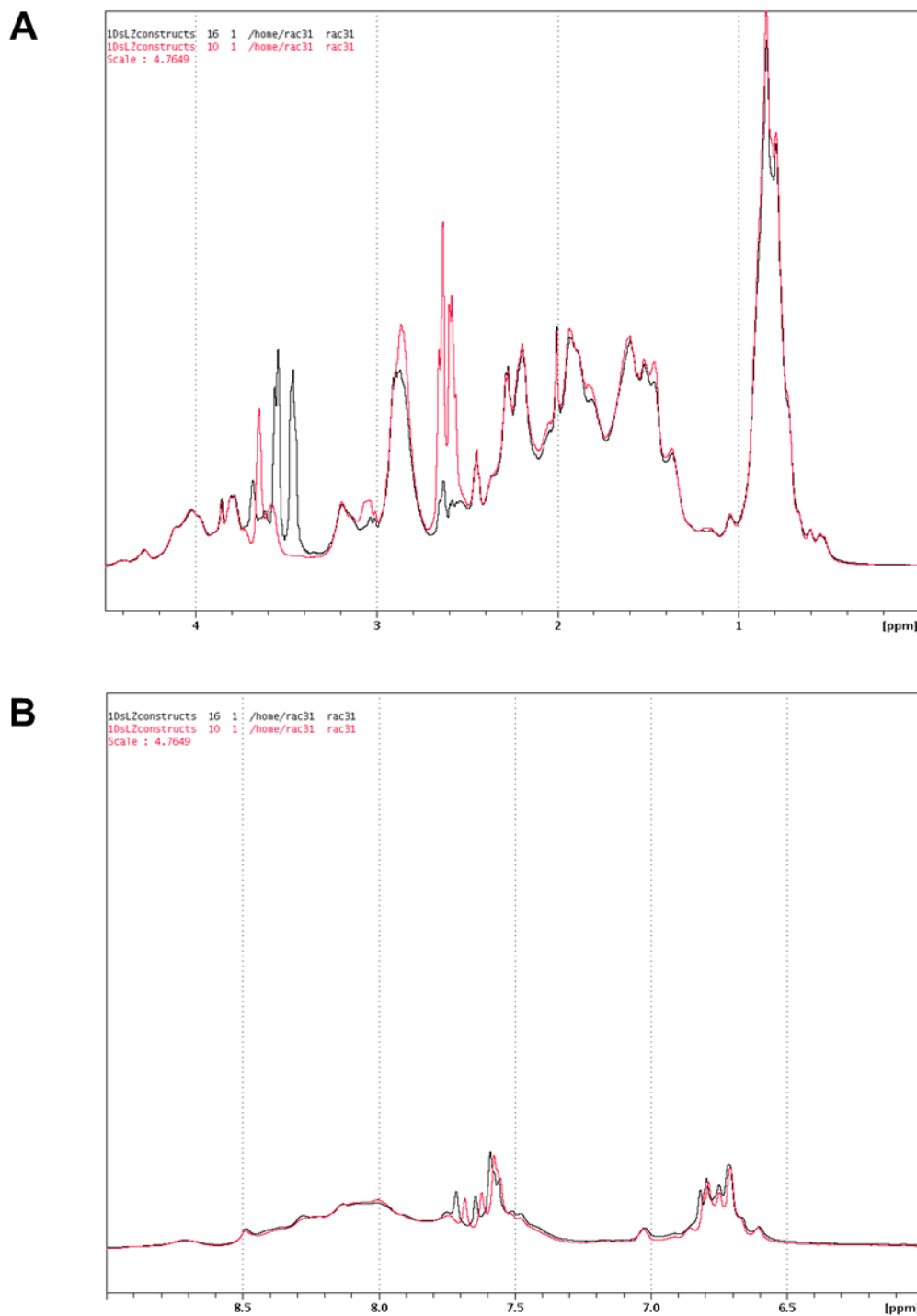


Figure 3.2 1D 1H NMR characterization of LZ0

An initial characterization using an unlabelled sample of the constructs leucine zipper 0 is shown, 1D experiments were performed at two protein concentrations of 1 mM (black) and 0.1 mM (red). The red spectrum is scaled up by a factor of approximately 4.8. A. The spectral region from 0 – 5.5 ppm is displayed containing the region of methyl and α protons. B. An enlargement of the spectral region from 5.5 – 9 ppm is shown indicating the line widths of amide protons in LZ0.

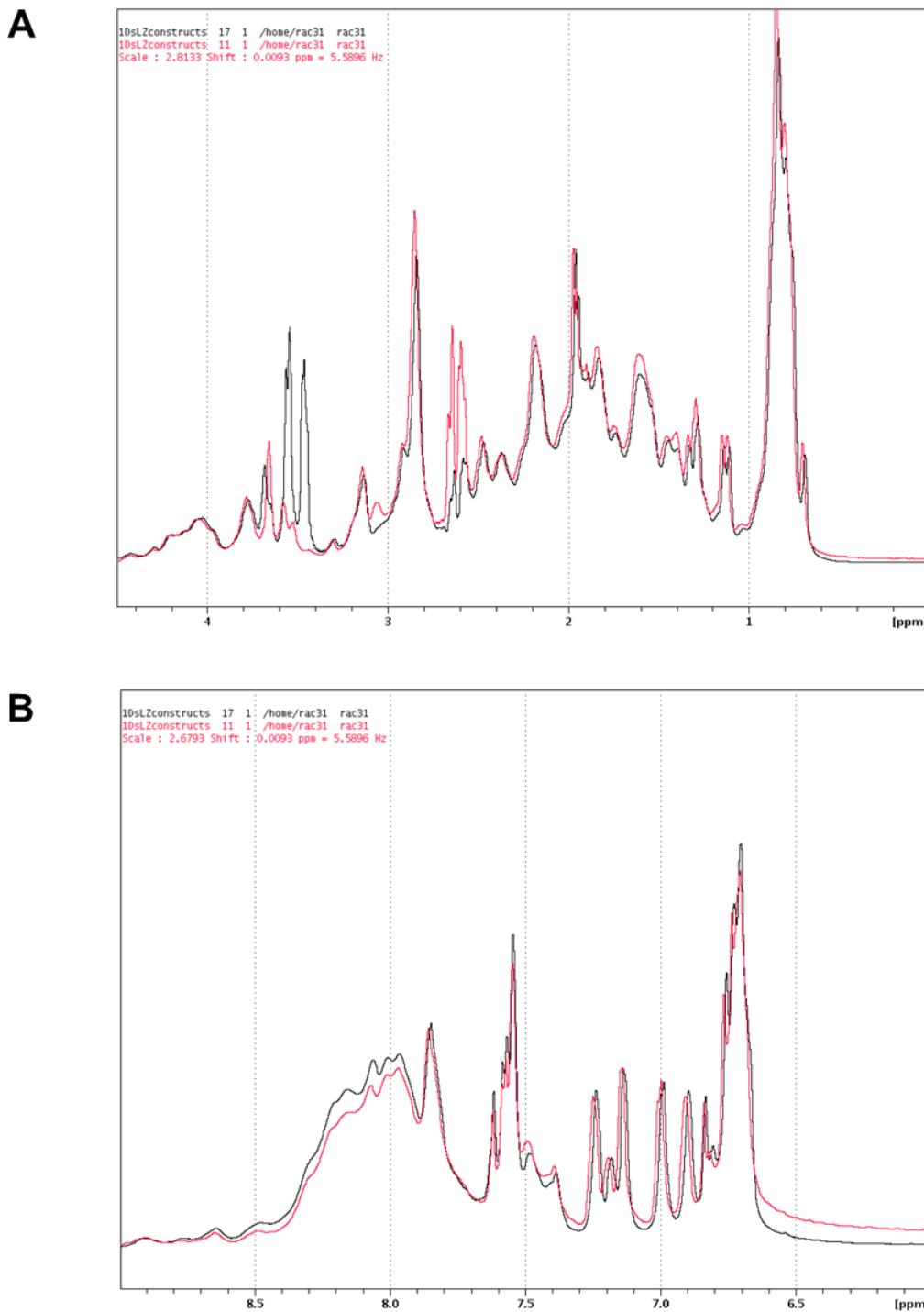


Figure 3.3 1D ^1H NMR characterization of LZ2

An initial characterization using an unlabelled sample of the construct LZ2 is shown, 1D experiments were performed at two protein concentrations of 1 mM (black) and 0.1 mM (red). A. The spectral region from 0 – 5.5 ppm is displayed containing the region of methyl and α protons, the red spectrum is scaled up by a factor of approximately 2.8. B. An enlargement of the spectral region from 5.5 – 9 ppm is shown indicating the line widths of amide protons in LZ2, the red spectrum is scaled up by a factor of approximately 2.7.

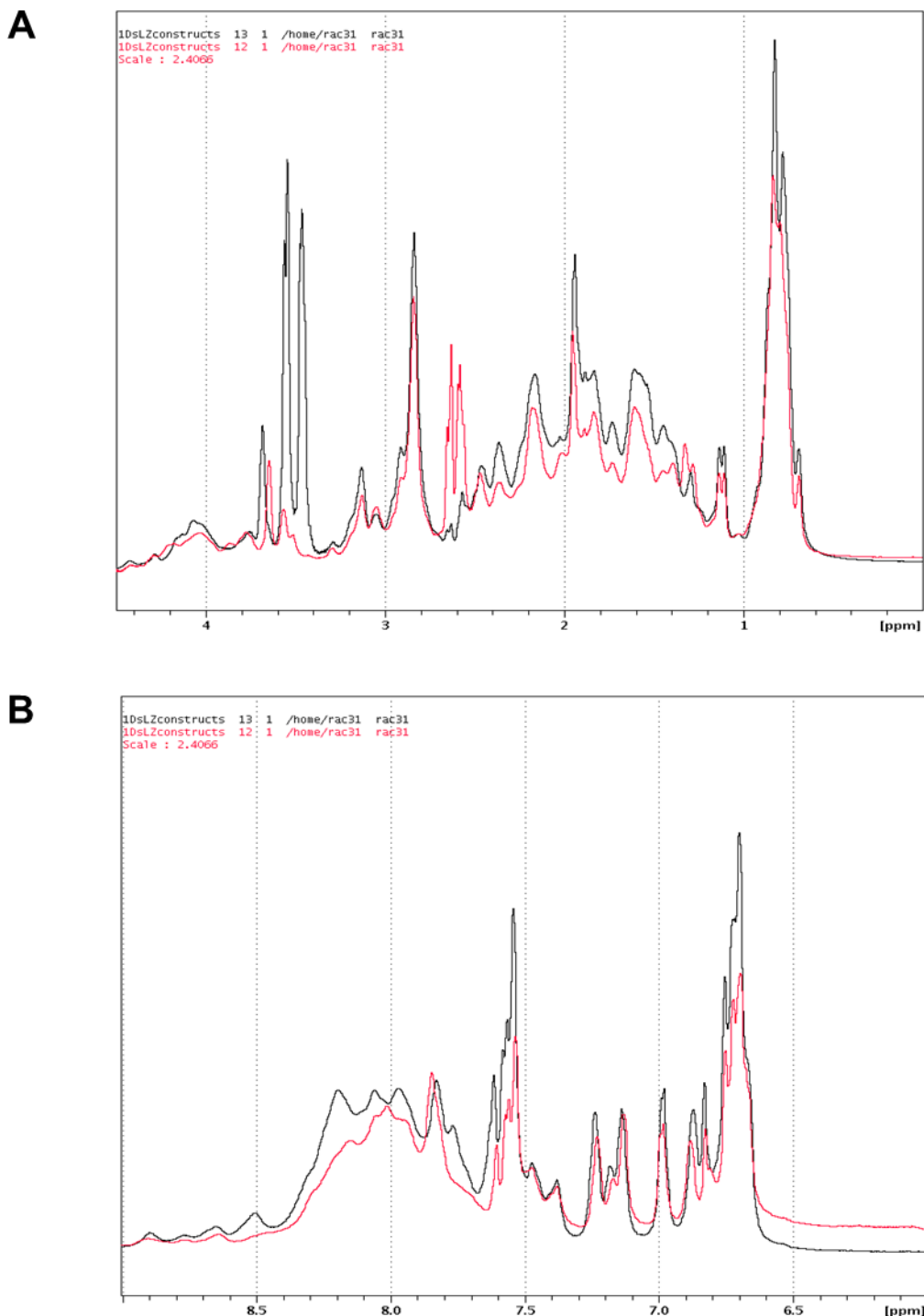


Figure 3.4 1D ^1H NMR characterization of LZ3

An initial characterization using an unlabelled sample of the construct LZ3 is shown, 1D experiments were performed at two protein concentrations of 1 mM (black) and 0.1 mM (red), the red spectrum is scaled up by a factor of approximately 2.4. A. The spectral region from 0 – 5.5 ppm is displayed containing the region of methyl and α protons,. B. An enlargement of the spectral region from 5.5 – 9 ppm is shown indicating the line widths of amide protons in LZ3.

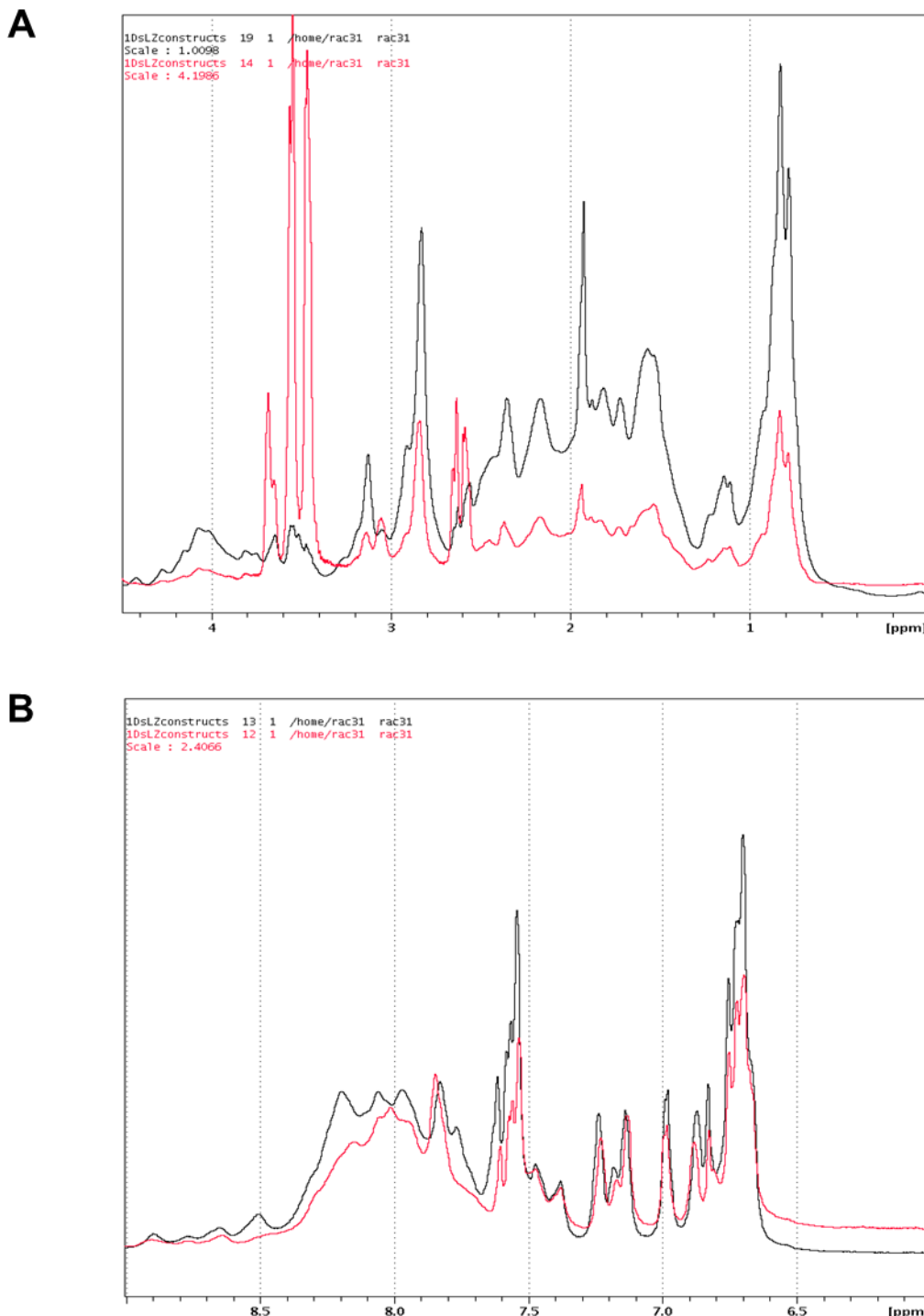


Figure 3.5 1D ^1H NMR characterization of LZ4

An initial characterization using an unlabelled sample of the construct LZ4 is shown, 1D experiments were performed at two protein concentrations of 1 mM (black) and 0.1 mM (red). A. The spectral region from 0 – 5.5 ppm is displayed containing the region of methyl and α protons, the red spectrum is scaled up by a factor of approximately 4.2. B. An enlargement of the spectral region from 5.5 – 9 ppm is shown indicating the line widths of amide protons in LZ4, the red spectrum is scaled up by a factor of approximately 2.4.

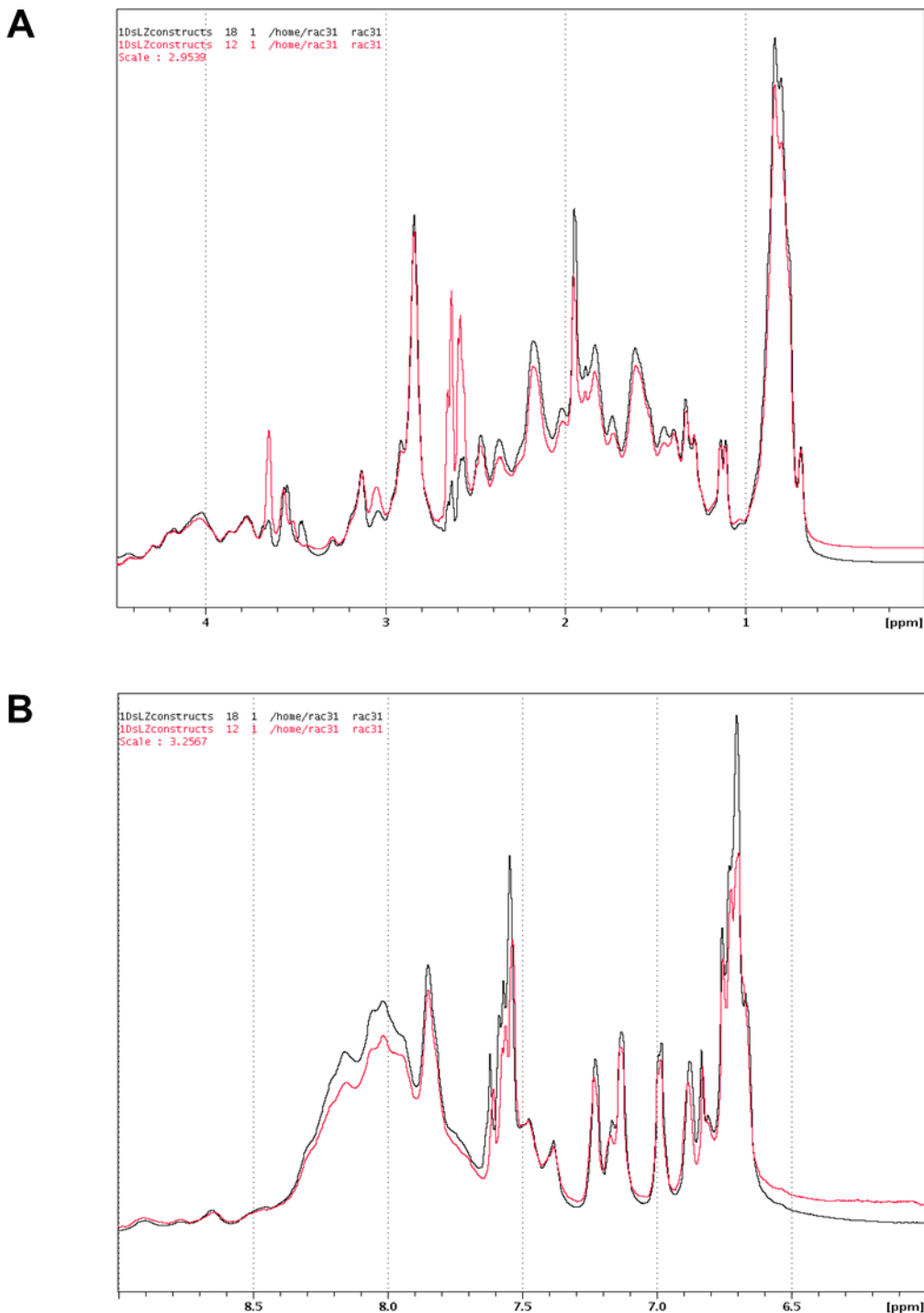


Figure 3.6 1D ^1H NMR characterization of LZ5

An initial characterization using an unlabelled sample of the construct LZ5 is shown, 1D experiments were performed at two protein concentrations of 1 mM (black) and 0.1 mM (red). A. The spectral region from 0 – 5.5 ppm is displayed containing the region of methyl and α protons, the red spectrum is scaled up by a factor of approximately 3.0. B. An enlargement of the spectral region from 5.5 – 9 ppm is shown indicating the line widths of amide protons in LZ5, the red spectrum is scaled up by a factor of approximately 3.3.

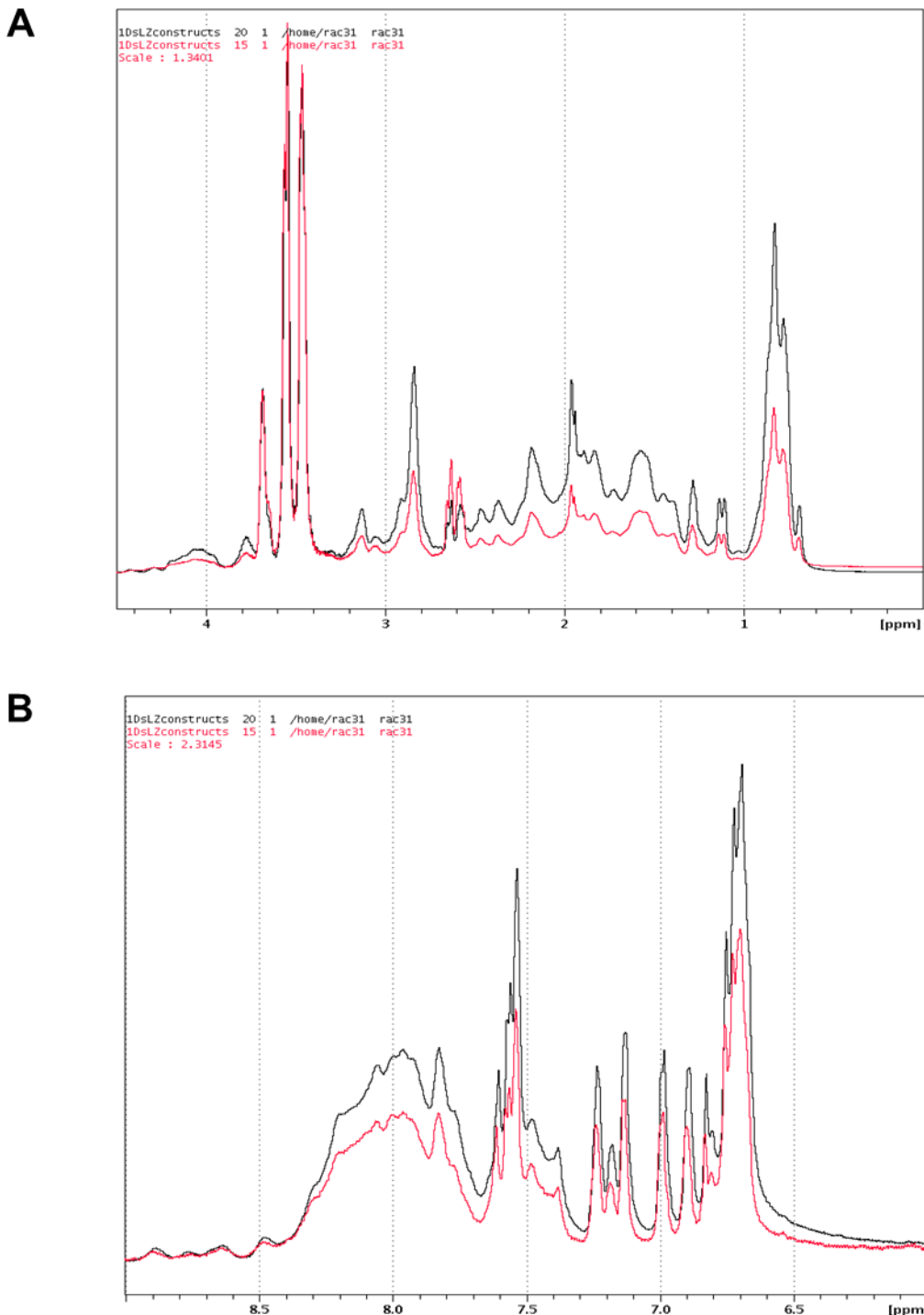


Figure 3.7 1D ^1H NMR characterization of LZ6

An initial characterization using an unlabelled sample of the construct LZ6 is shown, 1D experiments were performed at two protein concentrations of 1 mM (black) and 0.1 mM (red). A. The spectral region from 0 – 5.5 ppm is displayed containing the region of methyl and α protons, the red spectrum is scaled up by a factor of approximately 1.3. B. An enlargement of the spectral region from 5.5 – 9 ppm is shown indicating the line widths of amide protons in LZ6, the red spectrum is scaled up by a factor of approximately 2.3.

3.1.4 Generation of the Nek2 LZ5 domain mutants

To probe the possibility of conformational exchange (as seen by the presence of TOCSY-NOESY crosspeaks of equal intensity, in the previously acquired NOESY (80 ms mixing time) and TOCSY (50 ms) spectra), Nek2 LZ5 was engineered to include a cysteine residue at the N-terminus in the *a* position or *d* position. This intended to investigate the effects of locking the leucine zipper domain of Nek2 into either the HepI (leucines aligned in position *a*) or HepII (leucines in *d* position) conformation on dynamics (Figure 3.15B and C). The engineered cystines were also used to probe the orientation of the leucine zipper strands, only when the alpha helices of the leucine zipper were parallel would the disulphide bonds form. It has been documented that placing a cysteine residue close to the N- or C-terminus lead to an increase in melting temperature and therefore stability (Zhou et al., 1993). Two mutants of LZ5 were generated (Figure 3.8). The c-DNA of the plasmid pETM-11 containing the LZ5 gene was subject to mutagenesis using the QIAquick change site-directed mutagenesis (Stratagene). A two step mutational strategy was developed to incorporate two mutations into each of the two new constructs. The first mutation of the intrinsic C335A was performed to avoid subsequent interference by the formation of a disulphide bond with the newly incorporated engineered cysteine residues. The second round of mutagenesis was performed on residues K309C and E310C, to result in the generation of two novel c-DNA plasmids: LZ5 K309C/C335A and LZ5 E310C/C335A. Assuming that the Nek2 leucine zipper folds as a parallel coiled-coil, a disulphide bond could form between cystines in either the *a*-position (glutamate (E) mutated to cysteine – HepII “lock”) or the *d*-position (lysine (K)

mutated to cysteine – Hepl “lock”). Therefore, in oxidising buffer the K309C mutants should be ‘locked’ in the Hepl conformation and the E310C mutant in the HepII register.

3.1.5 Expression and purification of the Nek 2 Leucine zipper constructs

Plasmids encoding the leucine zipper constructs were transformed into the *E.coli* strain BL21 the cultures were plated onto LB-agar plates containing Kanamycin (Kan) (50 µg/ml) to enable selective growth of the pETM-11 plasmid (provided by EMBL Heidelberg) with Chloramphenicol (Cam) to limit bacterial growth to the BL21 Rosetta2pLysS strain (34 µg/ml). Each of the leucine zipper constructs were expressed using the protocol documented in section 2.3 of the materials and methods.

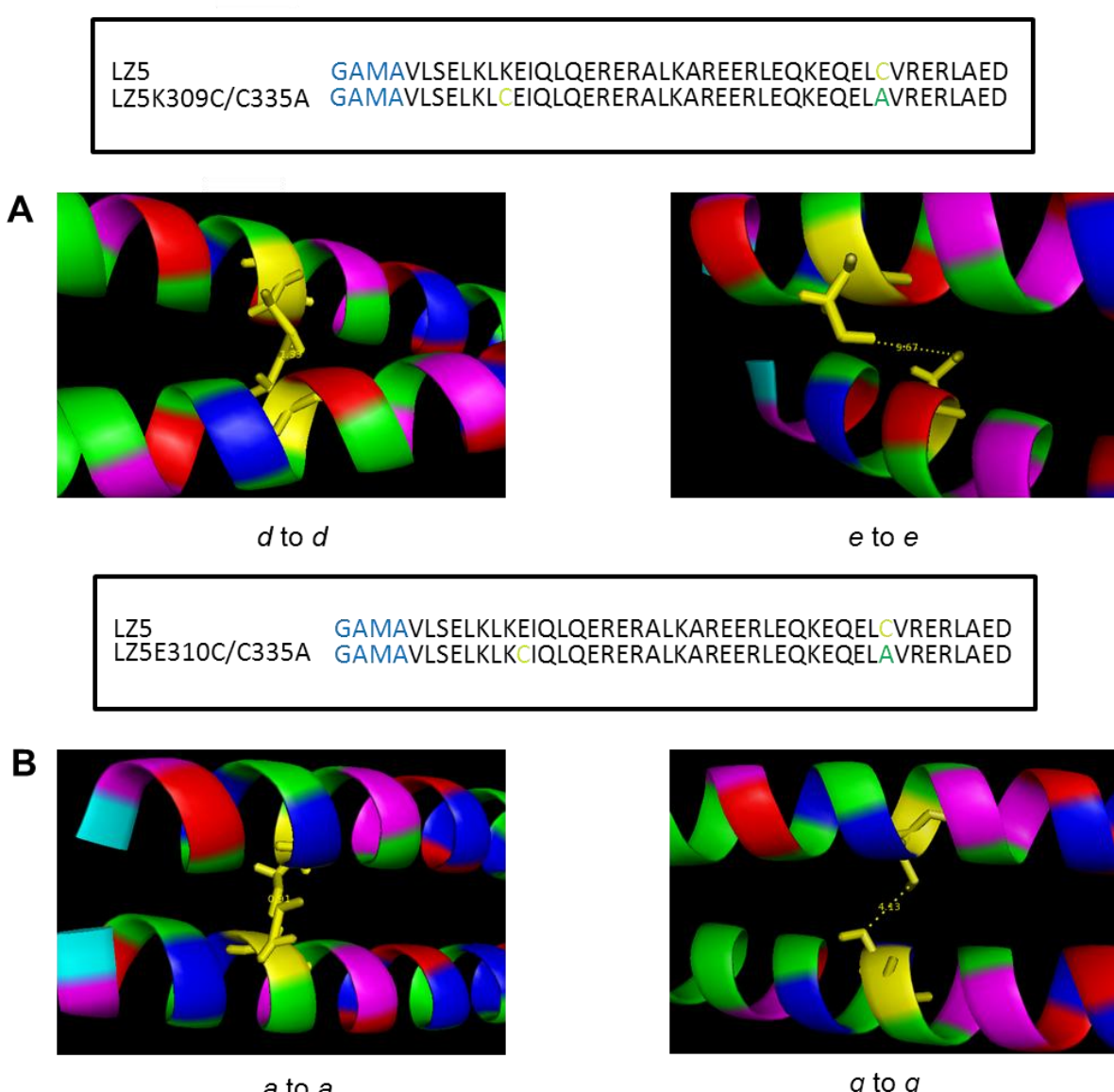


Figure 3.8 Mutagenesis to lock Hepl and HepII repeats in L25

A. The Hepl register of mutant LZ5K309C in a horizontal orientation with the N-terminal on the left side of the model is shown. The backbone is represented as a cartoon and the cystine side chain shown as a stick. Pymol was used to measure the distance between sulphhydryl groups of the mutant K309C and E310C. The lefthand side indicates the *d*-position interactions in Hepl and the right side indicates the HepII *e*-positions. B. The HepII register of LZ5E310C the formation of the disulphide bond between position *a* of the dimer in HepII and the inability of a disulphide bond to be formed in Hepl between position *a* of the leucine zipper dimer.

The variation in amino acid composition is displayed in Figure 3.9A. The proteins were purified in two stages. The presence of an N-terminal hexa-histidine tag allowed the different protein domains to be purified by affinity chromatography using Ni-NTA beads (GE healthcare), the flow-through, wash, and elution fractions were collected and 15 µL were analysed using an SDS-PAGE gel. The molecular weights of the leucine zipper constructs in kDa are as follows; LZ0 – 8.9, LZ2 and LZ2P298A – 5.7, LZ3 – 4.9, LZ4 – 5.2, LZ5 – 5.5 and LZ6 5.4. A second band is visible on the SDS-PAGE gel for all constructs and corresponds to the dimeric form of the leucine zipper domain which is resistant to denaturation by loading buffer (Figure 3.9B and C), indicating the formation of a highly stable dimer for all constructs regardless of the sequence variation.

A final polishing step of purification involved gel filtration, as shown in Figure 3.10A and B. Prior to SEC the Superdex 75 HiLoad 16/60 was calibrated using the gel filtration standard (BIORAD cat#151-1901), the molecular weight standard was loaded onto the column using the sample loop. The standard consists of five proteins thyroglobulin (670 kDa), γ -globulin (158 kDa), Ovalbumin (44 kDa), Myoglobin (17 kDa) and Vitamin B₁₂ (1.35 kDa). By cross-referencing the elution volume of the standard, especially the peaks corresponding to Ovalbumin (44 kDa at 52 ml), Myoglobin (17 kDa at 64 ml) and Vitamin B₁₂ (1.35 kDa at 88 ml) against the elution volume of the LZ proteins the approximate molecular weight could be interpreted. A typical chromatogram for LZ0 (Figure 3.10A, left panel), showed a double peak with fractions A6-A7 representing the dimeric form of LZ0 kDa. The predicted size of the LZ0 dimer including the hexa-histidine tag and linker region is 17.8 kDa (elution volume ≈ 65 ml) which is in agreement with the reference standard, with fractions A3-A4 being

higher molecular weight aggregates of more than 40 kDa. The purity of the LZ0 sample after gel filtration is approximately 90% and estimated using an SDS-PAGE gel (Figure 3.10A, right panel). A typical chromatogram for LZ2 showed a single peak with fractions A6-A8 representing the dimeric form of LZ2 (Figure 3.10B, left panel). The predicted size of the LZ2 dimer including the histidine tag and linker region is 11.4 kDa and the elution volume of \approx 63 ml confirmed that it existed as a dimer. For the construct LZ2 only a small peak can be seen in the chromatogram characteristic of the presence of higher order aggregates in fraction A3, whereas, in LZ0 a large peak indicating the presence of aggregates could be seen. It is possible that the differences in expression yield, with LZ0 expressing at an increased level to LZ2, could explain this observation. The purity of the sample of LZ2 was estimated using SDS-PAGE and was calculated to approximately 95% (Figure 3.10B, right panel).

A

LZ0 RQLGEPEKSQDDSSPVLSKLEIQLQERERALKAREERLEQKEQELCVRERLAEDKLARAENLLKNYSLL
LZ1 VEFHMSELKLKEIQLQERERALKAREERLEQKEQELCVRERL
LZ2 GAMASSPVLSKLEIQLQERERALKAREERLEQKEQELCVRERLAED
LZ3 GAMASELKLKEIQLQERERALKAREERLEQKEQELCVRERL
LZ4 GAMAVLSELKLKEIQLQERERALKAREERLEQKEQELCVRERL
LZ5 GAMAVLSELKLKEIQLQERERALKAREERLEQKEQELCVRERLAED
LZ6 GAMASSPVLSKLEIQLQERERALKAREERLEQKEQELCVRERL

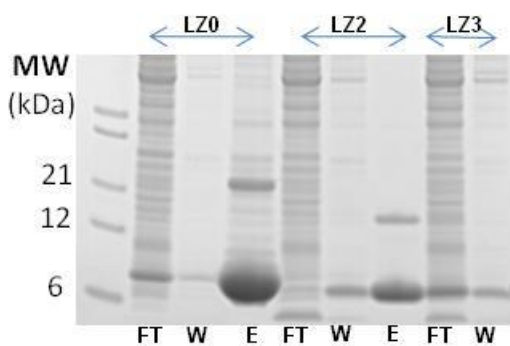
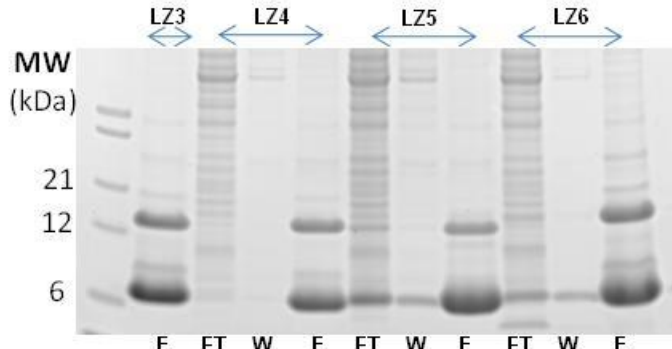
B**C**

Figure 3.9 Affinity Purification of LZ0-LZ6 using fast flow 6 Ni-NTA beads.

A. The amino acid variation in Nek2 LZ constructs are displayed, the blue coloured residues indicate the amino acids remaining post Actev cleavage which are not native to Nek2. B. A typical SDS PAGE gel displaying the flow-through (FT), washing (W) and Elution (E) stages of the Ni-NTA purification of the LZ constructs LZ0 to LZ2P301A are shown, C. Represents LZ constructs LZ3 – LZ6. The Mark 12 unstained standard (Invitrogen) was used to estimate molecular weights.

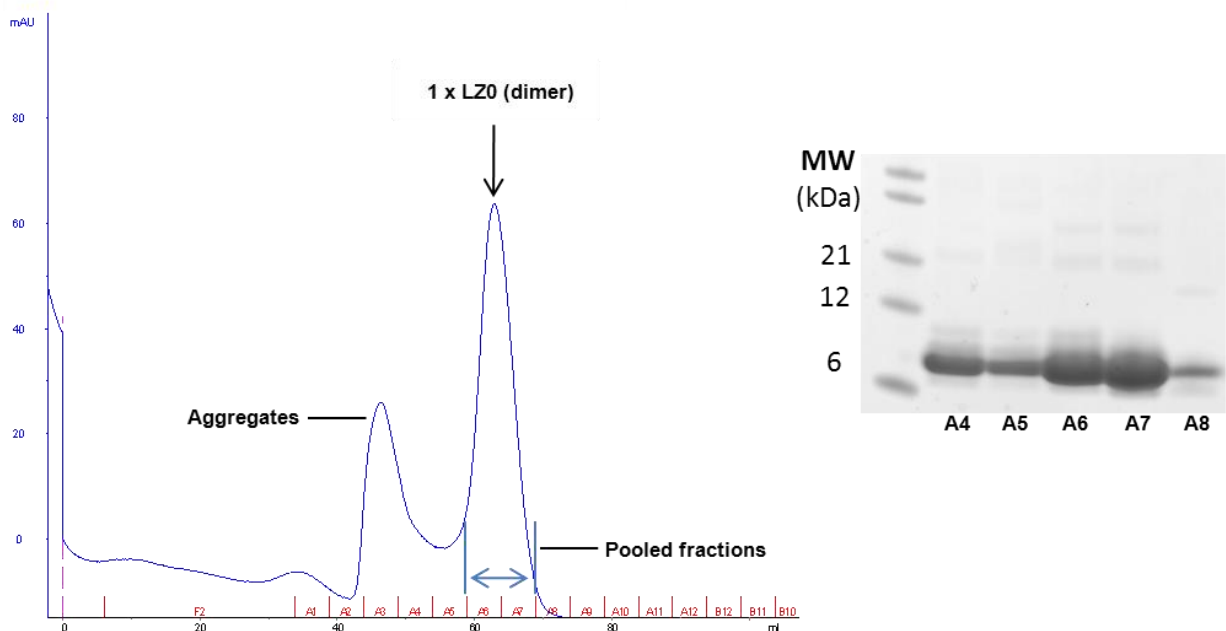
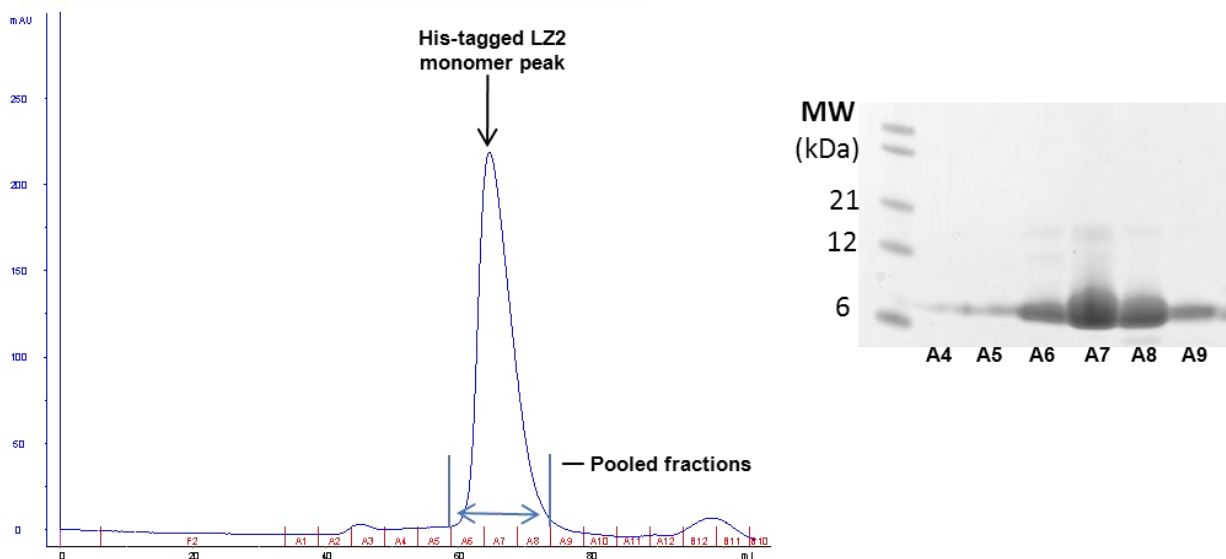
A**B**

Figure 3.10 Purification of leucine zipper constructs 0 and 2

A. An example of a FPLC elution profile attained by gel filtration on a superdex 75 16/60 column is displayed. On the left side an example chromatogram for LZ0 is displayed, with the pooled fraction from gel filtration highlighted. On the right hand side an SDS-PAGE gel performed after FPLC purification displaying the elution fractions and indicating the purity of the pooled fractions A6 and A7. B. The left side, represents a chromatogram of an example purification from LZ2, the pooled fraction are displayed. The right hand side depicts an SDS-PAGE gel of the specific fractions collected post-gel filtration. A high purity post gel filtration was observed for all LZ constructs. Mark 12 was used as a molecular weight marker in the SDS-PAGE.

3.1.6 Average expression yields of the Nek 2 leucine zipper constructs

The levels of expression were analysed to compare the effects of sequence variation to expression yield. Unfortunately due to the absence of aromatic residues A280 values could not be used to calculate concentrations. The bicinchoninic acid (BCA) assay was chosen to estimate concentrations. It has been previously documented that the BCA assay generates results consistent with amino acid analysis (Alterman et al., 2003), when glycosylation is not present (Fountoulakis et al., 1992). The LZ proteins expressed in *E.coli* are devoid of such post-translational modifications and therefore the BCA assay should yield accurate protein concentrations for the leucine zipper constructs. Initial protein determination experiments using the standard BCA assay from Pierce (Smith et al., 1985) proved to be unsuccessful. An overestimation of the protein concentration occurred. When the effect of DTT on the absorbance was analysed a linear relationship between DTT and absorbance occurred (Figure 3.11A). Therefore, a reliable protein assay was required which could estimate protein concentrations in the presence of 2 mM DTT in the NMR buffer and 1 mM DTT in the circular dichroism (CD) buffer. As the standard BCA estimation could not be used the Pierce® BCA Protein Assay Kit – Reducing Agent Compatible was assessed, which according to the manufacturer could tolerate up to 5 mM DTT before accuracy is reduced. Nobel and colleagues tested a panel of proteins, of a known concentration, against the BSA standard and found deviations from the actual protein concentrations due to amine accessibility (Nobel et al., 2007). To ensure accurate concentration determination, a 5 mg sample of Nek2 LZ2 was dialysed in water and lyophilized overnight; 2 mg of the protein was carefully weighed and resuspended in 1 ml of distilled H₂O. The LZ2 2 mg/ml solution was then used

as a standard to compare against the BSA provided by the manufacturer (Figure 3.11B). The results showed that the BSA standard measure at 3.6 times higher than the actual concentration of the LZ2 protein. Future experiments used the BSA standard, however reduced the absorbance readings by a factor of 3.6. A BCA reducing agent compatible experiment was performed to test the effects of 2 mM DTT in the BSA solution (Figure 3.12), triplicate data points were analysed and found that there was no significant effect of 2 mM DTT on the accuracy of the protein concentration.

The concentration of the expressed construct post affinity purification was measured and an average of three independent Ni-NTA purifications is shown for all constructs (Figure 3.13A). The level of LZ0 yield in 1L LB medium was 39.1 mg/L, LZ2 – 23.4 mg/L, LZ2P301A – 28.5 mg/L, LZ3 – 15.9 mg/L, LZ4 – 14.8 mg/L, LZ5 – 13.9 mg/L and LZ6 – 33.2 mg/L. The ranking of highest protein yield post affinity purification were as follows: LZ0; LZ6; LZ2P301A; LZ2; LZ3; LZ4; LZ5.

A graphical representation of the protein concentration post gel filtration is shown in figure 3.13B. An average of three independent gel filtration runs is shown for all constructs. The protein concentration for LZ0 post gel filtration was 24.7 mg/L, LZ2 – 15.6 mg/L, LZ2P301A - 17.2 mg/L, LZ3 - 10.4 mg/L, LZ4 – 12.2, LZ5 – 8.9, and finally for LZ6 – 21.7 mg/L. The percentage losses from affinity purification through to gel filtration due to aggregates and/or formation of higher order aggregates were for LZ0 – 37%, LZ2 – 33%, LZ2P301A – 40%, LZ3 – 35%, LZ4 – 18%, LZ5 – 36% and LZ6 – 35%. The calculated percentage losses correlate, with the highest expression levels showing an increased percentage loss of sample post gel filtration, excluding the construct LZ4 which showed over a 50% reduction in losses, when compared to the other leucine zipper constructs.

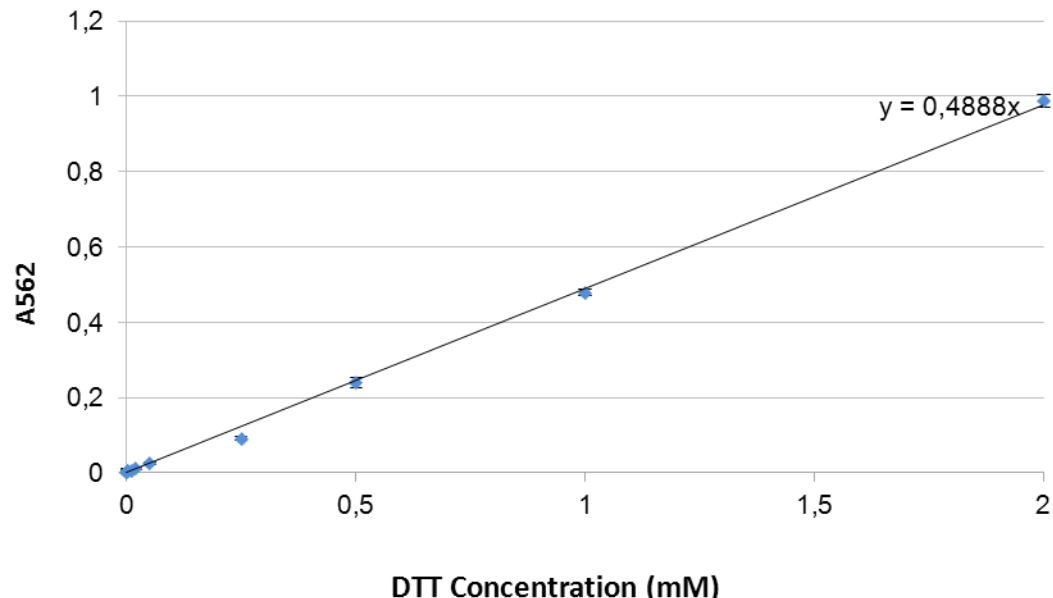
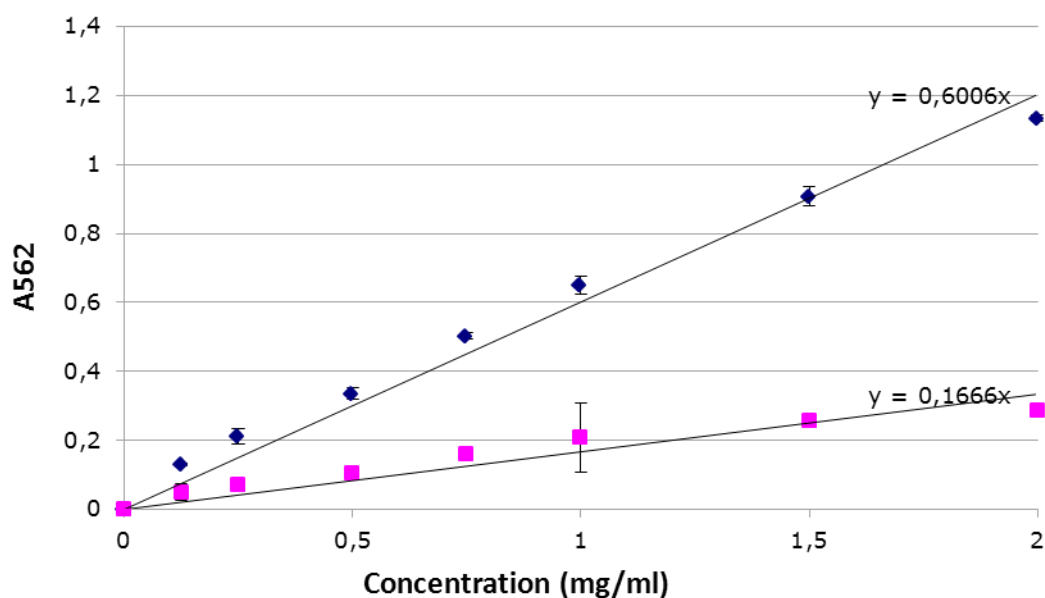
A**Effect of DTT concentration on the BCA Assay****B****BCA Reduced compatible calibration**

Figure 3.11 Calibrating the BCA protein assay to the Leucine zipper constructs

A. The effects of the addition of Dithiothreitol (DTT) to the LZ protein solutions before concentration were analyzed. A serial dilution of a 2 mM DTT to 0.5 µM were tested using the bicinchoninic acid assay (BCA assay). B. A lyophilized sample of LZ5 (H_2O) was used as a calibration standard for the BCA reduced compatibility assay (pink) and compared to the bovine serum albumin (BSA) standard provided by the manufacturer (Blue). A 3.6 fold difference between the LZ5 and BSA standards can be seen. Linear regression values are shown in black. The error bars indicate the standard deviations (SD) of triplicate data points.

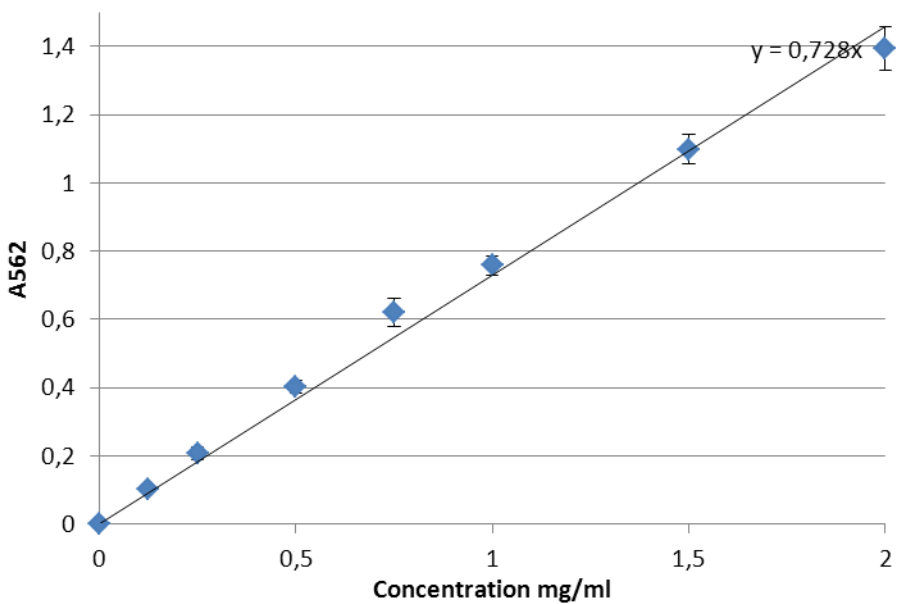


Figure 3.12 Reduced compatibility BCA assay calibration curve with 2 mM DTT

The effect of DTT addition to the BSA protein standard prior protein determination was performed. Six concentrations of BSA from 2 mg/ml to 0.125 mg/ml each with a concentration of 2 mM DTT were used. No significant effect of DTT addition was observed. Linear regression values are shown in black. The error bars indicate the standard deviations (SD) of triplicate data points.

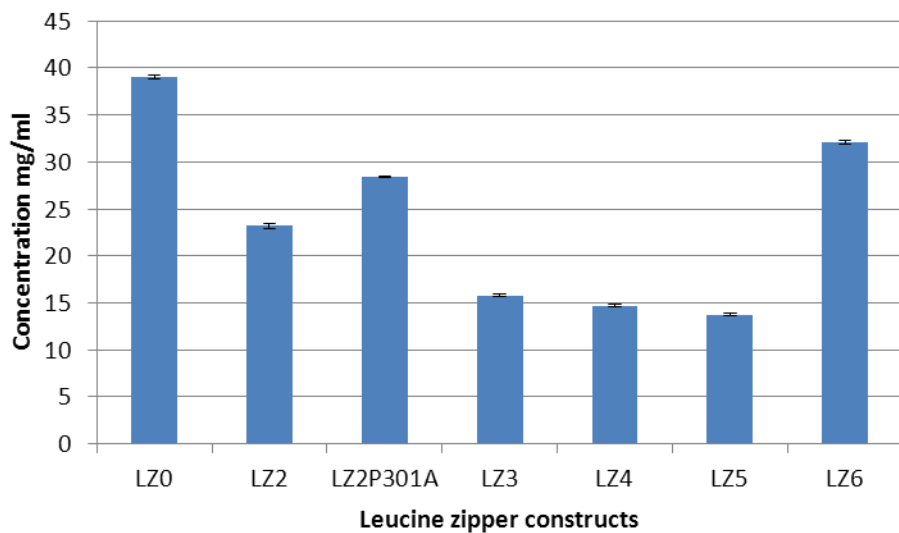
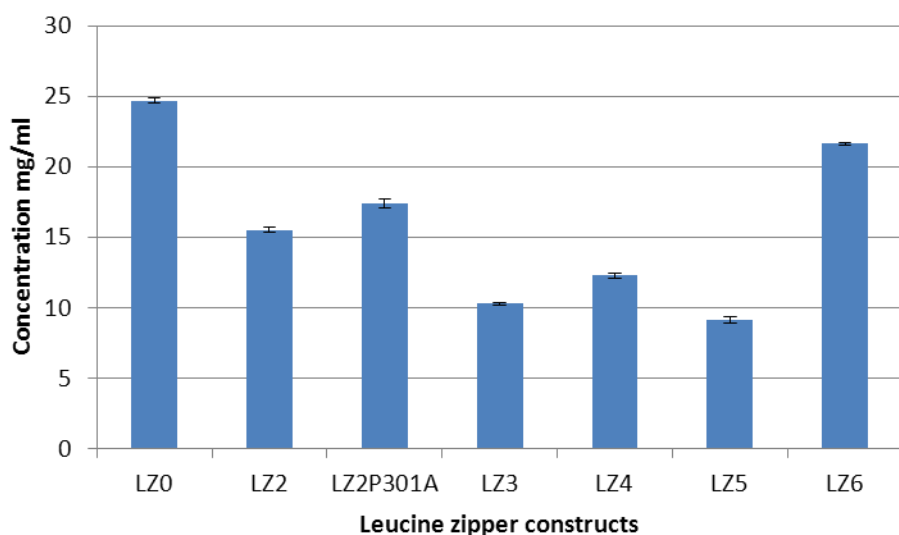
A**B**

Figure 3.13 Levels of protein expression between Nek2 leucine zipper constructs

A. The Nek2 leucine zipper constructs post Ni-NTA affinity chromatography are displayed, units of concentration are displayed as mg/ml. B. Concentrations of the LZ constructs post gel filtration using a Superdex 75 column are shown by the blue bars, the units of concentration are shown as mg/ml. All concentrations were determined using the Pierce BCA reduced compatibility assay.

The differences in expression levels after Ni-NTA purification are visible on an SDS-PAGE gel (figure 3.14A). In order of ranking from the highest protein recovery post gel filtration, LZ0 consistently displayed the highest yield, followed by LZ6, LZ2P301A, LZ2, LZ4, LZ3 and LZ5 (Figure 3.14B). A comparison of sequence composition indicates that the increase in expression or solubility could be due to the presence of the N-terminal amino acids SSPVL, the absence of these amino acids leads to a reduction in productivity (Figure 3.14C).

3.1.7 Bioinformatics analysis of the sequence of the Nek2 LZ domain

A bioinformatics analysis of the sequence of the Nek2 LZ domain was performed to determine the exact boundaries of the leucine zipper domain (Figure 3.15A). Meaningful leucine zipper scores provided by the program 2zip (Bornberg-Bauer et al., 1998) start around residue 305 and continue to approximately residue 335. The COILS software (Lupas et al., 1991) was used to predict coiled-coil scores, significant scores correlated with 2zip, beginning at around residue 305 spanning the leucine zipper until residue 335. The score values drop after residue 335 and return to significant levels between residues 340-355. A leucine zipper can be defined by the presence of leucine residue every seventh amino acid, in a so-called heptad repeat. In the conventional heptad repeat of a leucine zipper, a second position is also occupied by another leucine or equally compatible hydrophobic residue (V, A, I, M). In a repeating heptad *abcdefg*, positions *a* and *d* would normally both be occupied by hydrophobic residues. In the Nek2 leucine zipper, one of the conventional hydrophobic positions is missing, giving rise to the possibility to position the repeating pattern of leucine residues in either, the *a*-position as in Hepl (Figure 3.15B) or the *d*-position as in Hepll (Figure 3.15C). Conventionally, it is thought that the leucine residue occupies the *d*-position, but the energetic contribution to coiled-coil stability and the

frequency by which leucine is found in either position in leucine zipper sequences are very similar (Tripet et al., 2000). Regardless of the position of the leucine heptad repeat, charged residues would always occupy the second conserved position. In Hepl, lysine or arginine would occupy the *d*-position leading to the conservation of positively charged residues in the leucine zipper interface. Conversely, in HepII a conservation of negatively charged glutamate residues would occupy the *a*-position (Figure 3.16A). Interesting, previous data indicate that generally lysine and arginine prefer the *a*-position and glutamate is conserved in the *d*-position (Tripet et al., 2000; Straussman et al., 2007). Charged residues comprising the interface of a coiled-coil have been previously observed, for example, in myosin and also c-myc, however, the charged residue comprised stability and make the Nek2 leucine zipper a non-ideal coiled-coil. In the Nek2 leucine zipper, the consistent occupation of the *a*- and *d*-positions of the interface is interesting. Of the six *a*-positions in HepII, the first is occupied by leucine and the following five are occupied by glutamate, while in the case of Hepl, lysine and arginine both occupy three *d*-positions each. The degree of conservation of these positions suggests an important functional role for the non-ideal interface. An interesting but not proven combination of the heptad repeats suggests an ideal pairing of Hepl:HepII with relation to charge (Figure 3.16B).

To determine whether the Nek2 leucine zipper sequence permitted hetero-oligomerization, similarity searches were performed with a pattern search program (Bucher et al., 1996) using the pattern LXXR/KEXX repeated five times. No coiled-coil domain suitable to dimerization with the Nek2 leucine zipper domain, other than itself, were found, even allowing for up to two mismatches. Therefore, it is probably that the primary function of the Nek2 leucine zipper is to promote homodimerization (Fry et al., 1995).

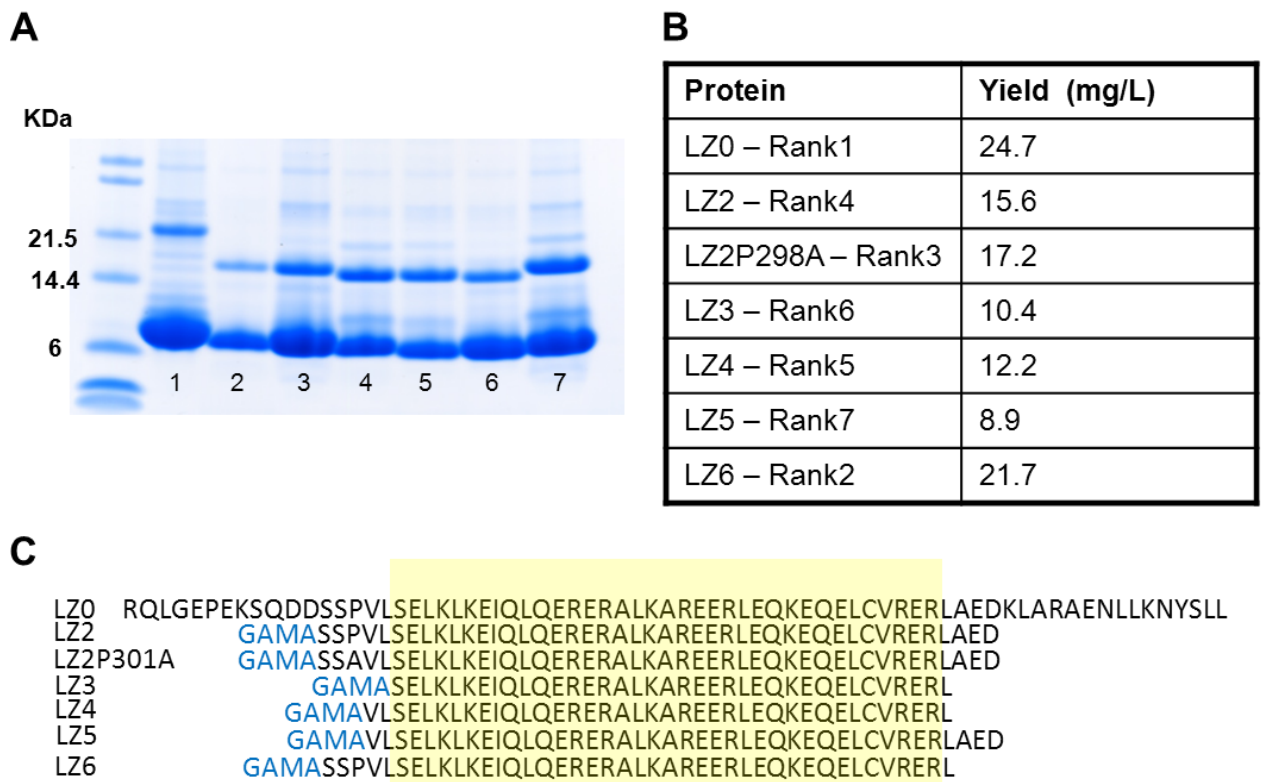


Figure 3.14 Levels of protein yield between Nek2 leucine zipper constructs

A. An SDS-PAGE of the Nek2 leucine zipper constructs post affinity purification Ni-NTA agarose beads is shown, the elution fraction only is shown in the case of all constructs. Lane 1 contains the LZ0 construct, 2-LZ2, 3-LZ2P301A; 4-LZ3; 5-LZ4; 6-LZ5 and 7-LZ6: B. A tabular format of the estimated protein concentrations after SEC using the BCA reduced compatibility assay is represented. C. The differences in amino acids composition of the expressed leucine zipper constructs used in the comparison of expression yield are indicated.

A

	290	300	310	320	330	340	350	360
seq :	L	C	P	E	I	S	T	S
HepI :	f	g	A	b	c	D	e	f
HepII :	b	c	D	e	f	g	A	b
Lzip :				L	Z	L	Z	L
cc :	0	0	0	0	0	0	0	0
agadir:	0	0	0	0	0	0	0	0
N-cap :		+	+			+		
C-cap :					+	++		
S-PO :		+	++				+	

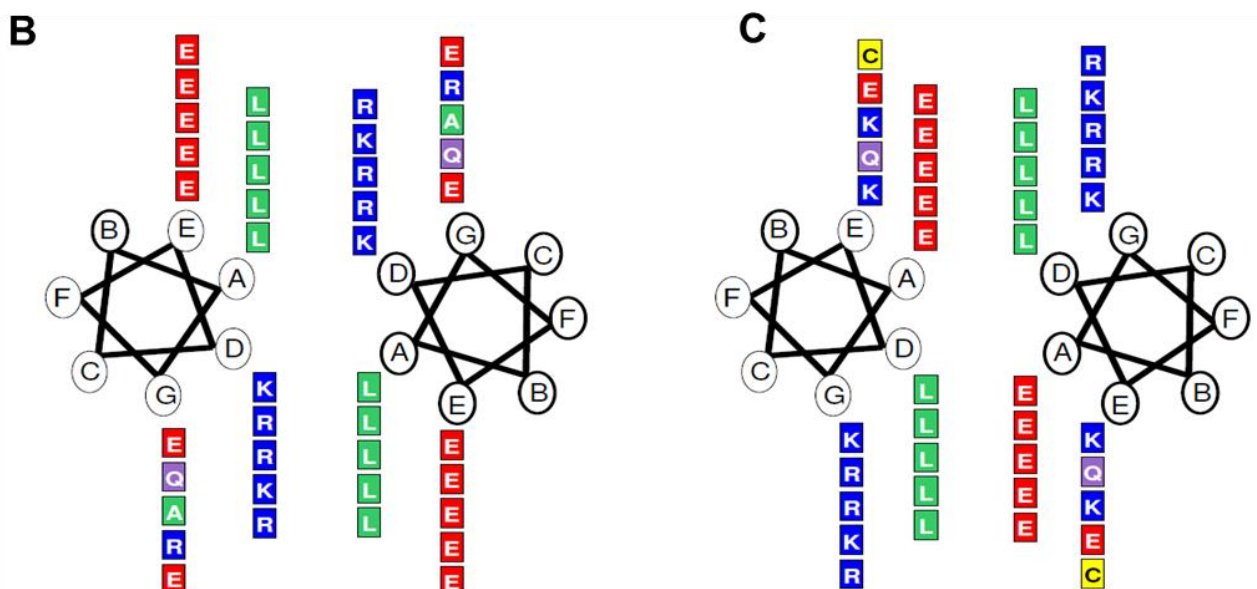


Figure 3.15 Sequence analysis of the Nek2 leucine zipper

A. The sequence of the leucine zipper colour coded by amino acid properties (green – hydrophobic; red – negatively charged; blue – positively charged; magenta – polar uncharged; yellow – cysteine) is shown. Directly below the sequence the two potential heptad repeats, HepI and HepII, are shown with the key a- and d-positions, marked in uppercase. The leucine zipper prediction by the program ZZIP is displayed (Lzip), followed by the coiled-coil prediction using COILS (cc). The following three lines were provided by the program AGADIR: probability of folding as an isolated α -helix (agadir) as well as putative N- and C-caps (N-cap:C-cap), and finally predicted serine phosphorylation sites (S-PO). B. A representation of helical wheel plots of the Nek2 leucine zipper domain for the theoretical HepI conformation is displayed. Amino acids are shown in boxes, coloured in alignment with panel A. Panel C represents a helical wheel plot for the leucine zipper conformation HepII.

A

HeptadI	Amino Acid				
<i>a</i> and <i>d</i>	LK	LR	LR	LK	LR
e and g	EQ	EA	ER	EE	EL
HeptadII					
<i>a</i> and <i>d</i>	LL	EL	EL	EL	EL
e and g	KK	QR	KR	EK	CR

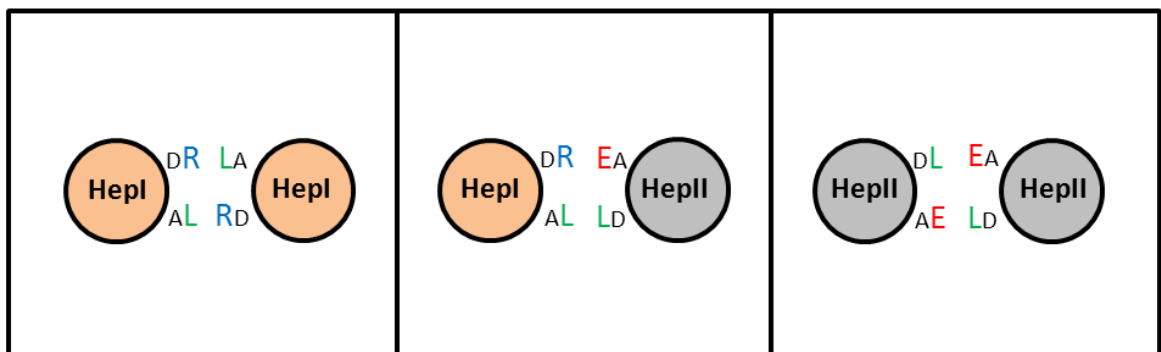
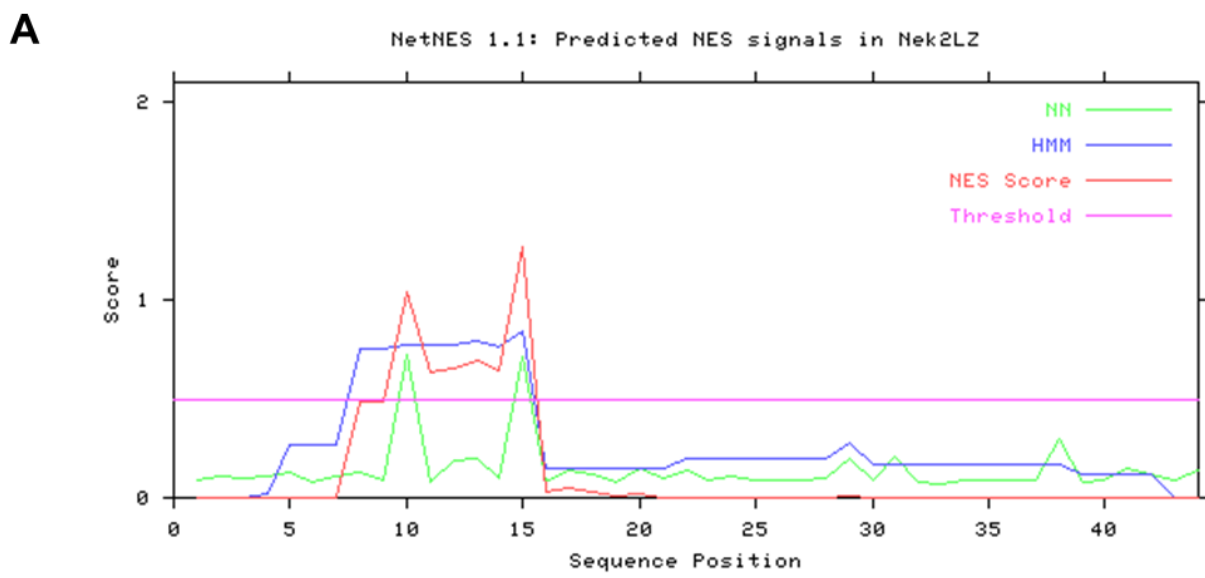
B

Figure 3.16 Sequence analysis of the potential interfaces of the Nek2 leucine zipper

A. A tabular form of the amino acids expected to interact in the Nek2 leucine zipper is shown. Direct amino acid interactions for conformers Hepl and HepII are displayed, residues in interface *a*- and *d*-positions, and also *e*- and *g*-positions to represent the side chain interactions are inserted. B. A schematic diagram indicating the theoretical dimerization of Hepl and HepII conformers of the Nek2 LZ is represented, the sequence of the leucine zipper interface is colour coded by amino acid properties (green – hydrophobic; red – negatively charged; blue – positively charged).

Analysis of the Nek2 leucine zipper domain using NetNES (la Cour et al., 2004), revealed the presence of a nuclear export signal (NES) (Figure 3.17A), comprising of residues LKEIQL (Figure 3.17B). The transport of macromolecules across the nuclear membrane is an active process regulated by a family of homologous transport receptors belonging to the importin family, also called karyopherin receptors or exportins (Strom and Weis, 2001). The presence of a NES in the Nek2 leucine zipper does not suggest that the Nek2 protein is constitutively exported from the nucleus. CRM1/Exportin1-mediated export is a regulated event, with several methods of regulation being reported; masking/unmasking of NESs (Li et al., 1998; Stommel et al., 1999; Seimiya et al., 2000; Heerklotz et al., 2001; Kobayashi et al., 2000; Craig et al., 2002); and also phosphorylation (Engel et al., 1998; Ohno et al., 2000; McKinsey et al., 2001; Zhang and Xiong, 2001; Brunet et al., 2002) and disulphide bond formation due to oxidation (Yan et al., 1998; Kudo et al., 1998; Kuge et al., 2001). All of these mechanisms are applicable to the Nek2 leucine zipper: the nature of the charged residues comprising the interface positions could be an inherent destabilizing mechanism to unmask the NES to allow export from the nucleus; the location of a phosphorylation site immediately upstream of the LZ domain (SSP) could potentially destabilize the dimerization of Nek2 sufficiently to expose the NES; and finally the cysteine residue in position 335 is located on the solvent exposed face of the LZ in Hepl and is partially accessible to solvent in HepII (Figure 3.17B).



B LZ2 SSPVLSELKL**K**E**I**QLQERERALKAREERLEQKEQELCVRERLAED

Figure 3.17 Nek2 LZ sequence analysis of a potential nuclear export signal (NES)

A. The sequence of the Nek2 Leucine zipper construct LZ2 inputed into the NetNES 1.1 software from the Technical University of Denmark is displayed. The green line represent the neural network algorithm (NN) used to predict the presence of a NES combined with the blue line which represents the Hidden Markov model algorithm (HMM), to give the overall NES score shown by the red line. The threshold value is indicated by the magenta line at a score of 0.5. B. The region of the Nek2 LZ in which the predicted NES sequence is located as highlighted in orange.

3.1.8 Circular dichroism (CD) of the wild-type Nek2 leucine zipper constructs

To understand the wild-type conformation of the Nek2 leucine zipper domain the biophysical technique of CD spectroscopy was performed using LZ0 and LZ5 polypeptides. The spectra were virtually identical and contained minima at 208 and 222 nm typical with that of an α -helix, with the minima at 208 nm slightly more pronounced than that of 222 nm (Figure 3.18A). The molar ellipticities at 222 nm of around $-22,000 \text{ deg mol}^{-1}\text{cm}^{-2}$ suggested the presence of approximately 70% α -helix, in agreement with expectation. The melting curves, performed at 222 nm, showed a reasonably cooperative thermal unfolding with relatively high melting temperatures of 57°C for LZ5 and a slightly higher value of 66°C for LZ0 (Figure 3.18B), suggesting that the core leucine zipper sequences as in LZ5 is sufficient to assume a proper fold and the additional coiled-coil between residues 340-355 in LZ0 had only a marginal effect on stability. The estimation of helical content was performed using mathematica, the equation used for the calculation is shown below:

$$\text{fff} = (\text{Ffold} + \text{m_f} * \text{x} + (\text{Funfold} + \text{m_u} * \text{x}) * \text{Exp}[(\text{x} - \text{T}_m) * \text{m}]) / (1 + \text{Exp}[(\text{x} - \text{T}_m) * \text{m}])$$

fff = signal measured (Ellipticity at 222nm)

Ffold = signal expected for 100% folded

Funfold = signal expected for 100% unfolded

x = temperature

T_m = melting temperature

m = slope at unfolding transition

m_f = slope of curve _before_ unfolding

m_u = slope of curve _after_ the protein is unfolded.

3.1.9 Circular dichroism (CD) of the mutated Nek2 leucine zipper constructs

Thermal melting temperatures of the LZ5 K309C/C335A mutant were generated using CD spectroscopy to investigate what effect ‘locking’ the leucine zipper into the HeplI conformation had upon stability. The thermal melting curves, performed at 222 nm, showed that in oxidised buffer LZ5 K309C/C335A had a T_m of 47°C, (Figure 3.19A) and in reduced buffer (Figure 3.12B) a T_m of approximately 26°C, indicating, that while the stability of LZ5 did not increase with mutation, a reduced cysteine in the *d*-position destabilized the Nek2 LZ5 polypeptide (Zhou et al., 1993).

The E310C/C335A mutant was also analysed to examine what effect mutation of the *a*-position had upon the stability of the leucine zipper. The mutation was designed to ‘lock’ the LZ5 domain into the Hepl register. Thermal unfolding of the LZ5 E310C/C335A mutant revealed that in oxidised buffer the T_m of 49°C was equivalent to that of the K309C/C335 mutant and offered no additional stabilizing effects (Figure 3.20A). A T_m of 33°C in reduced buffer was observed, indicating that although the mutation in the *a*-position reduced stability, the presence of a reduced cysteine in the *d*-position had an increased destabilizing effect than when in the *a*-position.

The CD raw data is included in the appendix (A1).

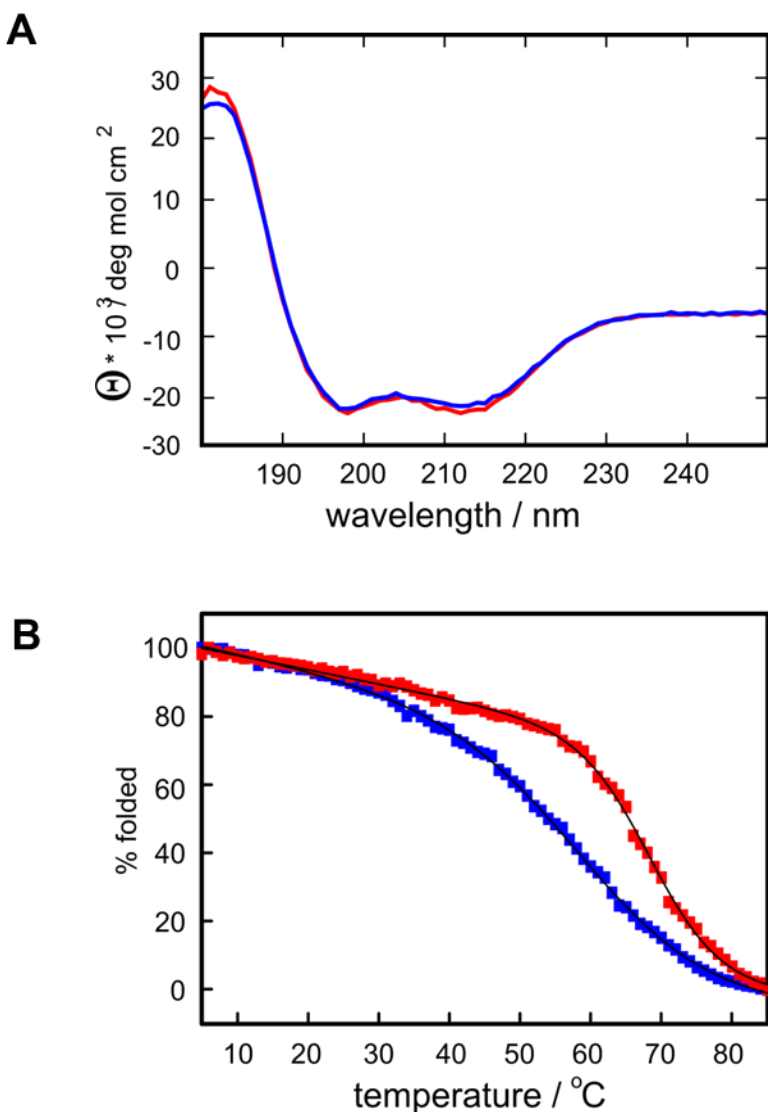


Figure 3.18 Circular dichroism (CD) comparison of leucine zipper constructs LZ0 and LZ5

A. An overlay of CD spectrum of molar ellipticity vs wavelength for the Nek2 leucine zipper constructs LZ0 (red) and LZ5 (blue), T=298K, concentration 50 μM , at a pathlength of 1 mm is displayed. B. A representation of a thermal melting curve measured at a wavelength of 222 nm. Melting temperatures were generated from the fitting of the curves to a two state cooperative unfolding equation (Mathematica). LZ0 – $T_m = 66.6 \pm 0.2^\circ\text{C}$ with a T_m of LZ5 = $57.8 \pm 0.2^\circ\text{C}$

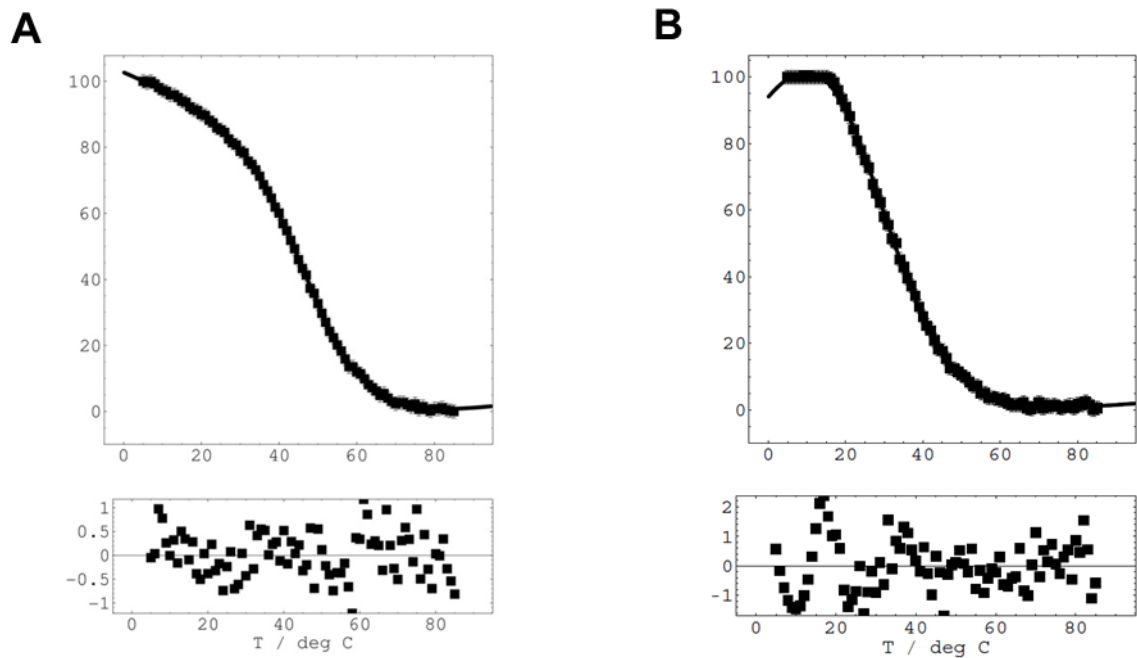


Figure 3.19 Thermal melting temperature of the Nek2 LZ5 mutant K309C

A. A thermal melting curve measured at a wavelength of 222 nm for the construct LZ5 K309C/C335A in oxidising buffer is shown. $T_m = 47.2 \pm 0.3^\circ\text{C}$. B. A representation of the thermal melting curve of LZ5 K309C/C335A in reducing buffer is displayed. $T_m = 25.7 \pm 0.5^\circ\text{C}$. Melting temperatures were generated from the fitting of the curves to a two state cooperative unfolding equation (Mathematica). Spectra were measured at concentration of 50 μM and at a pathlength of 1 mm.

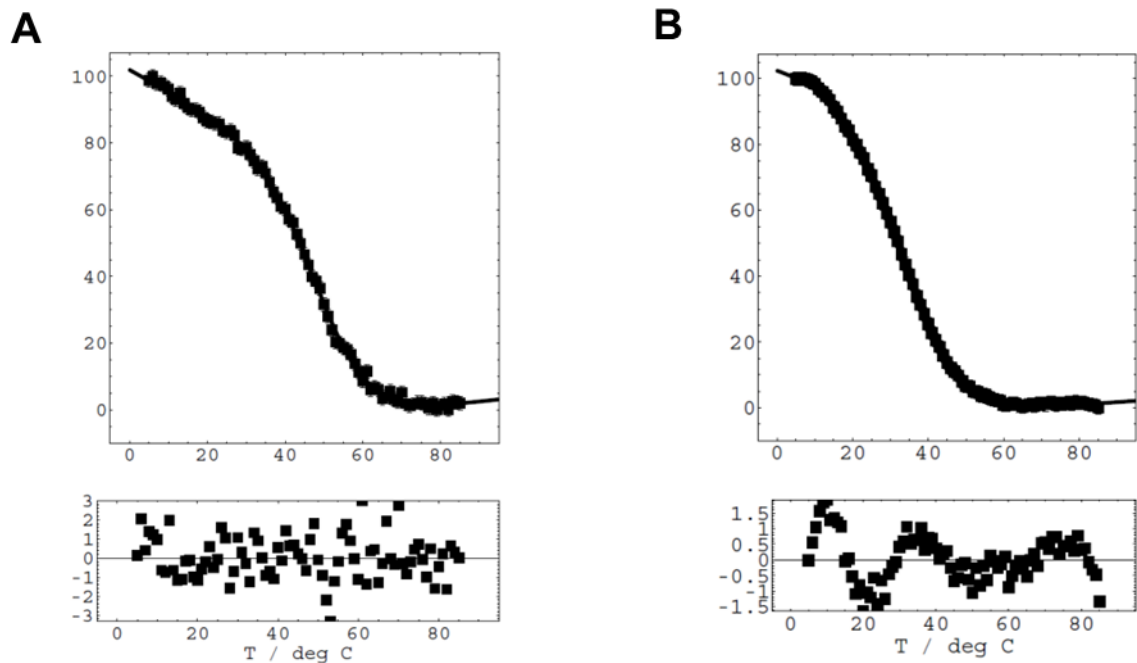


Figure 3.20 Thermal melting temperature of the Nek2 LZ5 mutant E310C

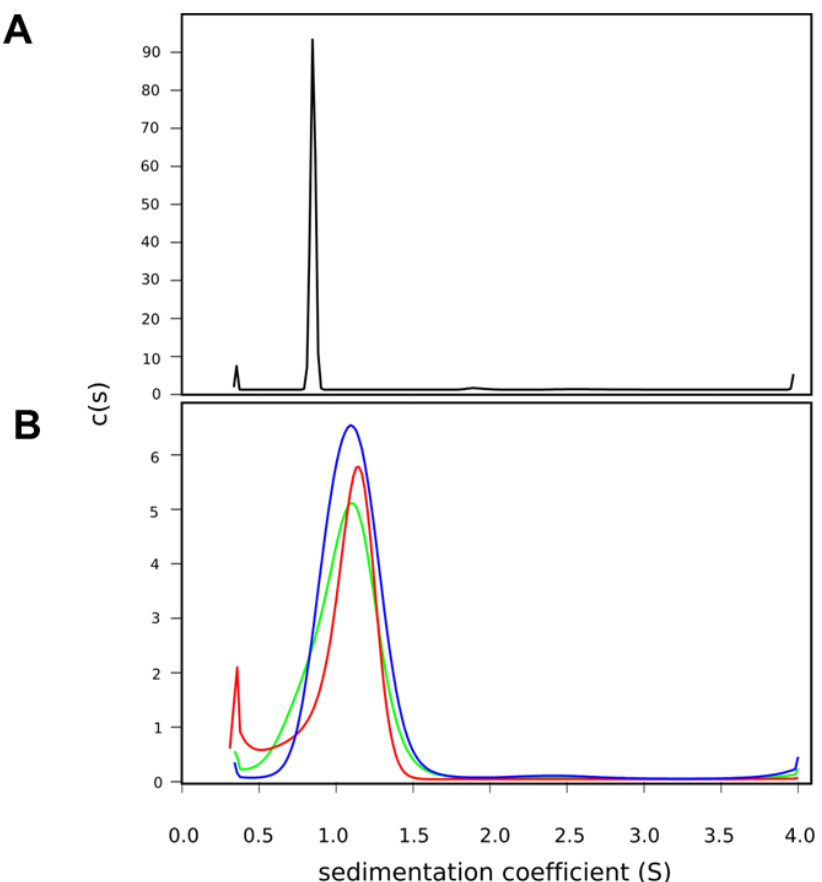
A. The thermal melting curve measured at a wavelength of 222 nm for the construct LZ5 E310C/C335A in oxidising buffer is shown. $T_m = 49.3 \pm 0.2^\circ\text{C}$. B. A representation of the thermal melting curve of LZ5 E310C/C335A in reducing buffer is displayed. $T_m = 32.7 \pm 0.3^\circ\text{C}$. Melting temperatures were generated from the fitting of the curves to a two state cooperative unfolding equation (Mathematica). Spectra were measured at a concentration of 50 μM and at a pathlength of 1 mm.

3.1.10 Analytical ultracentrifugation of Nek2 LZ domain

To determine the oligomerization state of wild-type Nek2 leucine zipper polypeptides and mutated polypeptides sedimentation velocity analytical centrifugation (AUC) was performed at the ISMB biophysics centre, University of London by Tina Daviter. Sedimentation velocity AUC show the concentration changes that occur in an ultracentrifuge cell, initially the molecules are evenly distributed and when a centrifugal force is applied a moving boundary of molecules is formed between the solvent and solution, the boundary travels down the cell with a velocity determined by the sedimentation velocity of the macromolecule. The sedimentation coefficient can be measured by following the boundary motion as a function of time. The sedimentation coefficient (S) was calculated using the Svedberg equation (Teller et al., 1979), since S is dependent on the partial specific volume, density of the solvent and the frictional coefficient which are directly dependent on the temperature and the buffer used a second value $S_{20,w}$ is calculated based on the viscosity of water at 20°C to provide a standardised system of representing the sedimentation coefficient.

f corresponds to the experimental frictional coefficient and f_0 to the minimal frictional coefficient. The results supported the conclusion that the LZ0 and LZ5 wild-type proteins were predominantly dimeric over a concentration range of 10-250 μM (Figure 3.21A). The sedimentation analysis for LZ0 indicated that the main peak estimated at 17,000 was within 500 Da of the actual size of the domain at 17,468 Da (Figure 3.21B). The AUC data generated using the LZ5 E310C/C335A mutant unfortunately could not be interpreted indicating the possibility that the mutation disrupted correct folding and/or the presence of aggregation. The LZ5 wild-type and the LZ5 K309C/C335A mutant, although displaying

peaks which were not exactly symmetrical, were predominantly in solution as dimeric species, regardless of oxidation state for the mutants.



Construct	S_{app}	$S_{20,w}$	f/f_0	Monomer MW (kDa)	Apparent MW (kDa)
LZ0, 228 μM	0.86	1.40	1.7	8.7	17.0
LZ0, 29 μM	0.89	1.40	1.7	8.7	17.7
LZ5	1.10	1.11	1.5	5.4	10.7
LZ5 C335A, K309C	1.07	1.08	1.5	5.4	10.0
LZ5 C335A, E310C	1.05	1.06	1.6	5.4	10.1

Figure 3.21 Sedimentation velocity AUC of LZ0, LZ5 and LZ5K309C/C335A

c(s) distributions are displayed for: A. LZ0 at a concentration of 228 μM indicating an apparent sedimentation coefficient in Svedberg units (S) of 0.86 is shown. B. LZ5 (blue) and LZ5K309C/C335A in reducing (red) and non-reducing buffer (green) at a concentration of 224 μM are indicated. The apparent S values were 1.10, 1.07 and 1.05, respectively. C. A representation of the AUC data acquired in tabular form. Analysis of LZ0 at a high concentration of 228 μM and at a low concentration of 29 μM indicated that LZ0 molecular weight which was consistent with that of a dimer. The LZ5 and the LZ5 mutant K309C/C335A in reduced and non-reduced buffer, at a concentration of 224 μM, displayed the apparent molecular weight of a dimer.

3.2 Discussion

3.2.1 Biophysical analysis of Nek2 leucine zipper

Seven new LZ constructs were generated and cloned into the pETM-11 vector containing a cleavable N-terminal 6 x His tag. Two of the seven constructs, specifically the LZ5 mutants (K309C and E310C) were produced using site-directed mutagenesis. The total number of existing leucine zipper constructs was therefore: LZ0, LZ2, LZ3, LZ4, LZ5, LZ5-K309C/C335A, LZ5-E310C/C335A and LZ6. A preliminary characterization of the LZ proteins was performed using a combination of 1D ^1H NMR, analysis of protein expression and purification, CD spectroscopy and AUC.

1D ^1H NMR spectroscopy performed on the LZ polypeptides LZ0, LZ2, LZ3, LZ4, LZ5 and LZ6 generated spectra with significant line broadening and no regions of sharp well resolved peaks over the entire spectral range, usually this is indicative of proteins with a high molecular weight, aggregated molecules or oligomeric protein and is a hallmark of globular unfolded proteins (Wüthrich, 1986). However, the leucine zipper motif when recombinantly expressed is subject to a slow-intermediate exchange process (as previously shown for LZ1 using TOCSY-NOESY NNR analysis), the 1D ^1H NMR showed that after analysing a number of constructs, even LZ0 the only fragment which remains after proteolytic digestion of the whole Nek2 protein kinase (Croasdale et al., 2011), the line broadening could not be improved and the exchange persisted in all constructs.

Quantification of protein yields was used to gain an insight into the stability of the leucine zipper constructs, amongst the panel of LZ molecules LZ0 and LZ6 had the highest

expression, however, both of these constructs also had significant levels of high molecular weight aggregates indicating the possibility that a percentage of the usable protein was lost due to misfolding or aggregation due to the high levels of soluble protein generated by the *E. Coli*. Overall, the leucine zipper constructs were present in the soluble fraction and not in inclusion bodies and all except LZ3 could be ¹⁵N isotope labelled without problems. LZ5 was chosen to perform the major characterization using NMR due to it possessing the least number of amino acids whilst maintaining suitable expression levels.

A previous study performed by Frank Ivins (unpublished data) reported that when analyzed by circular dichroism (CD), the construct LZ0 did not show any differences in structure or stability in the presence of increase ionic strength (1 M NaCl). One would expect that a domain with such a high composition of charged residues that the increased ionic strength would serve to destabilized the leucine zipper. However, the increased ionic strength may increase hydrophobicity at the interface to counteract the destabilizing effect.

CD spectroscopy was performed on all leucine zipper constructs LZ0 through to LZ6, all displayed spectra typical for a coiled coil with strong minima at 208 nm and 222 nm. The CD spectra showed no differences in the percentage helix of LZ0 and LZ5 indicating that serine 300 is not the location of the N-cap in the leucine zipper domain as predicted by AGADIR (Figure 3.15A). The absence of the N-cap residues would lead to a reduction in stability and therefore helical content. Both LZ0 and LZ5 had spectra consistent with a cooperative curve and a wide transition area with thermal melting temperatures a similar range, however, the T_m of LZ0 was higher than that of LZ5 indicating a little extra stability as a result of the extended domain boundaries, possibly due to the presence of the existence of the short helix at the extreme C-terminus (Fry et al., 1999)

The LZ5 K309C and E310C mutants had a T_m of within 2 degrees indicating that the effect of the insertion of the cysteine residue in the interface position was inconsequential with respect to the *a*- or *d*-position. Interestingly, upon reduction both mutants suffered approximately a 10 degree drop in thermal stability. This signified that firstly, the disulphide bond could be formed in both cases due to the drop in thermal stability in the presence of reducing agent, and secondly that the disulphide bonds had formed in both Hepl:Hepl and HepII:HepII displayed in figure 3.8. Demonstrating that both theoretical models of Hepl and HepII could be correct or the leucine zipper domain is highly flexible and one construct contains mispaired disulphide bonds i.e. not between positions *a* or *d* respectively.

Hydrodynamic assessment by sedimentation velocity AUC indicated that LZ0, LZ5 and the LZ5 mutants existed as a dimeric complex in solution and gave a determined frictional coefficient (f/f_0) of between 1.5-1.7. The f/f_0 of a globular protein/sphere is equal to 1, so the values generated for the LZ0 and LZ5 constructs indicate that the leucine zipper domain is elongated. These results confirm that the Nek2 leucine zipper is a tightly bound elongated dimer with no other detectable aggregation state. Although the SEC chromatogram showed the presence of high molecular weight aggregates, the AUC data indicates by the absence of oligomers, that after pooling the known dimeric fractions post SEC, the LZ0 and LZ5 do not undergo further aggregation or oligomerization. The high molecular weight peak in the SEC could be due to LZ protein that is partially folded and aggregated but is removed by stringent pooling of the protein fractions.

In summary, further analysis of the amino acid composition of the Nek2 leucine zipper which deviates from the classical coiled-coil structures is necessary. The determination of the three-dimensional structure of the Nek2 leucine zipper is essential to gain an insight into

the interesting salt-bridge interactions between the *a-g'* and/or *d-e'* positions. Mutational analysis could provide some understanding into what relevance the presence of a high number of charged residues have on the oligomerization state and specificity, but the 3D structure is of increasing importance.

CHAPTER 4

CHARACTERIZATION OF THE DYNAMIC NATURE OF THE NEK2 LEUCINE ZIPPER USING NMR

4.1 Results

4.1.1 Rationale to explore the dynamics of the leucine zipper domain

Initial $^1\text{H}/^{15}\text{N}$ HSQC experiments performed with the constructs LZ1 and LZ2 gave more than the expected number of peaks for the leucine zipper domain combined with poor line widths. This indicated that a slow exchange process on the chemical shift time scale due to conformational heterogeneity is occurring. To evaluate this NMR experiments to ascertain the R_1 and R_2 relaxation rate were planned specifically NOESY, TOCSY and a specialised heteronuclear correlation experiment designed to estimate site to site rate constants for two species in slow exchange (Farrow et al., 1994). In parallel to this the effects of concentration, temperature and the addition of the solvent acetonitrile was attempted to either increase or decrease the chemical shift timescale to analyse the effects on linewidth and the number of visible peaks in the spectra. Two mutants were designed as previously described in 3.1.5, to analyse the orientation of the leucine zipper dimer i.e. parallel or anti-parallel and to ‘lock’ the leucine zipper into either Hepl or Hepll dimeric conformations.

4.1.2 ^{15}N LZ5 Expression and Purification

A pETM-11 vector incorporating the amino acid residues 299-343 of the Nek2 leucine zipper domain termed LZ5, was used to express the polypeptide in *E.coli*. The complex was purified in two stages. The presence of a polyhistidine tag at the N-terminal of LZ5 allowed the protein domain to be purified by nickel affinity chromatography. A final polishing step of purification involved gel filtration, as shown in figure 4.1A and B. The typical chromatogram showed a double peak with fractions A6 and A7 representing the dimeric fraction of LZ5 (Figure 4.1A). The predicted size of the LZ5 construct including the histidine tag and linker

region is 8.4 kDa (Figure 4.1B), with fractions A2-A5 being higher molecular weight aggregates or possibly multimers of LZ5. The presence of a TEV protease site enabled the removal of the polyhistidine tag before analysis by NMR. This was performed using acTEV protease according to the manufacturers protocol (Invitrogen), the molecular weight of LZ5 after cleavage with TEV was 5.5 kDa (Figure 4.1C). In lanes 2 and 3 of fig. 4.1C an extra band at 16.8 kDa and 11 kDa can be seen on the SDS-PAGE gel. This band is due to the dimeric form of LZ5 remaining intact after incubation with loading buffer according to the standard manufacturers protocol, indicating the presence of a stable dimer after cleavage of the histidine tag. Typical yields of ^{15}N LZ5 after cleavage were between 2-2.5 mg per 1 L M9 minimal medium (Marley et al., 2001).

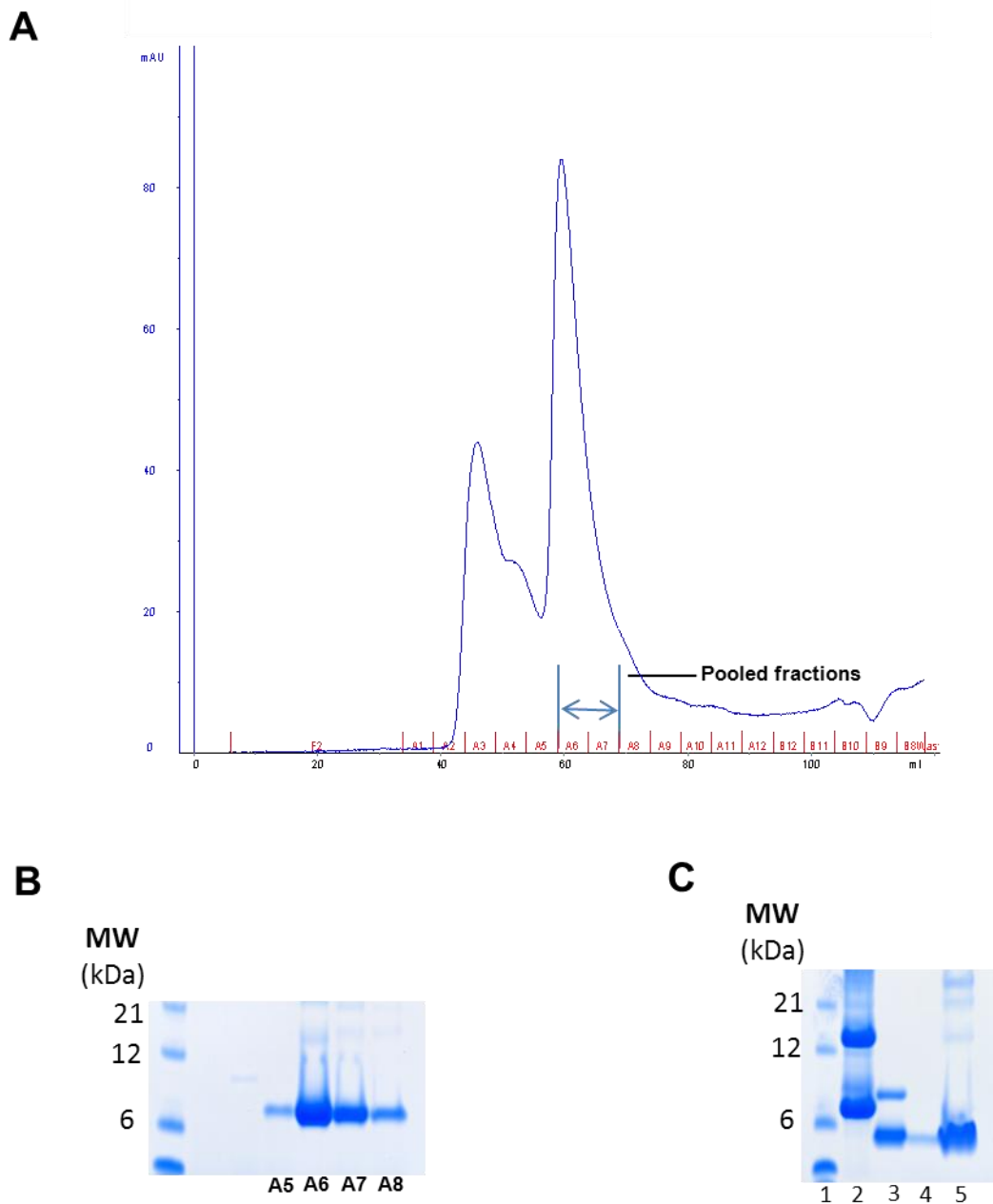


Figure 4.1 Purification of the His-tagged 15N Nek2 leucine zipper domain 5.

A. An example of a FPLC elution profile attained by gel filtration on a superdex 75 16/60 column is shown. Gel filtration was performed after Ni-NTA purification, the pooled fractions are also highlighted. B. An SDS-PAGE gel performed after FPLC purification displaying the elution fractions and indicating the purity of the pooled fractions A6 and A7 is displayed. C. An SDS-PAGE gel of the fractions obtained by acTEV protease digestion is represented. Lane 1 contains the Mark 12 unstained standard molecular weight marker, lane 2 the undigested 15NLZ5 protein as a control, lane 3 flow through after Ni-NTA purification post acTEV digestion showing incomplete reduction prior to loading band at 9 kDa, lane 4 the wash fraction from the Ni-NTA column and lane 5 represent the Histidine tag following elution from the Ni-NTA column using 500 mM Imidazole. Lane 3 was used for subsequent NMR analysis.

4.1.3 2D homonuclear TOCSY/NOESY with LZ2

Early experiments consisted of homonuclear TOCSY/NOESY. The presence of “twins” of resonances as shown in figure 4.2 indicate that there are at least 10 amide protons which have exchange specific crosspeaks (TOCSY) which mostly originate from neighbours in close proximity. The region of the spectrum from 7.4-9.0 ppm displays mainly the amide backbone NH protons. The two observed exchanging species of LZ2 exists in equal populations indicated by the peaks of the ‘twins’ of resonances being of similar intensity. Slow chemical exchange is present indicated by the presence of the unusual TOCSY exchange crosspeaks. To probe the dynamic state of LZ2, T_1 and T_2 relaxation rates for selected amino acids, and heteronuclear NOE experiments were used to analyse the molecular tumbling of the molecule as described in 2.4.2.7 using the Model free analysis. For LZ2 at a concentration of 1-2 mM surprisingly short values of R_1 around $0.7\text{--}0.8 \text{ s}^{-1}$ (Figures A2 & A4) combined with very fast R_2 rates approximated to 30 s^{-1} indicated a rotational correlation time of 20 ns (Figures A6 & A8), which corresponds to an approximate molecular weight of 30 kDa. However, there was considerable discrepancy between the R_1 and R_2 values as a result of the intermediate timescale dynamics or chemical shift anisotropy when calculating on only two residues and not the average relaxation rates of the whole molecule (Appendix I, Figure A2 - A9). With the T_2 values being artificially shortened, a combination of T_1 and heteronuclear NOE gave a value of $\tau_c = 14 \text{ ns}$, consistent of a tetramer. The high molecular weight obtained by NMR in contrast to AUC may be due to the shape of the molecule which is elongated and not globular. To further investigate the oligomerisation state of LZ2 using NMR, a repeat of the relaxation experiments using LZ2 at

a concentration diluted 1:4 was performed. If concentration dependent oligomerisation were present the relaxation experiments would indicate this by a reduction in estimated MW, a reduction in τ_c , a reduction in R_2 , and an increase in R_1 . Upon dilution all values were reduced but surprisingly R_1 remained constant at 0.77 s^{-1} for residue 17 but for residue 18 increased to 1.1 s^{-1} (Figures A3 & A5). For a precise tetramer the expected value would be $0.8-1\text{ s}^{-1}$ whilst a dimer would have an R_1 value of 1.4 s^{-1} . The results indicate that the construct LZ2 is a tetramer, whereas the AUC consistently indicates only the presence of a dimer. R_2 dropped from 30 s^{-1} to 21.9 s^{-1} indicating that the exchange process was reduced, but the oligomerisation state investigated by NMR may not be reliable due to the shape of LZ2 being an elongated alpha helix which may confuse interpretation (Figures A7 & A9).

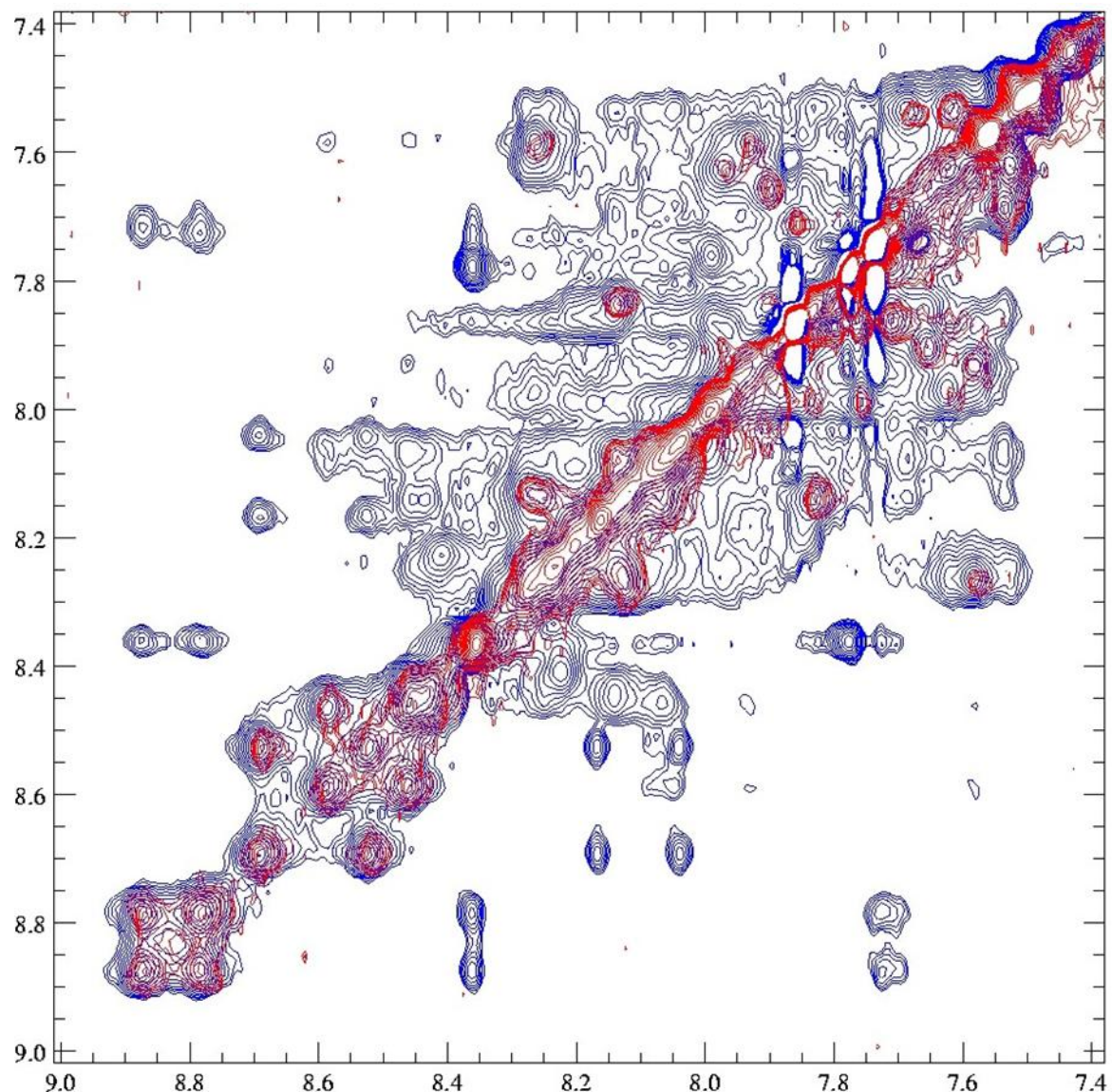


Figure 4.2 2D TOCSY/NOESY ^{15}N Nek2 leucine zipper domain 2 (LZ2).

The superimposition of the NOESY (blue) and TOCSY (red) for LZ2 is shown above in the amide region of the spectrum. The NOESY spectrum indicates the nuclei which are correlated in close space, an NOE between two nuclei indicates a close distance. The TOCSY peaks indicate the transfer of magnetisation via J-couplings, 4 bond J-couplings are unusual and indicate a chemical exchange process.

4.1.4 ^{15}N HSQC reference spectra

For each leucine zipper construct a $^1\text{H}/^{15}\text{N}$ HSQC NMR experiment was performed (described in 2.4.2.9). The construct LZ0 with the highest number of amino acids displayed an HSQC spectrum with fewer peaks than the 70 expected with a large area of unresolved peaks (Figure 4.3). The $^1\text{H}/^{15}\text{N}$ HSQC of LZ1 showed more than the expected number of peaks estimated to be 49 (Figure 4.4). LZ2 also showed more than the estimated number of peaks (Figure 4.5). The $^1\text{H}/^{15}\text{N}$ HSCQ spectrum of LZ4 was of significantly lower quality than for the other leucine zipper constructs (Figure 4.6), in that hardly any of the N-H peaks were resolved yielding a large area of unresolved peaks in the region 8.3-7.6 characteristic of unfolded proteins (Rehm et al., 2002). The spectrum of LZ5 again showed more than the expected number of peaks (Figure 4.7), and the figures 4.8 and 4.9 indicate the effects of engineering a cysteine residue into either the *a* or *d* position of the N-terminus. For LZ5 C335AK309C oxidised a decrease in the number of peaks can be seen and the peak dispersion is significantly improved. For the oxidised form of this protein the peak dispersion is extremely poor worse than for the HSQC using the native LZ5. The second mutant of LZ5 C335AE310C oxidised did not show the same reduction in overlap as in the mutant LZ5 C335AK309C oxidised (Figure 4.10) with the LZ5 C335AE310C reduced spectra looking typical of an unfolded protein (Figure 4.11).

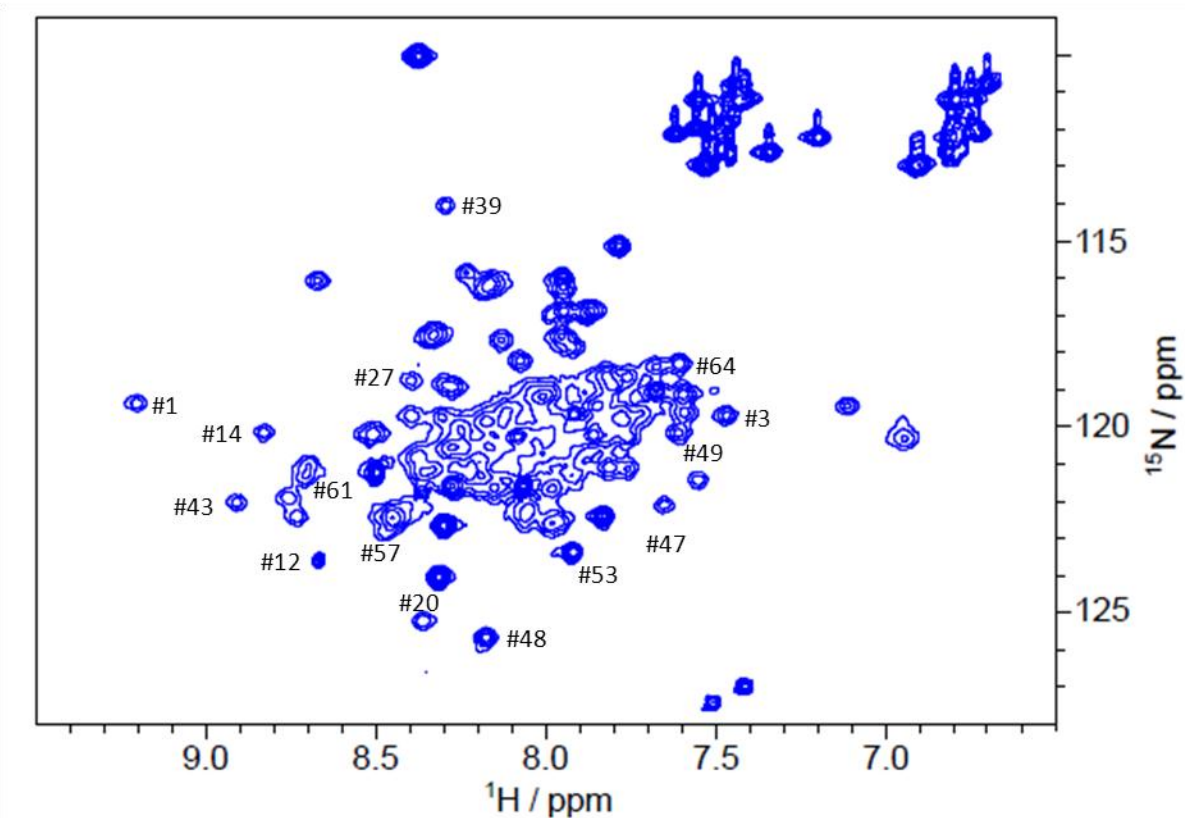


Figure 4.3 2D ¹H/¹⁵N HSQC of Nek2 LZ0

The spectrum shown was recorded at a temperature of 298 K with 128 scans. The figure displays an HSQC of ¹⁵N_LZ0 at a concentration of 2 mM. N-H chemical shifts were assigned a number for uses as a reference depicted as # followed by the number.

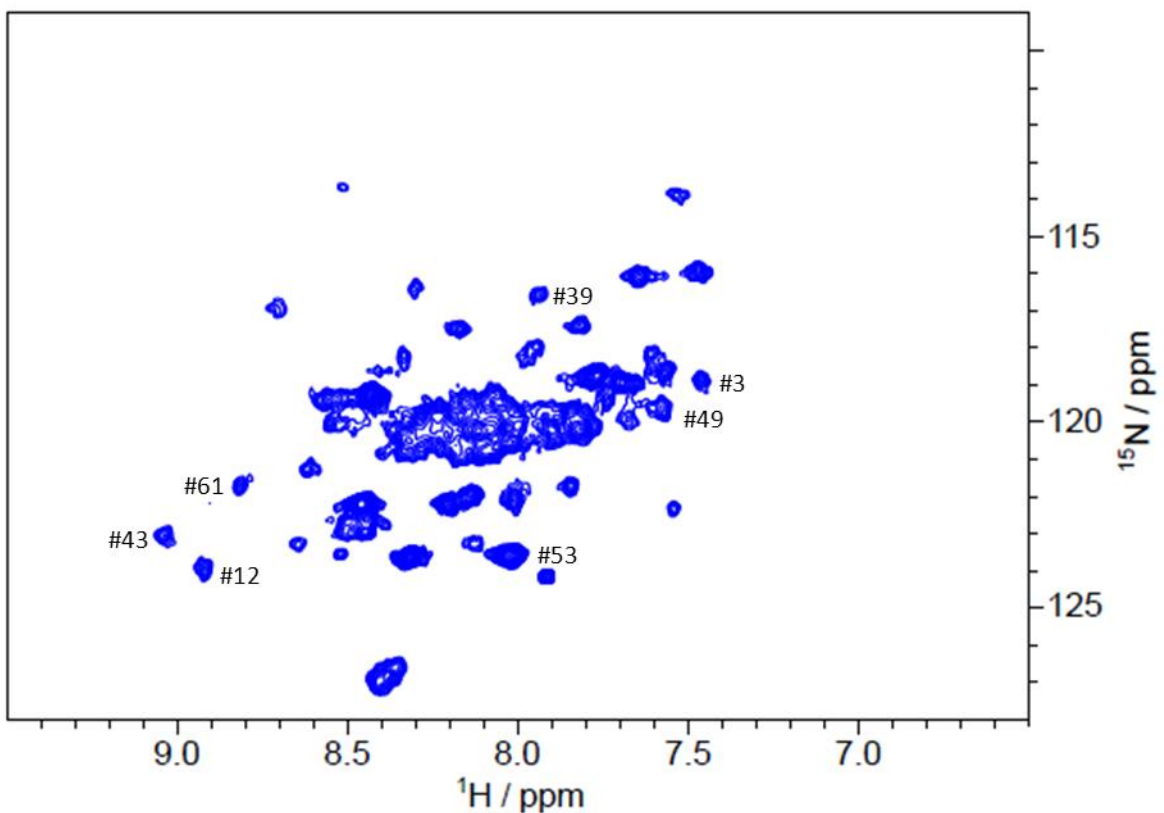


Figure 4.4 2D $^1\text{H}/^{15}\text{N}$ HSQC of Nek2 LZ1

The spectrum shown was recorded at a temperature of 298 K with 128 scans. The figure displays an HSQC of $^{15}\text{NLZ1}$ at a concentration of 2 mM. N-H chemical shifts were assigned a number for uses as a reference depicted as # followed by the number.

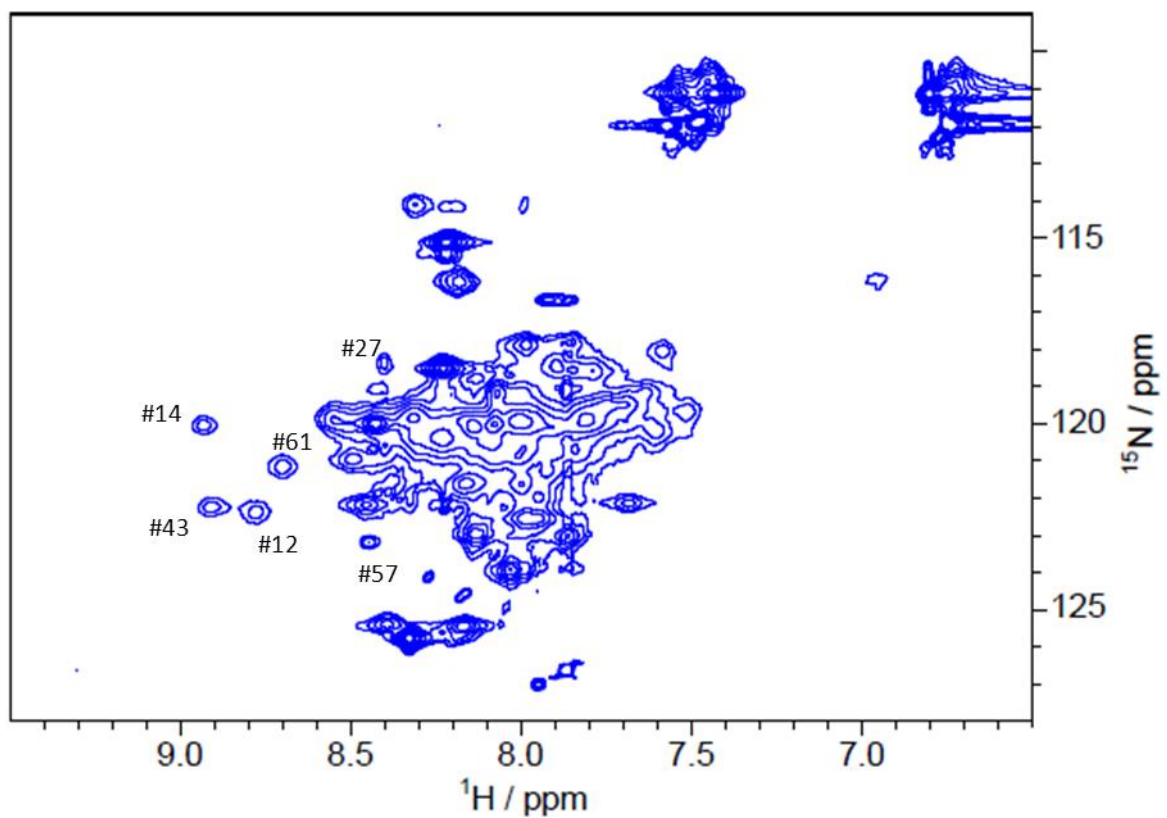


Figure 4.5 2D $^1\text{H}/^{15}\text{N}$ HSQC of Nek2 LZ2

The spectrum shown was recorded at a temperature of 298 K with 128 scans. The figure displays an HSQC of $^{15}\text{NLZ2}$ at a concentration of 2 mM. N-H chemical shifts were assigned a number for uses as a reference depicted as # followed by the number.

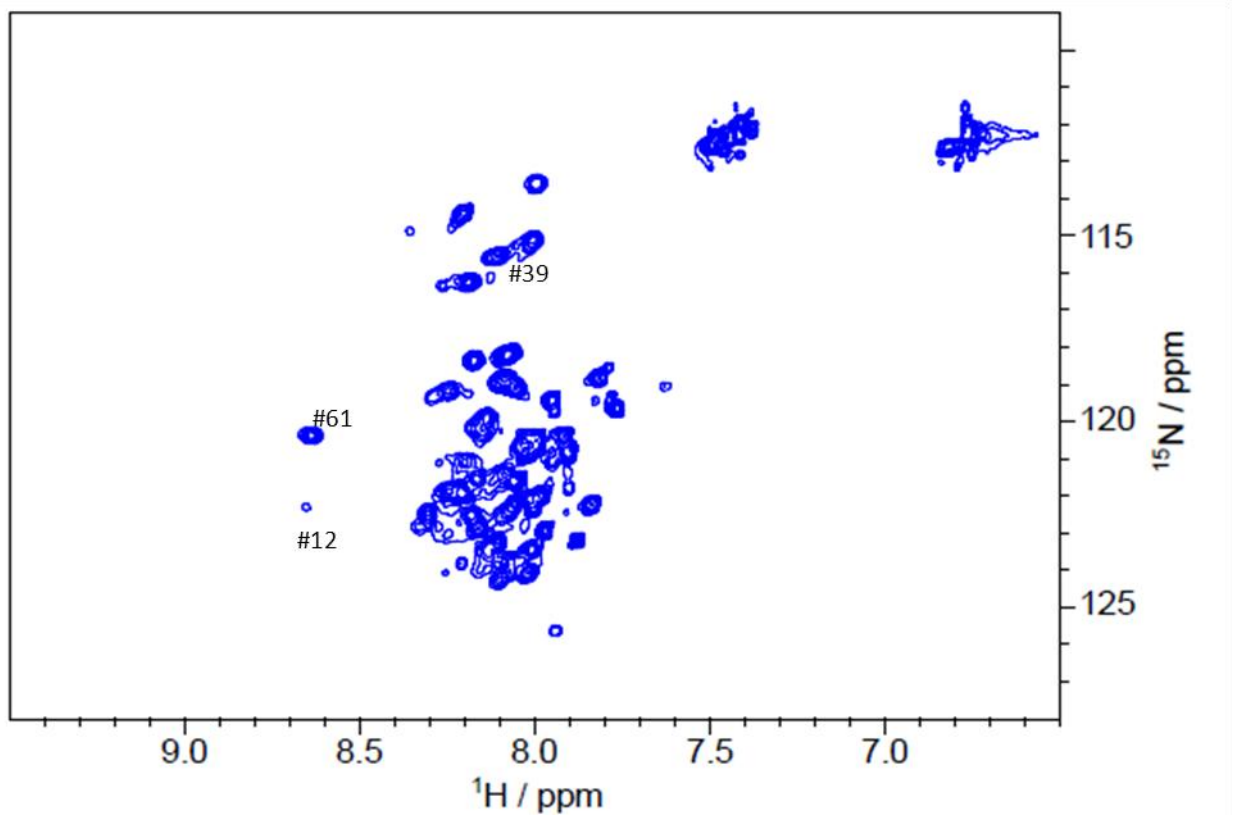


Figure 4.6 2D $^1\text{H}/^{15}\text{N}$ HSQC of Nek2 LZ4

The spectrum shown was recorded at a temperature of 298 K with 128 scans. The figure displays an HSQC of $^{15}\text{NLZ4}$ at a concentration of 2 mM. N-H chemical shifts were assigned a number for uses as a reference depicted as # followed by the number.

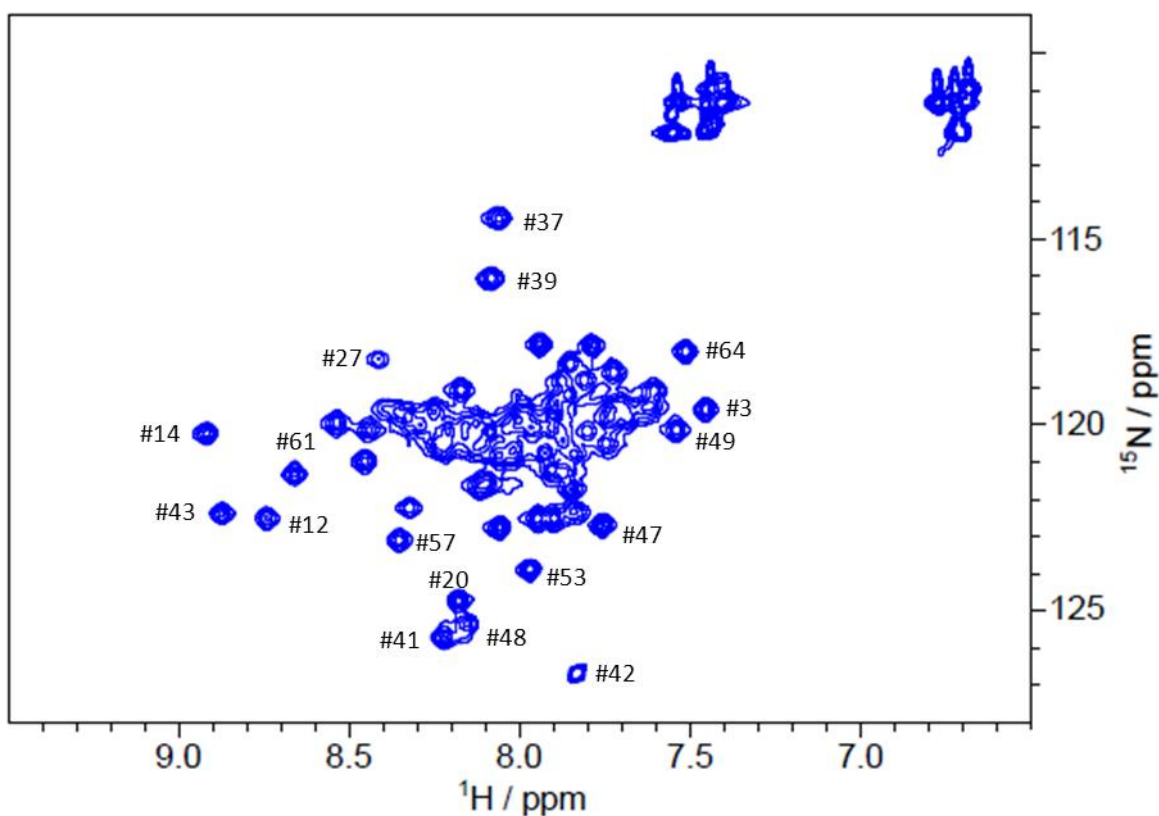


Figure 4.7 2D $^1\text{H}/^{15}\text{N}$ HSQC of Nek2 LZ5

The spectrum shown was recorded at a temperature of 298 K with 128 scans. The figure displays an HSQC of $^{15}\text{NLZ5}$ at a concentration of 2 mM. N-H chemical shifts were assigned a number for uses as a reference depicted as # followed by the number.

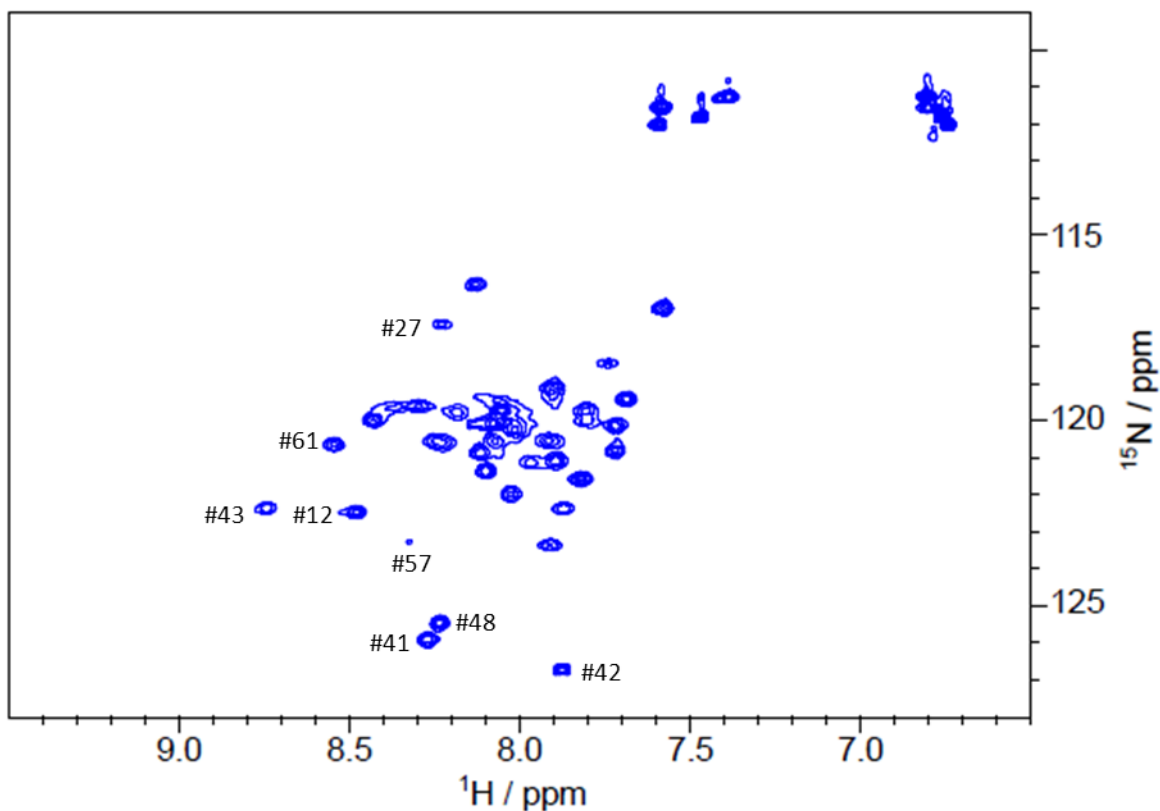


Figure 4.8 2D $^1\text{H}/^{15}\text{N}$ HSQC of Nek2 LZ5 C335AK309C oxidised

The spectrum shown was recorded at a temperature of 298 K with 128 scans. The figure displays an HSQC of $^{15}\text{NLZ5 C335AK309C}$ at a concentration of 2 mM. N-H chemical shifts were assigned a number for uses as a reference depicted as # followed by the number.

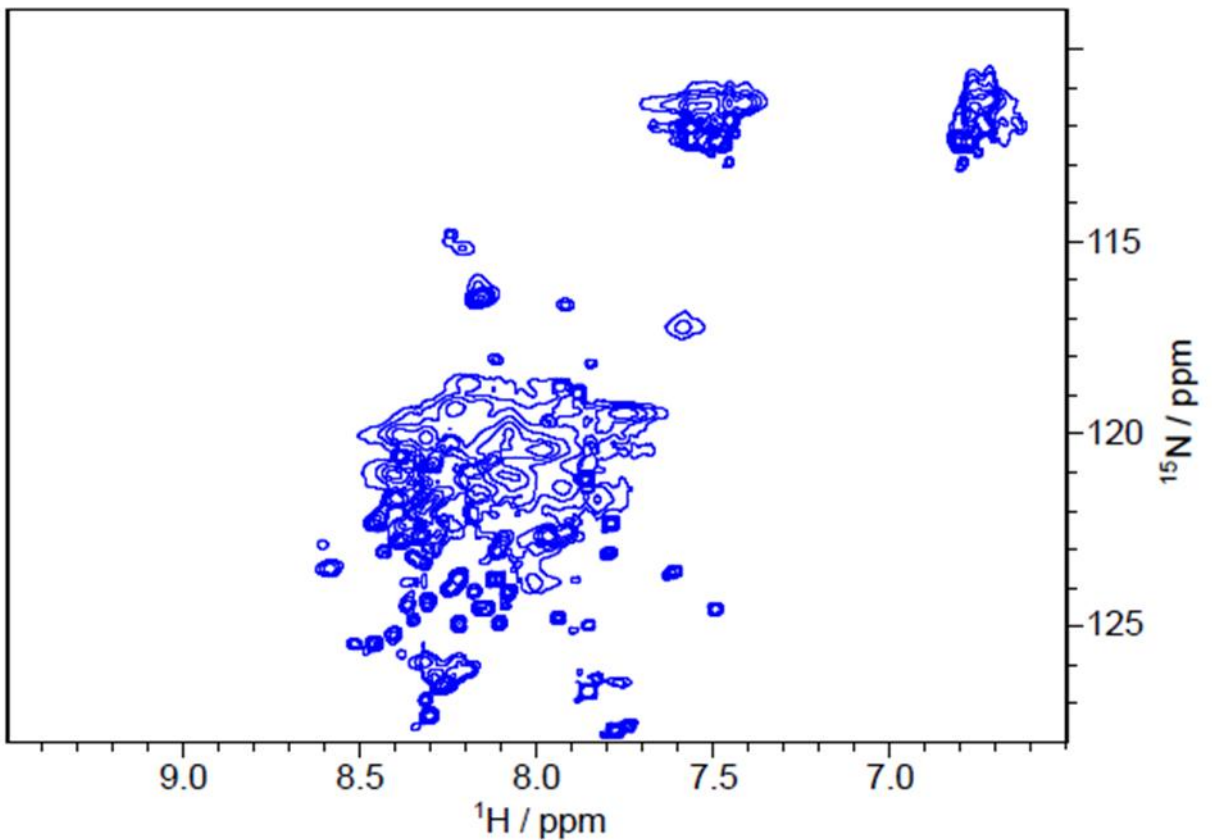


Figure 4.9 2D $^1\text{H}/^{15}\text{N}$ HSQC of Nek2 LZ5 C335AK309C reduced

The spectrum shown was recorded at a temperature of 298 K with 128 scans. The figure displays an HSQC of ^{15}N LZ5 C335AK309C reduced at a concentration of 2 mM. N-H chemical shifts were not assigned a number for uses as a reference due to the poor peak dispersion.

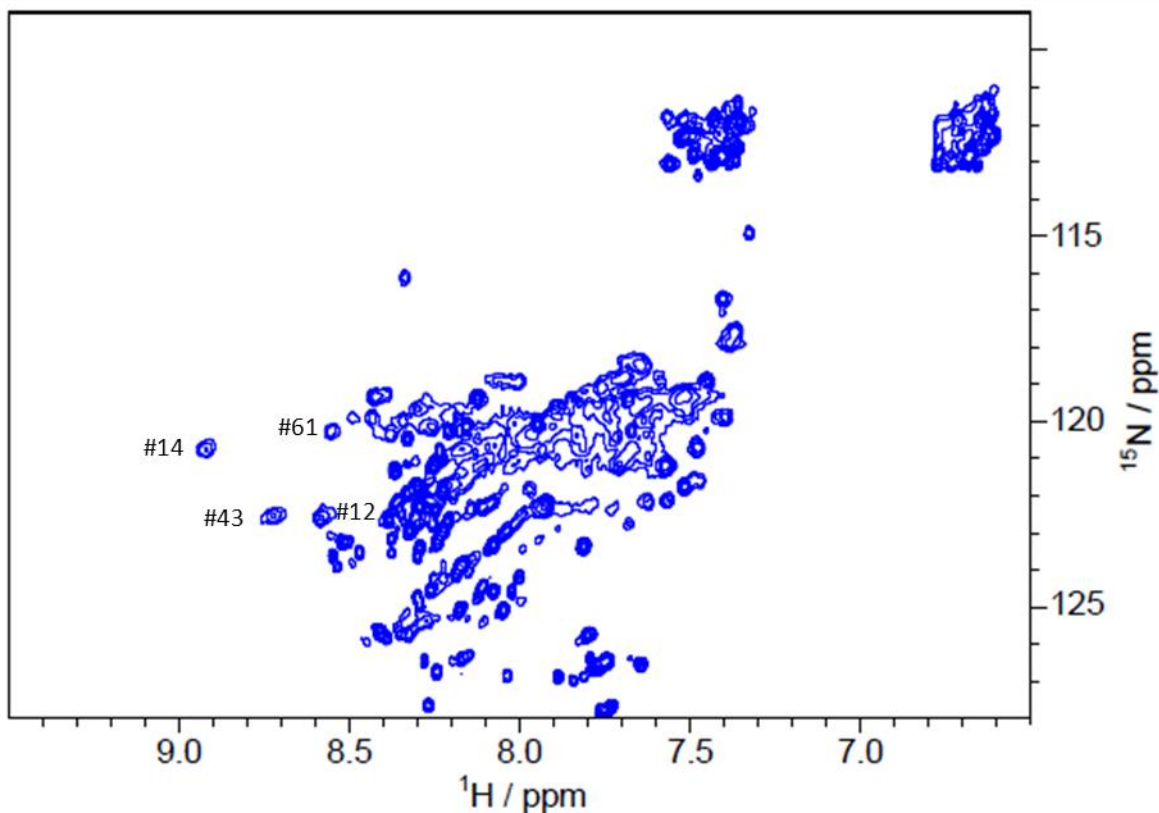


Figure 4.10 2D $^1\text{H}/^{15}\text{N}$ HSQC of Nek2 LZ5 C335AE310C oxidised

The spectrum shown was recorded at a temperature of 298 K with 128 scans. The figure displays an HSQC of ^{15}N LZ5 C335AE310C oxidised at a concentration of 2 mM. N-H chemical shifts were assigned a number for uses as a reference depicted as # followed by the number.

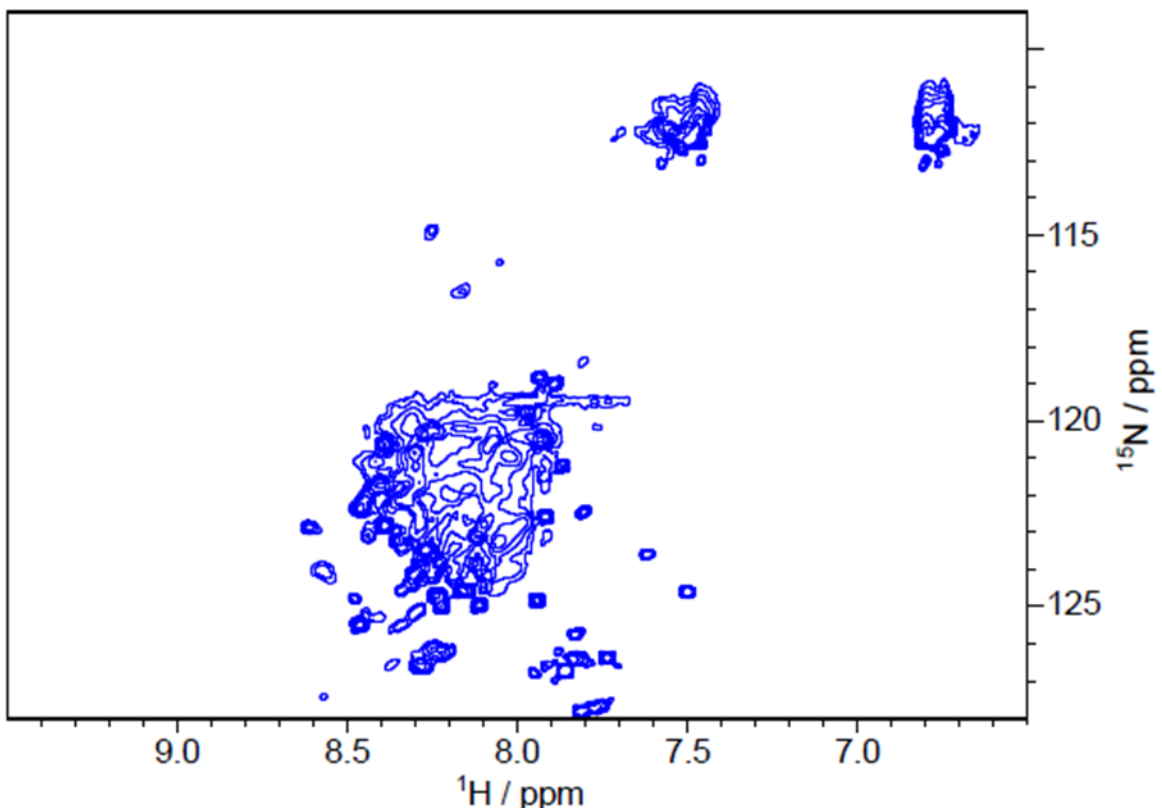


Figure 4.11 2D $^1\text{H}/^{15}\text{N}$ HSQC of Nek2 LZ5 C335AE310C reduced

The spectrum shown was recorded at a temperature of 298 K with 128 scans. The figure displays an HSQC of ^{15}N LZ5 C335AE310C reduced at a concentration of 2 mM. N-H chemical shifts have not been assigned a number for uses as a reference due to the poor peak dispersion.

4.1.5 ^{15}N HSQC showing the effect of dilution on LZ5

To investigate further the effects of possible oligomerization seen previously in the construct LZ2 a series of ^{15}N HSQC was acquired using different concentrations of LZ5 (Figure 4.12). Dilutions of LZ5 were prepared and a serial dilution was made ranging from 2 mM, 1 mM, 0.5 mM, 0.25 mM and 0.125 mM and an HSQC for each different protein concentration was acquired. In previous HSQC experiments too many peaks were observed and if the increased number of peaks were due to aggregation/oligomerization dilution could reduce the peak numbers. In these experiments peak number #14 at 120.2/8.94ppm was used as a predictor of oligomerisation state as it had previously been observed that in LZ2 when diluted peak #14 disappeared at lower concentrations. However, the exact concentration had never been determined due to the inherent problems in estimating the exact protein concentration of the leucine zipper constructs (discussed in 3.1.7). Diluting LZ5 down to a concentration of 0.125 mM had no effect on the chemical exchange. At concentrations from 2 mM - 0.125 mM the LZ5 protein exists as a dimer and oligomer which are not affected by this concentration range.

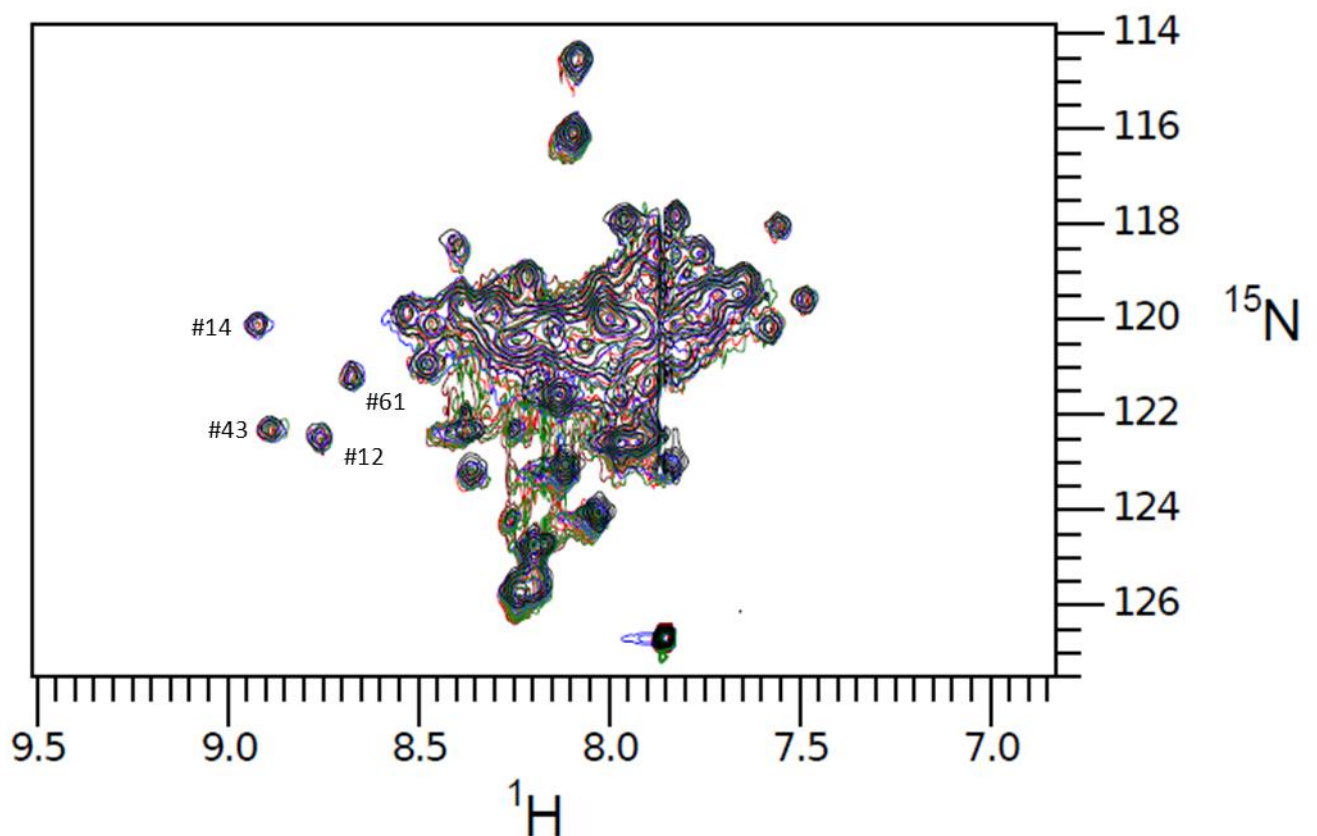


Figure 4.12 2D ¹H/¹⁵N HSQC of Nek2 LZ5

The spectrum shown was recorded at a temperature of 298 K with 128 scans. The figure displays an HSQC of ¹⁵N LZ5 at a concentration from 2 (black), 1 (blue), 0.5 (red), 0.25 mM (green) to 0.125 mM (brown). #14 is closely observed for the disappearance of the peak at lower concentrations.

However, in the ^{15}N HSQC where the LZ5 protein was diluted to 0.1 mM as shown in figure 4.13 peak #14 had completely disappeared indicating that at 0.1 mM higher order oligomerisation has been inhibited and that LZ5 was a dimer. Preliminary work performed using LZ3 by Arthur Rowe (University of Nottingham) showed that Nek2 LZ3 had the potential to revert back to a monomeric state at low concentrations 0.053 - 0.068 mM. The AUC also indicated that at concentrations above 0.073 mM LZ3 was dimeric. The disappearance and appearance of peaks, without increased resolution in the overlapping central region of the spectra confirms the presence of a concentration dependent oligomerisation. At a concentration of 0.1 mM the AUC indicates that the LZ5 complex is dimeric.

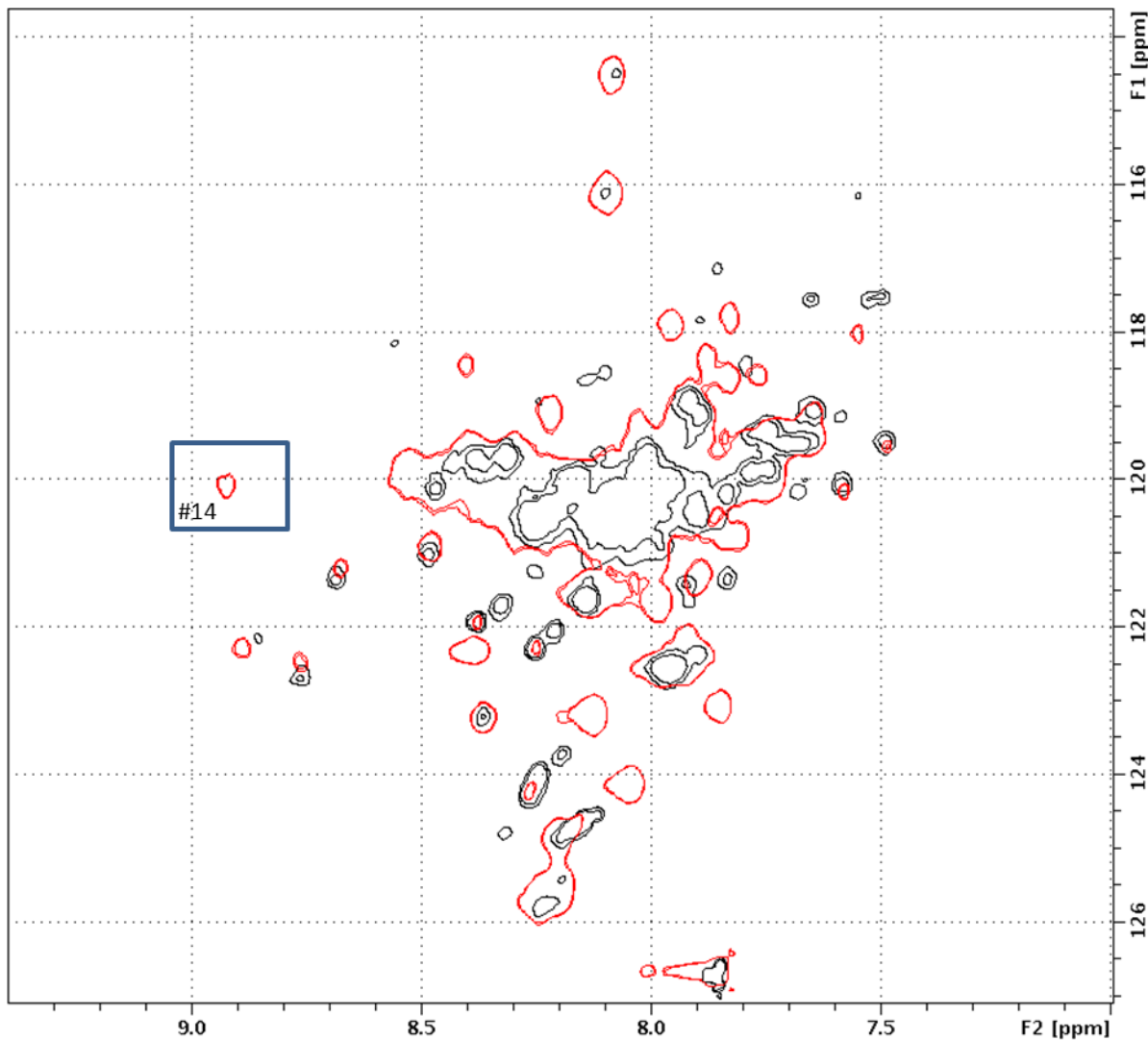


Figure 4.13 2D 1H/15N HSQC of the Nek2 LZ5 showing the effect of dilution on oligomerisation.

All of the above spectra were recorded at a temperature of 298 K with 128 scans. The red spectrum shows an HSQC of 15NLZ5 at a concentration of 1 mM, the black spectrum represents the 15NLZ5 at a concentration of 0.1 mM, Peak #14 indicated by the blue box at 120.2/8.94 ppm represents a residue previously identified to be highly susceptible to oligomerisation, upon dilution to 0.1 mM the peak is not present (Black).

4.1.6 ^1H 1D showing the effect of dilution on LZ2

A 1D of Nek2 LZ2 at was acquired at two different temperatures. Focusing on peak #14 in the proton spectrum, this peak was shown to be absent from the spectra of LZ5 at 0.1 mM concentration. The peak can be seen in the 1D when LZ2 is at a concentration of 0.5 mM (Figure 4.14A) This confirms what had been seen in the ^{15}N HSQC with LZ5 at 0.5 mM. However, when LZ2 is at a concentration of 0.14 mM peak #14 is clearly visible (Figure 4.14B). Previous analysis with LZ5 showed that peak #14 was still visible at 0.25 mM but disappeared at 0.1 mM, indicating that at concentrations between 0.25 mM and 0.1 mM the oligomerisation process persisted. For LZ2 even at concentrations replicating similar conditions at which the oligomerization in LZ5 was not perturbed (i.e. 0.14 mM) the same effect occurs with no reduction in oligomerisation in LZ2. However, when LZ2 is diluted to 0.1 mM the same effect as described for LZ5 (the disappearance of the peak #14 at 8.9 ppm) can be seen in a 2D HSQC (Figure 4.15). This would indicate that for both LZ2 and LZ5 at a concentration of approximately 0.1 mM the oligomerization is inhibited.

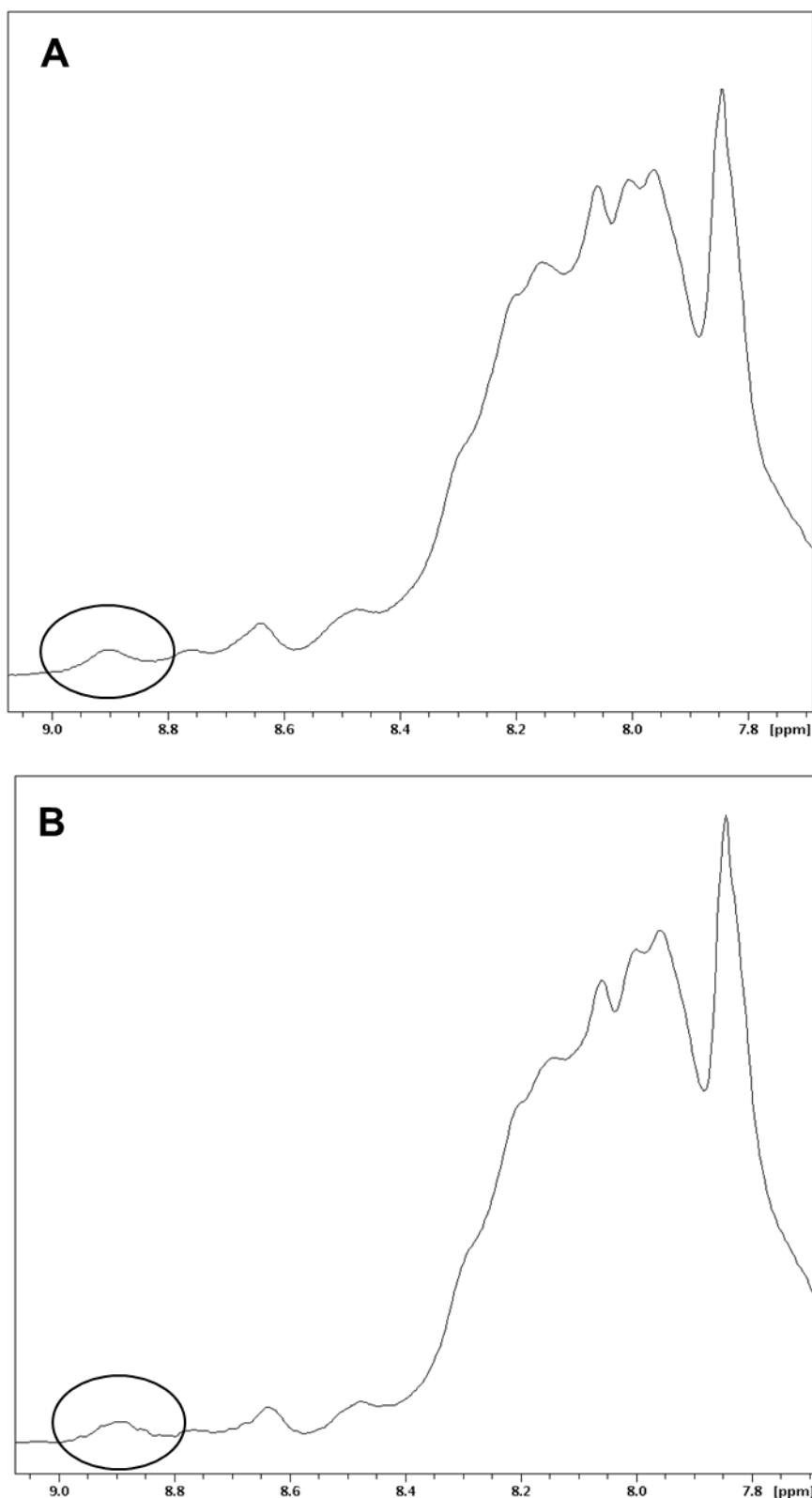


Figure 4.14 ¹H 1D spectrum of the Nek2 LZ2 showing the effect of dilution on oligomerisation.

The above spectra were recorded at a temperature of 298 K. A. LZ2 at a concentration of 0.5 mM at this concentration peak #14 (8.8 ppm) is visible and encircled in black is shown. B. LZ2 diluted approximately 5 fold to a concentration of 0.1 mM the peak #14 at 8.8 ppm remains visible and is encircled in black is displayed. Peak #14 has been shown to disappear when diluted to 0.1 mM, in this case the peak can clearly be seen at 0.5 mM and 0.1 mM.

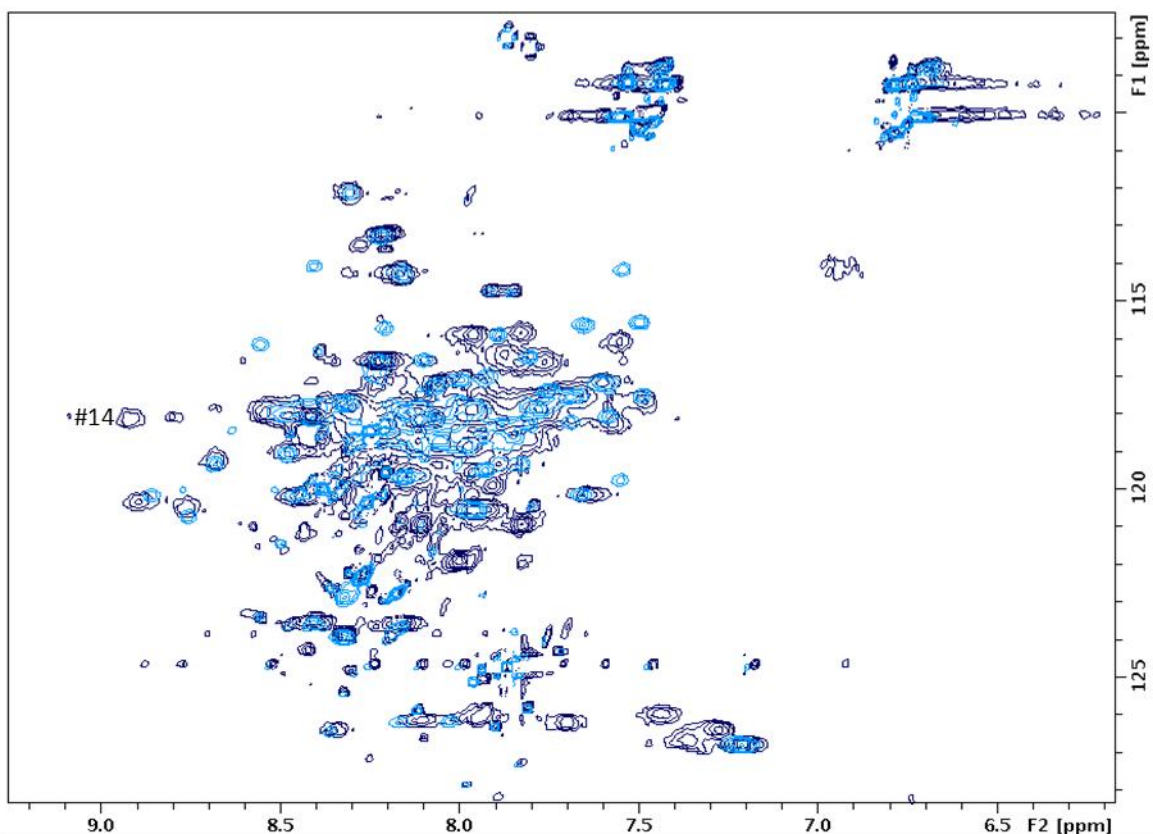


Figure 4.15 2D 1H/15N HSQC spectra of the Nek2 LZ2 showing the effect of dilution on oligomerisation.

All of the above spectra were recorded at a temperature of 298 K with 128 scans. The dark blue spectrum shows an HSQC of 15NLZ2 at a concentration of 1 mM, the light blue spectrum represents the 15NLZ2 at a concentration of 0.1mM, peak #14 at 120.2/8.94 ppm represents a residue previously identified to be highly susceptible to oligomerisation, and upon dilution to 0.1 mM the peak is not present.

4.1.7 2D $^1\text{H}/^{15}\text{N}$ HSQC of LZ5 studying the effect of temperature upon exchange

It was previously documented that a temperature shift from 293 K (25°C) to 328 K (55°C) had an effect on the two most lowfield shifted peaks #14 and #43, in that at 310 K the two peaks begin to reach coalescence and from 320 K appear as a single species at 8.9 ppm (peak #14). A 2 mM sample of Nek2 LZ5 was used to analyse the effect of decreasing temperature on LZ5 chemical exchange, decreasing temperature would hypothetically move the equilibrium to favour slow rather than intermediate exchange due to the reduced rate of molecular tumbling. The spectra were recorded at 298 K and 283 K with a total of 128 scans (Figure 4.16). A decrease in temperature results a reduction of the rate of molecular tumbling and should therefore have an effect on line broadening. At 298 K the spectra shows significant line broadening and the complete loss of a signal for peak #27, the peak intensities highlight the significant amount line broadening by the reduced peak intensity. The spectra recorded at 283 K for the same number of scans shows a reduction in line broadening with the peak intensities increasing and the resolution also increasing. The appearance of peak #27 indicates a change in the conformational dynamics on the NMR timescale by the appearance of new peaks related to one of the species of LZ5. The area highlighted in figure 4.16 with the dashed box displays a cluster of three well resolved peaks which cannot be seen in the spectra recorded at a temperature 15 degrees higher. Reducing temperature has a positive effect on the peak intensity, as the temperature decreases τ_c increases and therefore the transverse relaxation rate R_2 becomes longer. Since the linewidth is also dependent on R_2 , when R_2 is longer with lower temperature the line

widths broaden. Therefore, the decreased temperature must serve to decrease the conformational exchange and improve the line widths.

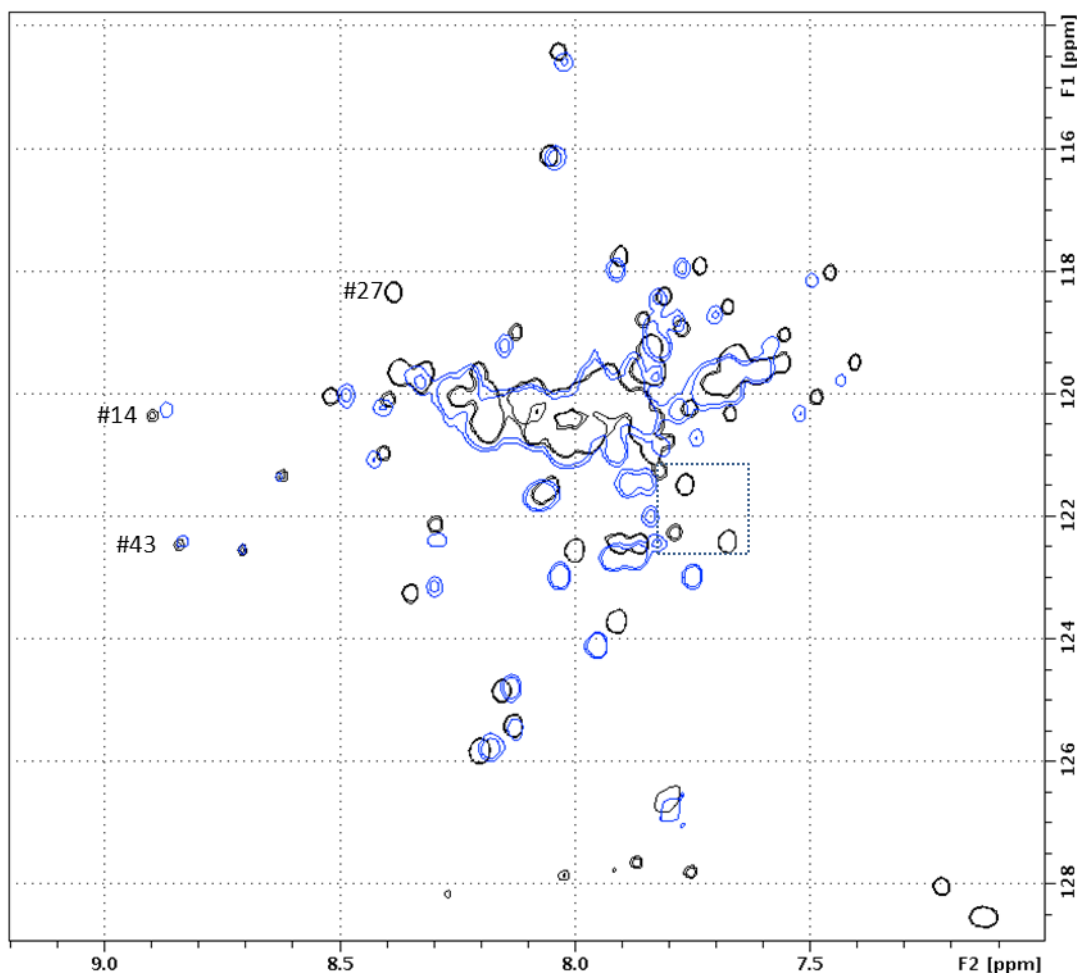


Figure 4.16 2D ¹H/¹⁵N HSQC of Nek2 LZ5 showing the effect of temperature.

The black spectrum was acquired at a temperature of 283 K with 128 scans. The spectrum shows an HSQC of 15NLZ5 at a concentration of 2 mM. The blue spectrum indicates the temperature at acquisition was 298 K. The effect of temperature on chemical exchange can be seen by a slight reduction in line broadening in the black spectrum and loss in resolution of the peaks in the central area of the spectrum at 298 K. The dashed box indicate the appearance of peaks at T = 283 K.

4.1.8 2D 1H/15N HSQC of LZ5 studying the effect of acetonitrile upon exchange

Acetonitrile is commonly used to induce helicity and to increase solvation of peptides and larger protein entities. Acetonitrile was used to limit self association/ aggregation at higher concentrations such as those used in NMR using LZ5. To determine if the exchange was due to aggregation in the alpha helix, high concentrations of up to 30% (v/v) acetonitrile should force the equilibrium towards pure dimeric state by buffering any exposed hydrophobic residues. Multiple HSQC spectra were recorded at 298 K with 128 scans using an Acetonitrile concentration gradient from 0 - 30% (v/v) (Figure 4.17). The concentration of LZ5 was kept constant at 2 mM throughout the experiment. At concentrations of 0, 5 and 10% acetonitrile there is no difference in the appearance of the spectra. At acetonitrile concentrations of 15% (v/v) the peak at 8.9/121 ppm is visibly reduced in intensity and in parallel two new resolved peaks upfield can be seen at 7.7/119 ppm and 7.55/119 ppm. Upon increasing the concentration of acetonitrile to 20% the peak #14 disappears, the same observation was made when the leucine zipper was diluted to 0.1 mM, and the peaks at 7.7/119 ppm and 7.55/119 ppm increase in intensity. This phenomenon continues up to an acetonitrile concentration of 30%.

1D projections taken from the nitrogen plane of the HSQC, indicate in detail the extent of the line broadening due to the change in acetonitrile concentrations. Figure 4.18A focuses on the peak which has been shown to be sensitive to changes in the concentration of LZ5 and at 0.1 mM is not present in the spectra of LZ2 and LZ5. The same effect occurs when the acetonitrile concentration reaches 20% for LZ5. At concentrations from 0 - 15% acetonitrile peak #14 starts to reduce in intensity, as the peak volume remains constant the

increasing concentration of acetonitrile results in the reduction of peak intensity and therefore an increase in line broadening. Figure 4.18B highlights a peak that is not visible at concentrations ranging from 0 and 5% of acetonitrile. At concentrations of 15% acetonitrile the peak at 7.6/117.5 ppm emerges from the baseline noise. Therefore, at concentrations of 15-30% (v/v) acetonitrile replicated the effects of dilution to 0.1mM, but indicated that the conformational exchange still persists and is not a result aggregation due to the presence of too many peaks in the HSQC spectrum.

4.1.9 The effect of increasing temperature at 30% acetonitrile concentration

The superimposed spectra (Figure 4.19) display spectra ran at increasing temperatures from 303, 310, 315 and 320 K at 600 MHz. The presence of acetonitrile caused the disappearance of one peak and the appearance of two peaks as previously described. However, the process of conformational exchange still occurs by the clear presence of more than 40 amide proton specific peaks, which constitute the backbone of LZ5. At 303 K peaks with large line broadening are seen with an obvious reduction as the temperature increases to 320 K (Figure 4.12A). In the 1D slice in the hydrogen dimension, one of the backbone amino acids for LZ5 can be shown as a doublet resonance (Figure 4.19B) as the temperature increases the peak begins to coalesce and at 315 K can be seen as one resonance although with a large linewidth. At 320 K in the presence of acetonitrile one resonance can be seen as the rate of the conformational exchange has increased and a weighted average of the individual species can be seen. However, observations of precipitation during experiments at 320 K of the LZ5 protein made longer more complex NMR experiments not viable.

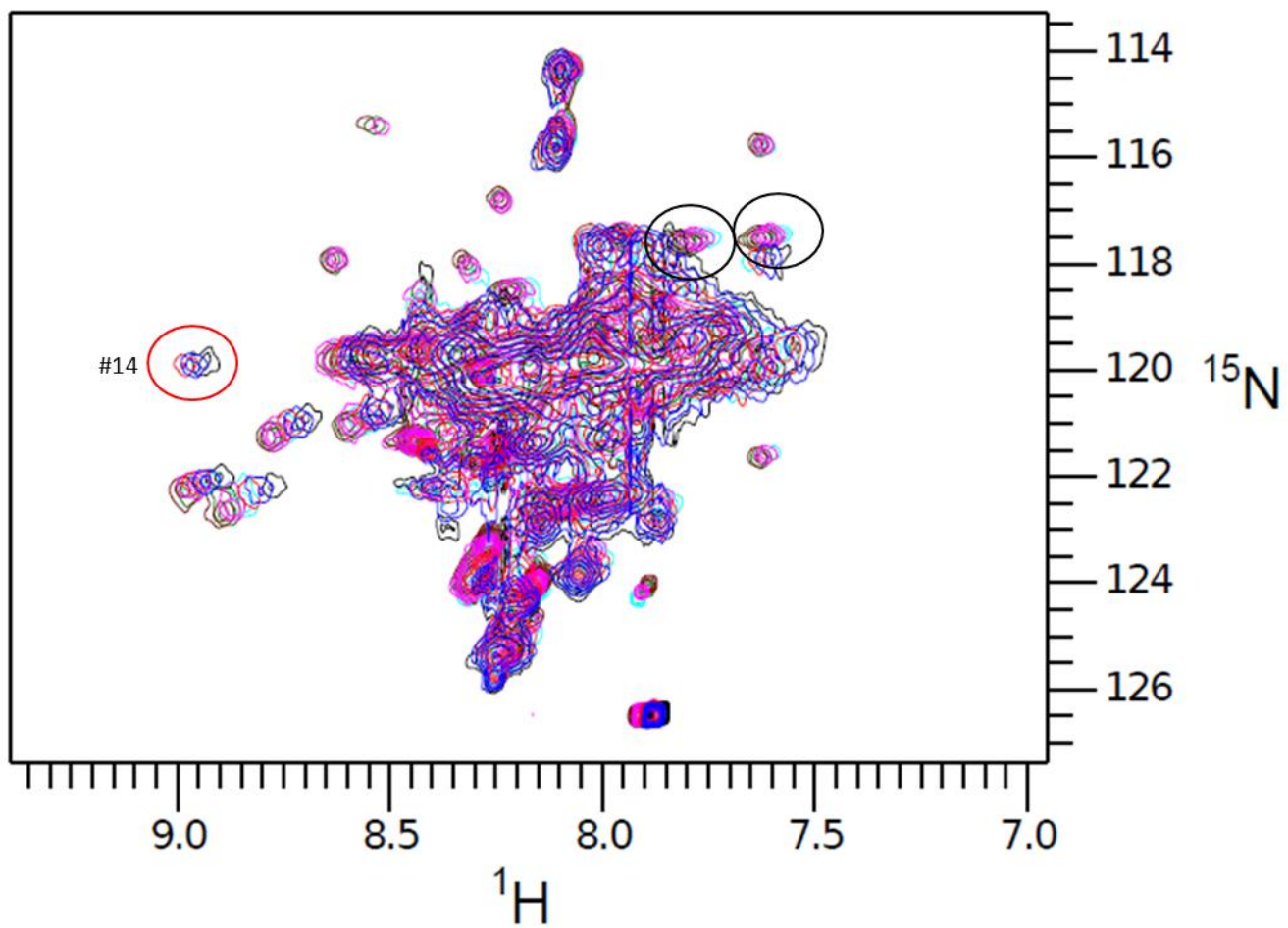


Figure 4.17 2D $^1\text{H}/^{15}\text{N}$ HSQC of Nek2 LZ5 showing the effect of acetonitrile concentration.

All the above spectra were recorded at a temperature of 298 K with 128 scans, $^{15}\text{NLZ5}$ was at an initial concentration of 2 mM. The black spectrum shows an HSQC of $^{15}\text{NLZ5}$ at an acetonitrile (AN) concentration of 0% (v/v), blue = 5% (v/v), red = 10% (v/v), cyan = 15% (v/v), magenta = 20% (v/v), green = 25% (v/v) and the spring colour = 30% (v/v).

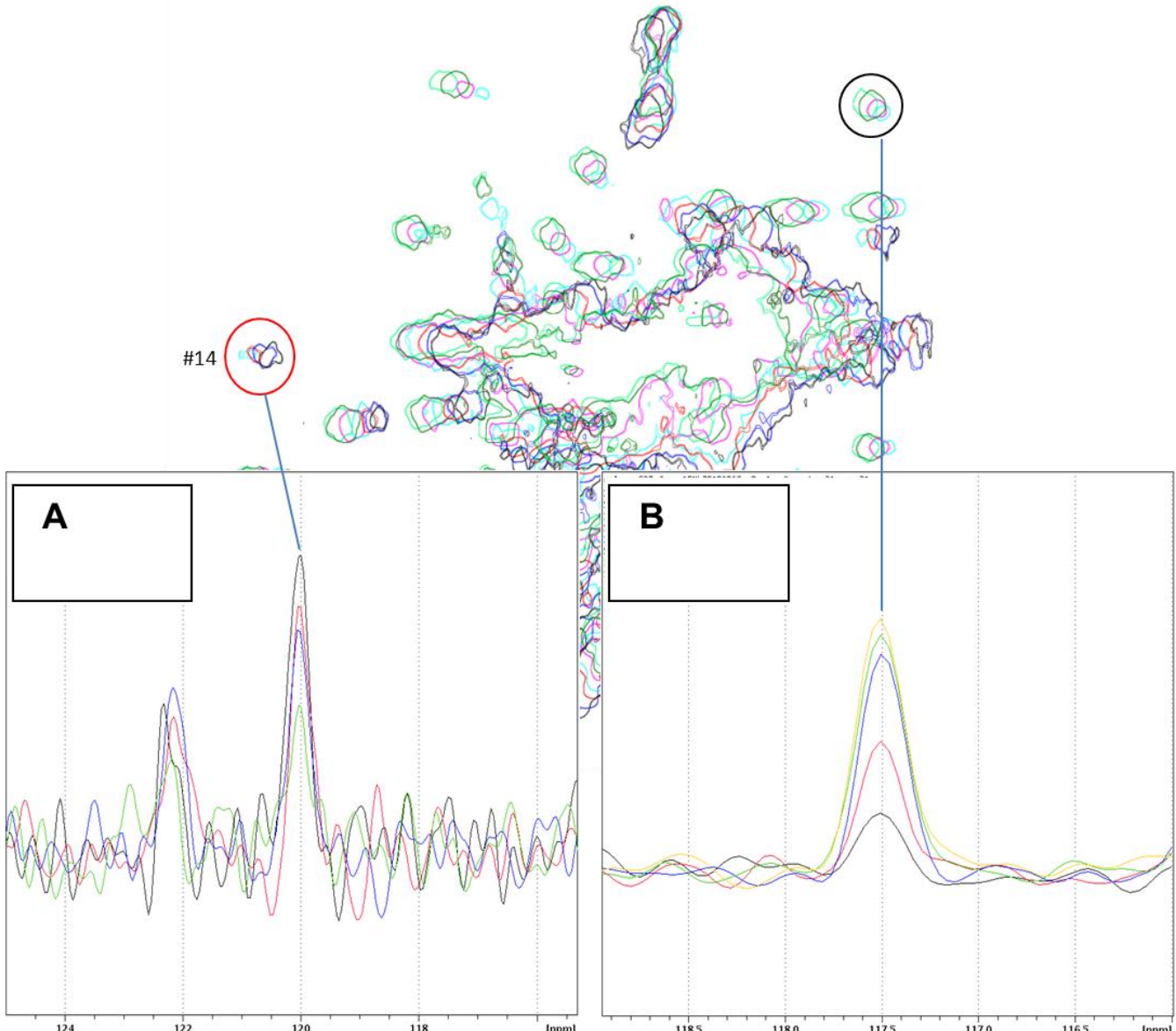


Figure 4.18 1D ^{15}N slice of LZ5 showing the effect of acetonitrile concentration upon line broadening.

All the above spectra were recorded at a temperature of 298 K with 128 scans, $^{15}\text{NLZ5}$ was at a concentration of 2 mM. A. Here a 1D slice through the H plane at 8.9 ppm peak #14 indicates the effect acetonitrile on peak intensity. At 0% acetonitrile (black), 5% (red), 10% (blue), 15% (green). B The appearance of a peak upon the addition of acetonitrile from 10% (black), 15% (red), 20% (blue), 25% (green) and 30% (yellow) encircled in black.

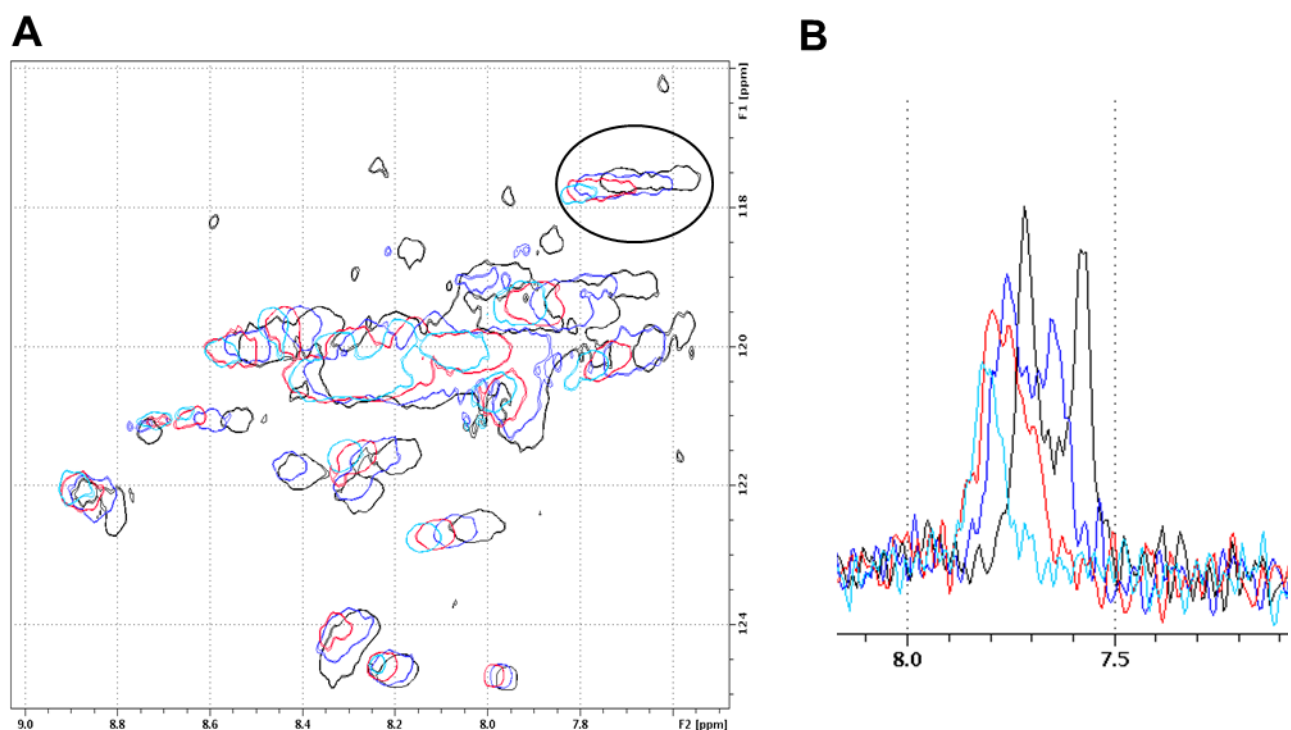


Figure 4.19 2D $^1\text{H}/^{15}\text{N}$ HSQC of LZ5 showing the effect of increasing temperature with 30% acetonitrile.

A. An overlay of $^{15}\text{NLZ5}$ recorded at differing temperatures is shown. The black spectrum was acquired at T=303 K, the blue spectrum was recorded at T=310 K, the red spectrum was acquired at T=315 K and finally the cyan spectrum at T=320 K. B. A 1D slice at 118.5 ppm in the nitrogen plane is displayed, here a peak transitions from a doublet to a singlet with increasing temperature (Black circle in panel A).

4.1.10 The effect of decreasing temperature at 30% acetonitrile concentration

Previous experiments showed that the addition of acetonitrile has the same effect on the spectra as reducing the concentration to 0.1 mM, in both experiments the disappearance of the peak #14 and two new resolved peaks upfield at 7.7/119 ppm and 7.55/119 ppm. Acetonitrile could serve to buffer any exposed hydrophobic residues leading to the observation of the same effect as dilution, in that, what we are observing is a concentration dependent oligomerization. However, what cannot be explained is that even at low protein concentrations and at high acetonitrile concentrations we still observe too many peaks corresponding to the backbone of the leucine zipper. Therefore, the chemical/conformational exchange process continues. To perturb possible oligomerisation and investigate the effect of temperature on LZ5, $^1\text{H}/^{15}\text{N}$ HSQC experiments were acquired with a 2 mM concentration of LZ5 and 30% acetonitrile concentration (v/v). Spectra were acquired at four different temperatures starting at 298, 293, 288 and 283 K. A superimposition of the four spectra (Figure 4.20) indicate that at temperatures of 288K (10°C) the peak intensities decrease when compared to the spectra acquired at 298K (25°C) but the same number of peaks can still be observed at both extremes of temperature. This indicates from observing the number of peaks present in the HSQC spectra, that at temperatures ranging from 298 K to 283 K the conformational dynamics is not significantly affected. Therefore, even under these conditions an inherent exchange process still persists.

A 1D slice into the hydrogen plane for a peak involved in chemical exchange (Figure 4.21A), the peak at 7.7/119ppm appears upon the addition of acetonitrile concentrations exceeding 15% (v/v). As the temperature decreases from 298K to 283K the shape of the does not

change greatly but does slightly reduce in peak height at lower temperatures due to the increase in R_2 and R_1 relaxation rates

The analysis of the effect of a second peak described as a peak that is not noticeably involved in oligomerisation and not subject to conformational exchange only to standard relaxation events as permitted by the pulse program (Figure 4.21B). What is evident is that the linewidth is reduced at lower temperatures however the signal intensity is also reduced at lower temperatures. The reduction in rotational correlation time would influence the relaxation rates and therefore the signal intensity.

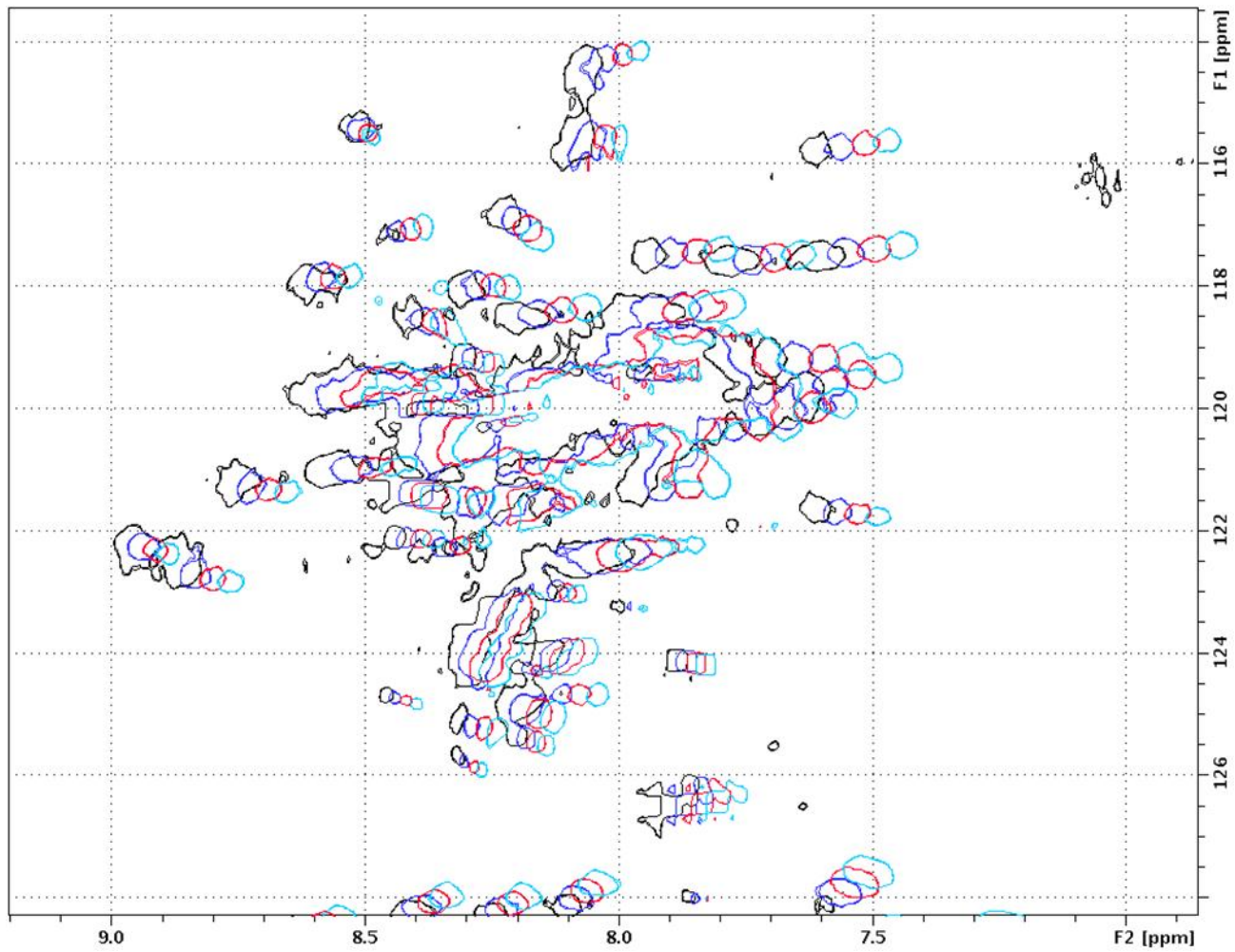


Figure 4.20 2D 1H/15N HSQC of LZ5 showing the effect of decreasing temperature with 30% acetonitrile.

An overlay of 15NLZ5 spectra recorded at differing temperatures. The black spectrum was acquired at T=298 K, the blue spectrum was recorded at T=293 K, the red spectrum was acquired at T=288 K and finally the cyan spectrum at T=283 K. As the temperature reduces from 298 K to 283 K a significant reduction in line broadening can be seen.

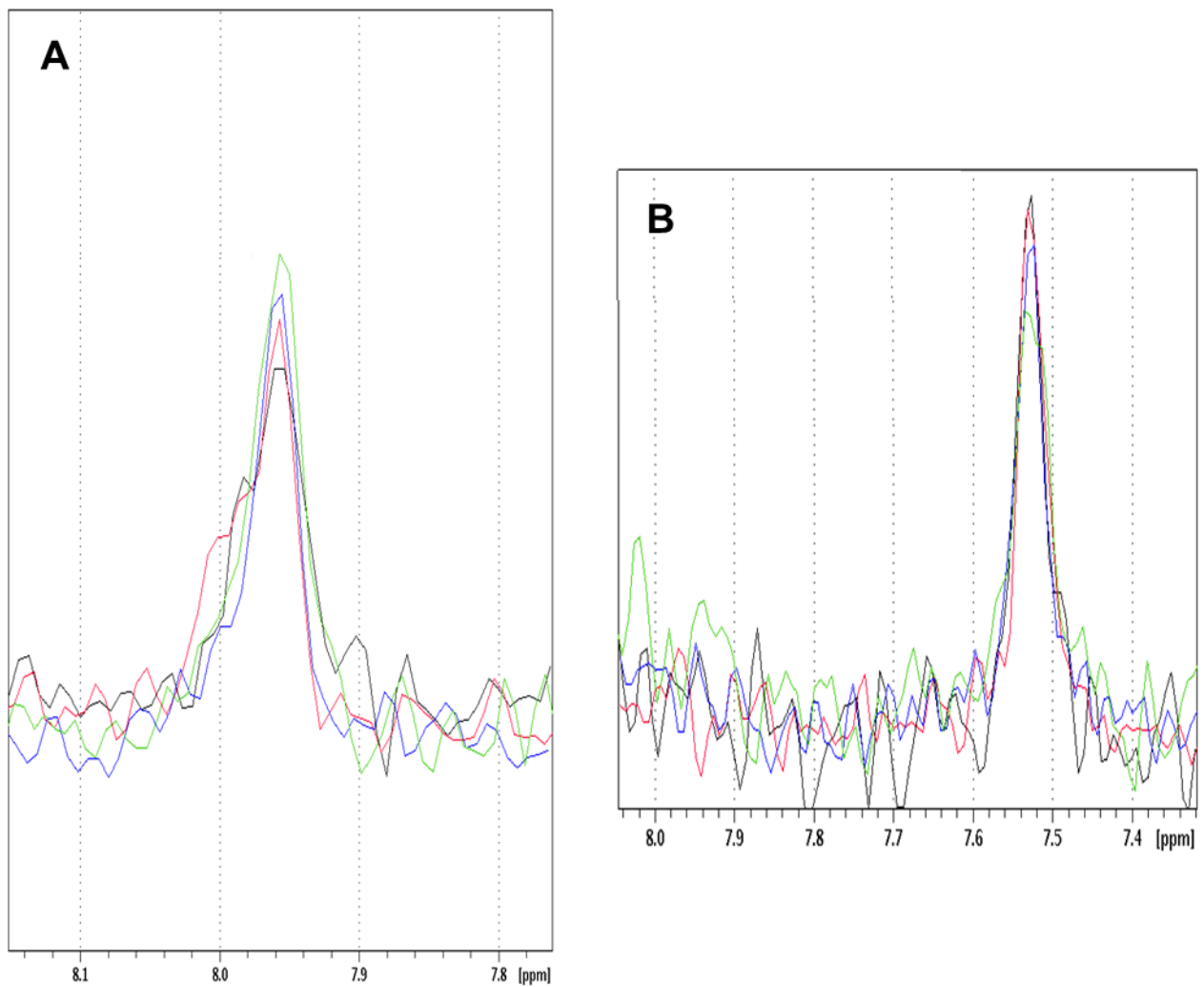


Figure 4.21 1D slice of an HSQC of LZ5 showing the effect of decreasing temperature with 30% acetonitrile.

A. An overlay of ^{15}N LZ5 recorded at differing temperatures is shown. The black spectrum was acquired at T=298 K, the red spectrum was recorded at T=293 K, the blue spectrum was acquired at T=288 K and finally the green spectrum at T=283 K. A. The effect of temperature on an exchanging peak is shown. B. The effect of temperature on a 'normal' peak is displayed.

4.1.11 The influence of pH upon HSQC line widths and the number of peaks present

Many early solution structures of alpha helices were elucidated at a low pH (Ciesla et al., 1991; Yamaguchi et al., 1998). Acidic pH was identified to aid helix formation and provides enhanced resolution to reduce spectral overlap, for example, the c Myc-Max heterodimeric leucine zipper NMR solution structure (Lavigne et al., 1998). The LZ5 construct was measured at physiological pH 7.0 and an acidic pH of 3.0 and the spectra from $^1\text{H}/^{15}\text{N}$ HSQC experiments were superimposed to analyse the effect of the reduction in pH. The LZ5 sample contained 30% acetonitrile to minimise any possibility of oligomerization (Figure 4.22). The superimposition of the spectra show major changes in the chemical shifts at pH 7 and at pH 3, however, the spectral overlap is not improved by the lower pH. In the presence of 30% acetonitrile and at pH 3 the chemical environment in which the LZ5 backbone resides is distinctly different than at pH 7. This is indicated by the extent of the chemical shift variation when the pH is lowered. It is difficult to postulate that this is due to the loss of helicity without the CD data to confirm the observation; however, it is possible that this effect could occur. CD data previously described showed a loss of helicity at lower pH units in the absence of acetonitrile, a co-operative thermal denaturation curve was absent at pH 3.0 transitioning to a linear gradient, unfold at lower temperatures. However, the % helix was not determined in the presence of acetonitrile.

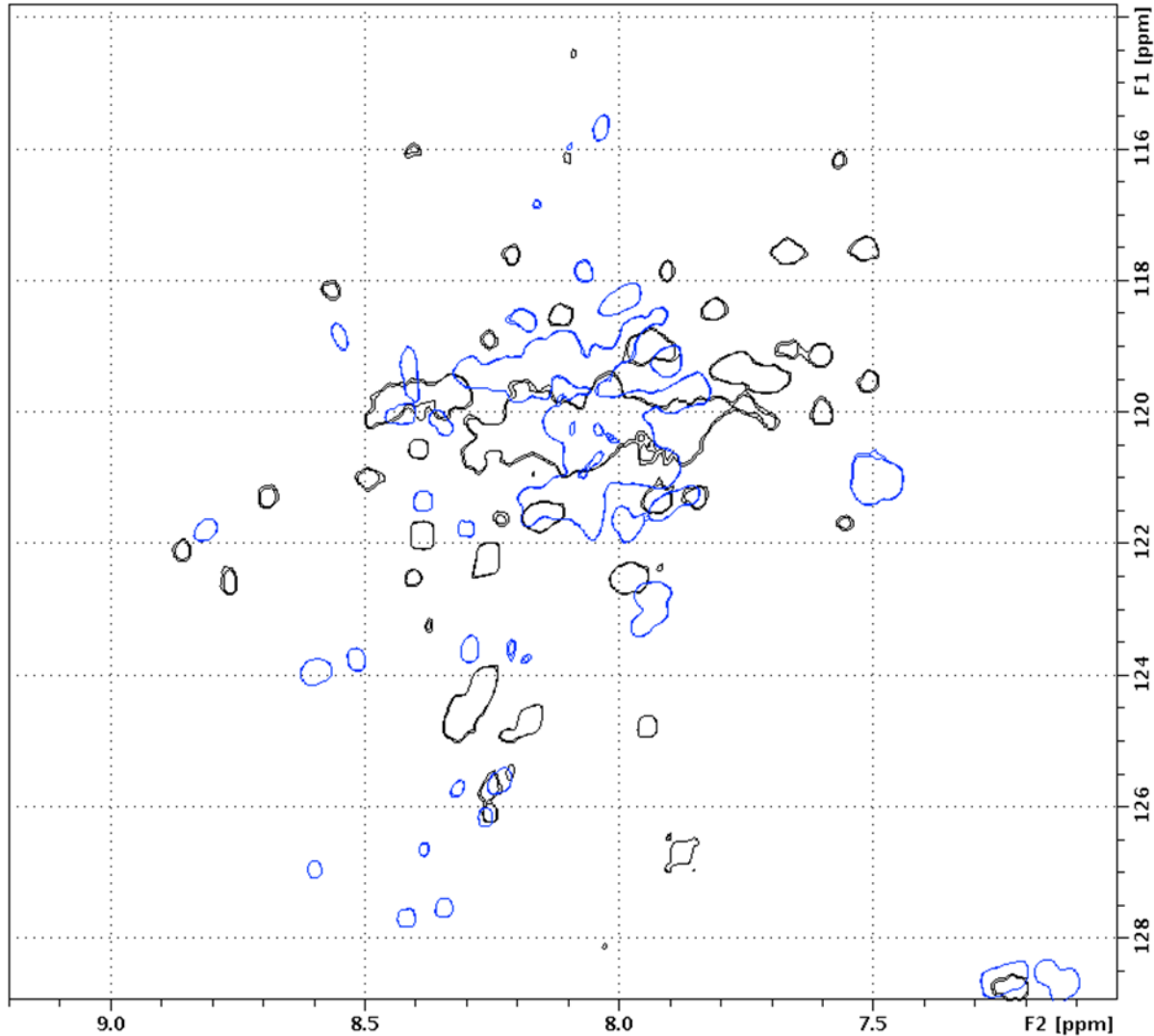


Figure 4.22 2D $^1\text{H}/^{15}\text{N}$ HSQC of LZ5 showing the effect of pH.

The above spectra were recorded at a temperature of 298 K with 30% acetonitrile. The black spectrum shows Nek2LZ5 at a concentration of 2 mM at a pH of 7.0. The blue spectrum was acquired at a pH of 3.

4.1.12 Investigating the nature of exchange in LZ5

To analyse the potential isoforms of LZ5 a ^{15}N labelled sample was prepared a reference HSQC is shown in figure 4.23 to indicate the peak numbers and peaks found to be connected through two site exchange. In an HSQC experiment, automatic peak peaking with CCPN analysis (Vranken et al., 2005) gave >75 peaks. The construct LZ5 has 46 residues in the backbone, from the analysis of this region of the spectrum giving almost double the number of expected peaks, confirms the presence of at least two forms of the protein (Figure 4.24A). To investigate if the two isoforms were in dynamic equilibrium, two NMR exchange experiments were recorded which is described in detail in section 2.4.2.13 (Farrow et al., 1994). The 2D spectrum has the appearance of an HSQC experiment because of the frequency labelling of the nitrogen in t1 (Figure 4.24B), or can take the form of a NOESY experiment with frequency labelling of the amide proton in t1 (Figure 4.24C). When taken together the experiments demonstrate that a substantial number of residues in LZ5 undergo slow exchange on a chemical shift time scale (Figures 4.24B and C). To improve characterisation of the nature of the exchange present in LZ5, both versions of the exchange experiment were combined into a 3D ^{15}N NOESY-HSQC (Figure 4.24D). The 2D correlation experiment was used to generate spectra which identify more than 34 exchange specific pairs of resonances, the total number of backbone amino acids present in the construct LZ5 are 46, suggesting that almost the entire length of the protein undergoes exchange (full peak lists for the exchange experiments are shown in A10 and A11). The number of exchange specific peaks indicates that only two isoforms are present in solution and the

presence of genuine amide-amide sequential NOE crosspeaks of equal intensity suggests that the isoforms are present in equal amounts.

A series of exchange experiments were performed with differing mixing times to elucidate the exchange rate (K_{ex}) and ^{15}N longitudinal relaxation rate (R_1). Qualitative analysis of exchange was generated by fitting cross- and diagonal peak intensities of pairs of exchanging resonances. Figure 4.17 displays one of the four pairs which was analysed. The values of K_{ex} were 18.2, 17.4, 16.9 and 17.2 s^{-1} , the average values could be determined because the values of K_{ex} were well within the error of the fitting procedure of the exchange rates, these gave a single rate constant of $17.4 \pm 1.7\text{ s}^{-1}$ indicating a single cooperative exchange event. ^{15}N R_1 values obtained for the same system were 1.5, 1.7, 1.4 and 1.6 s^{-1} , averaging $1.6 \pm 0.3\text{ s}^{-1}$. Fitting the peak intensities of resolved diagonal peaks directly to an exponential decay to obtain the effective R_1 gave values of 14.9, 16.8, 15.3 and 16.1 s^{-1} which averaged $15.8 \pm 1.6\text{ s}^{-1}$, approximately ten times the nominal value. The direct measurement of ^{15}N R_1 and R_2 values gave an average of $15.0 \pm 0.7\text{ s}^{-1}$ for R_1 and $30.4 \pm 0.8\text{ s}^{-1}$ for R_2 . Four exchanging spin systems were used to calculate the relaxation rates (Figure 4.25).

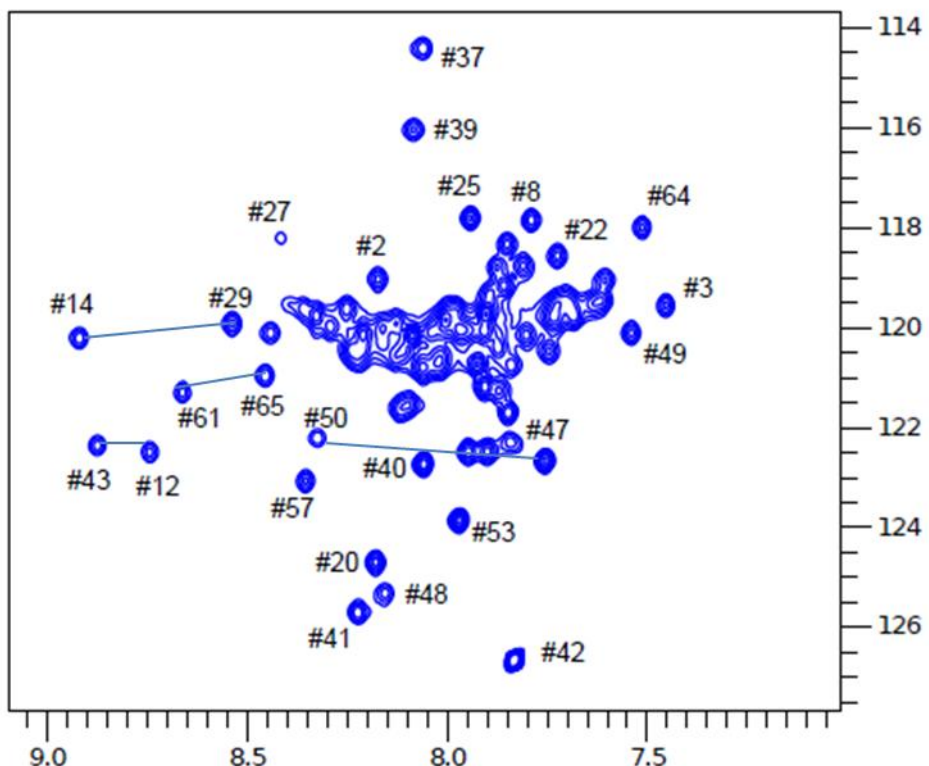


Figure 4.23 2D heteronuclear correlation experiment of Nek2 LZ5 reference HSQC

The spectrum shown was recorded at a temperature of 298 K with 128 scans. The figure displays an HSQC of 15NLZ5 at a concentration of 2 mM. N-H chemical shifts were assigned a number for uses as a reference depicted as # followed by the number. The peaks connected with a blue line were found to have exchange specific peaks when comparing the HSQC with the exchange HSQC and the two site exchange rates were calculated.

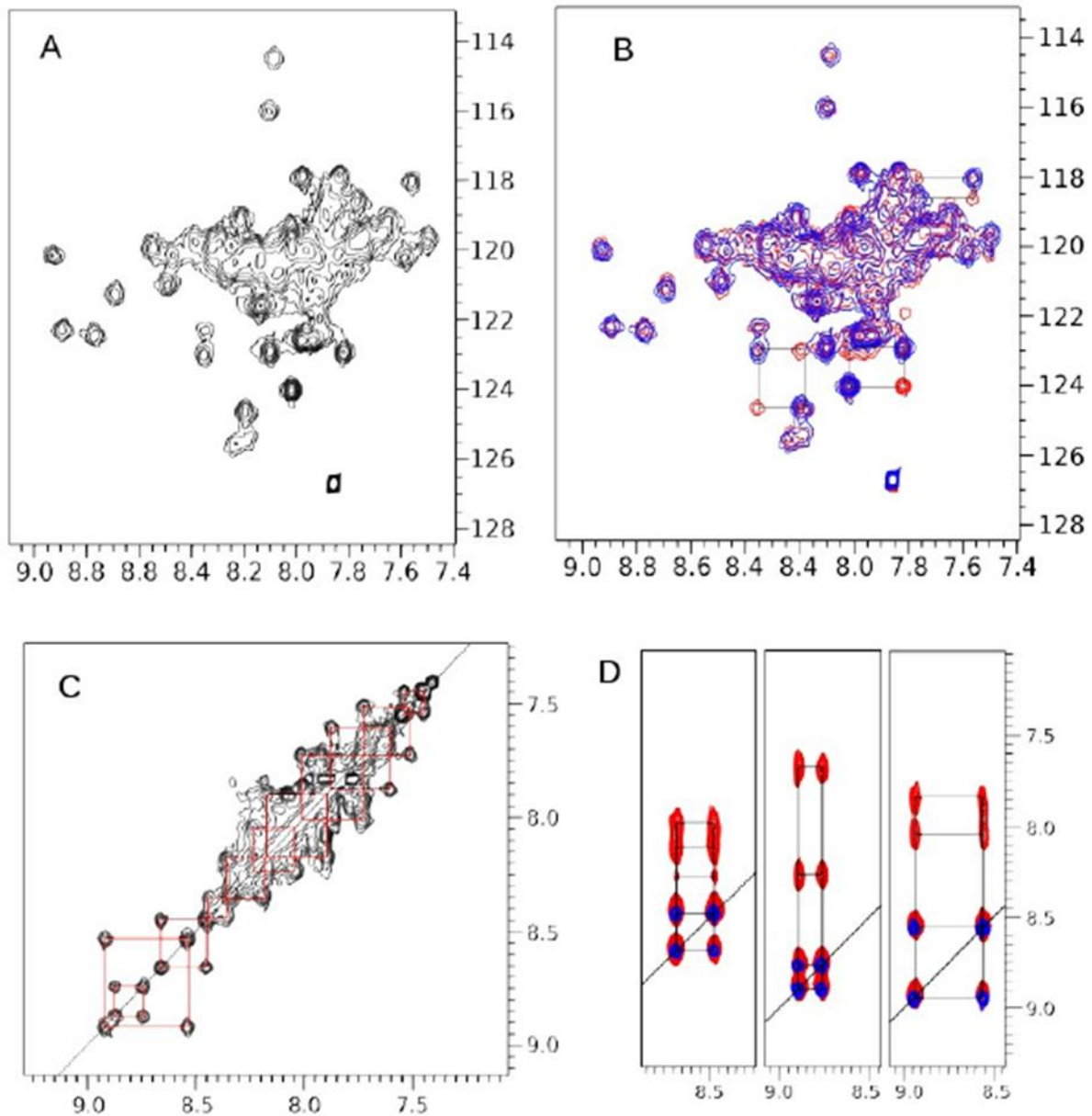


Figure 4.24 ^{15}N relaxation experiments using LZ5

A. The HSQC spectrum at 278 K, 600 MHz is shown. B. shows a ^{15}N heteronuclear correlation experiment shown as HSQC view (red), mixing time 60 ms, superimposed on HSQC (blue). Exchanging species are connected by black boxes for a few residues from the HSQC to the exchange HSQC. C. The ^{15}N heteronuclear correlation experiment shown in NOESY view with a mixing time of 60 ms is displayed. The red squares indicate exchange for eleven residues. D. The superimposition of 1H-1H slices of the ^{15}N heteronuclear correlation experiment with a 64 ms mixing time (blue) and a ^{15}N NOESY-HSQC with a 100 ms mixing time (red) (kindly processed by Mark Pfuhl).

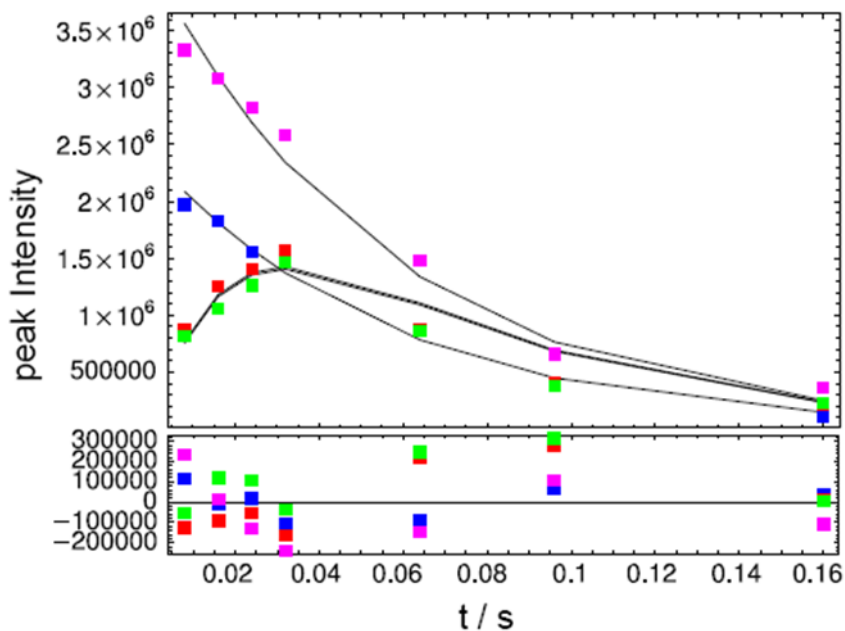


Figure 4.25 ^{15}N relaxation experiments using LZ5 for peaks #12 and #43

The figure indicates the time dependence of exchange (red, green) with a 64 ms mixing time and variable delay and diagonal auto peaks (pulse sequence without mixing time T (blue, magenta) intensity of a selected residue (boxes) compared to the results of fits (continuous lines). Fitting errors are shown. (kindly processed by Mark Pfuhl)

4.1.13 Investigation of the exchange in ‘locked’ LZ5 conformations through mutation

The presence of two possible conformations of the leucine zipper interface was discussed in detail in Chapter 3. Analysis of the secondary structure indicated that dimerization is possible by two independent interface interactions termed Hepl and HepII. Initial spectra showed the extensive overlap of peaks which is normal for coiled-coils, however, amplified by the presence of two similar isoforms of the same protein in solution. The chemical exchange is in the range of slow exchange but is close to the transition region to intermediate exchange, resulting in the further reduction of signal intensity.

Site-directed mutagenesis was performed on the construct LZ5 to generate mutants to ‘lock’ the isoforms into their respective leucine zipper register, either Hepl or HepII. In both mutants the natural cysteine residue in position 335 was mutated to alanine (C335A) to avoid the formation of wrongly paired cystine bridges. Two mutants were prepared: K309C to represent Hepl and E310C to represent HepII. ^{15}N labelled samples of the mutants were prepared and HSQC experiments acquired (Figure 4.26). For the mutant K309C a reduction in the overall number of peaks in the HSQC can be seen indicating a reduction in exchange. The HSQC experiment for E310C appears to be more complex the spectral resolution has been reduced giving a range of 7.73-8.5 ppm in the hydrogen dimension which would indicate that the addition of a cysteine residue in position 310 of LZ5 has a destabilising effect and results in incorrect folding. This was confirmed by the CD spectra demonstrating that in an oxidised buffer only a modest amount of α -helix at lower temperatures as previously described.

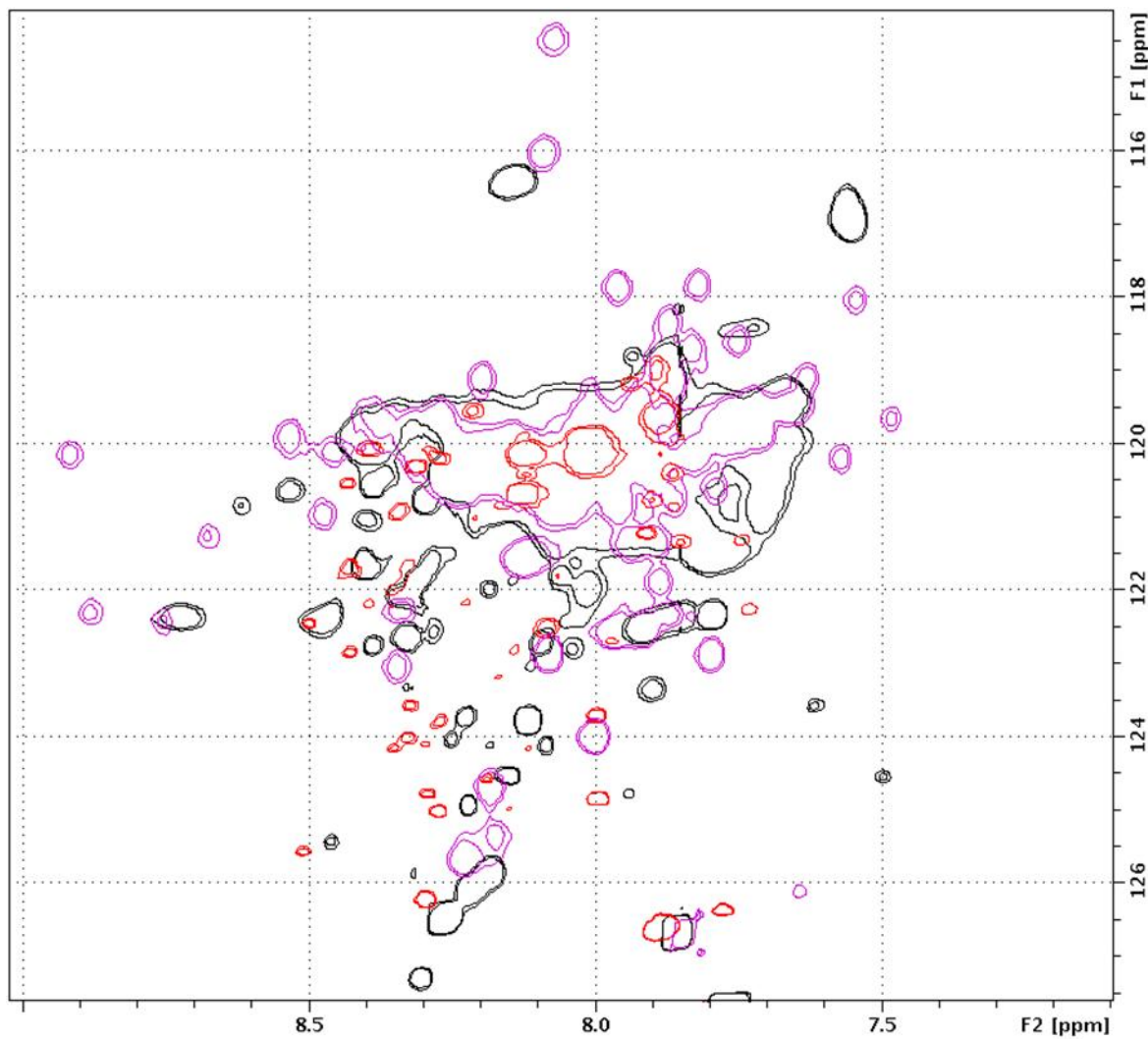


Figure 4.26 2D $^1\text{H}/^{15}\text{N}$ HSQC of LZ5, LZ5K309C and LZ5E310C

The above spectra were recorded at a temperature of 298 K at 500 MHz. The purple spectrum shows Nek2LZ5 at a concentration of 2 mM at a pH of 7.0. The black spectrum displays LZ5K309C at a concentration of 2 mM and a pH pH 7.0. The red spectrum was recorded with the construct LZ5E310C at a concentration of 2 mM also at a pH of 7.0.

To probe the effect of the addition of a disulphide bond in LZ5 K309C on the exchange dynamics, an HSQC spectrum was recorded in oxidising buffer (Figure 4.27A). The HSQC shows a reduction in the total number of peaks when compared to the wildtype LZ5. CCPN software produced a total of just over 40 peaks by automatic peak picking; in comparison the wild-type LZ5 yielded over 75, suggesting that the K309C mutant contained only one isoform. Direct comparison of LZ5C335A and LZ5C335AK309C (Figure 4.27B) revealed that in the resolved region on the left one peak of an exchanging pair had gone leaving only one peak (bracketed). The line broadening for the K309C spectrum was visibly reduced leaving well resolved sharp peaks, signalling that the exchange dynamics had been altered significantly by the mutation. The HSQC exchange spectrum displayed in the NOESY view (Figure 4.27C) of the mutant showed no exchange specific cross peaks, supporting the hypothesis that the K309C mutants locks one conformation and that the extensive line broadening observed with the wild-type LZ5 was due to conformational exchange.

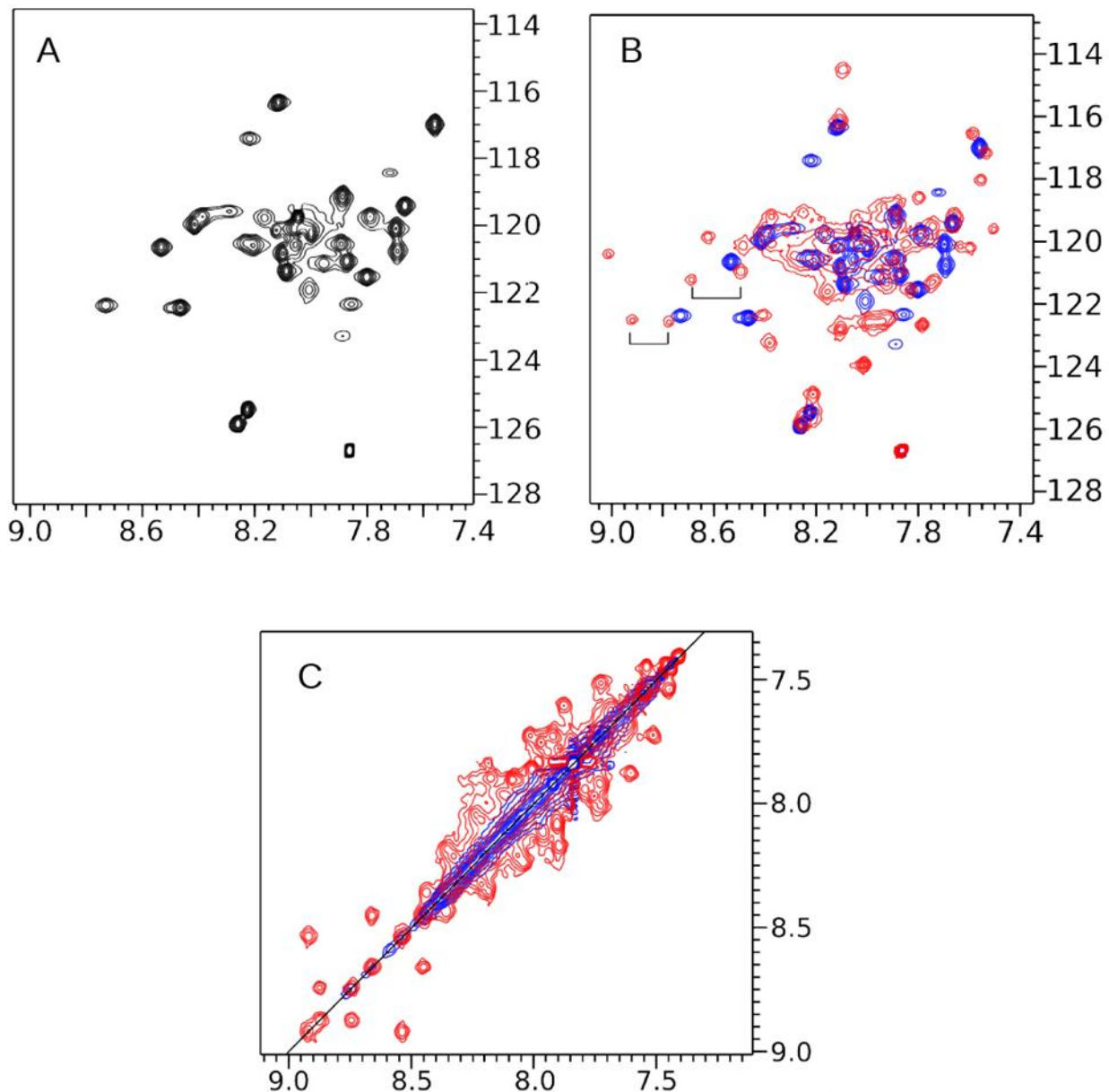


Figure 4.27 ^{15}N heteronuclear correlation experiments using LZ5K309C

A. ^{15}N HSQC of LZ5K309C in oxidised buffer at 298 K is represented. B. The wildtype LZ5 recorded in the same conditions as LZ5K309C is displayed, two sets of brackets indicate sets of well resolved exchanging pairs. C. A ^{15}N exchange experiment in the NOESY view of oxidised LZ5K309C (blue) superimposed on the same experiment for the wildtype LZ5 (red) is depicted.

4.2 Discussion

4.2.1 Exchange dynamics present in the Nek2 leucine zipper

The first indications that the Nek2 leucine zipper was subject to conformational exchange dynamics were generated from early experiments using $^1\text{H}/^{15}\text{N}$ TOCSY for the construct LZ2. The TOCSY experiment gave rise to crosspeaks between signals from backbone amide groups, which can only arise through chemical exchange processes (Feeney et al., 1991). The peaks were of equal intensity indicating that the exchanging species were present in equal populations. In the early experiments 2D NOESY experiments were used to probe the nature of the dynamics and pertain whether the exchange was due to oligomerization states. To do this measurement of relaxation time T_1 in the laboratory frame were performed. τ_c or the motional correlation time was determined for LZ2. However, due to the shape of the LZ2 protein or due to measuring too few peaks to average out the chemical shift anisotropy the estimated molecular weight was significantly greater than that estimated by SEC and AUC.

4.2.2 Investigation into the NMR oligomerization state of the Nek2 leucine zipper

Dilution of the LZ2 and LZ5 constructs lead the reduction in peaks but also conversely the appearance of peaks in the HSQC experiment, the same phenomenon occurred when acetonitrile was added at concentrations over 20% (Figures 4.13 and 4.17). Temperature adjustments were used to assess the effects of linewidth at increased and lower temperatures. Unfortunately the conformational exchange has a chemical shift timescale that is towards slow-intermediate exchange which could not be altered sufficiently to drive

the conformational dynamics into purely fast or purely slow exchange. Furthermore, pH had no significant effect on the conformational dynamics. Therefore, more complex 2D heteronuclear experiments were used to investigate the exact nature of the conformational dynamics. The two Nek2 mutants were analysed using 2D heteronuclear correlation spectroscopy where the two site exchanging spin systems were recorded with series of mixing times and cross referenced against an exchange experiment without a mixing time period T. The exchanging spin systems had R1 relaxation rate at ten-fold the ‘normal’ values when compared to the reference experiment, confirming that further investigation or elucidation of the structure of the Nek2 leucine zipper would not be possible using the non-engineered constructs. An HSQC exchange experiment was recorded for the mutant LZ5 C335K309C which did not show any exchange related cross peaks in the spectrum, indicating that if the 3D structure was required in future the construct LZ5 C335K309C would be a good candidate.

CHAPTER 5

FINAL DISCUSSION

5.1 Final discussion

5.1.1 Sequence specific interactions within the Nek2 leucine zipper

Sequence analysis indicates that the Nek2 leucine zipper is a non-ideal coiled-coil, the usual inclusion of hydrophobic residues in the *a* and *d* core residues are not conserved. The importance of non-polar residues at the core of coiled-coils is clear with the *a*- and *d*-positions contributing to oligomerization state and stability. The analysis of the effect of positioning on oligomerization state indicated that the γ -branched leucine residue is favoured in the perpendicular geometry, in the *d*-position for a dimer and the *a*-position for the tetramer (Harbury et al., 1993). A more recent statistical assessment indicated that the positioning of the leucine residue did not affect stability, and there was no statistical significance in frequency of occurrence in either position (Tripet et al., 2000). Taken together these data suggest that the presence of the polar amino acids as core residues in the Nek2 leucine zipper, influence the oligomerization state and stability significantly more than the conserved stretch of leucine residues.

Although coiled-coils existing with polar, charged residues in the core are a minority group they account for 20% of all coiled-coils studied to date (Akey et al., 2001). The function of such an interface is to increase specificity with the coiled-coil being the most common oligomerization subunit; with regards to cell division it is essential to maintain specificity. However, the inclusion of core polar residues to increase specificity simultaneously reduces stability. It was observed that leucine was favoured in the *d*-position (Woolfson and Alber, 1995), in the Nek2 leucine zipper it is hypothesised that this is occupied by: leucine in Hepl and glutamic acid in HepII, lysine exists in position *d* in Hepl and position *g* in HepII.

Modelling of the Nek2 leucine zipper domain, based on the assumption that leucine residues occupy the d-position and that the a-position is occupied by basic glutamic acid residues, suggested that the Nek2 leucine zipper would primarily adopt a parallel orientation. Although, not conclusively proven, modelling indicated that an antiparallel orientation would result in highly unfavourable juxtaposition of like-charges i.e. g-g' basic interactions (Fry et al., 1999). In the parallel orientation, substantial interactions are unlikely due to the e-position consisting primarily of uncharged residues, and residues with the same charge as in the g-position inducing electrostatic repulsion. Classical coiled-coil interactions between a-d and g-e positions are a well documented feature of coiled-coils, interestingly, modelling indicated that the probability of a-g' salt bridges were highly probably (Fry et al., 1995). A number of coiled-coils have been identified which contain a-g' and/or d-e' salt-bridges, these include, the bZIP transcription factors ATF-4 and C/EBP beta heterodimers (Estes et al., 1995), the Fos homodimer (O'Shea et al., 1992), tropomyosin (Gimona, 2008), and α -keratin (Steinert, 1990). Moreover, the cortexillin I coiled-coil contains charged residues at 10 a-positions and 6 d-positions (Lee et al., 2003). Fascinatingly, the crystal structure of the cortexillin I parallel homodimeric coiled-coil, revealed that a number of residues were involved in novel interhelical salt-bridges including d-e', g-a', and d-a'. The data acquired from the cortexillin I coiled-coil could give an insight into the type of interactions which are involved in the dimerization and stabilization of the leucine zipper domain, regardless of the heptad register assigned to it. Thorough analysis of the literature reveals that the charged residues located in the a- or d-position of the Nek2 leucine zipper are not unusual. However what is unique is the stretch of conserved glutamic acid residues in the a-position of HepII.

Significantly, a systematic mutational analysis of the *cFos-cJun* heterodimers indicated that when a mixture of mutated (*a:e/g* positions) were placed in solution, the highest percentage of correct recombination occurred with the least energetically stable mutants (Mason et al., 2009). With respect to the Nek2 leucine zipper, in which the classical positions of interaction are energetically unfavourable compared to that of the cJun-cFos interaction, it is interesting to speculate that due to the abundance of coiled-coil proteins located at and/or close to the centrosomes, the sequence variation from classical leucine zippers and coiled-coils is due to the fact that Nek2's main role is in centrosome disjunction where errors could prove lethal to the organism and that the sequence deviation is to maintain specificity and function in a location saturated with coiled-coil proteins.

5.1.2 The Nuclear export signal of the Nek2 protein

NetNES 1.1 software indicated that a nuclear export signal encompassing residues (LKEIQL) was present in the leucine zipper domain. The dual specificity phosphatase Cdc14 also contains a NES (Steigmeier et al., 2004); Cdc14 is held in the nucleus until the consecutive activation of two regulatory cascades – the Cdc Fourteen Early Anaphase Release (FEAR) and the Mitotic Exit Network (MEN), to carry out its role on a number of nuclear and cytoplasmic targets (Stegmeier et al., 2004). Is Nek2 subject to this form nuclear regulation? Located inside the leucine zipper domain of Nek2, consisting of six residues this motif would be masked by the dimerization of Nek2, regardless of which register the leucine zipper domain adopted. Daub et al., 2008 conducted a cell cycle orientated proteomics analysis determining residue specific phosphorylation events. Serine residues 299 and 300 were found to be phosphorylated in a cell cycle dependent manner, however, what effect if any this has upon the leucine zipper stabilization or destabilization to reveal the NES motif

remains to be elucidated. Interestingly, these two residues could include a polo-box domain (PBD) - S-(pS/pT)-(P/X) (Elia et al., 2003). Residues 299-301 correspond to a PBD consisting of SSP of which position 300 is known to be a *bona-fide* phosphorylation site. Analysis of mitotic regulators indicated that Cdc25, Wee1, Myt1, and INCENP also contain at least one PBD binding site. The Plk1 PBD mediated localization to substrates and centrosomes (Elia et al., 2003), analysis of Nek2 centrosomal localization indicated that residues 335-370 were involved (Hames et al., 2005), demonstrating that the PBD of Nek2 is not required for centrosomal location. However, one mechanism of regulation of NESs is by unmasking, these events occur in some proteins due to phosphorylation (Engel et al., 1998; Ohno et al., 2000; McKinsey et al., 2001; Zhang and Xiong, 2001; Brunet et al., 2002). It would be interesting to investigate if phosphorylation of the residue 300 in the PBD is sufficient to destabilize the leucine zipper.

5.1.3 Nek2 leucine zipper - a dynamic domain

The Nek2 leucine zipper domain is an atypical coiled-coil, the absence of hydrophobic residues in the core positions of the interface which are substituted for charged residues, functions to destabilized the leucine zipper but possible to increase specificity. This could be important due to the sub-cellular localization of Nek2 in relation to its function. The inherent dynamic properties of the leucine zipper domain were analysed using the powerful tool of NMR, and a slow exchange rate of 17 s^{-1} was observed, with ten-fold acceleration of R_1 relaxation. The detrimental effect upon NMR experiments was extreme, with enhanced relaxation rates so great that the acquisition of long experiments proved to be impossible. The exchange process was observed regardless of the construct used which indicates it could possibly be a feature of the Nek2 protein kinase *in vivo*. Mutagenesis of the Nek2

leucine zipper 5 domain resulted in the abolition of the exchange dynamics in the mutant LZ5 K309C/C335A, which were an inherent feature of the wild-type domain. A significant difference was observed between the oxidised and reduced states of both mutants when calculating the thermal melting temperature using CD (Figures 3.19 and 3.20). This indicated that the Nek2 leucine zipper can shift heptad register between two states Hepl and HepII, which encompasses the interchanging of a conserved stretch of basic and acidic residues in core positions of the interface, whilst the leucines were always situated in the core positions. Furthermore, this data confirmed the inherent flexibility of this domain in solution which could be observed experimentally in the wild-type leucine zipper domains using NMR. The use of acetonitrile proved that the exchange process was not due to unfolding of the leucine zipper domain, reinforced by the measured helical content of the domain being over 70% without the addition of acetonitrile (Figure 3.18).

The future elucidation of the structure of the Nek2 leucine zipper will be possible using the mutant LZ5 K309C/C335A, for which the relaxation rates are reduced sufficiently to enable structural determination. It is essential that the dimerization of this unusual domain is investigated to gain an insight into this novel mechanism of regulation of a eukaryotic protein.

The most well characterised consequence of Nek2 overexpression in cultured cells is premature centrosome disjunction. Elevated levels of Nek2 promote centrosome fragmentation, mitotic spindle multipolarity, cytokinesis failure, and aneuploidy. A loss of spindle bipolarity leads to a loss of genomic integrity. A multipolar spindle acting to segregate an aneuploid genome is thought to be the precursor of chromosomal instability (CIN). This genomic plasticity provides a heterogenous pool of tumour cells from which to

select for aggressive or drug-refractory tumour development. Increased levels of Nek2 may be central to initiating or maintaining CIN.

Though involvement of Nek2A in human neoplastic disease is clear, much of the mechanism remains unsolved. The substrates and pathways that convey an increase in Nek2 activity to malignancy are as yet unknown. However, enough is known to indicate that Nek2 should and is considered a strong candidate for therapeutic intervention. The generation of small molecule inhibitors proves challenging due to the lack of diversity in the nucleotide binding cleft of the catalytic sites of protein kinase domains, but the leucine zipper domain remains an attractive target for chemotherapeutic agents. The design of small molecules requires the elucidation of the structure, whereas, the use of peptide or peptidomimetics does not, the structure of coiled-coils are well characterized and the primary sequence of the Nek2 leucine zipper is known. The titration of the Nek2 leucine zipper into a variety of tumour cell lines would identify the optimum concentration for the competitive inhibition of Nek2 dimerization. The uptake of peptides through the cell membrane is an active process shown to be enhanced by the presence of positively charged residues (Vives and Lebleu, 2002; Bernal et al., 2007) and also by the helical propensity of the peptide (Bernal et al., 2007). The Nek2 leucine zipper not only has a high helical content of approximately 70%, but also a stretch of positively charged residues which due to the dynamic nature of the domain could be exposed enough to interact with the cell membrane to enhance membrane penetration. The dynamic behaviour has been observed in every construct used in this study, although, LZ0 could offer a possible resistance to degradation which has previously been observed in limited proteolysis (Frank Ivins, unpublished data). Alternatively, synthesised D-peptides

could offer enhanced properties over naturally occurring L-peptides, such as resistance to degradation and therefore low or no immunogenicity (Welch et al., 2007).

The effects of inhibiting the Nek2 kinase could serve to increase survival rates in cancer sufferers, through a small molecule inhibitor or the use of the leucine zipper peptide domain. It will be interesting to see what effect inhibiting a kinase involved in so many diverse roles essential in cellular proliferation has in humans.

5.1.4 Probing the oligomerization state of the Nek2 leucine zipper

Dilution of the LZ2 and LZ5 constructs lead to the identification of peaks susceptible to oligomerization, but unfortunately, dilution alone did not result in perturbation of the conformational exchange dynamics (Figure 4.12-4.15). At 0.1 mM in both LZ2 and LZ5 the oligomerization was reduced, however, slow-intermediate exchange persisted resulting in the loss of signal intensity and additional peaks for the majority of backbone amino acids. In order to solve the structure of the Nek2 leucine zipper methods needed to be developed to firstly, inhibit higher order oligomerization at high concentrations and secondly, to reduce conformational exchange.

Temperature can be used to adjust the rate of exchange, increasing the temperature for a molecule undergoing slow exchange can function to increase molecular tumbling and reduce R_2 relaxation rates. Therefore, an increased temperature pushes the equilibrium to favour fast exchange (Figure 5.1). As the motional correlation time becomes shorter (τ_c) R_1 and R_2 decrease. Initial experiments on LZ2 indicated that the exchange rate was in the range of slow-intermediate exchange at 10-100 ms. A reduction of temperature in an HSQC to 283 K using LZ5 resulted in a reduction in signal intensity due to the increase of relaxation effects with the decreased temperature (Figure 4.16). Furthermore, the inherent exchange

process at 283 K was not inhibited sufficiently to improve the line broadening. Adequate resolution of the HSQC was only possible when acquired with a large number of scans, indicating significant loss in both longitudinal and transverse relaxation at 283 K. Complex 3D experiments were still not possible under these conditions.

The isolated domain of LZ5 showed two interesting properties in solution, oligomerization at concentrations above 0.1 mM and chemical exchange independent of oligomerization hypothesised to originate from the unusual amino acid composition in the interface (Figure 5.2). To generate a method conducive to elucidate the structure the conformational exchange needed to be increased so that the peaks reached coalescence or inhibited. Attempts to solve the structure of the HIV-1 regulatory protein Vpr failed because of the strong tendency of the peptide to oligomerize in pure water (Bourbigot et al., 2005). The first solution structure of the Vpr domain was solved in the presence of 30% (v/v) trifluoroethanol (TFE), it was revealed that the Vpr domain contained three well defined α -helices adopting a U-shaped form (Wecker et al., 2002). However, when the 3D structure was obtained in the presence of 30% (v/v) acetonitrile the same three well defined α -helices were present folded around a hydrophobic core (Morellet et al., 2003), and may be involved in maintaining an intramolecular leucine zipper interaction (Wang et al., 1996). The data using TFE to reduce oligomerization suggests that the Vpr leucine zipper is forced into an unnatural U-shape which is not necessarily the native state of the domain; the use of acetonitrile reveals a more common formation of a three helix bundle centred around a hydrophobic core. Taking into account these factors it was decided to use acetonitrile to counteract the oligomerization process in LZ5. The ^{15}N HSQC suggests that use of acetonitrile indeed did not shift the leucine zipper into an unnatural conformation, as can be

seen by the spectra acquired in the acetonitrile titration containing only a slight change in chemical shift as the concentration of the solvent increases (Figure 4.17). At concentrations of 2 mM LZ5 and 20% acetonitrile the oligomerization effect is perturbed resulting in the disappearance of peak #14. This implies that in these conditions only the oligomerization is affected and not the secondary structure of the LZ5 domain, therefore, at conditions (concentrations) where NMR experiments are viable the oligomerization can be controlled. However, the chemical exchange persists resulting in a doubling of the expected backbone peaks and an accelerated decay of the magnetisation in both T_1 and T_2 relaxation (z and xy planes). Acetonitrile induces formation of secondary structure, the persistence of the rapid loss of signal below the baseline noise even at high concentrations of acetonitrile indicates that it is not a folding-unfolding transition which occurs, but rather highlights the effects of the Nek2 LZ having two possible heptad repeats, Hepl: with polar residues occupying the α -position and negatively charged residues occupying the d -position, and Hepll: with polar residues occupying the d -position and positively charged residues occupying the α -position (Figure 3.16B and C). Interestingly, the unusual composition of the interfaces could induce a ‘switch’ of register on a timescale of ms which would result in the type of enhanced relaxation seen in all NMR experiments undertaken with the Nek2 LZ domain.

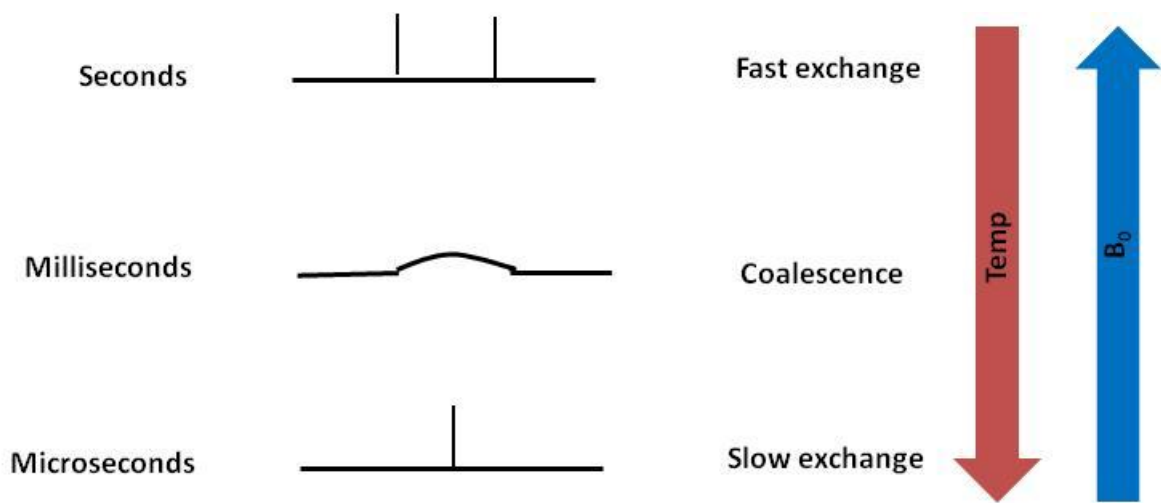


Figure 5.1 Example spectra displaying differing exchange rates related to chemical shift

The lower spectrum is an example of fast exchange where the chemical shift seen in the spectra is the weighted average of two fast exchanging peaks. In intermediate exchange, as seen in the spectrum immediately above, the two peaks begin to broaden as the average of the two chemicals shifts nears zero. At the upper end of the group of spectra, the spectrum displayed indicates the transition out of intermediate exchange and into fast chemical exchange, as the reaction time increases only one peak is now visible. The schematic diagram on the right indicates the effects of magnetic field strength (B_0) and temperature upon relaxation.

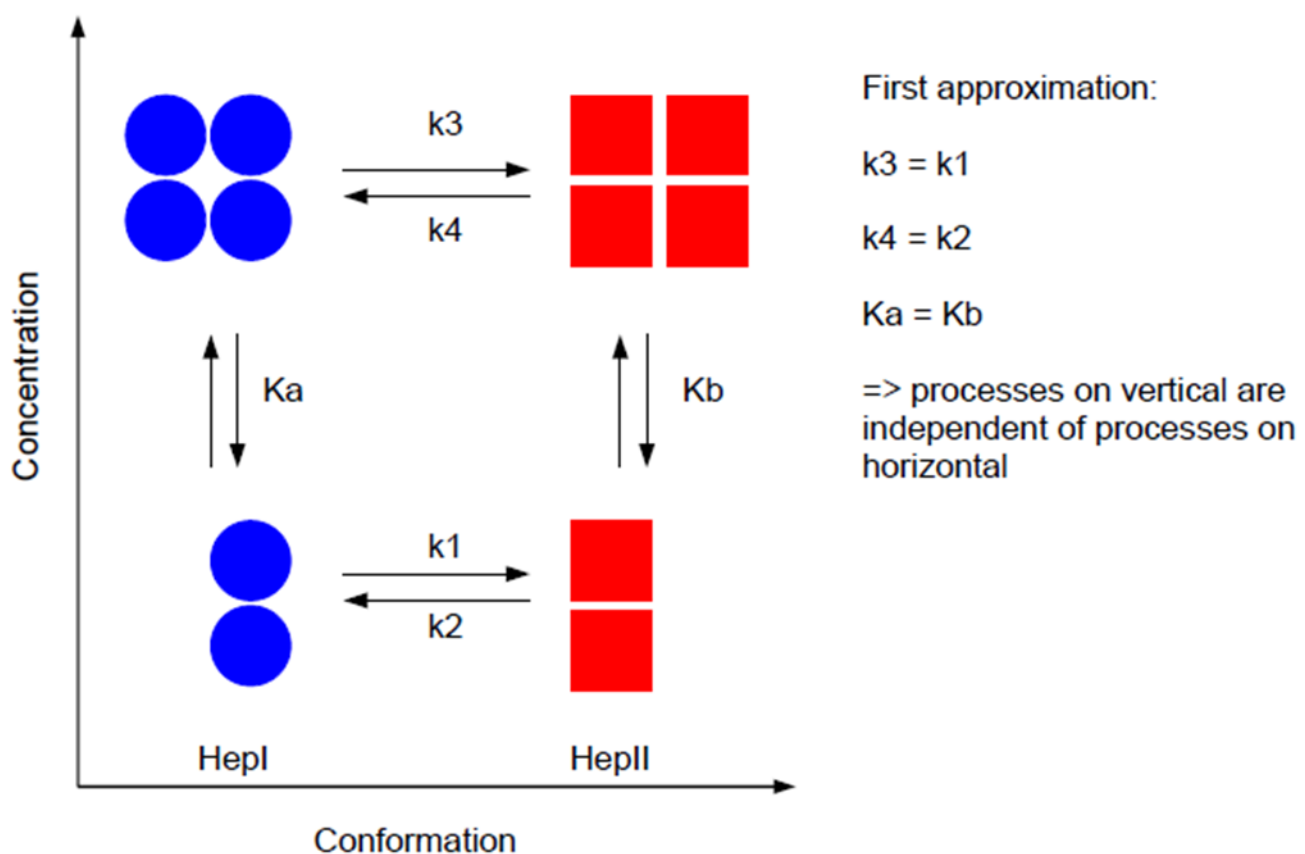


Figure 5.2 Two state dynamic process involving the Nek2 leucine zipper

A graphical model representing the two state dynamic process involving oligomerisation and conformational exchange. As the concentration increases along the y axis, this increases the K_a rate. The leucine zipper, therefore, forms higher order oligomers at increased concentrations. Progression along the x axis indicates the conformational exchange dynamics present at lower concentration and continuing regardless of concentration variations.

5.1.5 Manipulation of the kinetic equilibrium using temperature

Increasing temperature in the presence of 30% acetonitrile did indeed change the kinetics of the reaction; at 320 K peaks began to coalesce to reveal a weighted average of the two isoforms present in the spectra (Figure 4.19B). However, although it would have been an ideal situation to have one species to interpret in the spectra the equilibrium was not shifted far enough to overcome the transition from intermediate to fast exchange as can be seen by the linewidth of the peaks present. After 128 scans at 320 K in the presence of acetonitrile, it was observed that the solution had become cloudy and white precipitates had begun to form. Temperatures above 320 K were not attempted because of the detrimental effects to the protein sample.

Decreasing temperature to move the equilibrium of the exchange further towards slow exchange, away from intermediate exchange, yielded the expected results. The line widths were reduced but not significantly to increase the resolution of the spectra and had no effect on reducing overlap. Coiled-coils represent the worst case scenario for distinguishing between intra- and inter-molecular connectivities in multidimensional spectra containing NOEs (Nilges, 1993), due to the presence of the identical dimeric interface extending over the whole length of the domain, and the helical nature of the individual helices which minimise long range NOEs and causes significant overlap and therefore reduced resolution in the spectrum. The doubling of peaks due to the presence of two isoforms makes identification of connectivities even more challenging.

The use of acidic pH and acetonitrile at 30% reduced the spectral overlap (Figure 4.22), but the exchange dynamics persisted resulting in the observation of more than 40 amide

specific peaks in the spectrum. For the Nek2 leucine zipper simply lowering the pH and inhibiting the oligomerization did significantly affect exchange dynamics.

5.1.6 Frequency of exchange dynamics observed by NMR

Exchange dynamics have been previously observed in coiled coils domains in the *Bacillus subtilis* RNase P protein studied using NMR a folding intermediate has been characterized using NMR (Chang et al., 2010). Here significant R_{ex} values, the conformational exchange contribution of R_2 , was found for a few residues in the N and C-terminal. These regions were found to be unfolded in the intermediate state. However, significant R_{ex} values for residues in the RNR motif of P protein were found to be not due an unfolding process in the intermediate conformation. Hydrogen exchange for ribonuclease P protein was found to be dependent on ligand concentration and a ligand induced folding model was proposed (Henkels and Oas, 2006). However, the intermediate fold was not considered and the hydrogen exchange experiments exchange were predicted to be more significant because of the reduction of shielding from the solvent, in the follow up experiments some four years later (Chang et al., 2010). Comparison of the crystal and NMR structures for the first well characterised leucine zipper GCN4, revealed exchange on a fast chemical shift timescale (Saudek et al., 1990; Saudek et al., 1991). Similar observations were made for the c-jun leucine zipper (Junius et al., 1995; Junius et al., 1996). This family of transcription factors contain an asparagine (Asn) residue in the a-position which is hypothesised to enable the rapid exchange of zipper strands *in vivo*, it is thought that this would lead to the dimerization of bZIP strands to be under kinetic rather than thermodynamic regulation (Wendt et al., 1995).

Slow chemical exchange has been previously reported for the Mnt repressor, here the protein undergoes folding transitions on a slow chemical shift timescale (Nooren et al., 1999). The tetrameric leucine zipper exists in two conformations which are generated by the assembly of two coiled-coil dimers which pack into a distorted four helical assembly. Multicoil analysis indicates that the Nek2 leucine zipper has meaningful scores for the formation of a dimer but not trimeric or tetrameric structures, AUC also indicated that leucine zipper forms a dimeric structure *in vitro*.

Early work on the GCN4p1 reported two sets of peaks in NMR experiments (Saudek et al., 1991; Lovett et al., 1996), which have been attributed to a partially ordered conformation of GCN4p1 which exists in equilibrium with the coiled coil state (Nikolaev and Pervushin, 2007). Par4, a pro-apoptotic factor which is upregulated in prostate cancer cells, also contains a leucine zipper. NMR analysis of this domain indicated that dimerization is subject to changes in conformational state: from a partially ordered monomer to a coiled-coil dimer (Schwalbe et al., 2010). Interestingly, the Par4 leucine zipper has inferior thermodynamic properties (a lower melting temperature) than the Nek2 LZ5 construct with the T_m below the value of 57 °C which can indicate a lower stability, but the GCN4p1 leucine zipper has a T_m comparable to LZ5 at 53 °C (Harbury et al., 1993). What the Nek2 leucine zipper does not have in common with both the Par4 and GCN4p1 leucine zipper is the highly unusual interface, containing charged residues in the *a*- or *d*-positions depending on which heptad register is used, resulting in destabilisation of the leucine zipper (Figure 4.22), however, in Par4 charged side chains in the *e*- and *g*-position are thought to be adequate to destabilise dimerization, in the presence of a classical hydrophobic leucine zipper interface.

NMR experiments using Nek2 leucine zipper domain proved to be challenging, the detrimental effects of an exchange rate of 17 s^{-1} , although slow in a chemical shift timescale, resulted in extensive line broadening evident in all HSQC experiments (Figure 4.5). For a protein small protein such as LZ5, the unusual line broadening indicates that transverse relaxation rates are enhanced by the exchange. The direct measurement of R_2 values of 30 s^{-1} , for well structured residues, confirmed this theory. The measured values correspond to a protein of approximately 40 kDa, five-fold more than the 6 s^{-1} expected for a protein of 10 kDa. Additionally, longitudinal relaxation rates are enhanced (Figure 4.25), for the Nek2 LZ5 construct of 10 kDa R_1 relaxation rates of around 1.7 s^{-1} were expected, which was confirmed by the fits of the cross- and diagonal peaks in the exchange experiments. Unfortunately, the effective R_1 values were close to 16 s^{-1} a ten-fold increase of longitudinal decay. Therefore, a five-fold increase in the R_2 relaxation rates and a ten-fold increase in the R_2 relaxation rates resulted in the decay being too fast for the triple resonance experiments required to solve the solution structure.

The solution structure of the Mnt repressor could be obtained because the exchange rate was 1 s^{-1} , ten times slower than with LZ5. Conversely, the solution structure of the GCN4 transcription factor could be solved due to the fast exchange present. In both cases the exchange kinetics were not detrimental to the relaxation rates of the signals. However, for the Par4 leucine zipper with estimated exchange rates of 10 s^{-1} (Wendt et al., 1995), the solution structure has yet to be elucidated.

5.1.7 Characterization of the Nek2 mutants

To prove the hypothesis that the two heptad registers Hepl and HepII interconvert on a timescale of 17 s^{-1} , two construct were generated by mutagenesis to lock the conformers

into either Hepl or HepII. The use of a disulphide bond in the respective interface was thought to be an elegant method to probe the dynamics. Disulphide bonds naturally occur in some coiled-coils (Blankenfeldt et al., 2006) and the stabilising effect on leucine zippers has been investigated (Zhou et al., 1993). Position K309 was chosen for mutation to cysteine in the Hepl register and position E310 was chosen for the HepII register, both residues were thought to lie in the interface and modelling confirmed that the distance was sufficient for disulphide bond formation (Figure 4.23) and the possibility of bonding occurring in the opposite heptad register. In oxidising buffer, the formation of a disulphide bond should prevent conformational exchange. Mutant K309C/C335A in oxidising buffer, which represents a disulphide bond placed in the *d*-position of the leucine zipper, reduced the number of peaks in the HSQC to that expected, approximately 40 peaks, and the line widths of the peaks reflected a protein of 10 kDa. An exactly matching superimposition of the peaks was not expected due to the double mutation and the changes in environment introduced by the disulphide bond, although, the majority of peak were overlapping the wild-type spectrum. However, mutant E310C/C335A did not behave as initially predicted. In oxidising buffer the quality of the HSQC was poor and the line widths of the peaks did not reduce to the same extent as the K309C mutant.

A possible explanation for the different behaviour could be due to the position of the disulphide bond which is strongly influenced by sterical constraints (Zhou et al., 1993). A disulphide bond placed in any *d*-position of a leucine zipper has a stabilising effect. In the *a*-position only a slight stabilising effect results if the disulphide bond is placed at the extreme N- or C-terminal. The mutant E310C has the disulphide bond placed in the *a*-position and

located close to the central region; it is possible that this mutation has a destabilising effect rather than the predicted stabilizing effect.

The data generated with the K309C mutant is sufficient to confirm the hypothesis that the chemical exchange is due to the non-ideal interface of the Nek2 LZ interconverting on a timescale of 17s^{-1} , a rotation of approximately 20° about the long axis.

5.1.8 Functional relevance of the conformational dynamics of the Nek2 leucine zipper

The equilibrium of the two conformations is 50:50, as estimated by the peak intensities in the HSQC spectra, indicating that *in vitro* neither conformation is preferentially adopted. Interestingly, the surface charge of the interface could not be more different: Hepl has a highly positive charge density in the centre and negative charges on the edges, whereas, HepII has a highly negative charge density in the interface and positive charges on the outside (Figure 5.3A). The c-myc leucine zipper also has negatively charged residues in 3 out of 4 of the α -positions, mimicking the HepII register. The physiological effect of having the two registers and the differential charge densities is under investigation; however, it is likely that these differences could modulate protein-protein interactions involving Nek2. Interestingly, two serines (229 and 300) located close to the N-terminal of the leucine zipper, were reported to be phosphorylated in a cell cycle dependent manner (Daub et al., 2008). It is interesting to speculate that these could regulate the dimerization of the leucine zipper to favour one conformation *in vivo*. Serine 300 was predicted to be an N-cap residue by AGADIR analysis, phosphorylation of an N-cap residue has been shown to stabilize an isolated α -helix (Andrew et al., 2002). In Hepl, the position of a phosphate group leads to an unfavourable positioning of the backbone (Figure 5.4A), whilst in HepII no such constraints are predicted by the model (Figure 5.4B). Therefore, upon phosphorylation, the Hepl

conformation could be destabilized and the HeplI conformation stabilized. If only the HeplI conformation existed *in vivo*, and was destabilised in a cell cycle dependent manner due to phosphorylation of serine 300, it would reveal the nuclear export signal, predicted by NetNES, located in position 308-313 of the leucine zipper sequence (LKEIQL), which could influence transport into and out of the nucleus in relation to function. Therefore, in the unphosphorylated state it is interesting to speculate that the Nek2 leucine zipper could interact with c-myc, via the favourable pairing of the HeplI positively charged interface with the c-myc negatively charged interface. Upon phosphorylation and proposed destabilization of the leucine zipper domain, Nek2 could be export from the nucleus to perform a central role in centrosome disjunction, followed by degradation mediated by the APC/C via the degradation motif located at the extreme C-terminal of Nek2.

Rotational dynamics are a fundamental part of the function of transmembrane helices, it is required for enzymatic activity and regulated by substrate binding. One such example is CD39, where the active site is held down by two helices spanning the membrane, enzymatic control is tightly regulated by the rotation of the helices in relation to one another, rotation is mediated by substrate binding and also changes in the composition of the lipid bilayer (Grinthal and Guidotti., 2006). The HAMP domain, commonly found in a range of transmembrane proteins has also been found to rotate in response to externally triggered stimuli (Hulko et al., 2006). However, such an extreme variation away from the normal constitution of a leucine zipper interface sequence as found in Nek2 has not previously been documented, and it is of increasing importance that this mechanism of regulation is investigated further. Therefore, the elucidation of the structure of the Nek2 leucine zipper is of high importance to understand how this protein contributes to cancer progression and

genetic instability, how does the Nek2 kinase become fully activated through the leucine zipper interaction and what role does the conformational dynamics play *in vivo*.

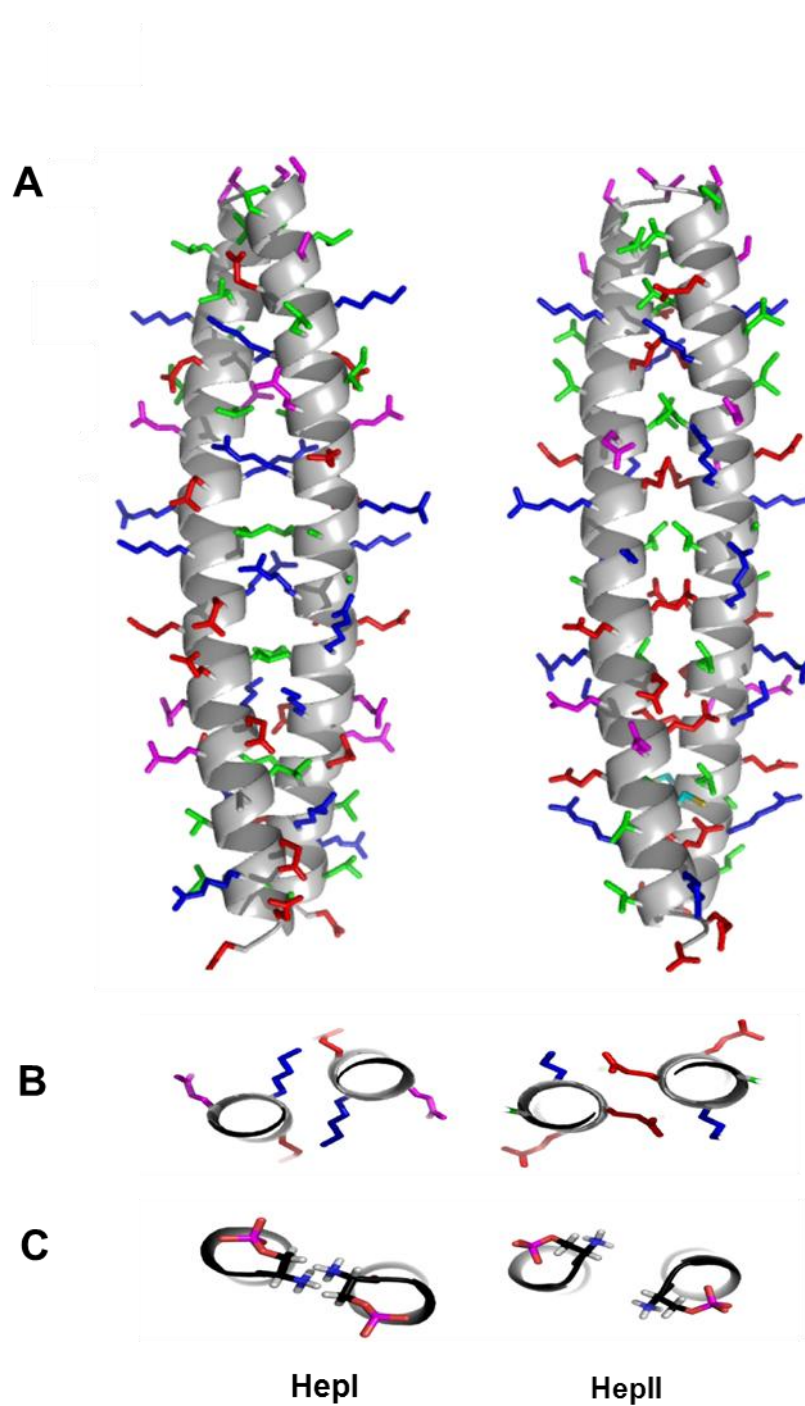


Figure 5.3 Model depicting the theoretic conformations of the Nek2 leucine zipper

A. The Nek2 leucine zipper vertically is displayed, with the N-terminal at the top and the C-terminal at the base. The backbone is shown as a helical cartoon with the side chains indicated using the stick setting. Hydrogens were omitted from the model. Amino acids are coloured according to their properties. B. The packing of the sidechains in relation to the proposed heptad repeat register is shown, as a slice through the central region. C. A view of the N-terminal N-cap after phosphorylation on Serine 299 is shown. The dihedral angles of the side chains, after phosphate addition using Pymol, were adjusted to allow the formation of hydrogen bonds. HepI depicts the potential clash of backbone atoms favourable sterical constraints are shown in HepII.

LZ5

GAMAVLSELKL**K**EIQLQERERALKAREERLEQKEQELCVRERLAED
 GAMAVLSELKL**C**EIQLQERERALKAREERLEQKEQEL**A**VRERLAED

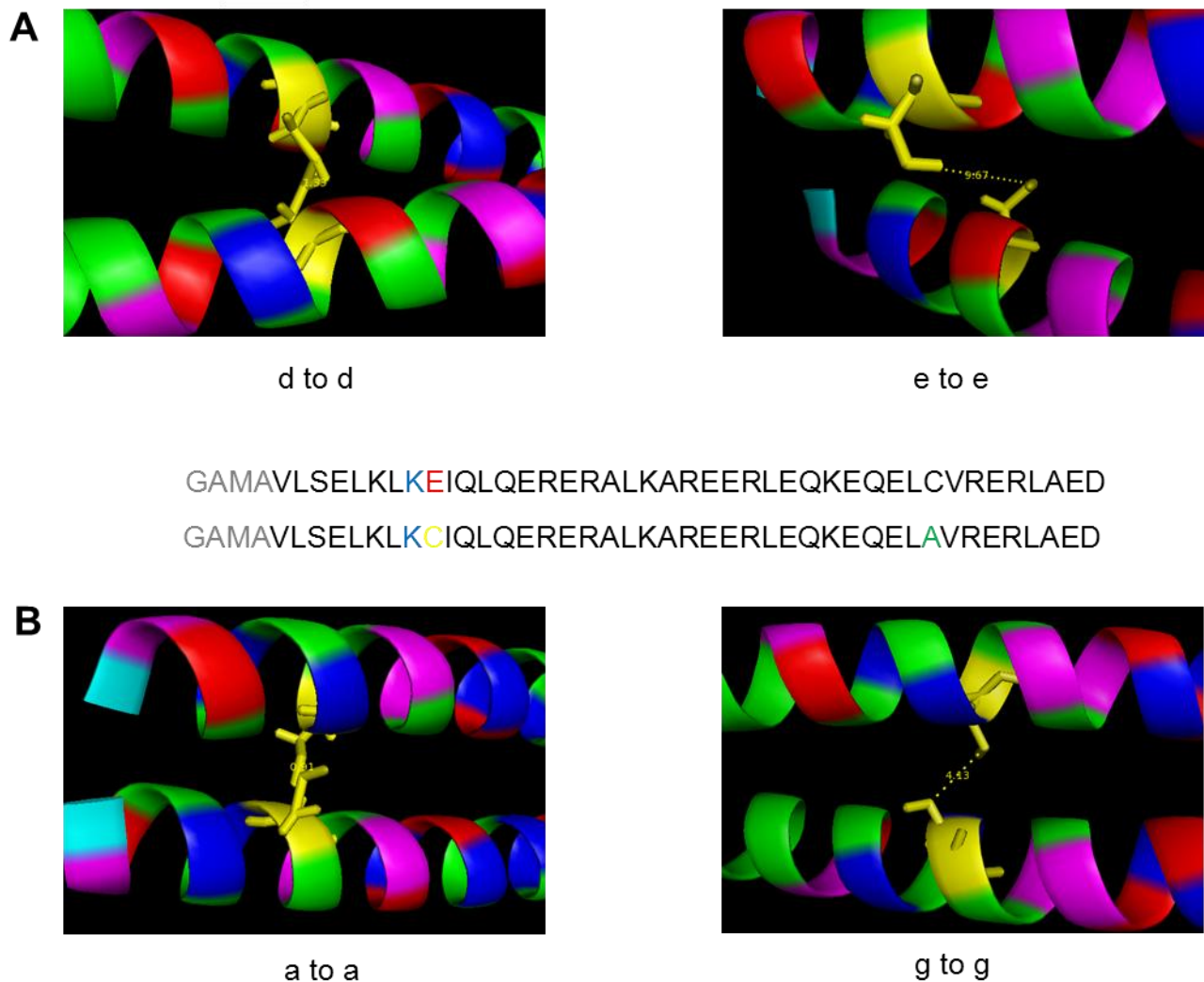


Figure 5.4 Mutagenesis to lock Hepl and HepII repeats in LZ5

A. The Hepl register of LZ5 in a horizontal orientation with the N-terminal on the left side of the model is shown. The backbone is represented as a cartoon and the cystine side chain shown as a stick. Pymol was used to measure the distance between sulphhydryl groups of the mutant K309C. The lefthand side indicates the d-position interactions in Hepl and the right side indicates the HepII e-positions.

B. A cartoon representation of, to the left, the a-position interactions in HepII and on the right the Hepl g-position cystine conformation is displayed. The sequence of LZ5 used in the modelling, including the positions of the wildtype sequence on the first line, and the positions of the respective mutations on the second, relating to the mutations K309C in panel A and E310C in panel B.

CHAPTER 6

BIBLIOGRAPHY

- ADAMSON, J. G., ZHOU, N. E. & HODGES, R. S. 1993. Structure, function and application of the coiled-coil protein folding motif. *Curr Opin Biotechnol*, 4, 428-37.
- AKEY, D. L., MALASHKEVICH, V. N. & KIM, P. S. 2001. Buried polar residues in coiled-coil interfaces. *Biochemistry*, 40, 6352-60.
- ALBER, T. 1992. Structure of the leucine zipper. *Curr Opin Genet Dev*, 2, 205-10.
- AL-ROMAIH, K., BAYANI, J., VOROBYOVA, J., KARASKOVA, J., PARK, P. C., ZIELENSKA, M. & SQUIRE, J. A. 2003. Chromosomal instability in osteosarcoma and its association with centrosome abnormalities. *Cancer Genet Cytogenet*, 144, 91-9.
- ANDERSEN, J. S., WILKINSON, C. J., MAYOR, T., MORTENSEN, P., NIGG, E. A. & MANN, M. 2003. Proteomic characterization of the human centrosome by protein correlation profiling. *Nature*, 426, 570-4.
- ANDERSEN, S. S. 1999. Molecular characteristics of the centrosome. *Int Rev Cytol*, 187, 51-109.
- ANDREW, C. D., WARWICKER, J., JONES, G. R. & DOIG, A. J. 2002. Effect of phosphorylation on alpha-helix stability as a function of position. *Biochemistry*, 41, 1897-905.
- AURORA, R. & ROSE, G. D. 1998. Helix capping. *Protein Sci*, 7, 21-38.
- BAHE, S., STIERHOF, Y. D., WILKINSON, C. J., LEISS, F. & NIGG, E. A. 2005. Rootletin forms centriole-associated filaments and functions in centrosome cohesion. *J Cell Biol*, 171, 27-33.
- BAKHOUM, S. F., GENOVESE, G. & COMPTON, D. A. 2009. Deviant kinetochore microtubule dynamics underlie chromosomal instability. *Curr Biol*, 19, 1937-42.
- BARTRAM, C. R., DE KLEIN, A., HAGEMEIJER, A., VAN AGTHOVEN, T., GEURTS VAN KESSEL, A., BOOTSMA, D., GROSVELD, G., FERGUSON-SMITH, M. A., DAVIES, T., STONE, M. &

- ET AL. 1983. Translocation of c-abl oncogene correlates with the presence of a Philadelphia chromosome in chronic myelocytic leukaemia. *Nature*, 306, 277-80.
- BERNAL, F., TYLER, A. F., KORSMEYER, S. J., WALENSKY, L. D. & VERDINE, G. L. 2007. Reactivation of the p53 tumor suppressor pathway by a stapled p53 peptide. *J Am Chem Soc*, 129, 2456-7.
- BERTHET, C., ALEEM, E., COPPOLA, V., TESSAROLLO, L. & KALDIS, P. 2003. Cdk2 knockout mice are viable. *Curr Biol*, 13, 1775-85.
- BLANKENFELDT, W., THOMA, N. H., WRAY, J. S., GAUTEL, M. & SCHLICHTING, I. 2006. Crystal structures of human cardiac beta-myosin II S2-Delta provide insight into the functional role of the S2 subfragment. *Proc Natl Acad Sci U S A*, 103, 17713-7.
- BOBINNEC, Y., KHODJAKOV, A., MIR, L. M., RIEDER, C. L., EDDE, B. & BORNENS, M. 1998. Centriole disassembly in vivo and its effect on centrosome structure and function in vertebrate cells. *J Cell Biol*, 143, 1575-89.
- BOREL, F., LOHEZ, O. D., LACROIX, F. B. & MARGOLIS, R. L. 2002. Multiple centrosomes arise from tetraploidy checkpoint failure and mitotic centrosome clusters in p53 and RB pocket protein-compromised cells. *Proc Natl Acad Sci U S A*, 99, 9819-24.
- BORNBERG-BAUER, E., RIVALS, E. & VINGRON, M. 1998. Computational approaches to identify leucine zippers. *Nucleic Acids Res*, 26, 2740-6.
- BORNENS, M. 2002. Centrosome composition and microtubule anchoring mechanisms. *Curr Opin Cell Biol*, 14, 25-34.
- BOURBIGOT, S., BELTZ, H., DENIS, J., MORELLET, N., ROQUES, B. P., MELY, Y. & BOUAZIZ, S. 2005. The C-terminal domain of the HIV-1 regulatory protein Vpr adopts an antiparallel dimeric structure in solution via its leucine-zipper-like domain. *Biochem J*, 387, 333-41.

- BRINKLEY, B. R. 2001. Managing the centrosome numbers game: from chaos to stability in cancer cell division. *Trends Cell Biol*, 11, 18-21.
- BRUNET, N., MORIN, A. & OLOFSSON, B. 2002. RhoGDI-3 regulates RhoG and targets this protein to the Golgi complex through its unique N-terminal domain. *Traffic*, 3, 342-57.
- BUCHDUNGER, E., CIOFFI, C. L., LAW, N., STOVER, D., OHNO-JONES, S., DRUKER, B. J. & LYDON, N. B. 2000. Abl protein-tyrosine kinase inhibitor ST1571 inhibits in vitro signal transduction mediated by c-kit and platelet-derived growth factor receptors. *J Pharmacol Exp Ther*, 295, 139-45.
- BUCHDUNGER, E., ZIMMERMANN, J., METT, H., MEYER, T., MULLER, M., DRUKER, B. J. & LYDON, N. B. 1996. Inhibition of the Abl protein-tyrosine kinase in vitro and in vivo by a 2-phenylaminopyrimidine derivative. *Cancer Res*, 56, 100-4.
- BUCHER, P. & HOFMANN, K. 1996. A sequence similarity search algorithm based on a probabilistic interpretation of an alignment scoring system. *Proc Int Conf Intell Syst Mol Biol*, 4, 44-51.
- BUFFIN, E., EMRE, D. & KARESS, R. E. 2007. Flies without a spindle checkpoint. *Nat Cell Biol*, 9, 565-72.
- CAHILL, M. T., STANCU, M. & ARROYO, J. G. 2002. Ataxia and vision loss: flow cytometric diagnosis of primary central nervous system lymphoma. *Br J Ophthalmol*, 86, 246-7.
- CHANG, W. H., CHEN, J. H. & HWANG, L. P. 2010. Single-sided mobile NMR apparatus using the transverse flux of a single permanent magnet. *Magn Reson Imaging*, 28, 129-38.
- CHEN, Y., RILEY, D. J., ZHENG, L., CHEN, P. L. & LEE, W. H. 2002. Phosphorylation of the mitotic regulator protein Hec1 by Nek2 kinase is essential for faithful chromosome segregation. *J Biol Chem*, 277, 49408-16.

- CIMINI, D. 2008. Merotelic kinetochore orientation, aneuploidy, and cancer. *Biochim Biophys Acta*, 1786, 32-40.
- CIMINI, D., HOWELL, B., MADDOX, P., KHODJAKOV, A., DEGRASSI, F. & SALMON, E. D. 2001. Merotelic kinetochore orientation is a major mechanism of aneuploidy in mitotic mammalian tissue cells. *J Cell Biol*, 153, 517-27.
- CIMINI, D., WAN, X., HIREL, C. B. & SALMON, E. D. 2006. Aurora kinase promotes turnover of kinetochore microtubules to reduce chromosome segregation errors. *Curr Biol*, 16, 1711-8.
- CLORE, G. M., DRISCOLL, P. C., WINGFIELD, P. T. & GRONENBORN, A. M. 1990. Analysis of the backbone dynamics of interleukin-1 beta using two-dimensional inverse detected heteronuclear ¹⁵N-¹H NMR spectroscopy. *Biochemistry*, 29, 7387-401.
- COHEN, C. & PARRY, D. A. 1998. A conserved C-terminal assembly region in paramyosin and myosin rods. *J Struct Biol*, 122, 180-7.
- CRAIG, P. O., URETA, D. B. & DELFINO, J. M. 2002. Probing protein conformation with a minimal photochemical reagent. *Protein Sci*, 11, 1353-66.
- CRICK, J. & JACKSON, H. 1953. The selective localization of p-radioiodophenyl-hydroxylamine in red cells: its relation to methaemoglobinaemia. *Br J Pharmacol Chemother*, 8, 87-92.
- CROASDALE, R., IVINS, F. J., MUSKETT, F., DAVITER, T., SCOTT, D. J., HARDY, T., SMERDON, S. J., FRY, A. M. & PFUHL, M. 2011. An undecided coiled coil: the leucine zipper of Nek2 kinase exhibits atypical conformational exchange dynamics. *J Biol Chem*, 286, 27537-47.
- D'ASSORO, A. B., LINGLE, W. L. & SALISBURY, J. L. 2002. Centrosome amplification and the development of cancer. *Oncogene*, 21, 6146-53.

- DE KLEIN, A., VAN KESSEL, A. G., GROSVELD, G., BARTRAM, C. R., HAGEMEIJER, A., BOOTSMA, D., SPURR, N. K., HEISTERKAMP, N., GROFFEN, J. & STEPHENSON, J. R. 1982. A cellular oncogene is translocated to the Philadelphia chromosome in chronic myelocytic leukaemia. *Nature*, 300, 765-7.
- DOBLES, M., LIBERAL, V., SCOTT, M. L., BENEZRA, R. & SORGER, P. K. 2000. Chromosome missegregation and apoptosis in mice lacking the mitotic checkpoint protein Mad2. *Cell*, 101, 635-45.
- DOXSEY, S. 2001. Re-evaluating centrosome function. *Nat Rev Mol Cell Biol*, 2, 688-98.
- DOXSEY, S. J. 2001. Centrosomes as command centres for cellular control. *Nat Cell Biol*, 3, E105-8.
- DZHINDZHEV, N. S., YU, Q. D., WEISKOPF, K., TZOLOVSKY, G., CUNHA-FERREIRA, I., RIPARBELLINI, M., RODRIGUES-MARTINS, A., BETTENCOURT-DIAS, M., CALLAINI, G. & GLOVER, D. M. 2010. Asterless is a scaffold for the onset of centriole assembly. *Nature*, 467, 714-8.
- ELIA, A. E., CANTLEY, L. C. & YAFFE, M. B. 2003. Proteomic screen finds pSer/pThr-binding domain localizing Plk1 to mitotic substrates. *Science*, 299, 1228-31.
- ELIA, A. E., RELLOS, P., HAIRE, L. F., CHAO, J. W., IVINS, F. J., HOEPKER, K., MOHAMMAD, D., CANTLEY, L. C., SMERDON, S. J. & YAFFE, M. B. 2003. The molecular basis for phosphodependent substrate targeting and regulation of Plks by the Polo-box domain. *Cell*, 115, 83-95.
- ENGEL, K., KOTLYAROV, A. & GAESTEL, M. 1998. Leptomycin B-sensitive nuclear export of MAPKAP kinase 2 is regulated by phosphorylation. *EMBO J*, 17, 3363-71.
- ERNST, R. R. 1987. Methodology of magnetic resonance imaging. *Q Rev Biophys*, 19, 183-220.

ESTES, D. M., HIRANO, A., HEUSSLER, V. T., DOBBELAERE, D. A. & BROWN, W. C. 1995.

Expression and biological activities of bovine interleukin 4: effects of recombinant bovine interleukin 4 on T cell proliferation and B cell differentiation and proliferation in vitro. *Cell Immunol*, 163, 268-79.

ETO, M., ELLIOTT, E., PRICKETT, T. D. & BRAUTIGAN, D. L. 2002. Inhibitor-2 regulates protein phosphatase-1 complexed with NimA-related kinase to induce centrosome separation. *J Biol Chem*, 277, 44013-20.

EUTENEUER, U. & MCINTOSH, J. R. 1981. Polarity of some motility-related microtubules.

Proc Natl Acad Sci U S A, 78, 372-6.

FARAGHER, A. J. & FRY, A. M. 2003. Nek2A kinase stimulates centrosome disjunction and is required for formation of bipolar mitotic spindles. *Mol Biol Cell*, 14, 2876-89.

FARDILHA, M., WU, W., SA, R., FIDALGO, S., SOUSA, C., MOTA, C., DA CRUZ E SILVA, O. A. & DA CRUZ E SILVA, E. F. 2004. Alternatively spliced protein variants as potential therapeutic targets for male infertility and contraception. *Ann N Y Acad Sci*, 1030, 468-78.

FARROW, N. A., MUHANDIRAM, R., SINGER, A. U., PASCAL, S. M., KAY, C. M., GISH, G., SHOELSON, S. E., PAWSON, T., FORMAN-KAY, J. D. & KAY, L. E. 1994. Backbone dynamics of a free and phosphopeptide-complexed Src homology 2 domain studied by ¹⁵N NMR relaxation. *Biochemistry*, 33, 5984-6003.

FARROW, N. A., ZHANG, O., FORMAN-KAY, J. D. & KAY, L. E. 1994. A heteronuclear correlation experiment for simultaneous determination of ¹⁵N longitudinal decay and chemical exchange rates of systems in slow equilibrium. *J Biomol NMR*, 4, 727-34.

FEENEY, R. E., OSUGA, D. T. & YEH, Y. 1991. Effect of boronic acids on antifreeze proteins. *J*

Protein Chem, 10, 167-70.

FERRE-D'AMARE, A. R., PRENDERGAST, G. C., ZIFF, E. B. & BURLEY, S. K. 1993. Recognition by

Max of its cognate DNA through a dimeric b/HLH/Z domain. *Nature*, 363, 38-45.

FLETCHER, L., CERNIGLIA, G. J., YEN, T. J. & MUSCHEL, R. J. 2005. Live cell imaging reveals distinct roles in cell cycle regulation for Nek2A and Nek2B. *Biochim Biophys Acta*, 1744, 89-92.

FOUNTOULAKIS, M., JURANVILLE, J. F. & MANNEBERG, M. 1992. Comparison of the Coomassie brilliant blue, bicinchoninic acid and Lowry quantitation assays, using non-glycosylated and glycosylated proteins. *J Biochem Biophys Methods*, 24, 265-74.

FRIEDBERG, E. C., AGUILERA, A., GELLERT, M., HANAWALT, P. C., HAYS, J. B., LEHMANN, A. R., LINDAHL, T., LOWNDES, N., SARASIN, A. & WOOD, R. D. 2006. DNA repair: from molecular mechanism to human disease. *DNA Repair (Amst)*, 5, 986-96.

FRY, A. M. 2002. The Nek2 protein kinase: a novel regulator of centrosome structure. *Oncogene*, 21, 6184-94.

FRY, A. M., ARNAUD, L. & NIGG, E. A. 1999. Activity of the human centrosomal kinase, Nek2, depends on an unusual leucine zipper dimerization motif. *J Biol Chem*, 274, 16304-10.

FRY, A. M., DESCOMBES, P., TWOMEY, C., BACCHIERI, R. & NIGG, E. A. 2000. The NIMA-related kinase X-Nek2B is required for efficient assembly of the zygotic centrosome in *Xenopus laevis*. *J Cell Sci*, 113 (Pt 11), 1973-84.

FRY, A. M., MAYOR, T., MERALDI, P., STIERHOF, Y. D., TANAKA, K. & NIGG, E. A. 1998. C-Nap1, a novel centrosomal coiled-coil protein and candidate substrate of the cell cycle-regulated protein kinase Nek2. *J Cell Biol*, 141, 1563-74.

FRY, A. M., MERALDI, P. & NIGG, E. A. 1998. A centrosomal function for the human Nek2

protein kinase, a member of the NIMA family of cell cycle regulators. *EMBO J*, 17, 470-81.

FRY, A. M. & NIGG, E. A. 1995. Cell cycle. The NIMA kinase joins forces with Cdc2. *Curr Biol*, 5, 1122-5.

FRY, A. M., SCHULTZ, S. J., BARTEK, J. & NIGG, E. A. 1995. Substrate specificity and cell cycle regulation of the Nek2 protein kinase, a potential human homolog of the mitotic regulator NIMA of *Aspergillus nidulans*. *J Biol Chem*, 270, 12899-905.

FURNESS, G., DEMAGGIO, M. & WHITESCARVER, J. 1975. Morphological changes induced during fixation of *Mycoplasma mycoides* for electron microscopy. *Tex Rep Biol Med*, 33, 415-22.

GALLANT, P., FRY, A. M. & NIGG, E. A. 1995. Protein kinases in the control of mitosis: focus on nucleocytoplasmic trafficking. *J Cell Sci Suppl*, 19, 21-8.

GAMBACORTI-PASSERINI, C., ANTOLINI, L., MAHON, F. X., GUILHOT, F., DEININGER, M., FAVA, C., NAGLER, A., DELLA CASA, C. M., MORRA, E., ABRUZZESE, E., D'EMILIO, A., STAGNO, F., LE COUTRE, P., HURTADO-MONROY, R., SANTINI, V., MARTINO, B., PANE, F., PICCIN, A., GIRALDO, P., ASSOULINE, S., DUROSINMI, M. A., LEEKSMA, O., POGLIANI, E. M., PUTTINI, M., JANG, E., REIFFERS, J., VALSECCHI, M. G. & KIM, D. W. 2011. Multicenter independent assessment of outcomes in chronic myeloid leukemia patients treated with imatinib. *J Natl Cancer Inst*, 103, 553-61.

GASCOIGNE, K. E. & TAYLOR, S. S. 2008. Cancer cells display profound intra- and interline variation following prolonged exposure to antimitotic drugs. *Cancer Cell*, 14, 111-22.

GHADIMI, B. M., SACKETT, D. L., DIFILIPPANTONIO, M. J., SCHROCK, E., NEUMANN, T., JAUHO, A., AUER, G. & RIED, T. 2000. Centrosome amplification and instability occurs exclusively in aneuploid, but not in diploid colorectal cancer cell lines, and correlates

- with numerical chromosomal aberrations. *Genes Chromosomes Cancer*, 27, 183-90.
- GIANANTI, M. G., BONACCORSI, S., BUCCIARELLI, E. & GATTI, M. 2001. Drosophila male meiosis as a model system for the study of cytokinesis in animal cells. *Cell Struct Funct*, 26, 609-17.
- GIMONA, M. 2008. Dimerization of tropomyosins. *Adv Exp Med Biol*, 644, 73-84.
- GRINTHAL, A. & GUIDOTTI, G. 2006. CD39, NTPDase 1, is attached to the plasma membrane by two transmembrane domains. Why? *Purinergic Signal*, 2, 391-8.
- GRZESIEK, S. & BAX, A. 1993. Amino acid type determination in the sequential assignment procedure of uniformly ¹³C/¹⁵N-enriched proteins. *J Biomol NMR*, 3, 185-204.
- GRZESIEK, S. & BAX, A. 1993. Measurement of amide proton exchange rates and NOEs with water in ¹³C/¹⁵N-enriched calcineurin B. *J Biomol NMR*, 3, 627-38.
- HABEDANCK, R., STIERHOF, Y. D., WILKINSON, C. J. & NIGG, E. A. 2005. The Polo kinase Plk4 functions in centriole duplication. *Nat Cell Biol*, 7, 1140-6.
- HAHN, W. C., DESSAIN, S. K., BROOKS, M. W., KING, J. E., ELENBAAS, B., SABATINI, D. M., DECAPRIO, J. A. & WEINBERG, R. A. 2002. Enumeration of the simian virus 40 early region elements necessary for human cell transformation. *Mol Cell Biol*, 22, 2111-23.
- HALUSKA, F. G., TSUJIMOTO, Y. & CROCE, C. M. 1987. The t(8;14) chromosome translocation of the Burkitt lymphoma cell line Daudi occurred during immunoglobulin gene rearrangement and involved the heavy chain diversity region. *Proc Natl Acad Sci U S A*, 84, 6835-9.
- HAMES, R. S., CROOKES, R. E., STRAATMAN, K. R., MERDES, A., HAYES, M. J., FARAGHER, A. J. & FRY, A. M. 2005. Dynamic recruitment of Nek2 kinase to the centrosome involves microtubules, PCM-1, and localized proteasomal degradation. *Mol Biol Cell*, 16, 1711-24.

- HAMES, R. S. & FRY, A. M. 2002. Alternative splice variants of the human centrosome kinase Nek2 exhibit distinct patterns of expression in mitosis. *Biochem J*, 361, 77-85.
- HAMES, R. S., WATTAM, S. L., YAMANO, H., BACCHIERI, R. & FRY, A. M. 2001. APC/C-mediated destruction of the centrosomal kinase Nek2A occurs in early mitosis and depends upon a cyclin A-type D-box. *EMBO J*, 20, 7117-27.
- HANAHAN, D. & WEINBERG, R. A. 2000. The hallmarks of cancer. *Cell*, 100, 57-70.
- HARBURY, P. B., PLECS, J. J., TIDOR, B., ALBER, T. & KIM, P. S. 1998. High-resolution protein design with backbone freedom. *Science*, 282, 1462-7.
- HARBURY, P. B., ZHANG, T., KIM, P. S. & ALBER, T. 1993. A switch between two-, three-, and four-stranded coiled coils in GCN4 leucine zipper mutants. *Science*, 262, 1401-7.
- HARRISON, L. M., RALLABHANDI, P., MICHALSKI, J., ZHOU, X., STEYERT, S. R., VOGEL, S. N. & KAPER, J. B. 2008. Vibrio cholerae flagellins induce Toll-like receptor 5-mediated interleukin-8 production through mitogen-activated protein kinase and NF-kappaB activation. *Infect Immun*, 76, 5524-34.
- HAVEL, T. F. & WUTHRICH, K. 1985. An evaluation of the combined use of nuclear magnetic resonance and distance geometry for the determination of protein conformations in solution. *J Mol Biol*, 182, 281-94.
- HAYES, M. J., KIMATA, Y., WATTAM, S. L., LINDON, C., MAO, G., YAMANO, H. & FRY, A. M. 2006. Early mitotic degradation of Nek2A depends on Cdc20-independent interaction with the APC/C. *Nat Cell Biol*, 8, 607-14.
- HAYWARD, D. G., CLARKE, R. B., FARAGHER, A. J., PILLAI, M. R., HAGAN, I. M. & FRY, A. M. 2004. The centrosomal kinase Nek2 displays elevated levels of protein expression in human breast cancer. *Cancer Res*, 64, 7370-6.
- HAYWARD, D. G. & FRY, A. M. 2006. Nek2 kinase in chromosome instability and cancer.

Cancer Lett, 237, 155-66.

- HEALD, R., TOURNEBIZE, R., HABERMANN, A., KARSENTI, E. & HYMAN, A. 1997. Spindle assembly in Xenopus egg extracts: respective roles of centrosomes and microtubule self-organization. *J Cell Biol*, 138, 615-28.
- HEERKLOTZ, D., DORING, P., BONZELIUS, F., WINKELHAUS, S. & NOVER, L. 2001. The balance of nuclear import and export determines the intracellular distribution and function of tomato heat stress transcription factor HsfA2. *Mol Cell Biol*, 21, 1759-68.
- HELPS, N. R., LUO, X., BARKER, H. M. & COHEN, P. T. 2000. NIMA-related kinase 2 (Nek2), a cell-cycle-regulated protein kinase localized to centrosomes, is complexed to protein phosphatase 1. *Biochem J*, 349, 509-18.
- HENKELS, C. H. & OAS, T. G. 2006. Ligation-state hydrogen exchange: coupled binding and folding equilibria in ribonuclease P protein. *J Am Chem Soc*, 128, 7772-81.
- HIDAKA, H., INAGAKI, M., KAWAMOTO, S. & SASAKI, Y. 1984. Isoquinolinesulfonamides, novel and potent inhibitors of cyclic nucleotide dependent protein kinase and protein kinase C. *Biochemistry*, 23, 5036-41.
- HINCHCLIFFE, E. H., LI, C., THOMPSON, E. A., MALLER, J. L. & SLUDER, G. 1999. Requirement of Cdk2-cyclin E activity for repeated centrosome reproduction in Xenopus egg extracts. *Science*, 283, 851-4.
- HINCHCLIFFE, E. H., MILLER, F. J., CHAM, M., KHODJAKOV, A. & SLUDER, G. 2001. Requirement of a centrosomal activity for cell cycle progression through G1 into S phase. *Science*, 291, 1547-50.
- HOCHEGGER, H., DEJSUPHONG, D., SONODA, E., SABERI, A., RAJENDRA, E., KIRK, J., HUNT, T. & TAKEDA, S. 2007. An essential role for Cdk1 in S phase control is revealed via chemical genetics in vertebrate cells. *J Cell Biol*, 178, 257-68.

- HULKO, M., BERNDT, F., GRUBER, M., LINDER, J. U., TRUFFAULT, V., SCHULTZ, A., MARTIN, J., SCHULTZ, J. E., LUPAS, A. N. & COLES, M. 2006. The HAMP domain structure implies helix rotation in transmembrane signaling. *Cell*, 126, 929-40.
- HULL, W. E. & SYKES, B. D. 1975. Fluorotyrosine alkaline phosphatase: internal mobility of individual tyrosines and the role of chemical shift anisotropy as a 19F nuclear spin relaxation mechanism in proteins. *J Mol Biol*, 98, 121-53.
- INNOCENTI, P., CHEUNG, K. M., SOLANKI, S., MAS-DROUX, C., ROWAN, F., YEOH, S., BOXALL, K., WESTLAKE, M., PICKARD, L., HARDY, T., BAXTER, J. E., AHERNE, G. W., BAYLISS, R., FRY, A. M. & HOELDER, S. 2012. Design of potent and selective hybrid inhibitors of the mitotic kinase Nek2: structure-activity relationship, structural biology, and cellular activity. *J Med Chem*, 55, 3228-41.
- JONES, S., ZHANG, X., PARSONS, D. W., LIN, J. C., LEARY, R. J., ANGENENDT, P., MANKOO, P., CARTER, H., KAMIYAMA, H., JIMENO, A., HONG, S. M., FU, B., LIN, M. T., CALHOUN, E. S., KAMIYAMA, M., WALTER, K., NIKOLSKAYA, T., NIKOLSKY, Y., HARTIGAN, J., SMITH, D. R., HIDALGO, M., LEACH, S. D., KLEIN, A. P., JAFFEE, E. M., GOGGINS, M., MAITRA, A., IACOBUSIO-DONAHUE, C., ESHLEMAN, J. R., KERN, S. E., HRUBAN, R. H., KARCHIN, R., PAPADOPOULOS, N., PARMIGIANI, G., VOGELSTEIN, B., VELCULESCU, V. E. & KINZLER, K. W. 2008. Core signaling pathways in human pancreatic cancers revealed by global genomic analyses. *Science*, 321, 1801-6.
- JUNIUS, F. K., MACKAY, J. P., BUBB, W. A., JENSEN, S. A., WEISS, A. S. & KING, G. F. 1995. Nuclear magnetic resonance characterization of the Jun leucine zipper domain: unusual properties of coiled-coil interfacial polar residues. *Biochemistry*, 34, 6164-74.
- JUNIUS, F. K., O'DONOUGHUE, S. I., NILGES, M., WEISS, A. S. & KING, G. F. 1996. High

resolution NMR solution structure of the leucine zipper domain of the c-Jun homodimer. *J Biol Chem*, 271, 13663-7.

KARNOUB, A. E. & WEINBERG, R. A. 2008. Ras oncogenes: split personalities. *Nat Rev Mol Cell Biol*, 9, 517-31.

KAY, L. E., TORCHIA, D. A. & BAX, A. 1989. Backbone dynamics of proteins as studied by 15N inverse detected heteronuclear NMR spectroscopy: application to staphylococcal nuclease. *Biochemistry*, 28, 8972-9.

KHODJAKOV, A., COLE, R. W., OAKLEY, B. R. & RIEDER, C. L. 2000. Centrosome-independent mitotic spindle formation in vertebrates. *Curr Biol*, 10, 59-67.

KHODJAKOV, A. & RIEDER, C. L. 2001. Centrosomes enhance the fidelity of cytokinesis in vertebrates and are required for cell cycle progression. *J Cell Biol*, 153, 237-42.

KNIGHTON, D. R., XUONG, N. H., TAYLOR, S. S. & SOWADSKI, J. M. 1991. Crystallization studies of cAMP-dependent protein kinase. Cocrystals of the catalytic subunit with a 20 amino acid residue peptide inhibitor and MgATP diffract to 3.0 Å resolution. *J Mol Biol*, 220, 217-20.

KNIGHTON, D. R., ZHENG, J. H., TEN EYCK, L. F., ASHFORD, V. A., XUONG, N. H., TAYLOR, S. S. & SOWADSKI, J. M. 1991. Crystal structure of the catalytic subunit of cyclic adenosine monophosphate-dependent protein kinase. *Science*, 253, 407-14.

KNIGHTON, D. R., ZHENG, J. H., TEN EYCK, L. F., XUONG, N. H., TAYLOR, S. S. & SOWADSKI, J. M. 1991. Structure of a peptide inhibitor bound to the catalytic subunit of cyclic adenosine monophosphate-dependent protein kinase. *Science*, 253, 414-20.

KNOWLTON, A. L., LAN, W. & STUKENBERG, P. T. 2006. Aurora B is enriched at merotelic attachment sites, where it regulates MCAK. *Curr Biol*, 16, 1705-10.

KOBAYASHI, Y., TAKASAKI, A., KUROSAKA, K., SAKURAI, Y., IWAMURA, M. & WATANABE, N.

2000. Cell-type specificity of L-leucyl L-leucine methyl ester. *Biochem Biophys Res Commun*, 272, 687-90.
- KONOPKA, J. B. & WITTE, O. N. 1985. Activation of the abl oncogene in murine and human leukemias. *Biochim Biophys Acta*, 823, 1-17.
- KOPS, G. J., KIM, Y., WEAVER, B. A., MAO, Y., MCLEOD, I., YATES, J. R., 3RD, TAGAYA, M. & CLEVELAND, D. W. 2005. ZW10 links mitotic checkpoint signaling to the structural kinetochore. *J Cell Biol*, 169, 49-60.
- KOZIELSKI, F., SACK, S., MARX, A., THORMAHLEN, M., SCHONBRUNN, E., BIOU, V., THOMPSON, A., MANDELKOW, E. M. & MANDELKOW, E. 1997. The crystal structure of dimeric kinesin and implications for microtubule-dependent motility. *Cell*, 91, 985-94.
- KRASINSKA, L., COT, E. & FISHER, D. 2008. Selective chemical inhibition as a tool to study Cdk1 and Cdk2 functions in the cell cycle. *Cell Cycle*, 7, 1702-8.
- KUGE, S., ARITA, M., MURAYAMA, A., MAETA, K., IZAWA, S., INOUE, Y. & NOMOTO, A. 2001. Regulation of the yeast Yap1p nuclear export signal is mediated by redox signal-induced reversible disulfide bond formation. *Mol Cell Biol*, 21, 6139-50.
- KUMAR, S. & BANSAL, M. 1998. Dissecting alpha-helices: position-specific analysis of alpha-helices in globular proteins. *Proteins*, 31, 460-76.
- KUMAR, S. & BANSAL, M. 1998. Geometrical and sequence characteristics of alpha-helices in globular proteins. *Biophys J*, 75, 1935-44.
- KUO, K. K., SATO, N., MIZUMOTO, K., MAEHARA, N., YONEMASU, H., KER, C. G., SHEEN, P. C. & TANAKA, M. 2000. Centrosome abnormalities in human carcinomas of the gallbladder and intrahepatic and extrahepatic bile ducts. *Hepatology*, 31, 59-64.
- LA COUR, T., KIEMER, L., MOLGAARD, A., GUPTA, R., SKRIVER, K. & BRUNAK, S. 2004.

Analysis and prediction of leucine-rich nuclear export signals. *Protein Eng Des Sel*, 17, 527-36.

LACEY, K. R., JACKSON, P. K. & STEARNS, T. 1999. Cyclin-dependent kinase control of centrosome duplication. *Proc Natl Acad Sci U S A*, 96, 2817-22.

LACROIX, E., VIGUERA, A. R. & SERRANO, L. 1998. Elucidating the folding problem of alpha-helices: local motifs, long-range electrostatics, ionic-strength dependence and prediction of NMR parameters. *J Mol Biol*, 284, 173-91.

LANDSCHULZ, W. H., JOHNSON, P. F. & MCKNIGHT, S. L. 1988. The leucine zipper: a hypothetical structure common to a new class of DNA binding proteins. *Science*, 240, 1759-64.

LAVIGNE, P., CRUMP, M. P., GAGNE, S. M., HODGES, R. S., KAY, C. M. & SYKES, B. D. 1998. Insights into the mechanism of heterodimerization from the ¹H-NMR solution structure of the c-Myc-Max heterodimeric leucine zipper. *J Mol Biol*, 281, 165-81.

LAVIGNE, P., KONDEJEWSKI, L. H., HOUSTON, M. E., JR., SONNICHSEN, F. D., LIX, B., SKYES, B. D., HODGES, R. S. & KAY, C. M. 1995. Preferential heterodimeric parallel coiled-coil formation by synthetic Max and c-Myc leucine zippers: a description of putative electrostatic interactions responsible for the specificity of heterodimerization. *J Mol Biol*, 254, 505-20.

LEE, D. L., IVANINSKII, S., BURKHARD, P. & HODGES, R. S. 2003. Unique stabilizing interactions identified in the two-stranded alpha-helical coiled-coil: crystal structure of a cortexillin I/GCN4 hybrid coiled-coil peptide. *Protein Sci*, 12, 1395-405.

LENGAUER, C., KINZLER, K. W. & VOGELSTEIN, B. 1998. Genetic instabilities in human cancers. *Nature*, 396, 643-9.

LI, R. & MURRAY, A. W. 1991. Feedback control of mitosis in budding yeast. *Cell*, 66, 519-31.

- LI, Y., BROWN, J. H., RESHETNIKOVA, L., BLAZSEK, A., FARKAS, L., NYITRAY, L. & COHEN, C. 2003. Visualization of an unstable coiled coil from the scallop myosin rod. *Nature*, 424, 341-5.
- LI, Y., YAMAKITA, Y. & KRUG, R. M. 1998. Regulation of a nuclear export signal by an adjacent inhibitory sequence: the effector domain of the influenza virus NS1 protein. *Proc Natl Acad Sci U S A*, 95, 4864-9.
- LINGLE, W. L., BARRETT, S. L., NEGRON, V. C., D'ASSORO, A. B., BOENEMAN, K., LIU, W., WHITEHEAD, C. M., REYNOLDS, C. & SALISBURY, J. L. 2002. Centrosome amplification drives chromosomal instability in breast tumor development. *Proc Natl Acad Sci U S A*, 99, 1978-83.
- LINGLE, W. L., LUTZ, W. H., INGLE, J. N., MAIHLE, N. J. & SALISBURY, J. L. 1998. Centrosome hypertrophy in human breast tumors: implications for genomic stability and cell polarity. *Proc Natl Acad Sci U S A*, 95, 2950-5.
- LINGLE, W. L. & SALISBURY, J. L. 1999. Altered centrosome structure is associated with abnormal mitoses in human breast tumors. *Am J Pathol*, 155, 1941-51.
- LINGLE, W. L. & SALISBURY, J. L. 2000. The role of the centrosome in the development of malignant tumors. *Curr Top Dev Biol*, 49, 313-29.
- LOU, Y., XIE, W., ZHANG, D. F., YAO, J. H., LUO, Z. F., WANG, Y. Z., SHI, Y. Y. & YAO, X. B. 2004. Nek2A specifies the centrosomal localization of Erk2. *Biochem Biophys Res Commun*, 321, 495-501.
- LOVETT, E. G., D'AVIGNON, D. A., HOLTZER, M. E., BRASWELL, E. H., ZHU, D. & HOLTZER, A. 1996. Observation via one-dimensional ^{13}C alpha NMR of local conformational substates in thermal unfolding equilibria of a synthetic analog of the GCN4 leucine zipper. *Proc Natl Acad Sci U S A*, 93, 1781-5.

- LU, K. P. & MEANS, A. R. 1994. Expression of the noncatalytic domain of the NIMA kinase causes a G2 arrest in *Aspergillus nidulans*. *EMBO J*, 13, 2103-13.
- LUPAS, A. 1996. Coiled coils: new structures and new functions. *Trends Biochem Sci*, 21, 375-82.
- LUPAS, A., VAN DYKE, M. & STOCK, J. 1991. Predicting coiled coils from protein sequences. *Science*, 252, 1162-4.
- MARDIN, B. R., LANGE, C., BAXTER, J. E., HARDY, T., SCHOLZ, S. R., FRY, A. M. & SCHIEBEL, E. 2010. Components of the Hippo pathway cooperate with Nek2 kinase to regulate centrosome disjunction. *Nat Cell Biol*, 12, 1166-76.
- MARLEY, J., LU, M. & BRACKEN, C. 2001. A method for efficient isotopic labeling of recombinant proteins. *J Biomol NMR*, 20, 71-5.
- MARSCHALL, H. U. 2001. [Disturbances in cholesterol metabolism]. *Dtsch Med Wochenschr*, 126, 63-4.
- MARTIN-LLUESMA, S., STUCKE, V. M. & NIGG, E. A. 2002. Role of Hec1 in spindle checkpoint signaling and kinetochore recruitment of Mad1/Mad2. *Science*, 297, 2267-70.
- MASON, J. M. & ARNDT, K. M. 2004. Coiled coil domains: stability, specificity, and biological implications. *Chembiochem*, 5, 170-6.
- MATSUMOTO, M., FURIHATA, M., ISHIKAWA, T., OHTSUKI, Y. & OGOSHI, S. 1999. Comparison of deregulated expression of cyclin D1 and cyclin E with that of cyclin-dependent kinase 4 (CDK4) and CDK2 in human oesophageal squamous cell carcinoma. *Br J Cancer*, 80, 256-61.
- MATSUMOTO, Y., HAYASHI, K. & NISHIDA, E. 1999. Cyclin-dependent kinase 2 (Cdk2) is required for centrosome duplication in mammalian cells. *Curr Biol*, 9, 429-32.
- MAYOR, T., STIERHOF, Y. D., TANAKA, K., FRY, A. M. & NIGG, E. A. 2000. The centrosomal

protein C-Nap1 is required for cell cycle-regulated centrosome cohesion. *J Cell Biol*, 151, 837-46.

MAYOR, U., GUYDOSH, N. R., JOHNSON, C. M., GROSSMANN, J. G., SATO, S., JAS, G. S., FREUND, S. M., ALONSO, D. O., DAGGETT, V. & FERSHT, A. R. 2003. The complete folding pathway of a protein from nanoseconds to microseconds. *Nature*, 421, 863-7.

MCARTHUR, J. E. 1943. The Sulfonamides in Less Severe Infections. *Can Med Assoc J*, 48, 238-9.

MCDONALD, H. J. & DECHATELET, L. R. 1967. The effects of three oral hypoglycemic agents on the incorporation of leucine-C14 into protein by liver microsomes of normal and alloxan-diabetic rats. *Life Sci*, 6, 183-9.

MCKINSEY, T. A., ZHANG, C. L. & OLSON, E. N. 2001. Identification of a signal-responsive nuclear export sequence in class II histone deacetylases. *Mol Cell Biol*, 21, 6312-21.

MERALDI, P., HONDA, R. & NIGG, E. A. 2002. Aurora-A overexpression reveals tetraploidization as a major route to centrosome amplification in p53-/- cells. *EMBO J*, 21, 483-92.

MERALDI, P., LUKAS, J., FRY, A. M., BARTEK, J. & NIGG, E. A. 1999. Centrosome duplication in mammalian somatic cells requires E2F and Cdk2-cyclin A. *Nat Cell Biol*, 1, 88-93.

MITELMAN, F. 2000. Recurrent chromosome aberrations in cancer. *Mutat Res*, 462, 247-53.

MONTELIONE, G. T., WINKLER, M. E., BURTON, L. E., RINDERKNECHT, E., SPORN, M. B. & WAGNER, G. 1989. Sequence-specific ¹H-NMR assignments and identification of two small antiparallel beta-sheets in the solution structure of recombinant human transforming growth factor alpha. *Proc Natl Acad Sci U S A*, 86, 1519-23.

MORELLET, N., BOUAZIZ, S., PETITJEAN, P. & ROQUES, B. P. 2003. NMR structure of the HIV-1 regulatory protein VPR. *J Mol Biol*, 327, 215-27.

MUNOZ, V. & SERRANO, L. 1994. Intrinsic secondary structure propensities of the amino acids, using statistical phi-psi matrices: comparison with experimental scales. *Proteins*, 20, 301-11.

MUNOZ, V. & SERRANO, L. 1997. Development of the multiple sequence approximation within the AGADIR model of alpha-helix formation: comparison with Zimm-Bragg and Lifson-Roig formalisms. *Biopolymers*, 41, 495-509.

MUSACCHIO, A. & SALMON, E. D. 2007. The spindle-assembly checkpoint in space and time. *Nat Rev Mol Cell Biol*, 8, 379-93.

NIGG, E. A. 2002. Centrosome aberrations: cause or consequence of cancer progression? *Nat Rev Cancer*, 2, 815-25.

NIKOLAEV, Y. & PERVUSHIN, K. 2007. NMR spin state exchange spectroscopy reveals equilibrium of two distinct conformations of leucine zipper GCN4 in solution. *J Am Chem Soc*, 129, 6461-9.

NILGES, M. 1993. A calculation strategy for the structure determination of symmetric dimers by ¹H NMR. *Proteins*, 17, 297-309.

NOOREN, I. M., GEORGE, A. V., KAPTEIN, R., SAUER, R. T. & BOELENS, R. 1999. NMR structure determination of the tetramerization domain of the Mnt repressor: An asymmetric alpha-helical assembly in slow exchange. *J Biomol NMR*, 15, 39-53.

NOOREN, I. M., KAPTEIN, R., SAUER, R. T. & BOELENS, R. 1999. The tetramerization domain of the Mnt repressor consists of two right-handed coiled coils. *Nat Struct Biol*, 6, 755-9.

NOWELL, P. C. & HUNGERFORD, D. A. 1961. Chromosome studies in human leukemia. II. Chronic granulocytic leukemia. *J Natl Cancer Inst*, 27, 1013-35.

OAS, T. G., MCINTOSH, L. P., O'SHEA, E. K., DAHLQUIST, F. W. & KIM, P. S. 1990. Secondary

structure of a leucine zipper determined by nuclear magnetic resonance spectroscopy. *Biochemistry*, 29, 2891-4.

OHNO, M., SEGREF, A., BACHI, A., WILM, M. & MATTAJ, I. W. 2000. PHAX, a mediator of U snRNA nuclear export whose activity is regulated by phosphorylation. *Cell*, 101, 187-98.

ORTEGA, S., PRIETO, I., ODAJIMA, J., MARTIN, A., DUBUS, P., SOTILLO, R., BARBERO, J. L., MALUMBRES, M. & BARBACID, M. 2003. Cyclin-dependent kinase 2 is essential for meiosis but not for mitotic cell division in mice. *Nat Genet*, 35, 25-31.

O'SHEA, E. K., KLEMM, J. D., KIM, P. S. & ALBER, T. 1991. X-ray structure of the GCN4 leucine zipper, a two-stranded, parallel coiled coil. *Science*, 254, 539-44.

OSMANI, A. H., MCGUIRE, S. L., O'DONNELL, K. L., PU, R. T. & OSMANI, S. A. 1991. Role of the cell-cycle-regulated NIMA protein kinase during G2 and mitosis: evidence for two pathways of mitotic regulation. *Cold Spring Harb Symp Quant Biol*, 56, 549-55.

OSMANI, A. H., MCGUIRE, S. L. & OSMANI, S. A. 1991. Parallel activation of the NIMA and p34cdc2 cell cycle-regulated protein kinases is required to initiate mitosis in *A. nidulans*. *Cell*, 67, 283-91.

OSMANI, A. H., O'DONNELL, K., PU, R. T. & OSMANI, S. A. 1991. Activation of the nimA protein kinase plays a unique role during mitosis that cannot be bypassed by absence of the bimE checkpoint. *EMBO J*, 10, 2669-79.

OSMANI, S. A., ENGLE, D. B., DOONAN, J. H. & MORRIS, N. R. 1988. Spindle formation and chromatin condensation in cells blocked at interphase by mutation of a negative cell cycle control gene. *Cell*, 52, 241-51.

OSMANI, S. A., PU, R. T. & MORRIS, N. R. 1988. Mitotic induction and maintenance by overexpression of a G2-specific gene that encodes a potential protein kinase. *Cell*,

53, 237-44.

- PAGE, R., PETI, W., WILSON, I. A., STEVENS, R. C. & WUTHRICH, K. 2005. NMR screening and crystal quality of bacterially expressed prokaryotic and eukaryotic proteins in a structural genomics pipeline. *Proc Natl Acad Sci U S A*, 102, 1901-5.
- PETIT, S., BORSHCH, S. A. & ROBERT, V. 2004. Exchange interactions and theoretical analysis of (³¹P) NMR spectra in VO(HPO(4)).0.5H₂O. *Inorg Chem*, 43, 4210-5.
- PIHAN, G. A. & DOXSEY, S. J. 1999. The mitotic machinery as a source of genetic instability in cancer. *Semin Cancer Biol*, 9, 289-302.
- PIHAN, G. A., PUROHIT, A., WALLACE, J., KNECHT, H., WODA, B., QUESENBERRY, P. & DOXSEY, S. J. 1998. Centrosome defects and genetic instability in malignant tumors. *Cancer Res*, 58, 3974-85.
- PIHAN, G. A., PUROHIT, A., WALLACE, J., MALHOTRA, R., LIOTTA, L. & DOXSEY, S. J. 2001. Centrosome defects can account for cellular and genetic changes that characterize prostate cancer progression. *Cancer Res*, 61, 2212-9.
- PIHAN, G. A., WALLACE, J., ZHOU, Y. & DOXSEY, S. J. 2003. Centrosome abnormalities and chromosome instability occur together in pre-invasive carcinomas. *Cancer Res*, 63, 1398-404.
- PIOTTO, M., SAUDEK, V. & SKLENAR, V. 1992. Gradient-tailored excitation for single-quantum NMR spectroscopy of aqueous solutions. *J Biomol NMR*, 2, 661-5.
- QIU, X. L., LI, G., WU, G., ZHU, J., ZHOU, L., CHEN, P. L., CHAMBERLIN, A. R. & LEE, W. H. 2009. Synthesis and biological evaluation of a series of novel inhibitor of Nek2/Hec1 analogues. *J Med Chem*, 52, 1757-67.
- RAJAGOPALAN, H. & LENGAUER, C. 2004. Aneuploidy and cancer. *Nature*, 432, 338-41.
- RAPLEY, J., BAXTER, J. E., BLOT, J., WATTAM, S. L., CASENGHI, M., MERALDI, P., NIGG, E. A. &

- FRY, A. M. 2005. Coordinate regulation of the mother centriole component nlp by nek2 and plk1 protein kinases. *Mol Cell Biol*, 25, 1309-24.
- RELLOS, P., IVINS, F. J., BAXTER, J. E., PIKE, A., NOTT, T. J., PARKINSON, D. M., DAS, S., HOWELL, S., FEDOROV, O., SHEN, Q. Y., FRY, A. M., KNAPP, S. & SMERDON, S. J. 2007. Structure and regulation of the human Nek2 centrosomal kinase. *J Biol Chem*, 282, 6833-42.
- RIED, T., HESELMAYER-HADDAD, K., BLEGEN, H., SCHROCK, E. & AUER, G. 1999. Genomic changes defining the genesis, progression, and malignancy potential in solid human tumors: a phenotype/genotype correlation. *Genes Chromosomes Cancer*, 25, 195-204.
- RIEDER, C. L. & SALMON, E. D. 1994. Motile kinetochores and polar ejection forces dictate chromosome position on the vertebrate mitotic spindle. *J Cell Biol*, 124, 223-33.
- ROEGIERS, F., YOUNGER-SHEPHERD, S., JAN, L. Y. & JAN, Y. N. 2001. Two types of asymmetric divisions in the Drosophila sensory organ precursor cell lineage. *Nat Cell Biol*, 3, 58-67.
- SAMSO, M., RADERMACHER, M., FRANK, J. & KOONCE, M. P. 1998. Structural characterization of a dynein motor domain. *J Mol Biol*, 276, 927-37.
- SANTAMARIA, D., BARRIERE, C., CERQUEIRA, A., HUNT, S., TARDY, C., NEWTON, K., CACERES, J. F., DUBUS, P., MALUMBRES, M. & BARBACID, M. 2007. Cdk1 is sufficient to drive the mammalian cell cycle. *Nature*, 448, 811-5.
- SATO, N., MIZUMOTO, K., NAKAMURA, M., MAEHARA, N., MINAMISHIMA, Y. A., NISHIO, S., NAGAI, E. & TANAKA, M. 2001. Correlation between centrosome abnormalities and chromosomal instability in human pancreatic cancer cells. *Cancer Genet Cytogenet*, 126, 13-9.

- SAUDEK, V., PASTORE, A., CASTIGLIONE MORELLI, M. A., FRANK, R., GAUSEPOHL, H., GIBSON, T., WEIH, F. & ROESCH, P. 1990. Solution structure of the DNA-binding domain of the yeast transcriptional activator protein GCN4. *Protein Eng*, 4, 3-10.
- SAUDEK, V., PASTORE, A., MORELLI, M. A., FRANK, R., GAUSEPOHL, H. & GIBSON, T. 1991. The solution structure of a leucine-zipper motif peptide. *Protein Eng*, 4, 519-29.
- SCHNEEWEISS, A., SINN, H. P., EHEMANN, V., KHBEIS, T., NEBEN, K., KRAUSE, U., HO, A. D., BASTERT, G. & KRAMER, A. 2003. Centrosomal aberrations in primary invasive breast cancer are associated with nodal status and hormone receptor expression. *Int J Cancer*, 107, 346-52.
- SCHUCK, P. 2000. Size-distribution analysis of macromolecules by sedimentation velocity ultracentrifugation and lamm equation modeling. *Biophys J*, 78, 1606-19.
- SCHULTZ, S. J., FRY, A. M., SUTTERLIN, C., RIED, T. & NIGG, E. A. 1994. Cell cycle-dependent expression of Nek2, a novel human protein kinase related to the NIMA mitotic regulator of *Aspergillus nidulans*. *Cell Growth Differ*, 5, 625-35.
- SCHUYLER, S. C. & PELLMAN, D. 2001. Search, capture and signal: games microtubules and centrosomes play. *J Cell Sci*, 114, 247-55.
- SCHWALBE, M., DUTTA, K., LIBICH, D. S., VENUGOPAL, H., CLARIDGE, J. K., GELL, D. A., MACKAY, J. P., EDWARDS, P. J. & PASCAL, S. M. 2010. Two-state conformational equilibrium in the Par-4 leucine zipper domain. *Proteins*, 78, 2433-49.
- SEIMIYA, H., SAWADA, H., MURAMATSU, Y., SHIMIZU, M., OHKO, K., YAMANE, K. & TSURUO, T. 2000. Involvement of 14-3-3 proteins in nuclear localization of telomerase. *EMBO J*, 19, 2652-61.
- SHARP, D. J., ROGERS, G. C. & SCHOLEY, J. M. 2000. Roles of motor proteins in building microtubule-based structures: a basic principle of cellular design. *Biochim Biophys*

Acta, 1496, 128-41.

- SMITH, P. K., KROHN, R. I., HERMANSON, G. T., MALLIA, A. K., GARTNER, F. H., PROVENZANO, M. D., FUJIMOTO, E. K., GOEKE, N. M., OLSON, B. J. & KLENK, D. C. 1985. Measurement of protein using bicinchoninic acid. *Anal Biochem*, 150, 76-85.
- SOLANKI, S., INNOCENTI, P., MAS-DROUX, C., BOXALL, K., BARILLARI, C., VAN MONTFORT, R. L., AHERNE, G. W., BAYLISS, R. & HOELDER, S. 2011. Benzimidazole inhibitors induce a DFG-out conformation of never in mitosis gene A-related kinase 2 (Nek2) without binding to the back pocket and reveal a nonlinear structure-activity relationship. *J Med Chem*, 54, 1626-39.
- STEGMEIER, F. & AMON, A. 2004. Closing mitosis: the functions of the Cdc14 phosphatase and its regulation. *Annu Rev Genet*, 38, 203-32.
- STEINERT, P. M. 1990. The two-chain coiled-coil molecule of native epidermal keratin intermediate filaments is a type I-type II heterodimer. *J Biol Chem*, 265, 8766-74.
- STETEFELD, J., JENNY, M., SCHULTHESS, T., LANDWEHR, R., ENGEL, J. & KAMMERER, R. A. 2000. Crystal structure of a naturally occurring parallel right-handed coiled coil tetramer. *Nat Struct Biol*, 7, 772-6.
- STOMMEL, J. M., MARCHENKO, N. D., JIMENEZ, G. S., MOLL, U. M., HOPE, T. J. & WAHL, G. M. 1999. A leucine-rich nuclear export signal in the p53 tetramerization domain: regulation of subcellular localization and p53 activity by NES masking. *EMBO J*, 18, 1660-72.
- STRAUSSMAN, R., BEN-YA'ACOV, A., WOOLFSON, D. N. & RAVID, S. 2007. Kinking the coiled coil--negatively charged residues at the coiled-coil interface. *J Mol Biol*, 366, 1232-42.
- STROM, A. C. & WEIS, K. 2001. Importin-beta-like nuclear transport receptors. *Genome Biol*,

2, REVIEWS3008.

- TARAPORE, P., OKUDA, M. & FUKASAWA, K. 2002. A mammalian in vitro centriole duplication system: evidence for involvement of CDK2/cyclin E and nucleophosmin/B23 in centrosome duplication. *Cell Cycle*, 1, 75-81.
- TELLER, D. C., SWANSON, E. & DE HAEN, C. 1979. The translational friction coefficient of proteins. *Methods Enzymol*, 61, 103-24.
- TRIPET, B., WAGSCHAL, K., LAVIGNE, P., MANT, C. T. & HODGES, R. S. 2000. Effects of side-chain characteristics on stability and oligomerization state of a de novo-designed model coiled-coil: 20 amino acid substitutions in position "d". *J Mol Biol*, 300, 377-402.
- TSOU, M. F. & STEARNS, T. 2006. Controlling centrosome number: licenses and blocks. *Curr Opin Cell Biol*, 18, 74-8.
- TSOU, M. F. & STEARNS, T. 2006. Mechanism limiting centrosome duplication to once per cell cycle. *Nature*, 442, 947-51.
- TWOMEY, C., WATTAM, S. L., PILLAI, M. R., RAPLEY, J., BAXTER, J. E. & FRY, A. M. 2004. Nek2B stimulates zygotic centrosome assembly in *Xenopus laevis* in a kinase-independent manner. *Dev Biol*, 265, 384-98.
- UTO, K. & SAGATA, N. 2000. Nek2B, a novel maternal form of Nek2 kinase, is essential for the assembly or maintenance of centrosomes in early *Xenopus* embryos. *EMBO J*, 19, 1816-26.
- VRANKEN, W. F., BOUCHER, W., STEVENS, T. J., FOGH, R. H., PAJON, A., LLINAS, M., ULRICH, E. L., MARKLEY, J. L., IONIDES, J. & LAUE, E. D. 2005. The CCPN data model for NMR spectroscopy: development of a software pipeline. *Proteins*, 59, 687-96.
- WAGNER, G. & WUTHRICH, K. 1982. Amide protein exchange and surface conformation of

the basic pancreatic trypsin inhibitor in solution. Studies with two-dimensional nuclear magnetic resonance. *J Mol Biol*, 160, 343-61.

WAGNER, G. & WUTHRICH, K. 1986. Observation of internal motility of proteins by nuclear magnetic resonance in solution. *Methods Enzymol*, 131, 307-26.

WAI, D. H., SCHAEFER, K. L., SCHRAMM, A., KORSCHING, E., VAN VALEN, F., OZAKI, T., BOECKER, W., SCHWEIGERER, L., DOCKHORN-DWORNICZAK, B. & POREMBA, C. 2002. Expression analysis of pediatric solid tumor cell lines using oligonucleotide microarrays. *Int J Oncol*, 20, 441-51.

WALSHAW, J. & WOOLFSON, D. N. 2003. Extended knobs-into-holes packing in classical and complex coiled-coil assemblies. *J Struct Biol*, 144, 349-61.

WANG, L., MUKHERJEE, S., NARAYAN, O. & ZHAO, L. J. 1996. Characterization of a leucine-zipper-like domain in Vpr protein of human immunodeficiency virus type 1. *Gene*, 178, 7-13.

WECKER, K., BONNET, M. C., MEURS, E. F. & DELEPIERRE, M. 2002. The role of the phosphorus BI-BII transition in protein-DNA recognition: the NF-kappaB complex. *Nucleic Acids Res*, 30, 4452-9.

WELCH, P. A., SINHA, V. P., CLEVERLY, A. L., DARSTEIN, C., FLANAGAN, S. D. & MUSIB, L. C. 2007. Safety, tolerability, QTc evaluation, and pharmacokinetics of single and multiple doses of enzastaurin HCl (LY317615), a protein kinase C-beta inhibitor, in healthy subjects. *J Clin Pharmacol*, 47, 1138-51.

WENDT, H., BERGER, C., BAICI, A., THOMAS, R. M. & BOSSHARD, H. R. 1995. Kinetics of folding of leucine zipper domains. *Biochemistry*, 34, 4097-107.

WESTWOOD, J. A., MURRAY, W. K., TRIVETT, M., HAYNES, N. M., SOLOMON, B., MILESHKIN, L., BALL, D., MICHAEL, M., BURMAN, A., MAYURA-GURU, P., TRAPANI, J. A., PEINERT,

- S., HONEMANN, D., MILES PRINCE, H., SCOTT, A. M., SMYTH, M. J., DARCY, P. K. & KERSHAW, M. H. 2009. The Lewis-Y carbohydrate antigen is expressed by many human tumors and can serve as a target for genetically redirected T cells despite the presence of soluble antigen in serum. *J Immunother*, 32, 292-301.
- WHELLIGAN, D. K., SOLANKI, S., TAYLOR, D., THOMSON, D. W., CHEUNG, K. M., BOXALL, K., MAS-DROUX, C., BARILLARI, C., BURNS, S., GRUMMITT, C. G., COLLINS, I., VAN MONTFORT, R. L., AHERNE, G. W., BAYLISS, R. & HOELDER, S. 2010. Aminopyrazine inhibitors binding to an unusual inactive conformation of the mitotic kinase Nek2: SAR and structural characterization. *J Med Chem*, 53, 7682-98.
- WILLIAMS, C., PONTEN, F., AHMADIAN, A., REN, Z. P., LING, G., ROLLMAN, O., LJUNG, A., JASPERS, N. G., UHLEN, M., LUNDEBERG, J. & PONTEN, J. 1998. Clones of normal keratinocytes and a variety of simultaneously present epidermal neoplastic lesions contain a multitude of p53 gene mutations in a xeroderma pigmentosum patient. *Cancer Res*, 58, 2449-55.
- WOLF, E., KIM, P. S. & BERGER, B. 1997. MultiCoil: a program for predicting two- and three-stranded coiled coils. *Protein Sci*, 6, 1179-89.
- WOOLFSON, D. N. & ALBER, T. 1995. Predicting oligomerization states of coiled coils. *Protein Sci*, 4, 1596-607.
- WU, W., BAXTER, J. E., WATTAM, S. L., HAYWARD, D. G., FARDILHA, M., KNEBEL, A., FORD, E. M., DA CRUZ E SILVA, E. F. & FRY, A. M. 2007. Alternative splicing controls nuclear translocation of the cell cycle-regulated Nek2 kinase. *J Biol Chem*, 282, 26431-40.
- YAMAGUCHI, M., SUGAHARA, K., SHIOSAKI, K., MIZOKAMI, H. & TAKEO, K. 1998. Fine structure of hepatitis B virus surface antigen produced by recombinant yeast: comparison with HBsAg of human origin. *FEMS Microbiol Lett*, 165, 363-7.

- YANG, J., LIU, X., YUE, G., ADAMIAN, M., BULGAKOV, O. & LI, T. 2002. Rootletin, a novel coiled-coil protein, is a structural component of the ciliary rootlet. *J Cell Biol*, 159, 431-40.
- YANG, S., LIU, X., YIN, Y., FUKUDA, M. N. & ZHOU, J. 2008. Tastin is required for bipolar spindle assembly and centrosome integrity during mitosis. *FASEB J*, 22, 1960-72.
- YANG, Z., LONCAREK, J., KHODJAKOV, A. & RIEDER, C. L. 2008. Extra centrosomes and/or chromosomes prolong mitosis in human cells. *Nat Cell Biol*, 10, 748-51.
- YUNIS, J. J. 1986. Chromosome and oncogene rearrangements in leukemia and lymphoma. *Monogr Pathol*, 91-6.
- ZENG, X., SHAIKH, F. Y., HARRISON, M. K., ADON, A. M., TRIMBOLI, A. J., CARROLL, K. A., SHARMA, N., TIMMERS, C., CHODOSH, L. A., LEONE, G. & SAAVEDRA, H. I. 2010. The Ras oncogene signals centrosome amplification in mammary epithelial cells through cyclin D1/Cdk4 and Nek2. *Oncogene*, 29, 5103-12.
- ZHANG, H., MA, G., DONG, M., ZHAO, M., SHEN, X., MA, Z. & GUO, K. 2006. Epidermal growth factor promotes invasiveness of pancreatic cancer cells through NF-kappaB-mediated proteinase productions. *Pancreas*, 32, 101-9.
- ZHANG, Y. & XIONG, Y. 2001. A p53 amino-terminal nuclear export signal inhibited by DNA damage-induced phosphorylation. *Science*, 292, 1910-5.
- ZHOU, N. E., KAY, C. M. & HODGES, R. S. 1993. Disulfide bond contribution to protein stability: positional effects of substitution in the hydrophobic core of the two-stranded alpha-helical coiled-coil. *Biochemistry*, 32, 3178-87.
- ZHOU, W., TAKUWA, N., KUMADA, M. & TAKUWA, Y. 1993. Protein kinase C-mediated bidirectional regulation of DNA synthesis, RB protein phosphorylation, and cyclin-dependent kinases in human vascular endothelial cells. *J Biol Chem*, 268, 23041-8.

ZIMMERMANN, K. C., SARBIA, M., WEBER, A. A., BORCHARD, F., GABBERT, H. E. & SCHROR,

K. 1999. Cyclooxygenase-2 expression in human esophageal carcinoma. *Cancer Res*,

59, 198-204.

Grzesiek S and Bax A. (1993). Amino-acid type determination in the sequential assignment

procedure of uniformly C-13/N-15-enriched proteins. *J. Biomol. NMR*, **3**: 185-204

Braunschweiler L and Ernst RR. (1983). Coherence transfer by isotropic mixing - application

to proton correlation spectroscopy. *Journal of Magnetic Resonance*, **53**: 521-528.

Bodenhausen G and Ruben DJ. (1980). Natural abundance N-15 NMR by enhanced

heteronuclear spectroscopy. *Chemical Physics Letters*, **69**: 185-189.

Bax A, Clore GM and Gronenborn AM. (1990). H-1-H-1 correlation via isotropic mixing of C-

13 magnetization, a new 3-dimensional approach for assigning H-1 and C-13 spectra

of C-13-enriched proteins. *Journal of Magnetic Resonance*, **88**: 425-431.

Bax, A and Pochapsky, S., (1992). *J. Magn. Reson.* 99, 638

Ernst R, Bodenhausen, G and Wokaun A. (1987). Principles of Nuclear Magnetic Resonance

in One and Two Dimensions. Clarendon Press, Oxford.

Lipari, G., and A. Szabo. 1982a. Model-free approach to the interpretation of nuclear

magnetic resonance relaxation in macromolecules. 1. Theory and range of

validity. *J Am Chem Soc.* 104:4546- 4559.

Lipari, G., and A. Szabo. 1982b. Model-free approach to the interpretation of nuclear

magnetic resonance relaxation in macromolecules. 2. Analysis of experimental

results. *J Am Chem Soc.* 104:4559-4570.

A. Abraham, (1961) "Principles of Nuclear Magnetism," pp. 1-599, Clarendon Press, Oxford.

McConnell, H. M., (1956), *J. Chem. Phys.*, 24, 764.

McConnell, H. M., (1958) Reaction rates by nuclear magnetic resonance. *J Chem Phys*

28:430–431

Gutowsky, McCall, and Slichter, (1953) *J. Chem. Phys.* **21**, 279 .

H. S. Gutowsky and C. H. Holm, (1956). Rate Processes and Nuclear Magnetic Resonance Spectra. II. Hindered Internal Rotation of Amides. *J. Chem. Phys.* **25**, 1228

Overhauser, A.W., (1953). Polarization of Nuclei in Metals. *Phys. Rev.* 92, 411–415

Anderson, W. A.; Freeman, R. (1962). "Influence of a Second Radiofrequency Field on High-Resolution Nuclear Magnetic Resonance Spectra". *The Journal of Chemical Physics* **37** (1): 411–5

J. Jeener, B.H. Meier, P. Bachmann and R.R. Ernst (1979). "Investigation of exchange processes by two-dimensional NMR Spectroscopy.". *J. Chem. Phys* **71**: 4546–4553.

Macura, S and Ernst, R.R. (1980) *Mol. Phys.*, 41, 95-117.

Morris, GA, Freeman R. 1979. ENHANCEMENT OF NUCLEAR MAGNETIC-RESONANCE SIGNALS BY POLARIZATION TRANSFER. *Journal of the American Chemical Society.* 101:760-762

Kay, Torchia and Bax (1989) Backbone Dynamics of Proteins As Studied by ¹⁵N Inverse Detected Heteronuclear NMR Spectroscopy: Application to Staphylococcal Nuclease. *Biochemistry* 1989, 28, 8972-8979

Palmer, A. G.,Rance, M. & Wright, P. E. (1991) *J. Am. Chem. Soc.* **113**, 4371-4380.

S.H. Smallcombe, (1993). Solvent suppression with symmetrically-shifted pulses, *J. Am. Chem. Soc* 115

E. L. Hahn and D. E. Maxwell (1952). Spin Echo Measurements of Nuclear Spin Coupling in Molecules. *Phys. Rev.* 88, 1070–1084

T.M. Laue et al. (1992) Computer-Aided Interpretation of Analytical Sedimentation Data for Proteins pp 90-125 in "Analytical Ultracentrifugation in Biochemistry and Polymer

Sciences"

Demeler, B. UltraScan A Comprehensive Data Analysis Software Package for Analytical Ultracentrifugation Experiments. Modern Analytical Ultracentrifugation: Techniques and Methods. D. J. Scott, S.E. Harding and A.J. Rowe. Eds. Royal Society of Chemistry (UK) (2005) 210-229

CHAPTER 7

APPENDIX

A1. CD raw data for the leucine zipper mutants

LZ5-K309C oxidised at 100 µM

```
#XUNITS      Temperature [C]
#YUNITS      CD [mdeg]
#Y2UNITS     HT [V]
#FIRSTX      5.0000
#LASTX       85.0000
#NPOINTS     81
#FIRSTY      -55.95370
#MAXY        -17.17440
#MINY        -55.95370
#XYDATA
5.0000      -55.9537    351.183
6.0000      -55.6698    351.255
7.0000      -55.726     351.325
8.0000      -55.6955    351.512
9.0000      -55.2964    351.613
10.0000     -55.2807   351.767
11.0000     -54.7861   351.924
12.0000     -54.8117   352.053
13.0000     -54.3844   352.243
14.0000     -53.8848   352.385
15.0000     -53.7972   352.589
16.0000     -53.6009   352.695
17.0000     -53.0737   352.865
18.0000     -53.2595   353.051
19.0000     -52.922    353.238
20.0000     -52.9119   353.433
21.0000     -52.2173   353.632
22.0000     -52.0414   353.86
23.0000     -51.8173   354.11
24.0000     -51.5002   354.267
25.0000     -51.5538   354.485
26.0000     -51.2845   354.724
27.0000     -50.8427   354.813
28.0000     -50.2781   354.951
29.0000     -49.7414   355.095
30.0000     -49.0362   355.201
31.0000     -48.3684   355.365
32.0000     -47.9272   355.471
33.0000     -47.5902   355.67
34.0000     -46.7401   355.808
35.0000     -46.3709   355.943
36.0000     -46.2722   356.196
37.0000     -45.9817   356.414
38.0000     -44.7621   356.676
39.0000     -44.4839   356.896
40.0000     -44.586    357.156
41.0000     -43.1715   357.344
42.0000     -42.8321   357.591
43.0000     -42.5006   357.836
44.0000     -42.2071   358.072
45.0000     -41.1934   358.352
46.0000     -40.2376   358.565
```

47.0000	-39.6576	358.793
48.0000	-39.0492	359.054
49.0000	-38.3111	359.254
50.0000	-37.1376	359.53
51.0000	-36.2586	359.772
52.0000	-35.6727	360.002
53.0000	-34.5446	360.247
54.0000	-33.9723	360.494
55.0000	-32.354	360.793
56.0000	-31.686	360.995
57.0000	-30.7158	361.207
58.0000	-29.8712	361.542
59.0000	-28.5135	361.822
60.0000	-27.8494	362.103
61.0000	-27.2515	362.412
62.0000	-26.3914	362.646
63.0000	-25.5002	362.956
64.0000	-24.1601	363.335
65.0000	-23.5864	363.587
66.0000	-23.345	363.912
67.0000	-22.0827	364.343
68.0000	-21.2783	364.744
69.0000	-20.6139	365.148
70.0000	-20.3139	365.573
71.0000	-20.3338	366.154
72.0000	-19.8514	366.585
73.0000	-19.9123	367.08
74.0000	-19.0363	367.622
75.0000	-18.6547	368.103
76.0000	-18.6358	368.627
77.0000	-18.5686	369.22
78.0000	-18.0672	369.821
79.0000	-18.1541	370.371
80.0000	-17.5354	371.176
81.0000	-17.2264	371.682
82.0000	-17.3756	372.242
83.0000	-17.1744	372.913
84.0000	-17.415	373.66
85.0000	-17.1904	374.369

LZ5-K309C reduced at 100 µM

#XUNITS	Temperature [C]	
#YUNITS	CD [mdeg]	
#Y2UNITS	HT [V]	
#FIRSTX	5.0000	
#LASTX	85.0000	
#NPOINTS	81	
#FIRSTY	-52.69630	
#MAXY	-14.81860	
#MINY	-52.69630	
#XYDATA		
5.0000	-52.6963	444.571
6.0000	-52.3404	444.592
7.0000	-51.8146	445.087
8.0000	-51.3459	445.667
9.0000	-49.8517	446.415

10.0000	-49.7124	447.104
11.0000	-49.3269	447.815
12.0000	-48.2239	448.677
13.0000	-47.9739	449.479
14.0000	-45.9349	450.256
15.0000	-45.61	451.145
16.0000	-44.2096	451.975
17.0000	-43.2762	452.758
18.0000	-42.2055	453.774
19.0000	-41.4662	454.569
20.0000	-40.1954	455.43
21.0000	-38.3091	456.317
22.0000	-38.2284	457.451
23.0000	-36.5888	458.38
24.0000	-34.9754	459.183
25.0000	-34.122	460.176
26.0000	-33.7993	461.216
27.0000	-32.195	462.22
28.0000	-30.4294	463.182
29.0000	-29.9905	464.295
30.0000	-29.7114	465.307
31.0000	-27.685	466.313
32.0000	-27.1621	467.309
33.0000	-26.479	468.503
34.0000	-24.9192	469.669
35.0000	-23.3503	470.636
36.0000	-23.6808	471.884
37.0000	-23.5723	472.919
38.0000	-22.4825	474.156
39.0000	-20.8491	475.265
40.0000	-22.5748	476.46
41.0000	-20.4609	477.645
42.0000	-21.1573	478.868
43.0000	-20.9174	479.967
44.0000	-20.57	481.171
45.0000	-19.7669	482.347
46.0000	-18.1973	483.475
47.0000	-18.093	484.737
48.0000	-18.1292	485.694
49.0000	-18.1349	486.502
50.0000	-16.6991	486.937
51.0000	-17.6714	488.572
52.0000	-17.4394	490.721
53.0000	-18.6854	492.284
54.0000	-16.5622	494.082
55.0000	-17.5703	495.786
56.0000	-18.0504	497.363
57.0000	-17.5438	499.109
58.0000	-16.0299	500.976
59.0000	-16.1874	502.542
60.0000	-16.1591	504.251
61.0000	-17.2406	506.132
62.0000	-16.4311	507.858
63.0000	-15.8079	509.629
64.0000	-16.583	511.382
65.0000	-16.887	512.766
66.0000	-15.899	514.42
67.0000	-15.7045	516.455

68.0000	-16.209	518.237
69.0000	-15.0438	519.943
70.0000	-15.3244	522.138
71.0000	-16.6001	523.893
72.0000	-15.5963	525.494
73.0000	-15.7709	526.679
74.0000	-15.4427	528.735
75.0000	-15.9043	530.789
76.0000	-15.7132	532.873
77.0000	-16.0707	534.898
78.0000	-16.6896	537.017
79.0000	-17.1622	539.851
80.0000	-15.6217	542.152
81.0000	-16.3211	544.611
82.0000	-14.9384	546.64
83.0000	-16.4545	549.454
84.0000	-14.8186	551.9
85.0000	-16.2073	554.561

LZ5-K310C oxidised at 100 µM

#XUNITS	Temperature [C]
#YUNITS	CD [mdeg]
#Y2UNITS	HT [V]
#FIRSTX	5.0000
#LASTX	85.0000
#NPOINTS	81
#FIRSTY	-105.67800
#MAXY	-33.15400
#MINY	-105.67800
#XYDATA	
5.0000	105.678 392.54
6.0000	105.344 392.454
7.0000	105.625 392.492
8.0000	105.075 392.504
9.0000	104.282 392.507
10.0000	103.664 392.575
11.0000	103.467 392.607
12.0000	102.671 392.6
13.0000	102.695 392.685
14.0000	102.107 392.751
15.0000	101.303 392.795
16.0000	101.071 392.792
17.0000	100.062 392.927
18.0000	99.4323 392.92
19.0000	99.258 392.982
20.0000	98.3583 393.089
21.0000	98.184 393.083
22.0000	97.1296 393.175
23.0000	96.5494 393.254
24.0000	95.4146 393.216
25.0000	95.0129 393.321
26.0000	94.4278 393.384
27.0000	93.0047 393.387
28.0000	92.1579 393.473

29.0000	91.6625	393.49
30.0000	90.2918	393.555
31.0000	89.9679	393.566
32.0000	88.141	393.585
33.0000	87.416	393.702
34.0000	86.2052	393.75
35.0000	84.8023	393.775
36.0000	82.9681	393.806
37.0000	81.5907	393.887
38.0000	80.0106	393.908
39.0000	78.031	393.944
40.0000	76.7328	393.965
41.0000	74.3995	394.045
42.0000	72.8524	394.111
43.0000	70.7381	394.125
44.0000	68.8924	394.127
45.0000	66.4994	394.181
46.0000	64.5687	394.194
47.0000	63.1102	394.225
48.0000	60.1833	394.281
49.0000	59.1029	394.375
50.0000	56.8454	394.429
51.0000	54.709	394.442
52.0000	52.7465	394.553
53.0000	50.7501	394.639
54.0000	49.3527	394.698
55.0000	47.7684	394.811
56.0000	46.4283	394.837
57.0000	44.6796	394.978
58.0000	42.9874	395.082
59.0000	42.9491	395.207
60.0000	41.836	395.307
61.0000	41.4484	395.441
62.0000	40.3143	395.544
63.0000	39.0436	395.658
64.0000	38.3615	395.794
65.0000	37.6392	395.89
66.0000	36.6802	396.065
67.0000	37.0895	396.161
68.0000	36.0945	396.313
69.0000	35.346	396.441
70.0000	34.8365	396.662
71.0000	35.1343	396.866
72.0000	35.0803	397.103
73.0000	34.6867	397.29
74.0000	34.1634	397.538
75.0000	34.8154	397.79
76.0000	33.6317	398.004
77.0000	34.2108	398.218
78.0000	33.6092	398.375
79.0000	33.2592	398.605
80.0000	33.7534	398.812
81.0000	33.7005	398.992
82.0000	33.9494	399.147
83.0000	33.4996	399.433
84.0000	33.3284	399.513
85.0000	33.154	399.684

LZ5-K310C reduced at 100 µM

```
#XUNITS      Temperature [C]
#YUNITS      CD [mdeg]
#Y2UNITS     HT [V]
#FIRSTX      5.0000
#LASTX       85.0000
#NPOINTS     81
#FIRSTY      -93.80080
#MAXY        -40.71130
#MINY        -94.47580
#XYDATA
5.0000      93.8008    445.95
6.0000      94.4758    445.878
7.0000      93.2314    446.023
8.0000      93.3943    446.178
9.0000      92.9432    446.428
10.0000     92.4319    446.744
11.0000     91.1979    447.053
12.0000     90.7547    447.297
13.0000     91.8359    447.541
14.0000     90.051     447.87
15.0000     89.3779    448.15
16.0000     88.9921    448.497
17.0000     89.1021    448.727
18.0000     88.7095    448.993
19.0000     87.8133    449.327
20.0000     87.2814    449.597
21.0000     87.1572    449.922
22.0000     86.8906    450.192
23.0000     86.8315    450.572
24.0000     85.7451    450.869
25.0000     85.4503    451.126
26.0000     85.7893    451.495
27.0000     84.9352    451.731
28.0000     82.9088    452.05
29.0000     82.7391    452.388
30.0000     83.0263    452.727
31.0000     81.888     453.022
32.0000     80.8169    453.384
33.0000     79.4946    453.705
34.0000     80.0017    454.105
35.0000     78.8561    454.475
36.0000     77.3927    454.818
37.0000     75.8535    455.242
38.0000     74.853     455.61
39.0000     73.4585    456.027
40.0000     73.0898    456.553
41.0000     71.4077    456.958
42.0000     70.868     457.266
43.0000     69.0109    457.615
44.0000     67.5387    457.929
45.0000     65.7675    458.102
46.0000     64.0592    458.44
47.0000     62.1451    458.794
48.0000     61.4364    458.96
```

49.0000	60.2985	459.002
50.0000	57.7255	458.763
51.0000	55.7776	458.75
52.0000	53.6129	458.726
53.0000	51.6167	458.55
54.0000	51.4269	459.589
55.0000	50.753	460.599
56.0000	50.3949	461.007
57.0000	49.5892	461.357
58.0000	48.1604	461.699
59.0000	46.7848	462.066
60.0000	45.4149	462.41
61.0000	46.9446	462.769
62.0000	43.9746	463.126
63.0000	44.3675	463.216
64.0000	43.945	463.637
65.0000	42.6013	464.05
66.0000	42.7997	464.378
67.0000	43.698	464.774
68.0000	42.3962	465.168
69.0000	42.0161	465.635
70.0000	43.5269	466.011
71.0000	41.74	466.463
72.0000	41.3339	466.802
73.0000	41.5904	467.35
74.0000	41.8798	467.727
75.0000	41.9784	468.087
76.0000	41.5367	468.461
77.0000	41.0292	468.957
78.0000	41.8215	469.46
79.0000	40.7113	469.863
80.0000	41.3445	470.386
81.0000	41.733	470.96
82.0000	40.7686	471.563
83.0000	42.0359	472.065
84.0000	41.89	472.442
85.0000	41.7818	473.089

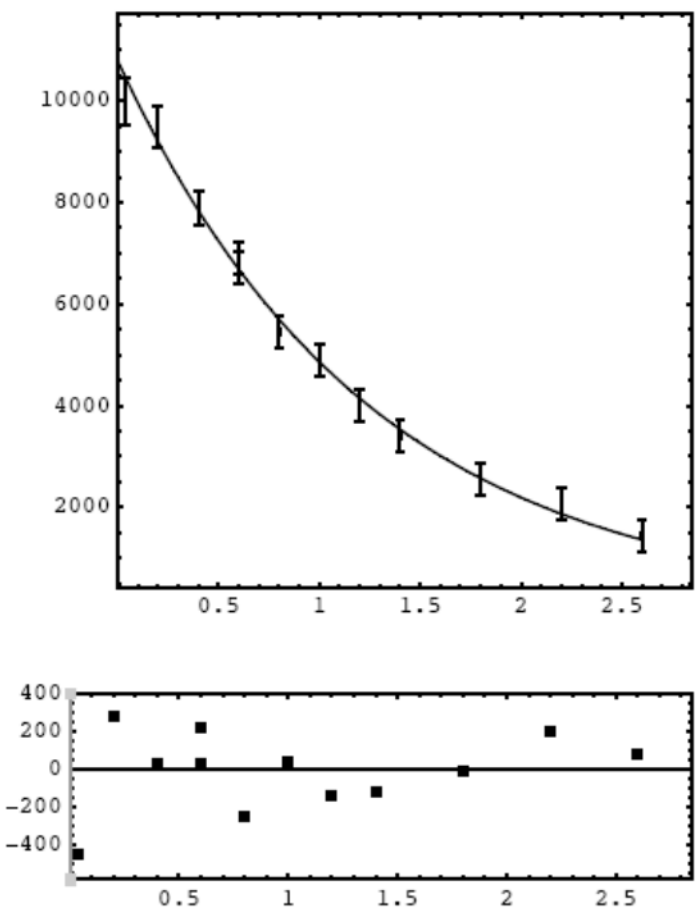


Figure A2 – R_1 fitting curve for LZ2 at 1mM for residue #12

Peak 17 was selected for fitting and Monte Carlo simulation. R_1 relaxation rates were determined to be $R = 0.797182 \pm 0.0216669 \text{ s}^{-1}$. 95% confidence interval from fit = 0.748905 to 0.845459 s^{-1} . Error in relaxation rate from Monte Carlo simulation = 0.0381496 s^{-1} . 95% confidence intervals from Monte Carlo simulation = 0.720883 to 0.87348 s^{-1} .

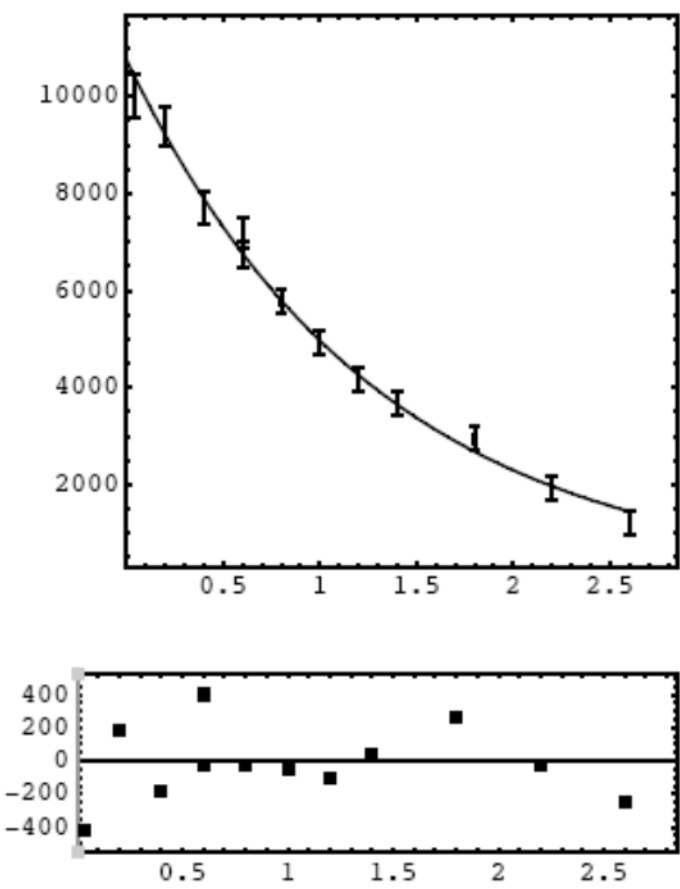


Figure A3 – R₁ fitting curve for LZ2 at 0.25mM for residue #12

Peak 17 was selected for fitting and Monte Carlo simulation. R1 relaxation rates were determined to be $R = 0.771876 \pm 0.0227225 \text{ s}^{-1}$. 95% confidence interval from fit = 0.721247 to 0.822505 s^{-1} . Error in relaxation rate from Monte Carlo simulation = 0.0307835 s^{-1} . 95% confidence intervals from Monte Carlo simulation = 0.710309 to 0.833443 s^{-1} .

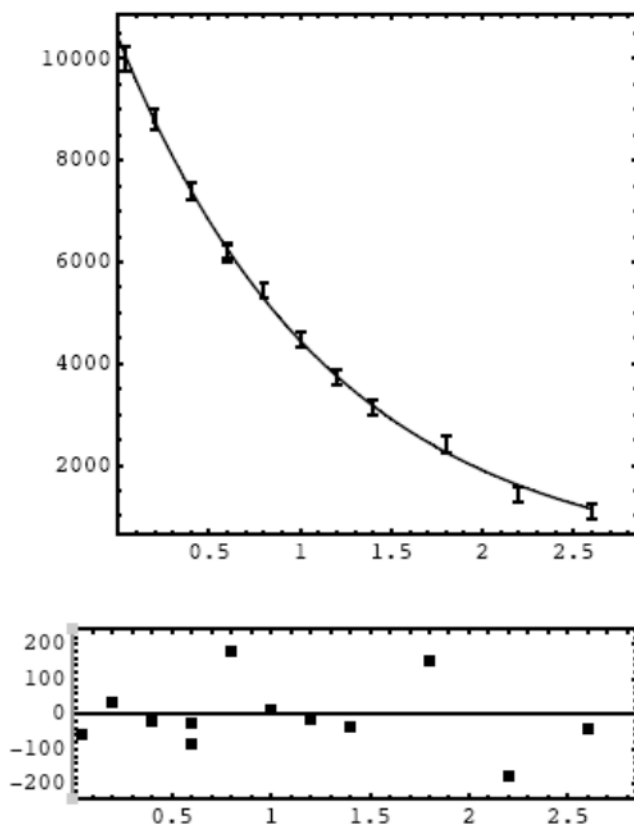


Figure A4 – R_1 fitting curve for LZ2 at 1mM for residue #20

Peak 18 was selected for fitting and Monte Carlo simulation. R_1 relaxation rates were determined to be $R = 0.849763 \pm 0.0131379 \text{ s}^{-1}$. 95% confidence interval from fit = 0.82049 to 0.879036 s^{-1} . Error in relaxation rate from Monte Carlo simulation = 0.0189228 s^{-1} . 95% confidence intervals from Monte Carlo simulation = 0.811917 to 0.887608 s^{-1} .

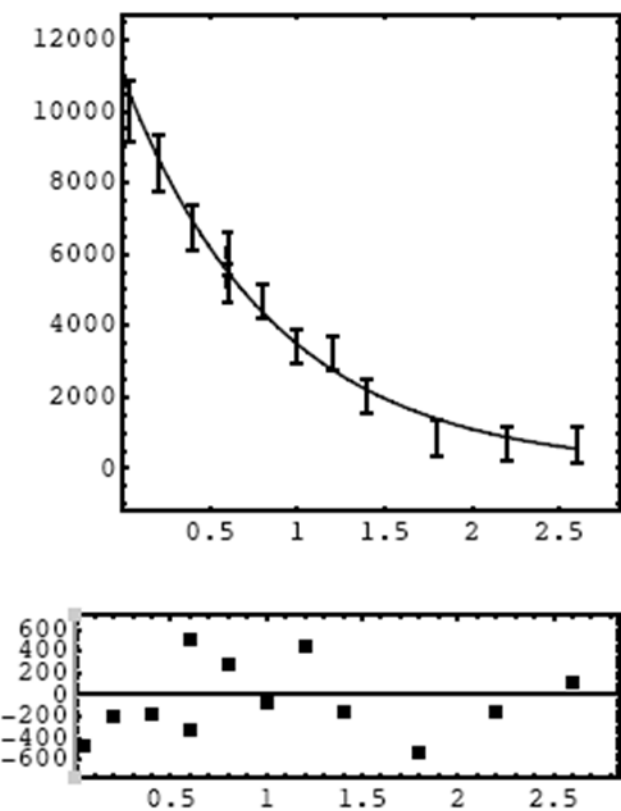


Figure A5 – R_1 fitting curve for LZ2 at 0.25mM for residue #20

Peak 18 was selected for fitting and Monte Carlo simulation. R_1 relaxation rates were determined to be $R = 1.14659 \pm 0.0576829 \text{ s}^{-1}$. 95% confidence interval from fit = 1.01806 to 1.27512 s^{-1} . Error in relaxation rate from Monte Carlo simulation = 0.0888761 s^{-1} . 95% confidence intervals from Monte Carlo simulation = 0.968838 to 1.32434 s^{-1} .

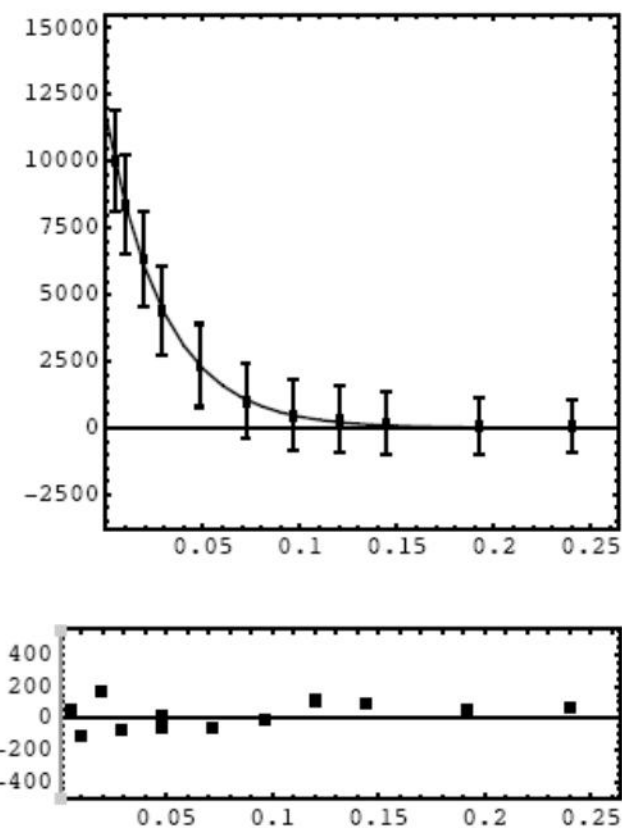


Figure A6 – R_2 fitting curve for LZ2 at 1mM for residue #12

Peak 17 was selected for fitting and Monte Carlo simulation. R_2 relaxation rates were determined to be $R = 33.1559 \pm 0.551414 \text{ s}^{-1}$. 95% confidence interval from fit = 31.9273 to 34.3846 s^{-1} . Error in relaxation rate from Monte Carlo simulation = 9.18548 s^{-1} . 95% confidence intervals from Monte Carlo simulation = 14.785 to 51.5269 s^{-1} .

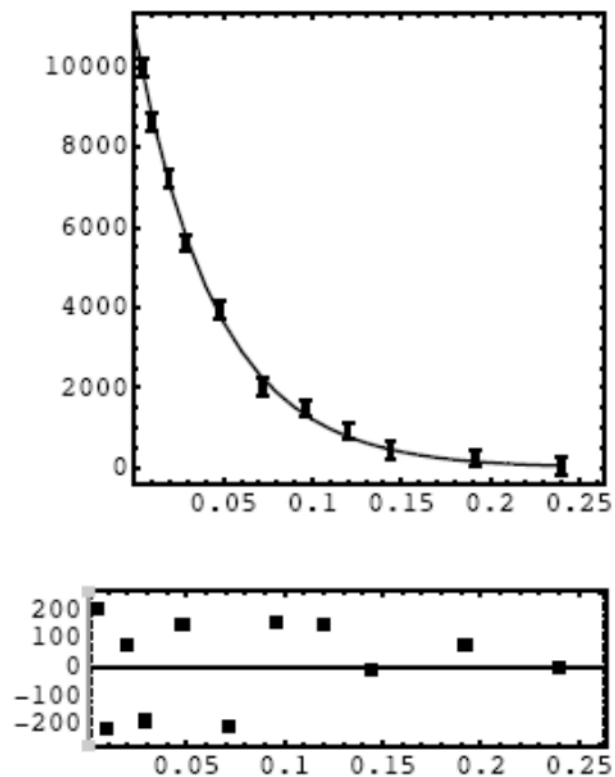


Figure A7 – R₂ fitting curve for LZ2 at 0.25mM for residue #12

Peak 17 was selected for fitting and Monte Carlo simulation. R₂ relaxation rates were determined to be $R = 21.9016 \pm 0.601841 \text{ s}^{-1}$. 95% confidence interval from fit = 20.5401 to 23.263 s^{-1} . Error in relaxation rate from Monte Carlo simulation = 0.844637 s^{-1} . 95% confidence intervals from Monte Carlo simulation = 20.2123 to 23.5908 s^{-1} .

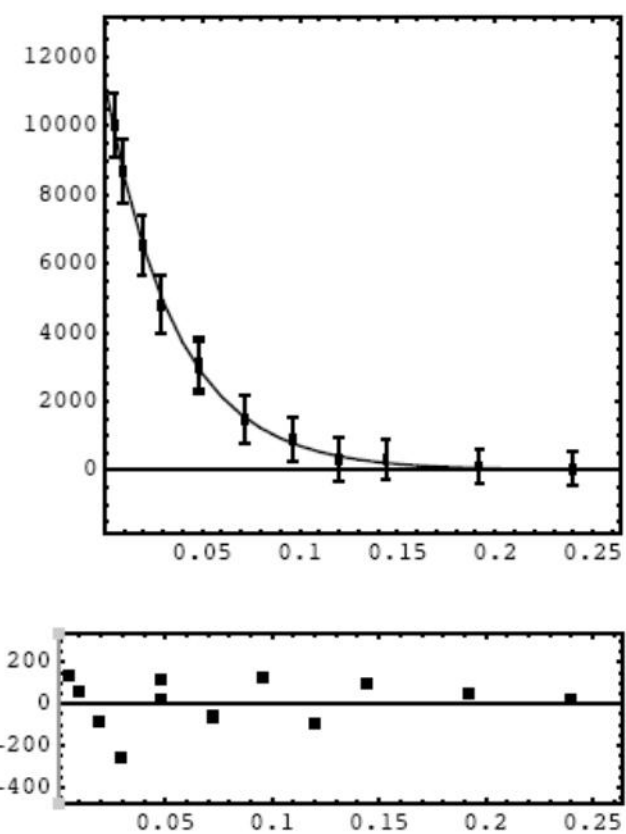


Figure A8 – R_2 fitting curve for LZ2 at 1mM for residue #20

Peak 18 was selected for fitting and Monte Carlo simulation. R_2 relaxation rates were determined to be $R = 27.7897 \pm 0.546369 \text{ s}^{-1}$. 95% confidence interval from fit = 26.5723 to 29.0071 s^{-1} . Error in relaxation rate from Monte Carlo simulation = 3.72508 s^{-1} . 95% confidence intervals from Monte Carlo simulation = 20.3395 to 35.2399 s^{-1} .

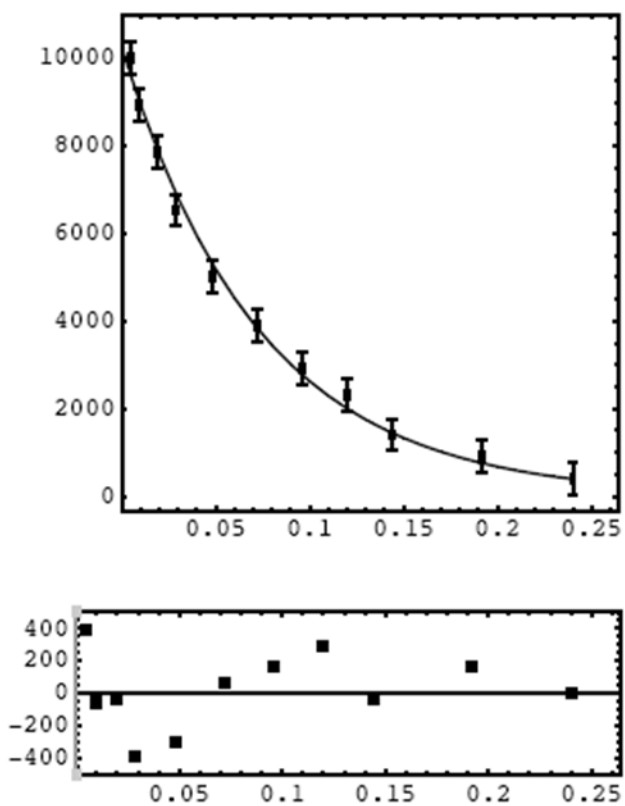


Figure A9 – R_2 fitting curve for L22 at 0.25mM for residue #20

Peak 18 was selected for fitting and Monte Carlo simulation. R_2 relaxation rates were determined to be $R = 13.6192 \pm 0.51024$ s⁻¹. 95% confidence interval from fit = 12.465 to 14.7735 s⁻¹. Error in relaxation rate from Monte Carlo simulation = 0.771826 s⁻¹. 95% confidence intervals from Monte Carlo simulation = 12.0756 to 15.1629 s⁻¹.

Position F1	Position F2	Assign F1	Assign F2	Height	Volume	Line Width F1 (Hz)	Line Width F2 (Hz)
7.92421	120.7562	{1}H[1]	{1}N[2]	2.40E+05	2.09E+06	22.79348	24.21912
8.17205	119.0555	{2}H[3]	{2}N[4]	1.16E+05	1.01E+06	24.01652	27.32651
7.45342	119.5819	{3}H[5]	{3}N[6]	1.10E+05	9.57E+05	22.54546	26.29167
8.32632	119.7919	{4}H[7]	{4}N[8]	1.96E+05	1.72E+06	24.53433	27.64336
7.90291	119.7599	{5}H[9]	{5}N[10]	5.20E+05	4.52E+06	21.20765	28.06162
8.23554	120.4801	{6}H[11]	{6}N[12]	2.03E+05	1.79E+06	47.24943	36.58448
7.63219	119.5402	{7}H[13]	{7}N[14]	1.56E+05	1.38E+06	43.60424	28.6314
7.78931	117.8793	{8}H[15]	{8}N[16]	1.30E+05	1.13E+06	22.71596	25.06597
7.94679	122.5165	{9}H[17]	{9}N[18]	2.00E+05	1.74E+06	24.36669	24.58367
7.89374	119.4038	{10}H[19]	{10}N[20]	1.32E+05	1.16E+06	28.95783	99.82374
8.06034	120.8209	{11}H[21]	{11}N[22]	2.72E+05	2.40E+06	56.68889	29.05556
8.74283	122.5166	{12}H[23]	{12}N[24]	7.97E+04	6.97E+05	25.53027	27.20627
7.87268	120.4215	{13}H[25]	{13}N[26]	1.36E+05	1.19E+06	29.66463	48.19999
8.91794	120.2375	{14}H[27]	{14}N[28]	9.09E+04	7.96E+05	26.05941	26.26572
8.09792	121.5782	{15}H[29]	{15}N[30]	1.66E+05	1.47E+06	37.67171	28.04301
7.90555	121.2079	{16}H[31]	{16}N[32]	2.06E+05	1.79E+06	22.78617	25.05198
8.35465	119.67	{17}H[33]	{17}N[34]	9.48E+04	8.40E+05	59.18784	31.21118
8.11121	121.6209	{18}H[35]	{18}N[36]	1.54E+05	1.37E+06	40.28644	29.8363
7.97979	119.7501	{19}H[37]	{19}N[38]	2.53E+05	2.25E+06	46.5869	58.56998
8.17812	124.7161	{20}H[39]	{20}N[40]	1.81E+05	1.57E+06	20.87366	24.42038
7.68443	119.7656	{21}H[41]	{21}N[42]	2.10E+05	1.85E+06	71.27383	42.68374
7.72407	118.5913	{22}H[43]	{22}N[44]	1.19E+05	1.04E+06	23.64528	26.75083
8.12757	119.9493	{23}H[45]	{23}N[46]	1.50E+05	1.33E+06	56.436	82.23292
7.73275	119.7875	{24}H[47]	{24}N[48]	2.85E+05	2.53E+06	36.05837	43.35589
7.94161	117.8392	{25}H[49]	{25}N[50]	1.59E+05	1.39E+06	21.83063	24.304
7.81026	118.7936	{26}H[51]	{26}N[52]	1.16E+05	1.02E+06	26.50401	27.93101
8.41395	118.2389	{27}H[53]	{27}N[54]	3.90E+04	3.42E+05	33.96935	28.31619
7.90646	120.0924	{28}H[55]	{28}N[56]	2.90E+05	2.56E+06	127.6734	57.76396
8.53666	119.9414	{29}H[57]	{29}N[58]	1.12E+05	9.80E+05	24.517	27.17622
7.61542	119.4835	{30}H[59]	{30}N[60]	1.69E+05	1.50E+06	39.5494	29.1523
8.03736	120.1137	{31}H[61]	{31}N[62]	1.85E+05	1.64E+06	244.1544	33.24214
7.89937	122.5068	{32}H[63]	{32}N[64]	1.85E+05	1.62E+06	26.93557	24.85659
7.7545	122.6943	{33}H[65]	{33}N[66]	2.52E+05	2.18E+06	20.12531	22.69598
8.00282	119.8734	{34}H[67]	{34}N[68]	5.09E+05	4.46E+06	25.86756	30.51499
7.9669	120.0685	{35}H[69]	{35}N[70]	4.28E+05	3.79E+06	66.85778	32.31122
8.16029	120.0463	{36}H[71]	{36}N[72]	1.61E+05	1.42E+06	129.5102	54.61786
8.05947	114.4443	{37}H[73]	{37}N[74]	9.33E+04	8.21E+05	29.29926	27.18531
7.8398	120.7798	{38}H[75]	{38}N[76]	9.08E+04	7.93E+05	35.29842	31.53983
8.08397	116.0699	{39}H[77]	{39}N[78]	1.07E+05	9.40E+05	27.21711	25.83783
8.05792	122.7575	{40}H[79]	{40}N[80]	3.09E+05	2.67E+06	19.05414	22.30617
8.2226	125.7245	{41}H[81]	{41}N[82]	1.43E+05	1.24E+06	23.77093	24.74258
7.83277	126.677	{42}H[83]	{42}N[84]	2.49E+06	2.14E+07	18.15893	18.02248
8.87284	122.3854	{43}H[85]	{43}N[86]	8.46E+04	7.42E+05	25.40075	25.67244
8.02073	120.7034	{44}H[87]	{44}N[88]	2.57E+05	2.28E+06	58.31369	37.04428
7.80166	120.174	{45}H[89]	{45}N[90]	1.22E+05	1.08E+06	28.31564	28.72707
7.72796	119.5833	{46}H[91]	{46}N[92]	2.43E+05	2.16E+06	55.77734	48.39756
7.84151	122.3199	{47}H[93]	{47}N[94]	8.66E+04	7.60E+05	35.38309	26.8482
8.15448	125.3376	{48}H[95]	{48}N[96]	8.39E+04	7.38E+05	27.73049	27.10528
7.53932	120.135	{49}H[97]	{49}N[98]	1.16E+05	1.02E+06	23.39969	26.44988
8.32334	122.2371	{50}H[99]	{50}N[100]	6.26E+04	5.53E+05	30.81259	26.63984
7.6985	119.5433	{51}H[101]	{51}N[102]	2.00E+05	1.79E+06	57.88027	46.04693
8.25056	119.6519	{52}H[103]	{52}N[104]	1.36E+05	1.20E+06	26.5126	31.72985
7.96938	123.8787	{53}H[105]	{53}N[106]	4.00E+05	3.45E+06	18.3717	21.19156
8.29137	120.0062	{54}H[107]	{54}N[108]	1.31E+05	1.15E+06	50.06991	31.26824
8.1613	120.2978	{55}H[109]	{55}N[110]	1.40E+05	1.24E+06	150.3393	59.39118
7.85785	119.1867	{56}H[111]	{56}N[112]	1.87E+05	1.63E+06	25.46193	26.9937
8.35344	123.0952	{57}H[113]	{57}N[114]	1.09E+05	9.54E+05	22.94836	26.22466
8.2125	120.4363	{58}H[115]	{58}N[116]	1.96E+05	1.75E+06	48.43422	61.70533
8.10982	120.4841	{59}H[117]	{59}N[118]	1.75E+05	1.55E+06	58.96146	55.21449
7.60562	119.0814	{60}H[119]	{60}N[120]	1.07E+05	9.41E+05	26.47048	61.45123
8.66067	121.3239	{61}H[121]	{61}N[122]	8.18E+04	7.17E+05	25.05791	27.32948
8.20951	120.1694	{62}H[123]	{62}N[124]	2.74E+05	2.40E+06	24.72962	49.91134
7.87511	118.8225	{63}H[125]	{63}N[126]	1.07E+05	9.38E+05	27.275	162.925
7.5126	118.0281	{64}H[127]	{64}N[128]	1.10E+05	9.64E+05	23.31057	25.95913
8.45362	120.986	{65}H[129]	{65}N[130]	9.67E+04	8.48E+05	25.59174	26.68547
7.84675	121.7272	{66}H[131]	{66}N[132]	1.39E+05	1.21E+06	23.56332	25.91574
8.44031	120.1387	{67}H[133]	{67}N[134]	8.67E+04	7.60E+05	27.53821	26.7403
7.84998	118.3581	{68}H[135]	{68}N[136]	1.21E+05	1.06E+06	23.78182	25.92409
7.87047	121.2917	{69}H[137]	{69}N[138]	1.12E+05	9.84E+05	57.19639	29.93836
7.74614	120.4975	{70}H[139]	{70}N[140]	1.11E+05	9.75E+05	26.0021	27.93851
8.08633	120.1909	{71}H[141]	{71}N[142]	5.86E+05	5.08E+06	20.16958	21.17794
7.73431	119.9145	{72}H[144]	{72}N[145]	2.13E+05	1.90E+06	34.42899	48.46371
8.13211	120.6188	{73}H[146]	{73}N[147]	1.41E+05	1.25E+06	47.19026	82.75548
8.22282	120.7413	{74}H[148]	{74}N[149]	1.07E+05	9.48E+05	34.45234	74.88163
8.25174	119.8659	{75}H[150]	{75}N[151]	6.87E+04	6.15E+05	230.954	109.8892
8.39007	119.5621	{76}H[152]	{76}N[153]	4.51E+04	4.04E+05	162.3568	32.36355

Figure A10 – Peak list for the HSQC experiment 2D heteronuclear correlation experiment

Peak heights were calculated using the equation (Farrow et al., 1994) and represent the auto peaks without a mixing time T, for pairs of nuclei known to undergo two site exchange.

Figure A11 – Peak list 3D exchange experiment

Peak heights were calculated using the equation (Farrow et al., 1994) and plotted against exchanging peaks with a range of mixing times T .